UNIVERSITY OF THESSALY, FACULTY OF ENGINEERING

DEPARTMENT OF MECHANICAL ENGINEERING

DEVELOPMENT OF METHODOLOGIES FOR PERFORMANCE ANALYSIS OF GRID-CONNECTED PHOTOVOLTAIC SYSTEMS

Elias Roumpakias, Dipl-Ing, MSc

Thesis Supervisor : Professor Anastassios Stamatelos

Volos, September 2019

Μέλη επταμελούς εξεταστικής επιτροπής

Πρώτος Εξεταστής (Επιβλέπων)	Σταματέλλος Αναστάσιος
Δεύτερος Εξεταστής	Τσιακάρας Παναγιώτης
Τρίτος Εξεταστής	Χαραλάμπους Γεώργιος
Τέταρτος Εξεταστής	Ανδρίτσος Νικόλαος
Πέμπτος Εξεταστής	Παντελής Δημήτριος
Έκτος Εξεταστής	Κτενά Αφροδίτη
Έβδομος Εξεταστής	Λιτσαρδάκης Γεώργιος

AKNOWLEDGMENTS

I would like to express my special thanks to my advisor Prof. Anastassios Stamatelos for his invaluable support in every aspect of this work and all the things that he taught me , starting from the courses from my Masters' degree. For the confidence he showed me in the assignment of this thesis and for keeping my morale in every difficulty we found in the course of this work. I would like to express my special thanks also , as he acted as a mentor for my professional career with his crucial consulting.

I wish to extend my sincere thanks to the other members of my supervising committee, namely, Prof. Panagiotis Tsiakaras and Prof. George Charalampous, for their valuable advice, support , help and motivations during the last years. Further, special thanks to Prof. Herricos Stapountzis as he was member of my supervising committee during the first six years and his advices were valuable.

Further, special thanks are due to Prof. Dimitrios Pantelis and Nicolaos Andritsos members of the examination board, for their valuable comments on the thesis manuscript.

I would like to express my special thanks to Prof. Aphrodite Ktena for her crucial comments and consulting in my Phd Thesis. Further, special thanks are due to Prof. George Litsardakis being a member of the examination board and for the chance that he gave me during my student years in Aristotle University Thessaloniki to study with energy issues and especially Photovoltaic technology.

From the personnel of Laboratory of Thermodynamics & Thermal Engines, special thanks are due to my colleague, Dr. Olympia Zogou for his help and support in my research and especially the first difficult years. Also, to Mr. Fotis Bouroutzikas for his assistance in experimental procedures.

Finally, I would like to appreciate my family for their support during the last difficult years.

Contents

Abstract

The growth of renewable energy - especially photovoltaic energy worldwide, and –more specifically- in Greece, is remarkable. There exist numerous grid-connected PV systems in Greek territory which have already completed ten years of operation. A challenging task for these systems is performance analysis, investigation of possible degradation in system's efficiency, formulation of a detailed solar potential record for each region and the study of factors which affect PV efficiency in each region. Furthermore, their inspection and maintenance needs are increasing fast. Thus, it becomes necessary to systematically characterize and classify the more important types of defects and correlate them to possible causes. This study has set five objectives which have been investigated through specific experimental and test set-ups. These set-ups comprise grid-connected PV installations in Thessaly and one off-grid experimental set-up in the University of Thessaly.

The first objective was to present real-world efficiency data for photovoltaic panels and photovoltaic parks, as function of air mass and environmental conditions. The experimental set-up consisted of a 2MWp grid-connected system as well as a single PV panel. The PV efficiency is observed to deteriorate quickly when the solar altitude is less than 45 degrees, or the solar insolation drops below 200 W/m^2.

The second objective was to attempt a systematic compilation of defects and devise a simple procedure to spot them by means of optical inspection, infrared inspection and electrical inspection. The experimental set-up consisted of five grid-connected 99,84kWp PV systems and one 9,88kWp rooftop installation. A methodology and guide for on-site PV inspection has been developed that may also be employed for screening newly installed PV panels on site.

The third objective was the formulation of an evaluation procedure for the photovoltaic plant's performance, based on routinely collected, real world system monitoring data. The role of air mass and clearness index variations in this context is well established and the analysis is conducted with the aid of these factors. The experimental set-up consists of a 99,84kWp grid connected PV system in Central Greece. The analysis has been carried out according to the following three directions: (i) evaluation of three existing models, (ii) performance ratio calculation and (iii) the formulation of an evaluation procedure based on normalization to Standard Reporting Conditions. A 10% fluctuation in yearly energy production was observed for the period 2013–2015. This fluctuation was investigated by means of performance ratio analysis, normalization procedure and model comparison. All results pointed to a decrease in PV panel's efficiency from the first year of operation. However, this was a small decrease covered by the terms of the manufacturer's warranty.

The fourth objective was to analyze the performance of a grid-connected 12,84 kWp PV system in central Greece for a six year period of operation. The analysis methodology was based on three axes: (i) calculation of the daily PR and yearly PR and their comparison for the 6 years of operation. The daily PR is further correlated with the averaged clearness index in order to assess the atmospheric effect on the PV performance. (ii) Application of a mathematic model, which describes PV power, to the available data. Computed values act as the reference values and deviation of the measured values thereof hint to probable changes in PV system performance. (iii) Computation of normalized efficiency to STC conditions. This included the computation of DC power from available AC data and inverters' efficiency, temperature

normalization according to the temperature coefficients of manufacturer and comparison of efficiency at various weather conditions and computation of yearly average values, respectively, with Air mass. The analysis results hint to a small performance deterioration over the years, with degradation rates ranging from 1 to 4%.

The fifth objective was the performance analysis of a grid-connected PV system with focus on the effects of dust accumulation on PV panels surface and aerosol mass concentration in Central Greece. The methodology of analysis developed in the previous objective is employed in combination with aerosol measurements. The results show that only heavily soiled surfaces have significant impact on PV performance and particularly a decrease of 5,6%. On the other hand, light or medium soiling have negligible impact on PV performance. As far as aerosol mass concentration is concerned, it does not significantly influence PV normalized efficiency in clear sky conditions.

`

Nomenclature

P_{AC} measured AC power [W]

P_{DC} computed DC power [W]

P_{STC} maximum DC power on STC [W]

P_{DC25} DC power normalized at 25°C [W]

G measured irradiance [W/m²]

G_{STC} irradiance on STC [W/m²]

G_{extra} extraterrestrial radiation on the plane normal to radiation on the nth day of year [W/m²]

G Measured irradiance [W/m²]

G_0 Extra-terrestrial solar intensity 1367 [W/m²]

k Irradiance factor [ ]

Kt Clearness index [ ]

T_C measured module temperature [K]

T_{STC} measured module temperature [K]

T_a ambient temperature [C°]

a temperature coefficient of P [%/ °C]

AM Optical path in air [relative air mass]

n_{INV} inverter efficiency [%]

n_{PV} array performance [%]

η_{STC} PV array performance on STC [%]

η_{DC25} PV array performance normalized at 25°C

E Energy [kWh]

H Total in plane irradiance[(Wh/m²)/ (W/m²)]

Y_F Specific yield factor [kWh/kW]

Y_R Reference yield [kWh/kW]

R_D Degradation Rate [%]

A Photovoltaic Panel surface area [m²]

P Local air pressure

P_0 Sea level air pressure

h Altitude of place [m]

Z_S Zenith angle [°]

E_t Equation of time

L_{LOC} Geographic Longitude

L_{STD} Time-zone of the location

t_{SOL} Solar time

t_{STD} Standard time

W_S Wind speed

Y_f System Yield [kWh/kWp]

Y_r Reference system Yield [kWh/kWp]

f_{PV} Photovoltaic panel derate factor

f_{DC} DC power derate factor

f_{AC} AC interconnection factor

f_{AGE} Age derate factor

f_{EXT} External derate factor

a_s Solar altitude angle[°]

β Slope of photovoltaic surface[°]

γ Solar azimuth surface[°]

γ_s Solar azimuth of sun[°]

δ Declination angle [°]

θ_z solar zenith angle [°]

ϕ Latitude

ω Hour angle

Abbreviations

EN European Norm

MPP Maximum Power Point

NOCT Normal operating cell temperature

STC Standard Test Conditions

PV Photovoltaic

IV Current- Voltage curve

PR Performance Ratio

CF Capacity Factor

GHI Global Horizontal Irradiation

AM Airmass

AM 1.5 Airmass 1.5 spectrum

AOI Angle of incidence

PID Potential Induced Degradation

PPC Public Power Corporation

DER Distributes energy resources

EPS Electrical power systems

List of Figures

List of Tables

1 Introduction

Renewable energy plays a central role in world energy production during the last decade, helping to attain ambitious legislated targets for CO_2 emission reduction and abatement of fossil fuel combustion. Solar power generation is one of the most common categories of renewable energy. Solar systems were expensive investments in the past, because of high costs of Photovoltaic cells. Government policies worldwide after year 2000 actively supported PV technologies by subsidization, feed in tariff systems, loans with small interest rates etc. Support of PV energy generation in combination with PV panels' technology evolution, reduced significantly the cost of initial investment. Another important factor that supported the growth of photovoltaic generation, especially in Europe, was European Union goals set for the energy sector. The first goal by 2020 was to reduce its greenhouse gas emissions by at least 20%, increase the share of renewable energy to at least 20% of consumption, and achieve energy savings of 20% or more. All EU countries must also achieve a 10% share of renewable energy in their transport sector [1]. Later, in October 2014, a new initiative was introduced with key targets: at least 40% cuts in greenhouse gas emissions (with reference to the 1990 levels), at least 32% share for renewable energy, at least 32.5% improvement in energy efficiency.

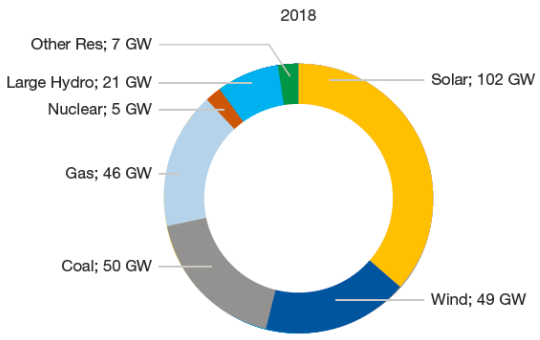

Figure 1 : Net power generating capacity added in 2018 by main technology [2]

Solar power plants exist both as standalone and grid-connected systems. Grid connected systems operate either as feed-in tariff or feed-in premium systems, according to the mode of transferring the electricity generated to the grid. Another popular policy is the net-metering, where part of the electrical consumption of residential and commercial clients is covered by solar generation and the rest from the grid, depending on the daily consumption and energy generation profiles. Finally, there are stand-alone PV systems, which operate in combination with energy storage systems to fully cover the electricity demand in remote places. For all these categories, it is important to appropriately size the PV installation, employ performance monitoring and performance evaluation. Appropriate sizing of the system, especially in net-metering and stand-alone applications, demands a very good knowledge of the region's solar potential. There are different models for estimating the solar potential using solar geometry and there exist specialized databases as PVGIS [3].

PV systems' installations in Greece expanded significantly during the last decade, profiting from the favorable feed-in tariff legislation. The Feed-in-Tariff (FiT) is a source of tariffs that implies the obligation on the part of a distribution company to buy the electricity generated by renewable energy (RE) producers in their service area . The price of this energy is set by energy policy and will be guaranteed for a determined period of

time[4].This includes not only PV park installations (2146 MWp total) but also building-top installations (351 MWp total) until 2018 [5]. Significant growth rates were observed until the end of 2013, when a correction of the legislated feed-in tariff was initiated. During the last three years, PV market priorities are shifting to net-metering, recently legislated in Greece, as well as to the maintenance and performance monitoring of existing PV parks. Due to the decrease in tariffs, depreciation of the investment cost of a PV park in a sensible period of time requires electricity generation with no significant deviations below the nominal production, which determined the initial sizing of the park, based on the expected average irradiance levels for its location.

The next step from net- metering was to keep the feed in tariff system for small scale PV installation and introduce feed in premium system through power auctions. The Premium tariffs or feed-in Premium (FiP) is a system of support for renewable energy that establishes a premium on the existing market electricity price. Thus, it generates two sources of income for the producers: one with the sale of energy in the electricity market and the other with the receipt of the premium. The premium varies based on the criteria applied in each country, energy source or technology used, size of the plant, electricity generation costs [6].

All of these support schemes and the reduction of initial cost of investment helped grid parity to be achieved quickly. Grid parity has emerged as a key indicator of the competitiveness of renewable electricity generation technologies. The term can generally be defined as the time point at which the decreasing cost of electricity from a renewable energy technology due to its technological advances intersects the cost of electricity generated from conventional fuels, such as coal and natural gas, and it is generally thought that, without any subsidies, a renewable energy technology will have cost-competitiveness [7].

In summary, solar energy is an important kind of renewable energy and especially for countries with adequate solar potential. The big growth observed during the last decade in this sector is expected to continue. Solar parks are capital intensive investments and it is very important to achieve a small payback time. This will be secured by the flawless operation of these system. In that context, a valid performance analysis is essential in order to check if PV manufacturers' warranties are met. This Phd thesis aims to formulate a methodology for performance analysis of grid-connected photovoltaic system under real world operating conditions.

1.1 Photovoltaic systems

1.1.1 Off-grid systems

Off-grid photovoltaic systems are usually combined with energy storage technology, but there are also systems that directly consume the energy produced. In cases of off-grid systems, a second source of energy is also used as back-up such as a wind turbine or a diesel generator. A typical stand-alone system consists of PV generators, an inverter, a charge regulator, batteries and electrical equipment for protection and control.

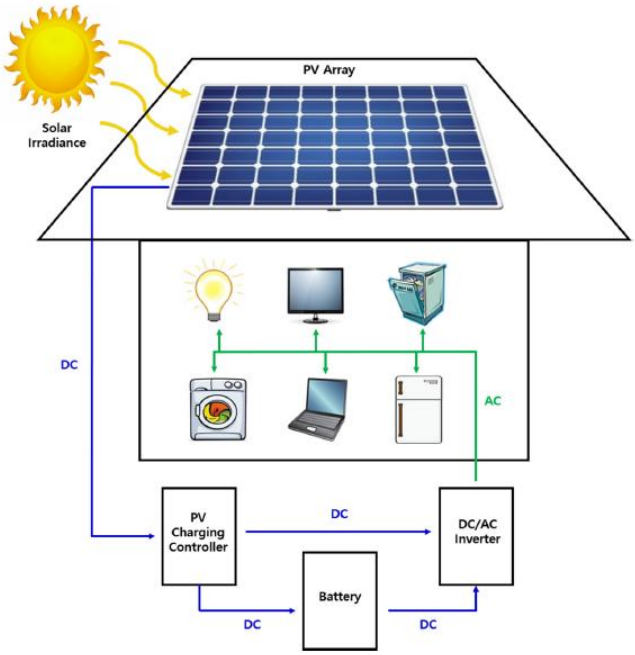

Figure 2 : Stand-alone PV system with battery back-up for residential building [8]

Off-grid systems provide significant solutions in cases where no public grid exists. Most often these systems are used in special applications to power antennas or isolated residential buildings. An appropriate energy scheduling is necessary in order to use electrical devices whenever sufficient electrical energy exists. D. Cho et al, propose a model for this purpose which is tested on four scenarios based on region and season [8]. An important factor for the appropriate sizing of these systems is a good knowledge of solar potential and other environmental variables affecting PV energy generation. The same type of information is important in cases with Hydrogen employed as back-up storage medium. C. Marino et al, study a stand-alone photovoltaic system with storage realized using electrolytic hydrogen, being converted to electricity in fuel cells. In this type of application it is important to achieve a positive annual balance between hydrogen production and consumption; moreover, the storage must meet periods with low production, such as winter. In addition, both the photovoltaic generator and storage tank must be adequately sized to avoid large production surplus that cannot be converted into hydrogen due to tank or battery capacity limitations [9].

1.1.2 Grid-connected PV systems

Grid-connected PV systems provide energy to the grid and are installed either on the ground or on rooftops. The main parts of these systems are the PV panels, inverter(s), And the distribution panel with the protection and control devices and the monitoring system (Figure 3). There are also solar tracking systems, able to follow the sun's path, by employing one-axis or two-axis tracking systems.

There are different types of PV cells, inverters and tracking systems which are analyzed in the following sections. Several factors, environmental, technical, sizing, faults, affect the PV system performance. Rao et al, summarize the factors that affect performance of grid-connected photovoltaic systems (Figure 4).

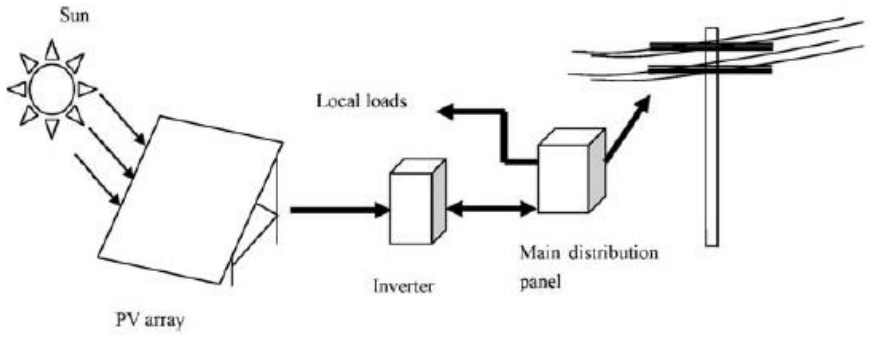

Figure 3 : Grid connected photovoltaic system[10]

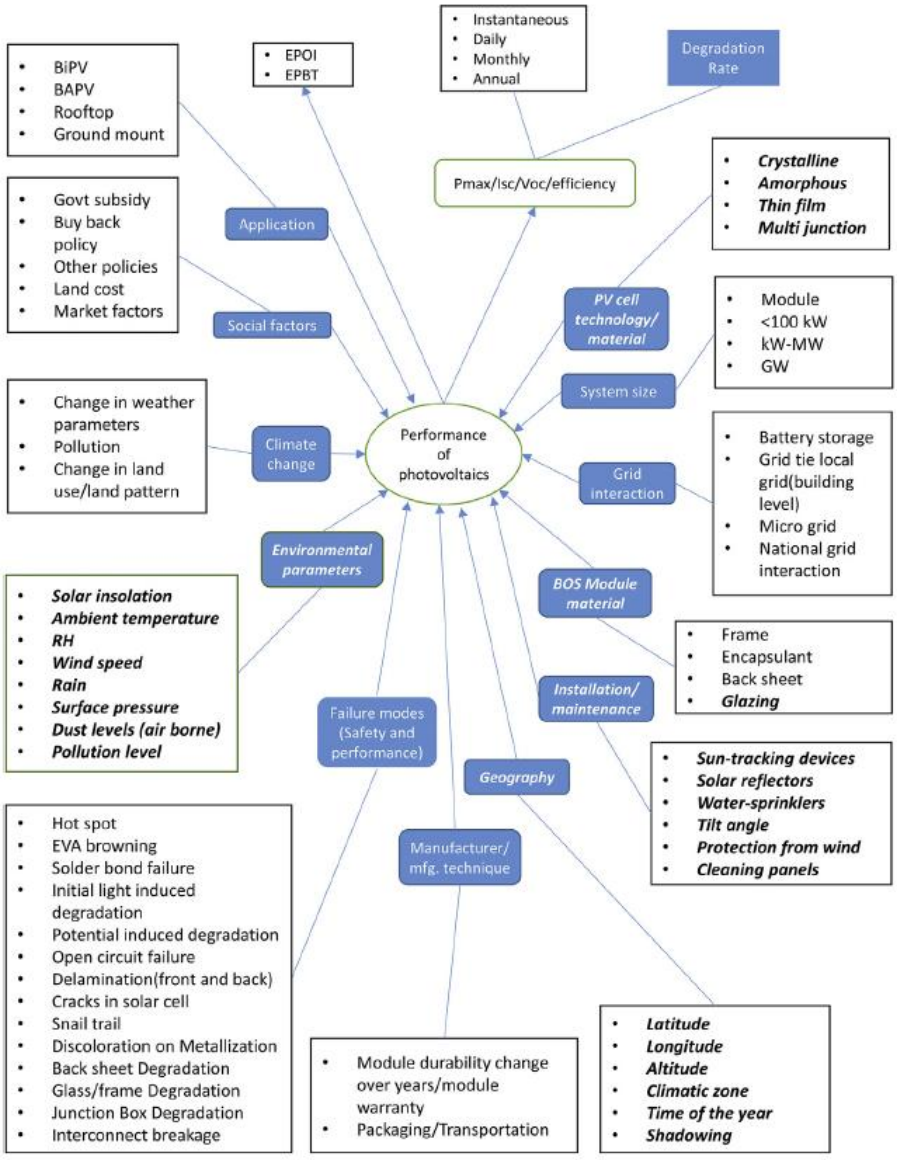

Figure 4 : Factors affecting PV performance [11]

1.1.3 Photovoltaic conversion

Specific semiconductors have the capacity to absorb light and deliver a portion of the energy of the absorbed photons to carriers of electrical current – electrons and holes. A semiconductor diode is formed when a p-type semiconductor and a n-type semiconductor are brought together to form a junction. These types of semiconductors are doped with specific impurities deliberately introduced in the crystalline lattice. The doping atoms may be Boron or Aluminium for p-type semiconductors and Phosphorus, Arsenic for n-type semiconductors.

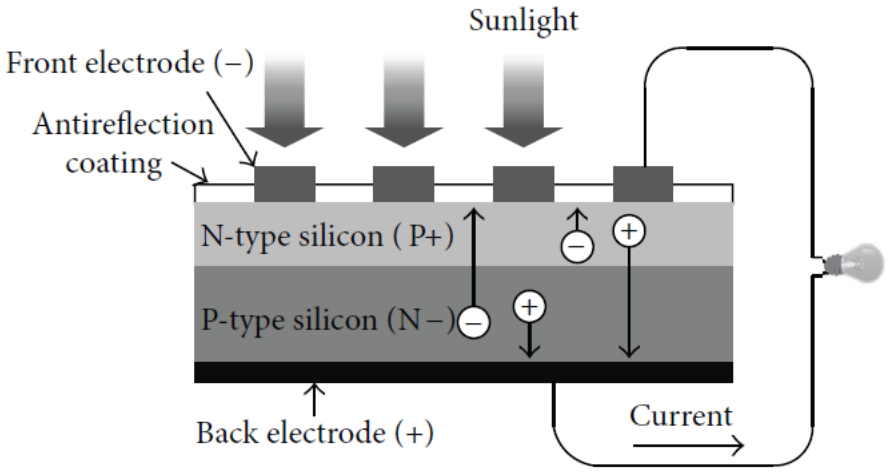

Figure 5: Crystalline silicon solar cell [12]

The junction of the two types of semiconductor create a region with free charge carriers. At this junction (Figure 5), electrons from the n-type semiconductor diffuse into the p-type, creating a zone (P+) of positively charged carriers (holes) in the n-type layer, and holes from the p-type semiconductor diffuse into the n-type, creating a zone (N+) of negatively charged carriers in the p-type layer. An electrical field is created that opposes the movement of the charge carriers. When the junction is exposed to light, photons are absorbed by valence electrons which acquire enough energy to break away from their atoms and leave behind a respective number of holes. Photons with sufficient energy create an electron–hole pair, that is, those with energy greater than the semiconductor band gap (E_G), will contribute to the energy conversion process. Then, electrons are moved into the n-region by the electrical field and holes are moved in the opposite direction of the junction, respectively. This carrier movement generates a current which is called the photovoltaic effect.

Solar cells are, usually, p-n semiconductors that operate under sunlight. However, there exist also solar cells made of n-p semiconductors, which present differences in ageing characteristics. Sunlight is composed of photons, which carry specific amounts of energy according to their frequency, determined by the spectral properties of their source. Photons also exhibit a wavelike character with the wavelength, λ, being related to the photon energy, E_λ, by

$$E_\lambda = \frac{h\,c}{\lambda} \qquad (1\text{-}1)$$

where h is Plank's constant and c is the speed of light.

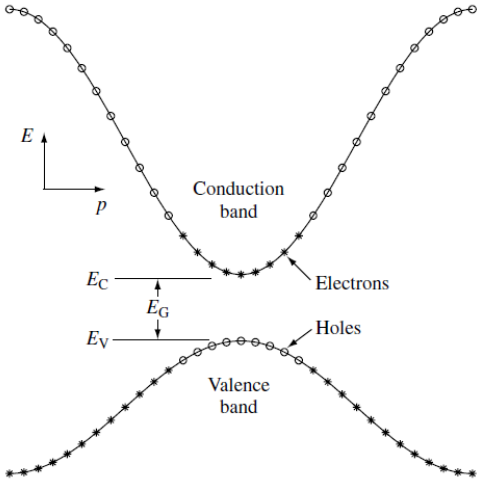

Figure 6 : Band gap energy of semiconductors [13]

1.1.4 Types of Photovoltaic technology

The most important semiconductor used for the manufacturing of PV cells is Silicon, which is the second most abundant element in the earth after oxygen. The two main forms of PV elements are wafers and thin films. The wafer-based PV elements are crystalline and divided into monocrystalline (mono) and polycrystalline (poly-si). Thin film PV technology includes amorphous silicon (a-si), microform silicon (m-si), (CIS), (CdTe), and dyes.

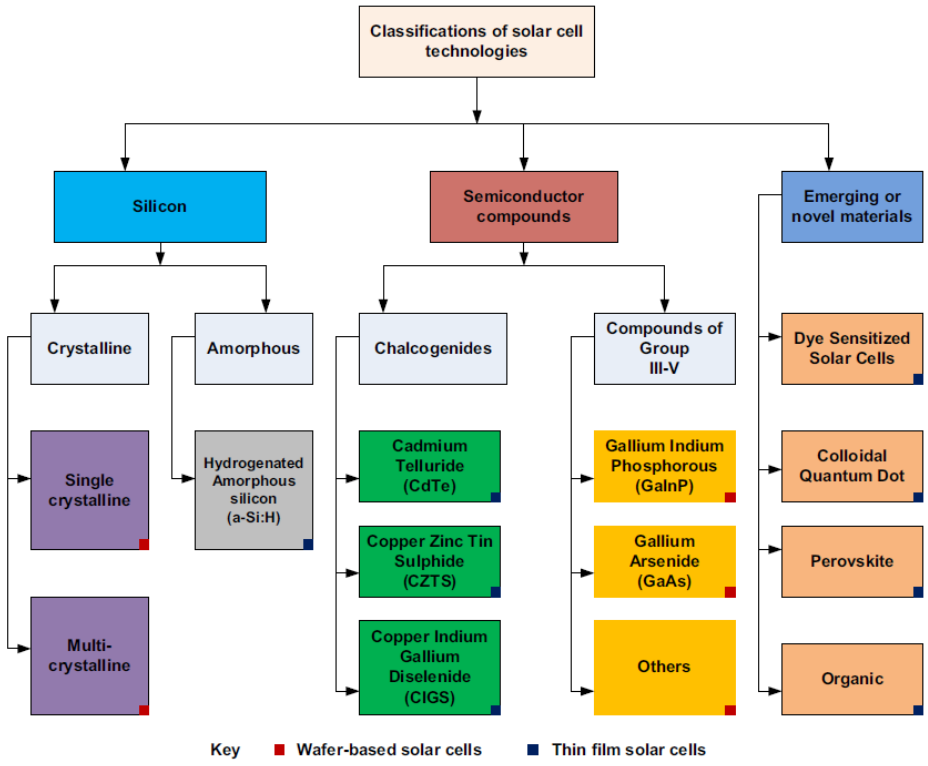

Figure 7 : Types of PV cells [14]

Figure 7 presents types of PV cells which are in the market and other types that are

under research and development studies. The most common PV types employed in commercial and residential applications are presented below.

Crystalline silicon [15]

Crystalline silicon solar cells and modules have dominated photovoltaic (PV) technology from the beginning, with more than 85% market share today. One of the reasons for this dominant position is the role of advances in microelectronics in silicon technology. The PV community has extensively benefited from the accumulated knowledge but also silicon feedstock and second-hand equipment have been acquired at reasonable prices. Conversely, Microelectronics has taken advantage of some innovations and developments proposed in Photovoltaics. For several decades, the terrestrial PV market has been dominated by p-type Czochralski silicon substrates. Continuous improvements in performance, yields and reliability have allowed important cost reductions and the subsequent expansion of the PV market.

The main categories of crystalline silicon are mono-si and poly-si solar cells. Monocrystalline solar cells attain a 15-18% energy conversion efficiency. Their shape may be square, circular or semicircular. Typical sizes of cells are 10x10cm^2, 12.5x12.5 cm^2, 15x15 cm^2 with typical thickness between 0,2-0,3 mm. The cells' color is black or deep blue. Polycrystalline solar cells usually attain 13-16% efficiency and their shape is square. Typical sizes of cells are 10x10cm^2, 12.5x12.5cm^2, 15x15cm^2, 15.6x15.6cm^2, 21x21 cm^2, with thickness 0.24-0.3mm. The cells' color is blue [16].

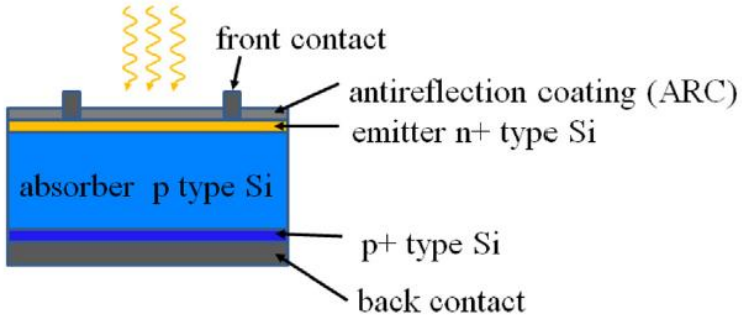

Figure 8 : Conventional crystalline cell [17]

Amorphous silicon(a-si)

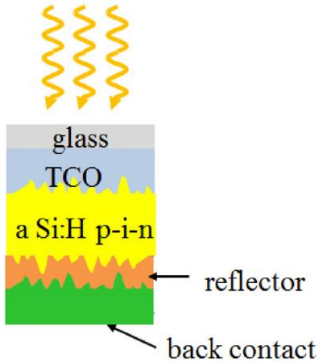

Figure 9 : Typical a-si solar cell [17]

Amorphous silicon is the most common thin film technology, with cell efficiencies in the range of 5–7% and double and triple-junction (Figure 10) designs, with enhanced

efficiency up to 8–10%. Some of the varieties of amorphous silicon are amorphous silicon carbide (a-SiC), amorphous silicon germanium (a-SiGe), microcrystalline silicon (c-Si), and amorphous silicon-nitride (a-SiN)[18].

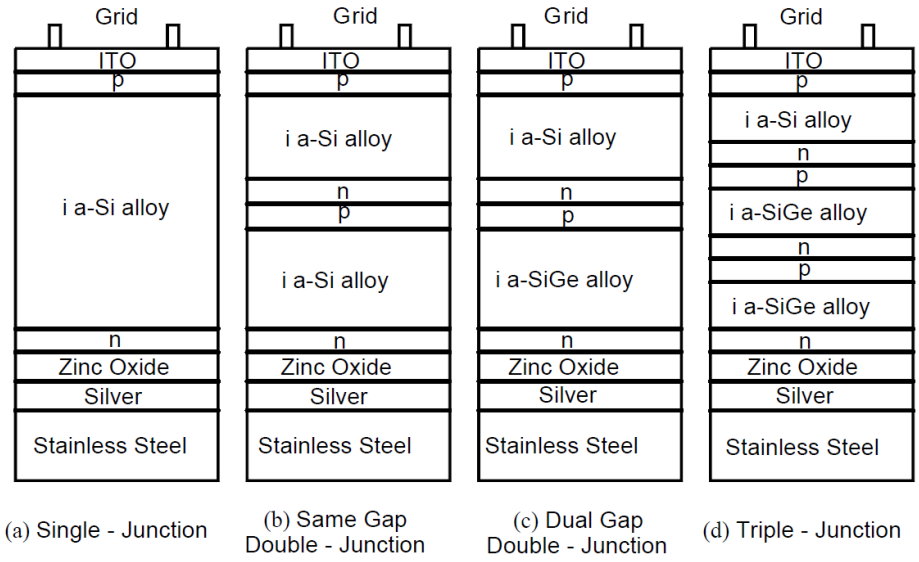

Figure 10 : Structures of a-si PV panels. Single, double and triple junction [19]

Two of the most important advantages of a-si PV panels are low cost and small temperature coefficients; however, this technology has low efficiency.

CIS

Of all the thin film materials, cells and modules made from alloys of copper indium diselenide (CIS) have achieved the highest efficiencies and have demonstrated long term outdoor stability. (This material can be alloyed with gallium and/or sulfur, resulting in a family of materials with the general formula of Cu(In,Ga)(Se,S)2, all of which will be referred to in this paper as CIS or CIS-based absorbers) [20].

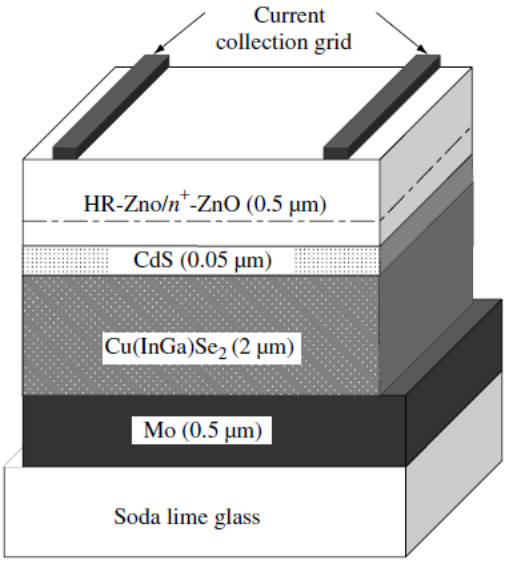

Figure11: Structure of CIS PV panels [13]

CdTe

CdTe PV cells are grown on a glass substrate with a transparent conduction layer made from indium tin oxide as the front contact. This is initially coated with an n-type CdS window layer before being coated with the p-type CdTe layer. CdTe has the lowest production cost among the thin-film PV cells [16].

CdTe PV cells are included in the thin film category and their performance is currently between 15-17%[21]. Research shows that they may achieve over 20% efficiency [22]. A typical structure of a CdTe PV panel is shown in Figure 12.

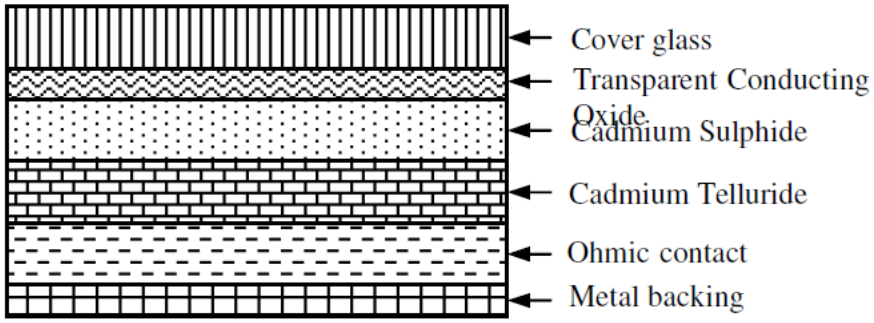

Figure 12: CdTe thin film PV cell [23]

Hybrid solar cells (HIT: heterojunction with intrinsic thin layer)

HIT solar cell is a combination of a crystalline and thin film solar cell. This comprises c-si and a-si that is bonded with an additional un-doped thin film (intrinsic layer). A mono-si wafer forms the core of the HIT cell and is coated on both sides with a thin layer of amorphous silicon. As intermediate layer, an ultra-thin undoped intrinsic layer made from a-si bonds the c-si wafer with each a-si layer. A p-doped a-si layer is deposited on the front side, which forms the p-n junction with the n-doped mono-si wafer. While in other crystalline technologies the same semiconductor is doped differently in order to create the p-n junction, HIT technology achieves it with two structurally different semiconductors [16].

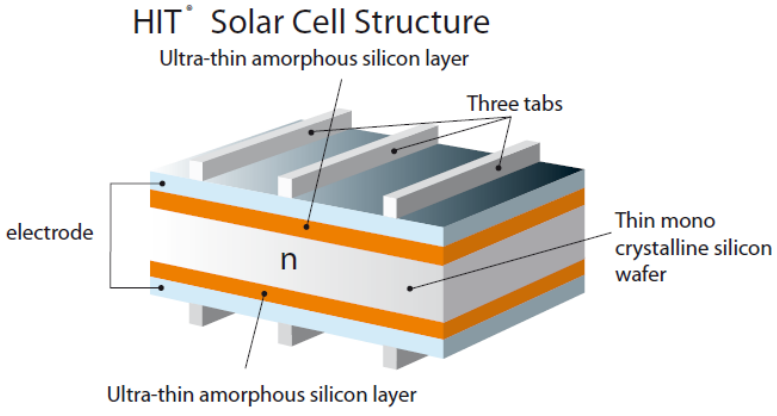

Figure 13: Hybrid (HIT) PV cells [24]

Table 1 presents commercial PV panels of various technologies. It can be observed that high efficiency rates are achieved for most technologies.

Table 1 : Performance of commercial PV panels

PV panel	Power (W)	Efficiency (%)	Manufacturer	Technology	Reference
ALEO P19	290-300	17.6-18.3	Aleo	Mono-si	[25]
ALEO S19	300-310	18.3-18.9	Aleo	Mono-si	[25]
CS6K-290-305-MS-FG	290-305	17.72-18.54	Canadian Solar	Mono-si	[26]
CS6K-290-305-MS-FG	300-315	18.33-19.24	Canadian Solar	Mono-si	[26]
CS6K-270-280P	270-280	16.5-17.11	Canadian Solar	Poly-si	[26]
CS6K-285-295-P-FG	285-295	17.33-17.94	Canadian Solar	Poly-si	[26]
LG340N1C-V5	345	19,8	LG	Mono-si	[27]
N-PEAK SERIES	310-300	18.6-19.8	REC	Mono-si	[28]
ECO LINE M60/300 - 320W	300-320	17.78-18.93	Luxor	Mono-si	[29]
ECO LINE P60/270 – 290W	270-290	16.21-17.49	Luxor	Poly-si	[29]
HiA-S300RG	300	18.44	Hyundai solar	Mono-si	[30]
HiA-S360RG	360	18.55	Hyundai solar	Mono-si	[30]
Maxeon 360	340-360	19.2-20.4	Sunpower	Mono-si	[31]
STP22524/Vfw-STP335 24/Vfw	325-335	16.7-17.2	Suntech	Poly-si	[32]
STP340- 24/Vfw-STP350-24/Vfw	340-350	17.5-18.0	Suntech	Poly-si	[32]
VBHN335KJ01	335	19.7	Panasonic	HIT	[33]
Q.PEAK BLK-G4.1 285-295	285-295	17.1-17.7	Qcells-Hanwha	Mono-si	[34]
Q.PEAKG4.1 290-305	290-305	17.4-18.3	Qcells-Hanwha	Mono-si	[34]
Q.POWER L-G5 315-335	315-335	16.2-17.2	Qcells-Hanwha	Poly-si	[34]
COE-280P60L	280	17,21	Trienergia	Poly-si	[35]
TRIxxxBC-WB	320-330	19,7-20,3	Trienergia	Mono-si	[35]
SFK185S	185	15.06%	Solar frontier	CIS	[36]
YGE 72 CELL SERIES 2 HSF SMART	320-345	16.1-17.4	Yingli Solar	Poly-si	[37]
YLM 60 CELL	285-315	17.4-19.2	Yingli Solar	Mono-si	[37]
ND-AK Series	270-275	16.6-16.9	Sharp solar	Poly-si	[38]
NU-AK Series	300	18.4	Sharp solar	Mono-si	[38]
FIRST SOLAR SERIES 6™	420-445	17-18%	First Solar	CdTe	[39]
U-EA TYPE	100-120	8.2-9.8%	Kaneka	a-si-μc-si	[40]

A large number of researchers investigate the performance behavior of different PV technologies. There exist several studies comparing the performance of various panels from each different technology. These comparisons are based either on real time operation systems or on off-grid experimental set-ups.

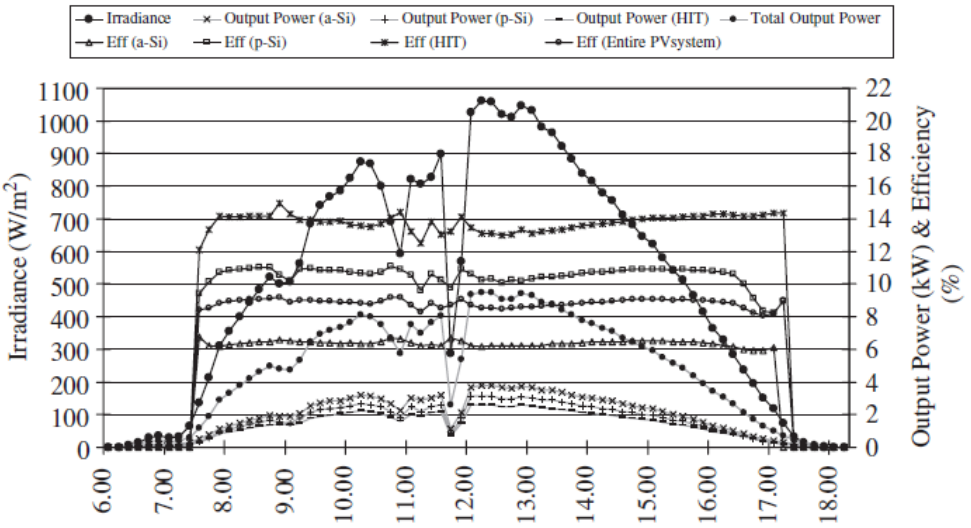

Figure 14 : Performance, Power, Solar irradiance of a PV system based on a-si, poly-si and Hybrid PV cells [41]

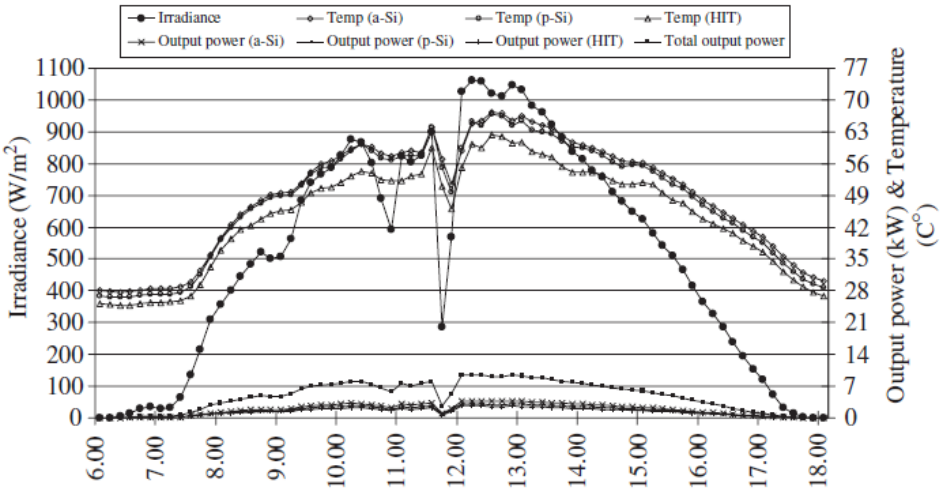

Figure 15 : Temperature, Power, Solar radiation of PV system which is consisted of a-si, poly-si and Hybrid PV cells [41]

Figure 14 and Figure 15 present a daily performance comparison of poly-si, a-si and hydrid type panels as function of temperature and solar radiation. Sasitharanuwat et al, observe that a-si PV cells performed better than poly-si and hybrid. As far as temperature is concerned, hybrid panels are heated less than poly-si and a-si PV cells [41]. S. Silvestre et al., studied performance and degradation rate of three different crystalline silicon-based photovoltaic (PV) modules mc-Si (multi-crystalline), c-Si (mono-crystalline, back contacted) and HIT (heterojunction with intrinsic thin-layer) in the Saharan environment after years of exposure. The results show a 6% total power reduction for the HIT PV module, while for the same period, the reduction of power observed in the c-Si PV module was 4.2% and mc-Si PV module has lower power reduction trend [42]. Tossa et al, conducted performance analysis between one monocrystalline PV panel, two polycrystalline and one PV panel of tandem structure

(micromorph) and observed that the micromorph panel presents the best performance on the site with an average performance ratio of 92% while monocrystalline and polycrystalline had averaged performance ratio of 84% and the fourth polycrystalline has the worst (an average performance ratio of 80%). According to this study the main reason of good performance of the micromorph was based on low temperature coefficients [43]. S. Kichou et al., studied the behavior of three different PV modules based on cadmium telluride (CdTe), monocrystalline (c-Si) and multicrystalline silicon (mc-Si) technologies deployed outdoor in a humid continental climate. The results show that the evolution of the calculated performance ratios (PR) of the three different PV module technologies confirm the stability of c-Si and mc-Si PV modules. The effects of the seasonal changes could be also observed in the trend of PR of crystalline silicon PV modules. It could be concluded that c-Si and mc-Si PV modules perform better in winter months rather than in summer months due to their high power temperature coefficient. In addition, if c-Si and mc-Si PV modules perform better than CdTe ones in winter, this fact can be related to their different tilt angles [44].

1.1.5 Characteristics of PV panels

The efficiency of PV panels is measured in the Laboratory with a standard solar simulator, according to ASTM Standard E 948 [45] and an associated bundle of standards.

The standard conditions refer to

- A panel temperature of 25° C
- A solar insolation of 1000 W/m²
- An air mass AM = 1.5 (ASTM G173 [46])

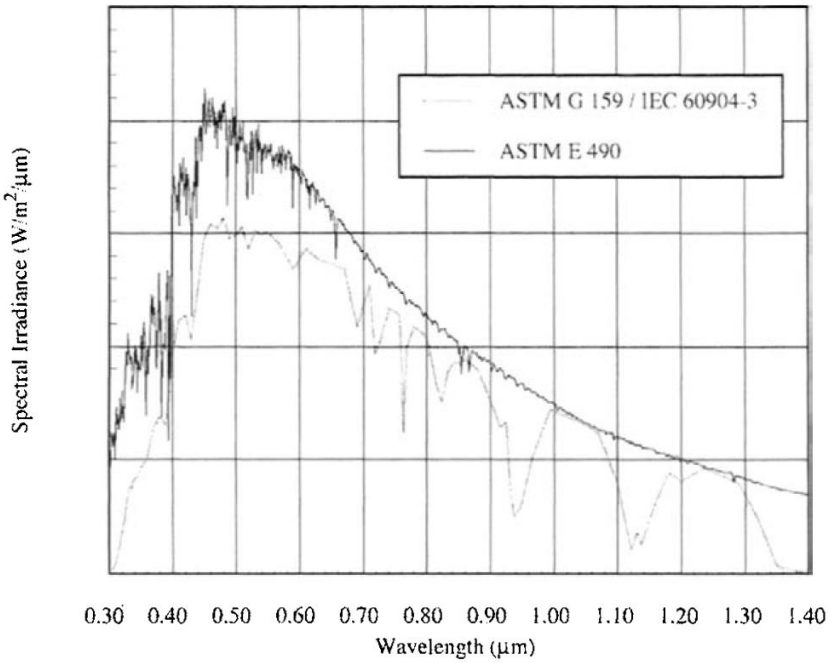

Figure 16 : Reference spectral irradiances for AM1.5, AM0 [47]

The main electrical characteristics of PV cell are short-circuit current, open circuit voltage, maximum current, maximum voltage and maximum power. Furthermore, PV panels manufacturers provide information in relation with temperature coefficients of maximum power, short-circuit current, and open circuit voltage. Another important information is irradiance reduction factor, typically denoted by k, which reflects the efficiency reduction with irradiance from 1000W/m² to 200W/m². However, this factor is not provided by all manufacturers in technical datasheets. Finally, several manufacturers provide spectral responses of their PV panels.

1.2 Performance of grid-connected Photovoltaic systems

Performance of grid-connected photovoltaic systems is affected by several factors. The main parts of a system are the photovoltaic panels, inverter and mounting system. Each of these parts affects the total PV systems performance. The aim of this study is the analysis of systems' performance and focus on PV panels performance. It is important to investigate how several factors influence performance. Thus, this section presents the main factors that affect PV panels performance and other parts of a PV system. According to PV panels characteristics (Section 1.1.5) the main factors that have direct impact in PV performance is solar radiation, spectrum and temperature. These factors are influenced by other indirect factors which are related to problems of each installation. Such factors are dust, shading, humidity that are related to characteristics of installations' location. Furthermore, inverter efficiency or type of mounting or tracking system influence the total PV systems' efficiency. All of these factors are analyzed in the following sections.

1.2.1 Solar radiation

As regards the effect of solar irradiance level, the manufacturers' data usually present efficiency values down to an insolation of 200 W/m². A significant drop in efficiency is reported when insolation drops from 1000 to 200 W/m² (about 6 efficiency percentage units' reduction). Obviously, this drop is non-linear with insolation levels and increases as we move to lower levels. It is mainly due to the effect of air mass increase which leads to a decrease in insolation under clear sky conditions. Thus, the effect of air mass is lumped inside the above figure of efficiency drop. For this reason, no separate reference exists in the manufacturers' datasheets on the effect of the air mass.

Silicon solar cells are not very sensitive to certain, low wavelength portions of the solar spectrum that are scattered in the atmosphere. The resulting spectrum at the Earth's surface matches more closely the band gap of silicon. For this reason, silicon solar cells are more efficient at Air Mass 1 than Air Mass 0 (extraterrestrial radiation spectrum). However, even though the efficiency is lower at AM 0, the total output for a typical solar cell is still highest at AM 0. On the other hand, the shape of the spectrum changes with further increases in atmospheric thickness, and hence cell efficiency drops for AM numbers significantly higher than 1.5. The light scattering mechanism by particles much smaller than the wavelength of light was first studied by Lord Rayleigh [48]. This was followed by Mie which formulated a more general approach based on the scattering of electromagnetic radiation by spherical particles of various sizes [49].

Analysis of monitoring data from a PV park in Greece during 2010 [50] indicates that 16% of the yearly electricity is produced before 10:00 and after 18:00. That is, a significant part of electricity is generated during the early morning and late afternoon

hours, at high air mass (and thus low insolation) conditions. For this reason, it is interesting to investigate in more detail the effect of air mass on the efficiency of PV panels. This investigation could also cover the effect of different atmospheric conditions.

Radiometric instrumentation is a crucial parameter in PV application as solar irradiance is a factor that affect PV performance either with absolute a values or with spectral content. Radiometers are divided in broadband instruments and spectral instruments. Broadband instruments measure in certain band and spectrally-integrating radiation from all wavelengths it contains, while spectral measure radiation at certain wavelengths. Broadband instruments contain pyranometers, pyrheliometers, pyrgeometers, UV meters, rotating shadow band radiometers and albedometers. Spectral instruments include scanning filter photometers (SFP) or sky scanners, sun-photometers, multi-filter rotating shadow band radiometers (MFRSR), rotating shadow band spectrometers (RSS), spectro-radiometers, interferometers and grating spectrometers [51].

1.2.2 Temperature

The electrical performance is primarily influenced by the type of PV used. A typical PV module converts 6-20% of the incident solar radiation into electricity, depending upon the type of solar cells and climatic conditions. The rest of the incident solar radiation is converted into heat, which significantly increases the temperature of the PV module and reduces the PV efficiency of the module [52]. As module temperature increases, the band gap of PV panels usually decreases, resulting in the absorption of longer wavelength photons, and the minority carrier lifetime generally increases. These factors slightly increase the light-generated current (I_{sc}) but lead to a reduction in the cell's open circuit voltage (V_{oc}), which results in PV panels' fill factor overall reduction [53].

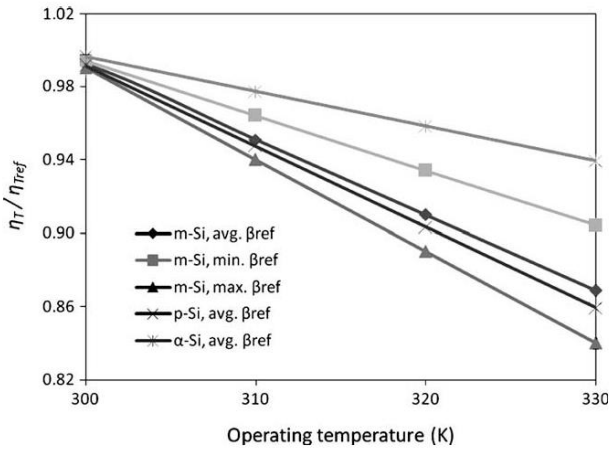

Figure 17 : Temperature effect on different types of photovoltaic technology [54]

Figure 17 presents the variation of PV panels performance as a function of operating temperature. The difference in behavior of each PV panel is expressed by a different slope of the curve. It is clear that a-si PV panels have smaller temperature losses.

As regards the effect of PV panel temperature, the manufacturers' data sheets usually give an efficiency reduction coefficient. Skoplaki and Palyvos [55] reviewed literature correlations of cell temperature with weather variables and material/ system-dependent properties. Alonso-Garcia and Balenzategui presented results of the application of existing international standards for the simulation of crystalline and thin-film module temperature from Nominal Operation Cell Temperature (NOCT), to different types of

PV modules [56]. Cueto studied the performance behavior of different PV technologies and observe that efficiency was strongly temperature-dependent and negative for c-Si, poly-c-Si, and CIS module types, while for a-Si temperature dependence is much weaker, and positive. Furthermore, efficiency for CdTe is not a simple function of temperature, and more likely a complicated function that includes spectral and low-light level effects in conjunction with temperature [57].

Table 2 : Temperature Coefficients of commercial PV panels

PV panel	Technology	Temperature coefficient of P	Temperature coefficient of I	Temperature coefficient of V	Reference
Aleo	Mono-si	-0.4%[%/K]	0.05%[%/K]	-0.29%[%/K]	[25]
Canadian solar	Mono-si	-0.39%[%/K]	0.05%[%/K]	-0.29%[%/K]	[26]
Canadian solar	Poly-si	-0.40%[%/K]	0.05%[%/K]	-0.29%[%/K]	[26]
Hyundai solar	Mono-si	-0.41[%/C°]	0.058[%/C°]	-0.33[%/C°]	[30]
LG	Mono-si	-0.30%[%/K]	0.037%[%/K]	-0.24%[%/K]	[27]
Luxor	Mono-si	-0.40%[%/K]	0.06%[%/K]	-0.30%[%/K]	[29]
Luxor	Poly-si	-0.41%[%/K]	0.05%[%/K]	-0.30%[%/K]	[29]
REC Solar	Mono-si	-0.37%[%/K]	0.04%[%/K]	-0.28%[%/K]	[28]
Sunpower	Mono-si	-0.36%[%/K]	0.05%[%/K]	-0.29%[%/K]	[31]
Suntech	Poly-si	-0.41%[%/K]	0.067%[%/K]	-0.33%[%/K]	[32]
Panasonic	HIT	-0.258%[%/K]	0.055%[%/K]	-0.235%[%/K]	[33]
Qcells-Hanwha	Poly-si	-0.40%[%/K]	0.04%[%/K]	-0.29%[%/K]	[34]
Qcells-Hanwha	Mono-si	-0.40%[%/K]	0.05%[%/K]	-0.31%[%/K]	[34]
Trienergia	Poly-si	-0.41%[%/K]	0.05%[%/K]	-0.31%[%/K]	[35]
Trienergia	Mono-si	-0.375%[%/K]	0.0405%[%/K]	-0.294%[%/K]	[35]
Solar forntier	CIS	-0.33%[%/K]	0.01%[%/K]	-0.27%[%/K]	[36]
Yingli	Mono-si	-0.38%[%/K]	0.04%[%/K]	-0.30%[%/K]	[37]
Sharp solar	Poly-si	-0.4%[%/K]	0.05%[%/K]	-0.29%[%/K]	[38]
Sharp solar	Mono-si	-0.41%[%/K]	0.055%[%/K]	-0.33%[%/K]	[38]
First solar	CdTe	-0.32%[%/K]	0.04%[%/K]	-0.28%[%/K]	[39]
Kaneka	a-si-μc-si	-0.35%[%/K]	0.056%[%/K]	-0.39%[%/K]	[40]

Table 2 shows temperature coefficients of commercial PV modules. It is remarkable that the lowest power temperature coefficients belongs to HIT technology , then CIS and CdTe modules.

1.2.3 Spectral response of PV panels

The spectral response of a solar cell permits an examination of how photons of different wavelengths contribute to the short-circuit current. The spectral response is defined as the short-circuit current, $I_{SC}(\lambda)$, resulting from a single wavelength of light normalized by the maximum possible current [13]. Spectral response of PV is a characteristic curve which shows behavior of PV in each wavelength. Figure 18 shows the spectral response of various PV technologies.

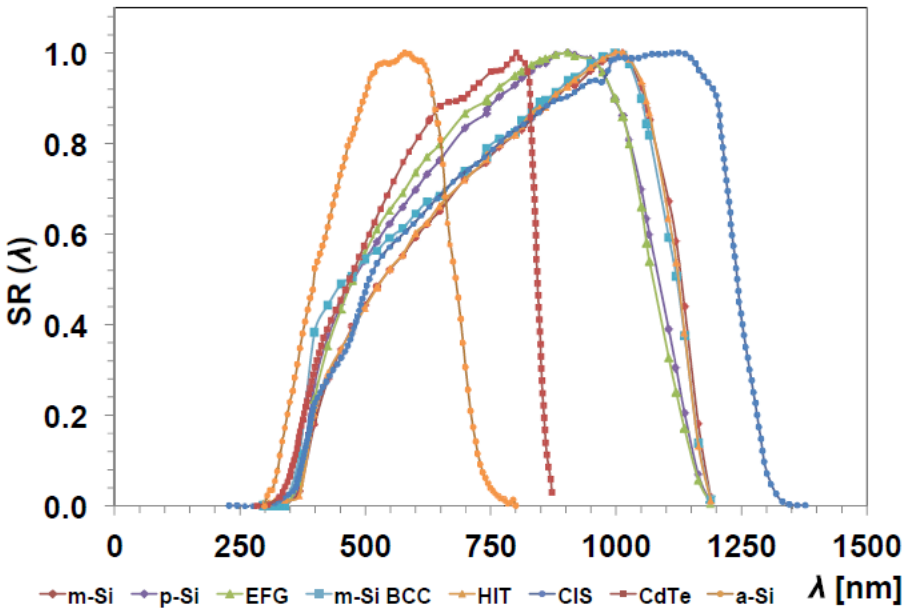

Figure 18 : Spectral response of different Photovoltaic technologies [58]

Spectral variation due to weather conditions or pollution is accounted for by means of the clearness Index K_t, defined as the ratio of the horizontal global irradiance to the corresponding extraterrestrial irradiance multiplied by the sinus of the sun height [59, 60]. K_t usually varies in the range 0.6-0.8 (clear weather conditions) [61, 62].

Therefore the Clearness Index K_t may be considered as an attenuation factor of the atmosphere. The influences of clearness index and air mass on the outdoor performance of single crystalline and amorphous-Si PV modules were analyzed by Nakada et al. in [63]. It was found that Average Photon Energy (APE) increases with decreasing the K_t and AM, with stronger effect on APE on the amorphous-Si PV modules. The overall performance of PV panels at high air mass conditions is complicated by the shape of the solar spectral response curve of the specific module type. Consequently it is useful to select a metric that is independent of the spectral response of any particular technology. Average Photon Energy (APE) is a metric for describing the spectral quality of solar irradiance. This is analogous to an average wavelength value but instead, it represents the average energy of all the photons impinging upon a target surface [64]. APE is calculated by the following equation:

$$APE = \frac{1}{q} \frac{\int E_\lambda d\lambda}{\int \Phi_\lambda d\lambda} \quad (1\text{-}2)$$

Where q [eV] is the electron charge, E_λ[W $m^{-2}nm^{-1}$] is the spectral irradiance at wavelength λ, and Φ_λ is the photon flux density at wavelength λ, calculated by the following equation.

$$\Phi_\lambda = \frac{1}{q} \frac{E_\lambda}{hc/\lambda} \quad (1\text{-}3)$$

Solar spectral response of the various types and designs of PV modules is routinely included in specialized publications, in the form of external quantum efficiency plots versus wavelength, either absolute values or normalized to the peak measured value

[65].

Perez-Lopez et al. presented results of solar spectral irradiance measurements performed in Madrid in the wavelength range 250–2500 nm (extending the spectral range far away from the wavelengths where PV semiconductors are active), during selected clear days covering the four seasons of the year [66].

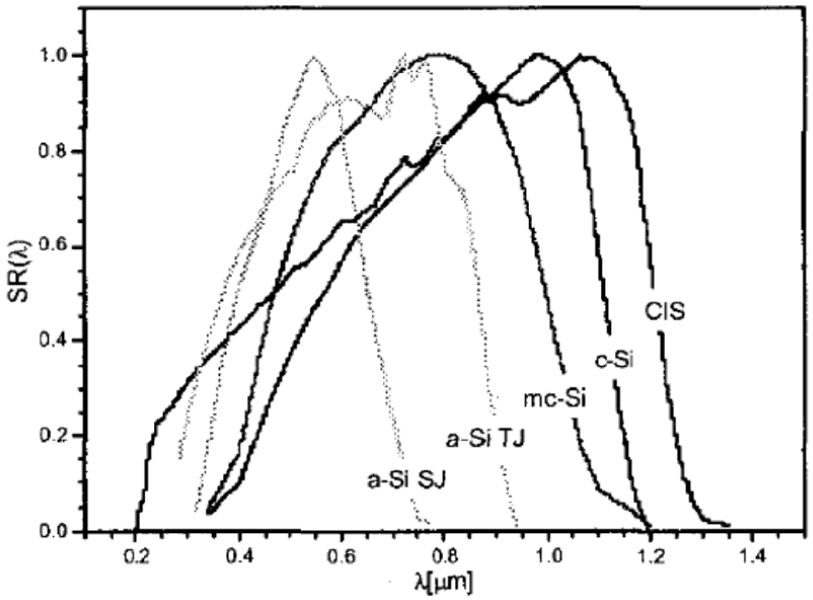

Figure 19 : Spectral response of PVcells a-si, μ-si, crystalline-si, CIS [67]

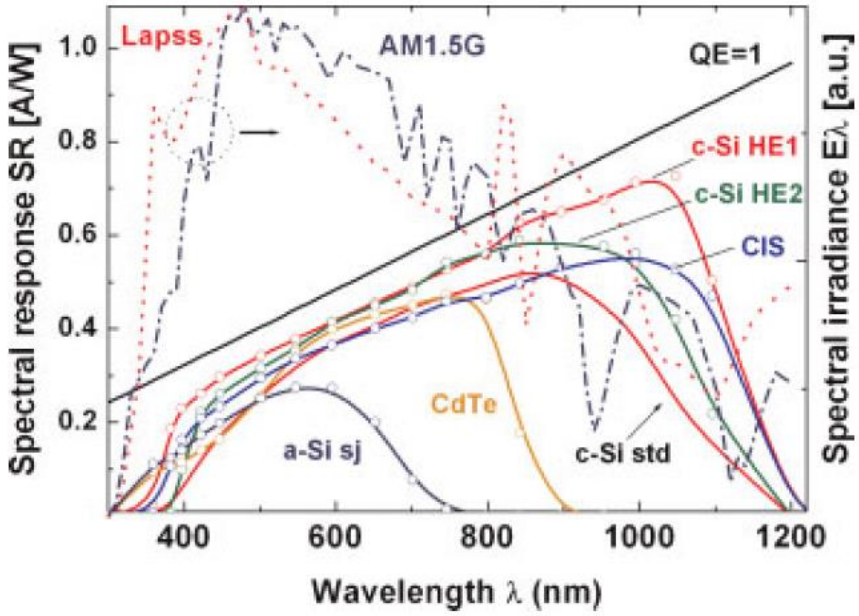

Figure 20: Spectral response of different type of PV cells in comparison with spectral irradiance [68]

1.2.4 Photovoltaic mounting systems

PV panels are based on aluminum or galvanized iron systems and are either fixed or tracking. Fixed systems are based on reinforced concrete bases, galvanized iron piles, or screwed foundations. The two main characteristics that affect performance of fixed systems are their slope and azimuth angle. The ideal values for the two angles depend on the location of the installation. Angle of tilt is related with latitude and consequently its optimization is related with the location. The optimal azimuthal angle for the northern hemisphere is zero (south orientation) while for the south is 180 degrees (north orientation). In case of installations where optimal orientation is not possible, the installation is placed with losses at another tilt angle, something that is happened in roof systems.

Tracking systems have the ability to move in one or two axles. Single axis systems can be driven as a pre-azimuth angle or frame angle. The first essentially follows the daylight trajectory and achieves up to 25% of the output of a fixed system in the same location. The latter simply optimize the tilt angle some times a year. However, higher yields are achieved by the two-axis systems, ie the azimuth angle and tilt angle. Control of tracking systems is done either by using an astronomical algorithm that gives the suns' path and drive the PV arrays in accordance with it. However, there are systems that receive solar radiation to find the optimum position that the PV array must have and constantly correct their position. Sensor-based systems can achieve higher yields because in days with high cloudiness they can switch properly and make better use of diffuse radiation.

Here is a diagram Figure 21 showing the extra energy generated by various types of mounting systems. Specifically, these are 7 different types of systems. Koussa et al, investigate the effect of using different sun tracking mechanisms on the flat plate photovoltaic system performances and the main parameters affecting the amount of their electrical energy output as well as those affecting their gains compared to the traditional fixed photovoltaic systems. The used systems are : **FY** fixed panel and its surface inclined at the yearly optimum slope, **FS** fixed panel and its surface inclined at the seasonal optimum slope, **OVY** single vertical rotating axis sun tracking system, where the panel surface is inclined at the yearly optimum slope, **OV**S single vertical rotating axis sun tracking system, where the panel surface is inclined at the seasonal optimum slope, **OIY** single inclined rotating axis sun tracking system, where the panel surface is inclined at the yearly optimum slope, **OIS** single inclined rotating axis sun tracking system, where the panel surface is inclined at the seasonal optimum slope, **DT** two-axis sun tracking system. Figure 21 shows the additional power output from each type of tracking system, as compared against the fixed system, during a clear sky day. It is found that for a completely clear day, the highest obtained gains are associated with two-axis sun tracker systems. For the partially clear days, the amount of gain depends on the clearness index and on the seasonal variation of day length Finally on a completely cloudy day, the results show that all considered systems produced around the same electrical energy [69].

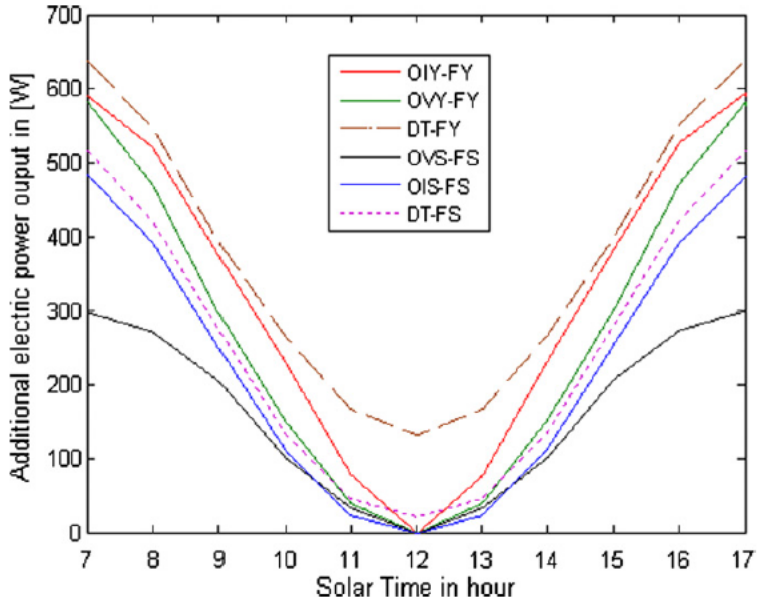

Figure 21 : Additional electrical power output of the tracked PV panel to that fixed Panel clear sky state [69].

Koussa et al, obtained similar results for cloudy days in a case study in an arid and hot climate. The performance of tracking systems shows significant increase when compared against fixed systems during clear sky days, while on cloudy days it fluctuated around the same levels [70]. Sidek et al. study the performance of a photovoltaic system based on a dual axis tracking system which is controlled with a Micro controller unit and Global positions system. This system is able to achieve 26,9% higher power than the fixed-systems under clear conditions. On the other hand, the system achieves 12,8% higher power under cloudy conditions [71].

1.2.5 Environmental conditions - Shading

Significant role in the performance of a PV plant plays the microclimate of the installation area. In particular, there are significant differences in systems that are installed in urban environments and those installed in rural areas. Higher temperatures and pollution are observed in systems installed in urban which means a reduction in system performance.

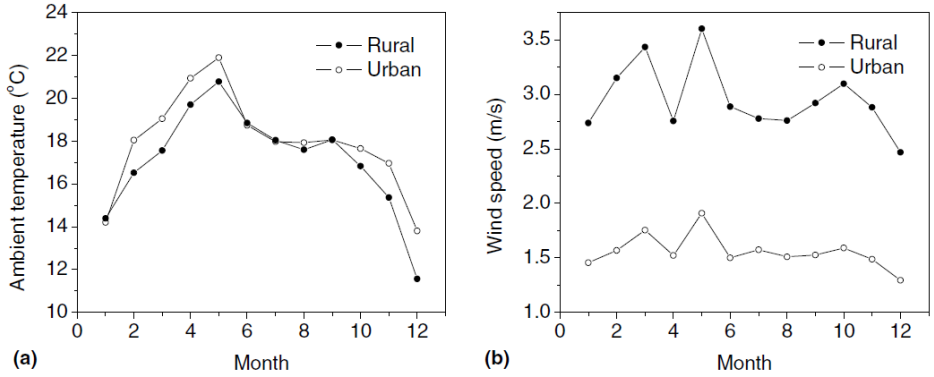

Figure 22 : Ambient temperature and air velocity in urban and rural environment during a year [72]

Besides ambient temperatures, PV panels' temperature is also affected by the air of the

area as it can help to temperature reduction. It is observed that levels of wind in the rural areas are higher than the urban ones. Something that positively affects the performance of systems installed in the countryside. Also, lower radiation values have been observed in the urban environment than in the countryside.

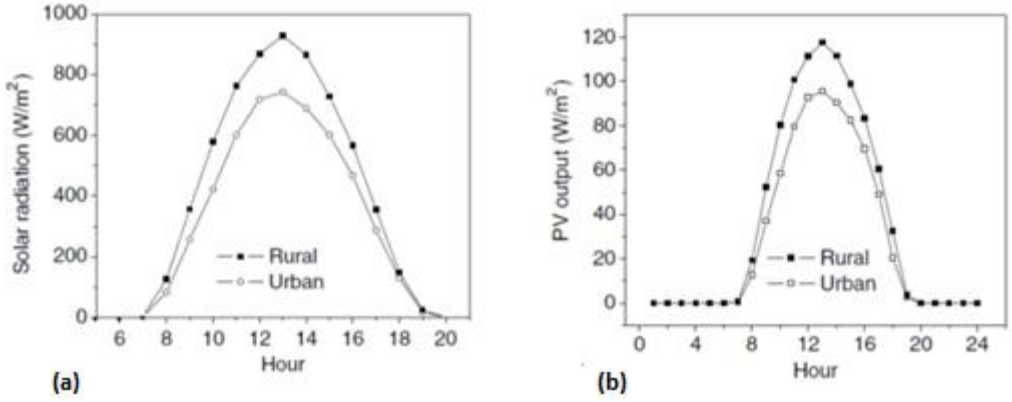

Figure 23 : Solar radiation and PV power output on rural and urban area [72]

In addition to meteorological factors affecting the performance of systems installed in urban environments, shading plays an important role too. Shading can be a negative factor in both systems' performance and degradation. Especially partial shading is a condition where, the panels in a photovoltaic (PV) array do not receive irradiation on whole surface. Shading causes mismatch in the electrical characteristics of the panels composing the PV array and results in significant reduction in the energy yield [73].

Because of the fact that PV cells are connected in different configurations, shading of one affects others and thus significantly reduces systems' performance. Possible configurations that are referred in literature are Series (S), Parallel (P), Series-Parallel (SP), Total-Cross-Tied (TCT), Bridged-Linked (BL), and Honey-Comb (HC) [74].

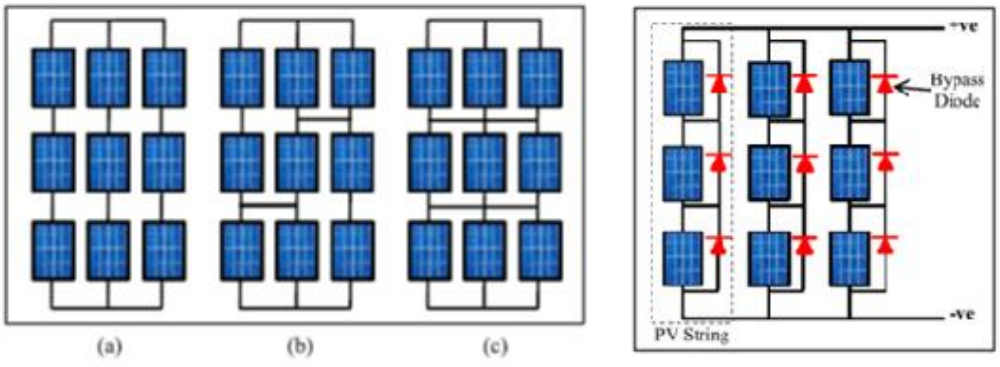

Figure 24 : Different configurations. (a) Series-Parallel (SP), (b)Bridge-Linked (BL), (c) Total Cross Tied (TCT). Schematic diagram of a 3x3 PV array[75]

Shading is an important factor for photovoltaic system efficiency, however its quantification is a difficult task that is analyzed by several researchers. Satpathy et al, studied partial shading for different configurations and shading conditions and observed that the array with SP configuration generated the lowest power output during all shading cases followed by BL and TCT [75].

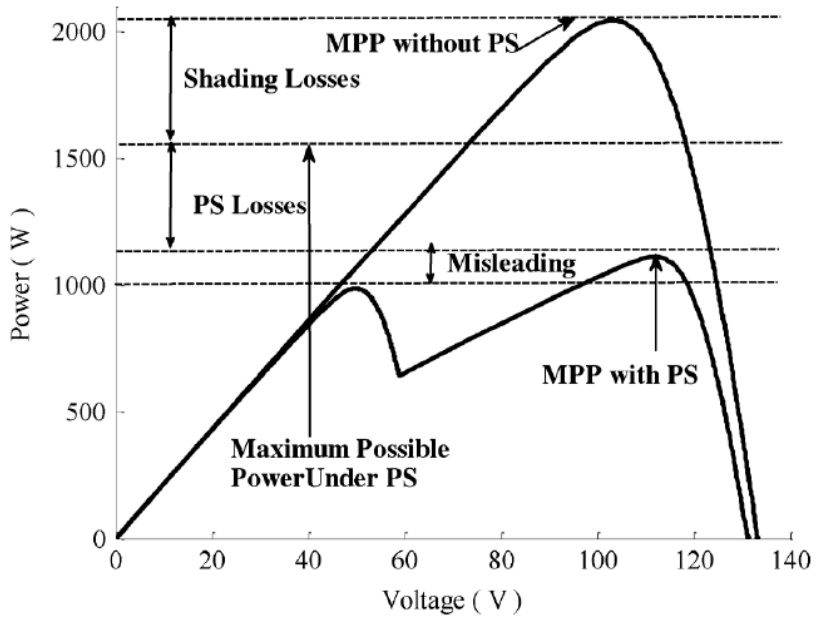

Figure 25 : Shading, partial shading, and misleading losses for a photovoltaic array [76]

Partial shading (PS) causes power losses through different mechanisms, the most severe one being the incoherence of the array's maximum power point (MPP) with the modules' MPPs [76]. Furthermore, partial shading for long time periods can cause temperature increase and possibly create a hot spot which leads to a faster degradation. Shading basically changes PV cells I-V curve, as shown in the figure below, so this can negatively affect maximum power point of inverter MPP tracker, something that affects negatively the inverters' performance and consequently total systems' performance.

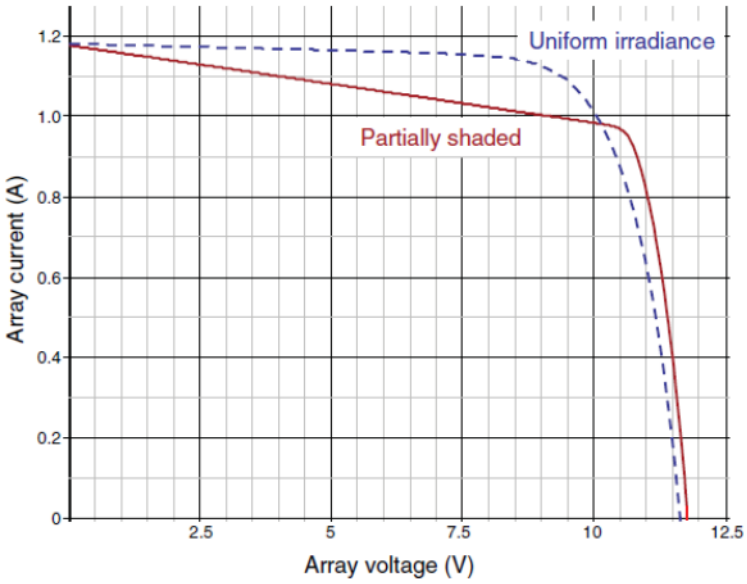

Figure 26: Impact of shading on I-V curve [77].

1.2.6 Inverter - sizing

The inverter is one of the most important parts affecting photovoltaic systems efficiency either for grid-connected applications or for off-grid systems. Inverters for grid-connected application have to meet a number of requirements, which concern levels of voltage, frequency and anti-islanding protection, in order to be connected to public grids.

One of the most important concerns in utilizing PVs in power system is islanding. Islanding happens when a line is disconnected and is energized by one (or multiple) DERs (distributed energy resources), whilst that section of the EPS(electric power systems) is electrically cut off from the remainder of the EPS. If this situation is not discovered quickly, it may deteriorate safety conditions. During unintentional islanding, the DER shall have the means to recognize the accidental island and discontinue to energize the EPS in less than two seconds of the island's creation [78].

There are four types of inverters for Grid-connected PV systems: (a) module, (b) string, (c) multi-string, and (d) central inverter [79]. Central inverters are usually used in large scale PV arrays which consist of PV modules divided into series connections known as strings to generate high voltage. These strings are connected in parallel, through string diodes, to generate high power. In string inverter, usually one single PV string is coupled to one inverter. The input voltage may be high enough to avoid voltage amplification. This topology has the minimum losses due to which it has the advantage of increased energy yield and enhanced supply reliability. Multi-string inverters are connected to several strings which are interfaced with their own DC-DC converter to a common DC-AC inverter. Every string can be controlled individually. The application area of the multi-string inverter covers PV plants of 3–10 kW. The module integrated inverter is used when an AC module consisting of a single solar PV panel and its own inverter is connected to the utility grid. It removes the mismatch losses between PV modules, as well as supports optimal adjustment between the PV module and the inverter. A control design for the module integrated PV and converter units under partial shading conditions is proposed [80].

Inverter sizing plays an important role in the performance of a photovoltaic system. Inverters' performance is related to its size. Moreover, appropriate sizing of the inverter expands its lifetime. Sangwongwanich et al, study the impacts of array sizing in inverters' lifetime and the results show a considerable impact of the PV array sizing on the reliability and lifetime of the PV inverter installed in Denmark, where the PV inverter thermal loading increases considerably with the oversized PV arrays.[81]

Operation of inverter based on MPP tracker algorithms and each manufacturer uses each algorithm. Maximum Power Point corresponds to the pair of current and voltage values on an I-V curve where power has its maximum value. The concept of MPP tracker operation is based on checking the voltage fluctuation from the maximum power point.

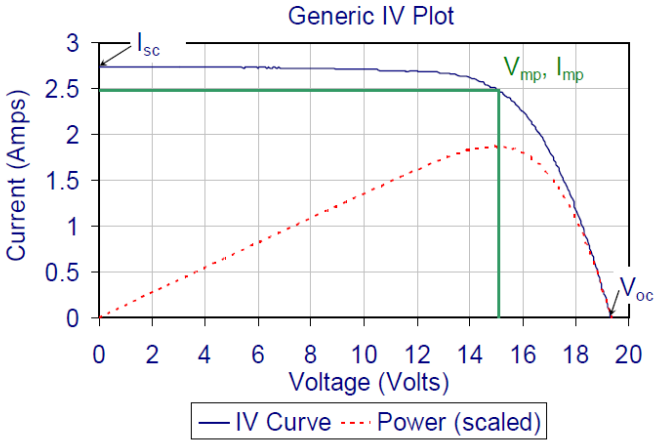

Figure 27 : I-V curve and maximum power point in Power curve [82]

As the MPP keeps on changing according to the varying irradiation levels, a MPPT method is used to track the MPP of the system. Various types of MPPT methods have been developed and implemented over the years which are categorized on the basis of many features including solar efficiency, dynamic response, convergence speed, sensors requirement, cost, complexity [83].

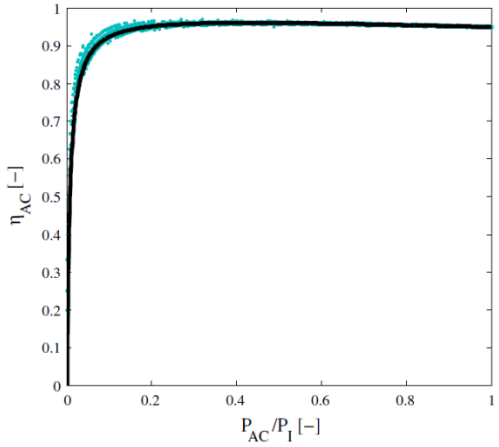

Figure 28: Typical performance curve of Inverter [84]

The optimal sizing of an inverter with respect to the peak power of the PV array rating at Standard Test Conditions (STC) depends on the local climate. It has been shown that the optimal sizing values are different for every month based on solar irradiation, and temperature received at this location [85]. However, according to inverters' efficiency curve and climatic conditions, the size of the inverter should be selected in order to achieve maximum performance during the year. In certain cases, because of low radiation levels and temperature conditions, a small under sizing or oversizing of the inverter power is desirable. Another important parameter is the cost of installation, as over-sizing of an inverter may reduce significantly the total cost for inverter installation.

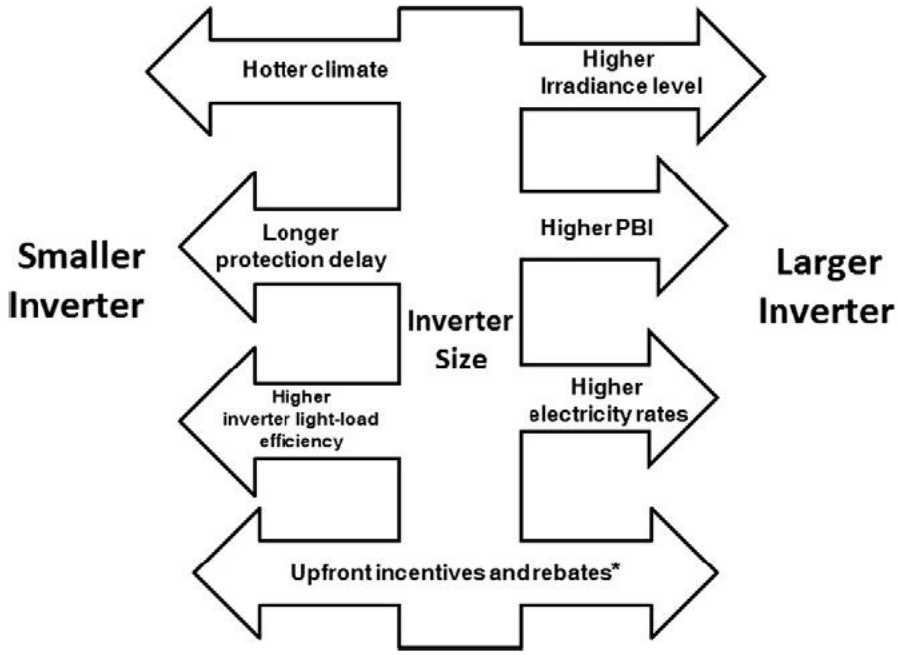

Figure 29 : Advantages of an oversized and undersized inverter [86]

An important parameter that defines the oversizing or undersizing is the sizing ratio which is defined as the ratio of the PV array capacity at standard test conditions (STC) to the rated inverter input DC power given and is described by the following equation [87] :

$$Sizing\ ratio = \frac{P_{PVRATED}}{P_{INVRATED}} \quad (1\text{-}4)$$

where, $P_{PV,rated}$ and $P_{inv,rated}$ represent rated PV capacity and rated inverter input power, respectively [87].

There are many studies that discuss optimal sizing of inverter according to site parameters as temperature and irradiance conditions. Luoma et al, observed that with sizing ratio 0.81 and 0.87 in San Diego, California, up to 6.5% of the monthly energy generation from a PV array and inverter system was lost due to inverter saturation [84]. Rodrigo et al, studied the operation of two grid-connected systems in Central Mexico in order to draw results for inverter sizing ratio based on climatic conditions, type of inverter and PV panel. The results showed that for optimally oriented systems, the recommended array-to-inverter power sizing ratio is 1.05 for c-Si and 0.95 for CdTe independently of the chosen inverter [88].

When designing PV installations, it is necessary to take into account the non-uniformity of the PV panels' connected in series in order to avoid losses of up to 4%. In order to mitigate this problem, sorting the PV panels according to power from flash reports is suggested. Whenever several strings are connected in parallel to form an array, due to the effect of the serial and parallel interconnection, power output of each module in an array will be affected by the weakest modules. The diagram of Figure 30 demonstrates how the performance of a string is affected by the presence of a bypass diode. The problematic operation of a PV panel may be due to shading or a defective or aged panel.

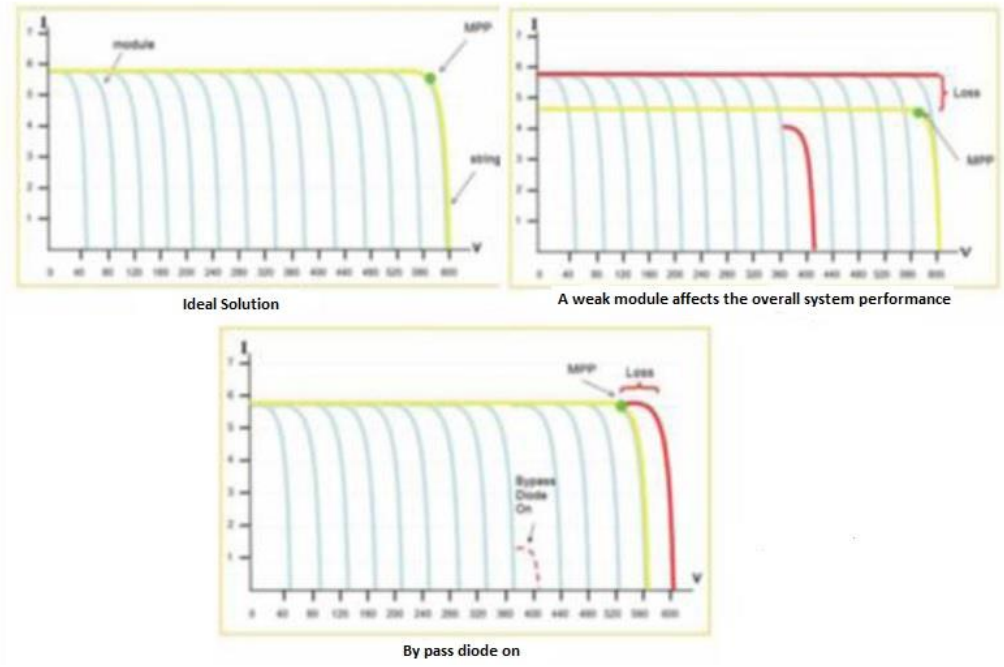

Figure 30 : Behavior of a string with a weak panel [89]

Finally, another factor that may affect the performance of photovoltaic systems is the appropriate sizing of DC and AC cables in order to reduce ohmic losses.

1.2.7 Dust and aerosol effects

The effect of dust accumulation is related to environmental conditions, size distribution of dust particles and tilt angles of the PV panels' surfaces. Several researchers study the effect of dust accumulation on energy generation in places with varying environmental conditions. Kaldellis et al, studied the effect in urban environment of Athens with systematic measurements on roof-top PV panels which were left exposed to natural air pollution for certain time periods and subsequently cleaned in order to be compare the panels' performance. The results showed a 6.5% drop in energy generation of the dusty panels [90]. The climate of each location affects the dust accumulation effect; in wet climate, rainfall, wind and gravity help cleaning of the panels' surface. In dry climate, on the other hand, accumulated dust is an important problem [91]. Ullah et al, studied the effect of soiling on energy production in Pakistan and showed that a lightly soiled panel had a 10% performance reduction, whereas a heavily soiled one could have a 40% reduction [92]. Several studies investigated the dust effect in desert areas with severe environmental conditions. Saidan et al, studied the dust effect on PV panels with direct exposure to weather conditions. The dusted panels were exposed indoors to solar simulator side-by-side with cleaned ones, in order to investigate the effect. The results show degradation of 6.24-18.74% depending on the exposure period [93]. Ramli et al, investigated dust effect in Indonesia using an experimental set up and a rule-based model to identify different experimental conditions. Results showed a 10.8% reduction in outdoor exposure [94]. The ground type of the site plays an important role in this process. Especially in desert areas this effect is stronger. Massi Pavan et al, studied the soiling effect using regression models and results show a 6.9% loss in a sandy site while losses of similar panels on a compact ground were 1.1% [95]. Pulipaka et al, studied effect of soiling on irradiance and observe that that soiling on a panel can decrease the

amount of horizontal irradiance received by the panel by causing angular losses ranging from 22% to 52% [96]. Beattie et al, proposed models of sand and dust particle accumulation on photovoltaic panels based on laboratory investigations on a glass surface. The results qualitatively describe existing field data and account for field conditions, including the effects of photovoltaic module tilt, humidity and wind speed [97]. Javed et al. studied the dust effect using artificial neural networks which indicate that the two most important environmental factors for PV soiling are wind speed and relative humidity [98].

The size distribution of the accumulated dust particles and their composition significantly affect the photovoltaic panels' efficiency. Abderrezek et al, investigated the effect of several types of dust (size and type) by employing a microscope, a spectrophotometer, an I-V photovoltaic modules analyzer and thermocouples. The results show that the dust material, its light transmissivity and the glazing temperature affect photovoltaic performance [99]. Adıgüzel et al., investigated the effect of size and weight of particles on the performance of PV modules, measuring voltage, current and power variation. The results show that the power loss increases with the weight of accumulated dust, assuming that average particle size remains the same. On the other hand with the assumption that particle weight remains the same, the power loss decreases as average particle size increases [100].

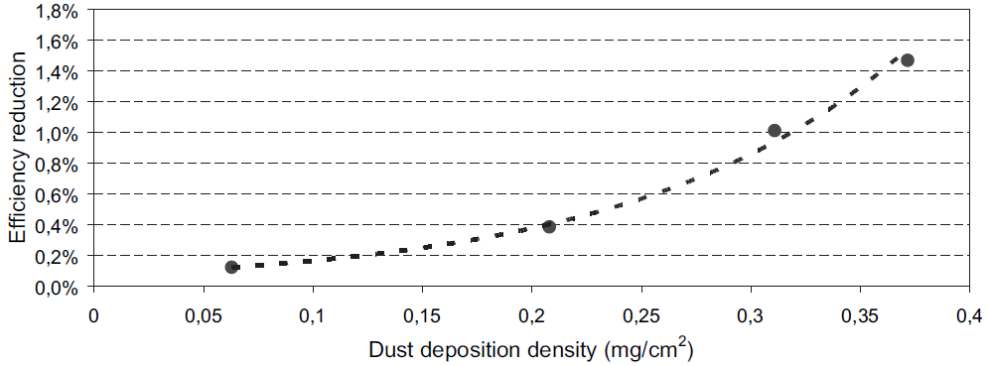

Figure 31 : Impact of soiling on PV efficiency [101]

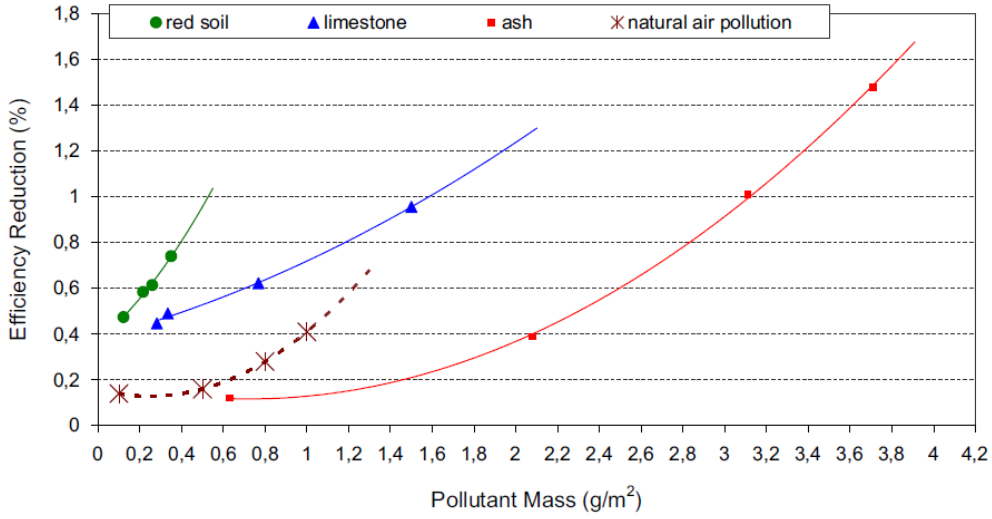

Figure 32: Impact of different kind of soiling on PV production 19 [102]

As referred above, significant role plays the type of dust. Dust contents are a mixture of different pollutants and many studies investigate the effect of each type outdoors and indoors. The pollutants which have remarkable impact according to literature are limestone, ash, red soil, calcium carbonate, silica, and sand [91]. Kaldelis et al, investigated the effect of different pollutants in PV efficiency in Figure 32. Experimental data concerning the effect of three representative air pollutants (i.e. redsoil, limestone and carbonaceousfly-ash particles) on the energy performance of PV installations are analyzed [102].

Another factor that possibly affects PV efficiency is aerosols. Spectral distribution can vary depending on the content of the atmosphere, thus different gases, humidity, particles or atmospheric pressure can have an impact on the spectrum of light reaching the ground [103]. Aerosols modify microphysical and radiative properties of clouds (aerosol indirect effect), but they also scatter and absorb radiation (aerosol direct effect), altering the radiative balance of the Earth-atmosphere system. The level of reduction is determined by absorption and scattering processes [104]. There are many studies which are focused on investigation of aerosol effect in PV performance. Gutiérrez et al, studied the impact of aerosols in PV production from seasonal to multi-decadal time scales The analysis based on aerosol and climate simulations and the results show significant differences in the average annual productivity from 12-16% depending the installation typology [105]. Neher et al, investigated the impacts of aerosols on PV production using an atmospheric radiative transfer and a PV power model. The study concerns a Sub-Saharan region and the results show reduction on PV yields from 2-48% [106].

Aerosols interact with clouds and modify their microphysical and radiative properties (aerosol indirect effect), but they also scatter and absorb radiation (aerosol direct effect), altering the radiative balance of the Earth-atmosphere system. The reduction in the intensity of a direct solar beam during its propagation through the atmosphere is determined by absorption and scattering processes.

1.2.8 Photovoltaic panels deterioration

Degradation in PV modules means a gradual deterioration of the component or system characteristics that can affect the ability to operate within the allowed tolerances. Manufacturers' quality assurance procedures usually consider a PV module as degraded, whenever its output power falls below 80% of nominal value [107]. PV modules' performance can be compromised by several factors, such as temperature, humidity, radiation and mechanical shock [108]. Each of these factors can cause various types of degradation. The IEC 61215 standard establishes the parameters for determining the modules degradation and performance. The tests include visual detection of defects in insulation and leakage currents [109]. It has been stated that the degradation rate of PV systems is less than 1% per year on the majority of the systems[110]. However there is a lack of adequate documentation about the effects of local climates on PV systems as the degradation rate may vary from region to region.

Jordan et al reported that degradation rates for all types of PV modules average 0.8% per year while for crystalline silicon modules were 0.7% per year and for thin film modules were 1.5% per year [110]. Limmanee et al, measured an average degradation rate of 6,1% per year for thin film modules compared to other technologies ranging between 1.2 - 1.8% per year [111]. On the other hand, Rajput et al, found that the rate of degradation of P_{MAX} of monocrystalline photovoltaic panels was 1.9% per year during 22 years of outdoor exposure in India [112]. Hun et al, observed that the median power degradation

of a PV system of 110 kWp, consisting of monocrystalline PV panels, was 1.54% per year [113].

1.2.9 Main types of faults in PV panels

Inspection of PV panels is a quality assurance procedure that is increasingly employed, in various forms, by several PV panel manufacturers, before the lamination process takes place. These inspection procedures are completed in less than 1 minute and spot the existence of micro cracks, cell edge deterioration, electrically inactive parts of cells, low generation cell areas, low generation cells (for mismatch), irregular distance between cells, crystal defect, ribbon misalignment etc. In case of spotting defects that exceed the performance limits set, the panel may be readily repaired before proceeding to the lamination.

On the other hand, an inspection procedure for the PV panels and electrical installation of in-use PV parks should be also embedded in a PV park monitoring process. This inspection process may lead to the detection of a number of faults that may be categorized as follows:

1. Damage to the PV panel or panel covers, of the following types:

- Breakage of the glass protective surface
- Bubbles and/or tears to the polymer (Tedlar) cover of the backsheet
- Corrosion of metallic frames
- Damage to the panel insulation
- Failed solder bonds of the PV cells

2. Hot spots to the panel surface, which are observable by infrared thermography. A hot spot is a PV cell or a group of cells being at significantly higher temperature than the rest of the cells of the panel, because it behaves as an ohmic load, draining energy produced by the neighboring series - connected cells. This behavior could be due to the following reasons:

- Deterioration of the PV current due to dust or dirt accumulated on its surface
- Damaged or broken up cells (mechanical damage, break of protective layers)
- Partially shaded cells (usually met in residential installations)
- shunt resistance problems
- resistive heating due to improper cell interconnect

3. Errors in the laying out of the electrical installation – bypass diode

4. PID effect (Potential Induced Degradation)

This phenomenon, first observed in the seventies, leads to a sudden decrease of PV panel efficiency. The general mechanism of PID is that voltage bias related with leakage currents pass from silicon active layer through the glass to the grounded module frame [114]. Module leakage current to the ground increases with ambient temperature and relative humidity [114]. PID degradation depends on polarity and potential difference between cell and ground [115]. The most common test to detect PID is electroluminescence imaging, thermal (IR) imaging, measurements of open-circuit and operating voltage, IV curves and dark IV curves [116]. There exist recovery methods for affected panels[116], therefore it is important to inspect the panels.

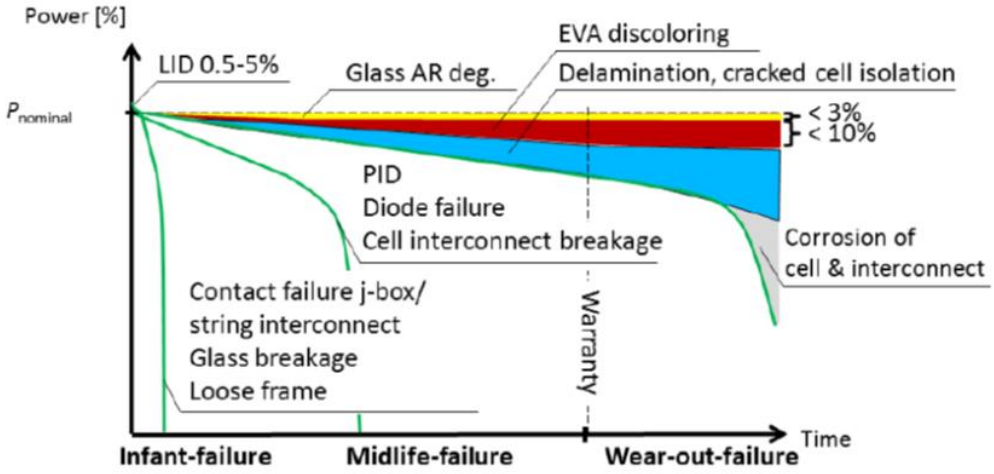

Figure 33 : Different faults in PV panels in correlation with years[117]

Factors that are able to decrease energy generation are described below: Grid faults of grid that most of the times happened because of PPC grid faults. PV panel's degradation (corrosion, discoloration, delamination breakage and cracking cells [107]. Faults of this category are not readily diagnosed. PID- affected cells is a common problem in cases with transformer-less inverters, that could lead to significant decrease in energy generation. Dust effects could be also a problem for particular locations, reported to cause up to 6.5% reduction in urban areas according to a specific study. Power loss due to partial shading and dust accumulation were investigated in a desert environment [118]. These problems can be avoided by optical inspections, monitoring, I-V measurements and IR thermography [119]. The respective standards and guidelines are discussed in [120].

The above facts point to the importance of a monitoring system that would cooperate with a mathematical model to diagnose faults in time, allowing the timely solution of the problems. The system should operate with a grid connected PV park, without loss in energy generation. Such a monitoring system is also important in evaluating conformance to the terms of manufacturer's warranty. Most manufacturers' warranties terms allow for a degradation of power output to 90% for the first 10 years and 80% for 25 years. The power output of every PV panel is defined and tested at STC Conditions (1000W/m^2, 25° C PV panel temperature, AM1.5 spectrum) and NOCT (800W/m^2, 20° ambient temperature, 1 m/s wind speed) conditions. Performance at these conditions allows measurement comparisons between different laboratories and different PV modules however it is not representative for outdoor conditions [121]. Thus, manufacturers data do not define the expected energy generation of PV panels under real insolation conditions [122]. The correlation of irradiance and panel temperature effects is feasible because of the existence of many mathematical models and adequate technical data from manufacturers. Especially, there are several correlations for panel temperature for various applications, so it is important to choose the most suitable for each case [55]. However, checking the third parameter, namely STC conditions performance, is a challenging task, as it involves spectral measurements and information about spectral response of PV panels, something that is not always provided in technical datasheets. Tian et al. discuss the effect of spectral distribution of irradiance, especially in urban areas [72].

1.3 Measurement equipment

Typical measurement equipment that can be used to evaluate a PV plant performance includes a irradiance sensor, an ambient temperature measurement sensor, a temperature sensor of the back panel surface, and a speed measuring sensor of the wind. Apart from the sensors for measuring the climatic data, some measuring instruments such as electrical voltages, electric currents and power are also required. Typically, important information can be obtained from the installation inverter.

1.3.1 Standard measurement systems

Measurement standards are described in standards below [123]:

- IEC 60904-1 "Photovoltaic devices – Part 1: Measurement of photovoltaic current-voltage characteristics"
- IEC 61724 "Photovoltaic System Performance Monitoring – Guidelines for Measurement, Data Exchange and Analysis"
- IEC 61829 "Crystalline Silicon Photovoltaic array – On-site Measurement of I-V Characteristics"
- ASTM E1036 "Standard Test Methods for Electrical Performance of Non concentrator Terrestrial Photovoltaic Modules and Arrays Using Reference Cells"
- ASTM E2527 "Standard Test Method for Electrical Performance of Concentrator Terrestrial Photovoltaic Modules and Systems Under Natural Sunlight"
- ASTM WK22009 "Reporting Photovoltaic Non-Concentrator System Performance " Sources of Uncertainty NREL's Approach

General Information of Standards [123]

IEC 60904-1

- Voltage and current measured with ±0.2 % uncertainty in open circuit voltage and short-circuit current
- Test and reference device coplanar within ±2° and normal to the sun within ±5°
- Reference cell and test device temperature measured with ±1 °C uncertainty
- Optionally test device temperature determined via equivalent cell temperature method (IEC 60904-5)
- Spectral mismatch error correction if matched reference cell not used (IEC 60904-7)
- If reference cell >2 °C from calibration temperature corrections applied
- Use IEC 60891 to translate for temperature and irradiance IEC

ASTM E1036

- Voltage and Current measured with ±0.1 % Uncertainty and 0.05% Resolution for open-circuit voltage and short-circuit current.
- Test and Reference device coplanar within ±2° and normal to the sun within ±10° or report incidence angle
- Reference cell and test device temperature measured with ±1 °C uncertainty, 0.1 °C resolution.
- Spectral mismatch error correction applied (ASTM E973)
- Temperature and irradiance corrections applied if temperature more than 2°C from reference temperature or irradiance > 5% from reference irradiance correct using bilinear method. Otherwise current corrected to constant irradiance.

- Average Wind speed for 5 min prior to test.

IEC 61724

Meteorology

- Total irradiance, in the plane of the array
- Ambient air temperature
- Wind speed

Photovoltaic array

- Output voltage
- Output current
- Output power
- Module temperature
- Mounting / tracker characteristics

Load

- Load voltage
- Load current
- Load power

Energy storage

- Operating voltage
- Current to/from storage
- Power to/from storage

Utility grid

- Utility voltage
- Each phase - Current to/from utility grid
- Power to/from utility grid

Back-up sources

- Output voltage
- Output current
- Output power

Total Irradiance

- Measured in plane of array
- Uncertainty including Instrumentation < 5%

Pyranometer

- Reference cell or cell in Module Package or Module (IEC 60904-2)
- Ambient Temperature –
- Representative of Array Location
- Uncertainty including Instrumentation < 1°C

Wind Speed

- Measured at Height and Location Representative of Array
- Uncertainty including Instrumentation < 0.5 m/s for Speeds < 5 m/s, and <10 % of the reading for Speeds > 5 m/s

Module Temperature

- Measured on back of 1 or more modules in representative of location
- Uncertainty including Instrumentation < 1°C
- location on module given in IEC 61829 method A (center of back surface of module in center of array field)
- Based upon V_{oc} and equivalent Cell temperature (IEC 60904-5)

Voltage and Current

- AC and or DC
- Uncertainty including Instrumentation < 1% of reading

Power

- DC Calculated based upon instantaneous and not averaged readings or directly measured with wattmeter
- AC power accounts for power factor and harmonic distortion
- Uncertainty including Instrumentation < 2%

Huld et al, proposed specific requirements for energy rating of photovoltaic modules. The minimum requirements for a meteorological data set for energy rating should contain broadband irradiance and air temperature. The current proposal of standard data sets consisting of "typical days" do not give realistic estimates of PV performance and thus is not sufficient as a rating standard. A dataset compromising between being significant for any location but not consisting of too much data is required. A method to generate such a dataset is presented, meeting all the requirements of an international standard while being sufficiently accurate to differentiate between different devices of different manufacturers. It is suggested to work with annual data-sets for specific climatic zones, and compare devices based on their module performance ratio [124].

1.4 Monitoring systems

1.4.1 1.1 Monitoring of PV parks

In the case of utility scale PV plants, monitoring typically serves for comparison of current plant performance with an initial energy yield assessment. To distinguish performance, one should filter the significant variability of insolation. Thus, monitoring should always include both the energy generated and the incoming irradiation. For electricity yield measurements, energy meters or true-rms power meters should be used. The inverter-integrated measurements are usually not sufficiently precise. Nevertheless they are useful for identifying relative changes over time. Figure 34 - Figure 36 show three different monitoring systems with measurement equipment and data recording systems.

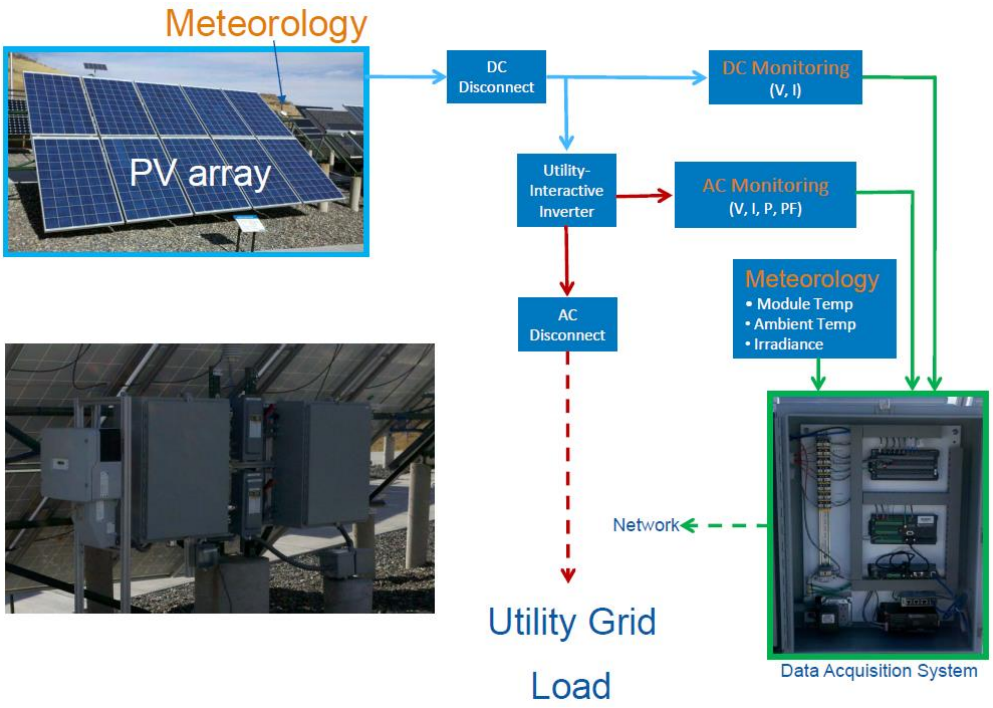

Figure 34 : Measurement equipment for photovoltaic installation of NREL[123]

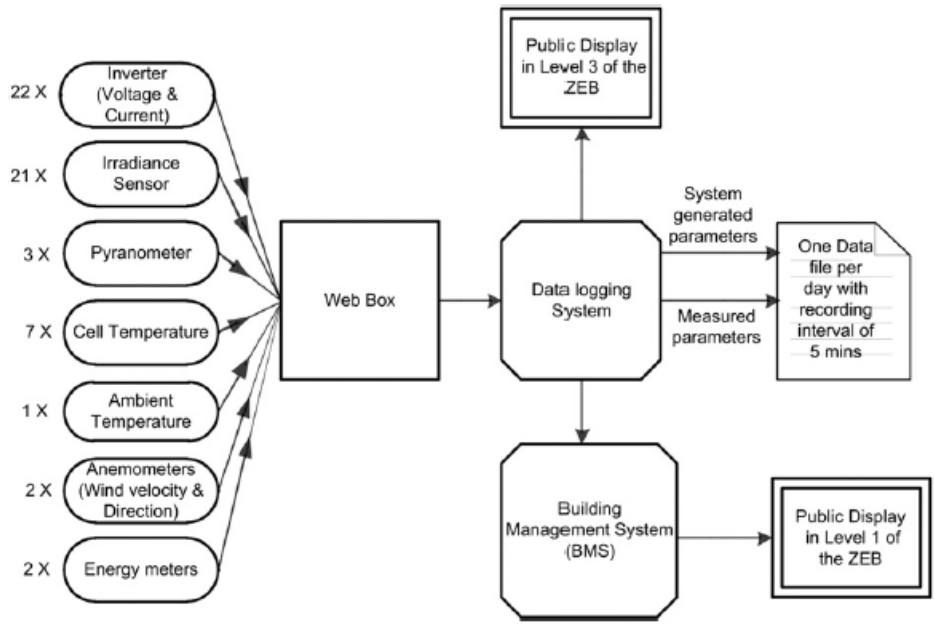

Figure 35: Monitoring System of a 142,5KWp PV system [125]

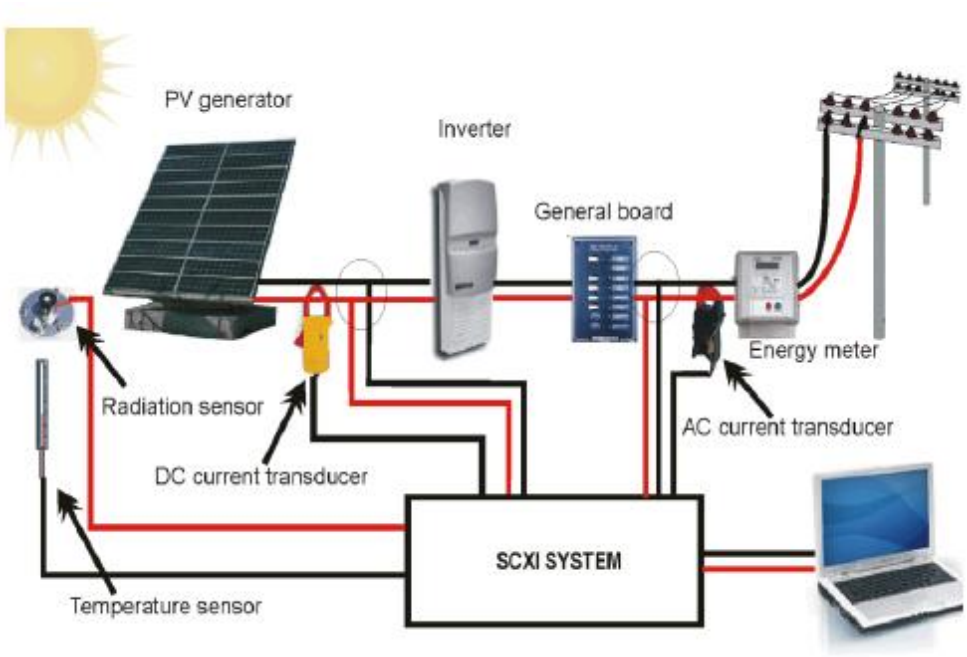

Figure 36: Monitoring system using LABVIEW [126]

1.4.2 Commercial monitoring systems

Typical measurement equipment which is provided by Inverters' manufacturers are irradiance sensors (calibrated reference cells), ambient or back panel temperature sensors, air velocity, recording system and a data set of inverters' inlet measurements. These measurements concern AC voltage, power and total energy, DC voltages and some of manufacturers provide DC current and power. These sets may differ for each manufacturer. In this section are presented equipment of typical monitoring systems of Inverters' manufacturers.

Fronius accompany its inverters with the Fronius sensorbox , irradiance, temperature and air velocity sensors, ambient temperature sensor with large range of measurement in order to cover ambient measurements.

Figure 37 Fronius Ambient temperature sensor

Table 3 : Fronius Ambient temperature sensor

Sensor	PT1000
Measuring range	-40°C to +180°C; -40 F to 356 F;
Accuracy	
Design	Sensor in a cylindrical housing of stainless steel

Dimensions	Length 50mm, 6mm
Cable	3m Cu-cable, 2x0,5 mm, silicon isolated, ferrules, UV-resistant
Max cable length	20m

PV panels temperature sensor

An adhesive sensor which measures PV panels temperature

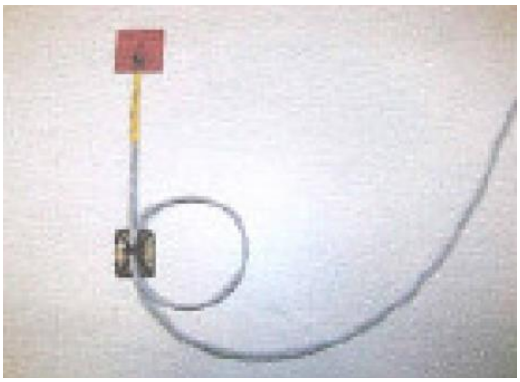

Figure 38 : Temperature sensor on back panel surface

Table 4 : Fronius Temperature sensor

Sensor	PT1000
Measuring range	-4° F to +302° F
Accuracy	± 0,45°C (im Bereich -20°C bis 150°C) 0,81° F (in the range –4° F to 302° F)
Design	Sensor on an adhesive film for measurement on surfaces
Dimensios	32x32mm
Cable	5m Cu,
Max cable length	20m

Solar irradiance sensor

It is a sensor that measures solar radiation and is positioned in the same slope as the inclination of the PV panels. The sensor is a small monocrystalline cell and its output gives an electrical voltage. The sensor is calibrated in order to measure solar irradiance.

Figure 39: Fronius Solar irradiance sensor

Table 5 : Fronius Solar irradiance sensor

Sensor	Mono crystalline Si-Sensor
Sensor voltage	approx. 75mV at 1000W/m2 (exact calibration voltage is written on the sensor)
Accuracy	± 5% (average over a year)
Ambient temperature	-40°C to +85°C; -40° F to 185° F
Design	Sensor is mounted on Z-shaped aluminium profile
Dimensions	l x w x h = 55 x 55 x 10 mm
Cable	3m Cu-cable; ferrules, UV-resistant
Cable Max. cable length (distance: Sensor Card/Box – sensor)	30m

Figure 40 : Fronius Air velocity sensor

Table 6 : Fronius Anemometer characteristics

Sensor	Cup Anemometer
Output signal Rectangle	Low ≤ 0,5V / High ≥3,5V
Calibration factor	5,22 Hz = 1km/h 18,79 Hz = 1m/s
Threshold	2,5m/s wind speed
Resolution	1m/s; 1km/h
Accuracy	± 5% at wind speed≥5m/s
Degree of protection	IP54
Ambient temperature	-20°C to +60°C; -4 F to 140 F
Dimensions	85 x 93 x 115 mm
Cable	2m Cu-cable; ferrules, UV-resistant
Max. cable length (distance: Sensor Card/Box – sensor)	30m

Another monitoring equipment set, which is provided by Kostal Piko inverters, consists of a irradiance sensor and a temperature sensor for back PV panel surface. Characteristics of this sensor set are presented in Figure 41, Table 7, Table 8.

Table 7 : Kostal irradiance sensor

Sensor	Mono crystalline Si-Sensor
Voltage range	0-3,125V
Range	0-1500W/m²
Accuracy	± 5% (average over a year)
Calibration	Solar simulator solar constant 1200,ISE

Table 8 : Kostal temperature sensor

Sensor	PT1000
Measuring range	-4° F to +302° F
Accuracy	± 0,45°C (im Bereich -20°C bis 150°C) 0,81° F (in the range –4° F to 302° F)
Design	Sensor on an adhesive film for measurement on surfaces
Dimensions	32x32mm
Cable	5m Cu,
Max cable length	20m

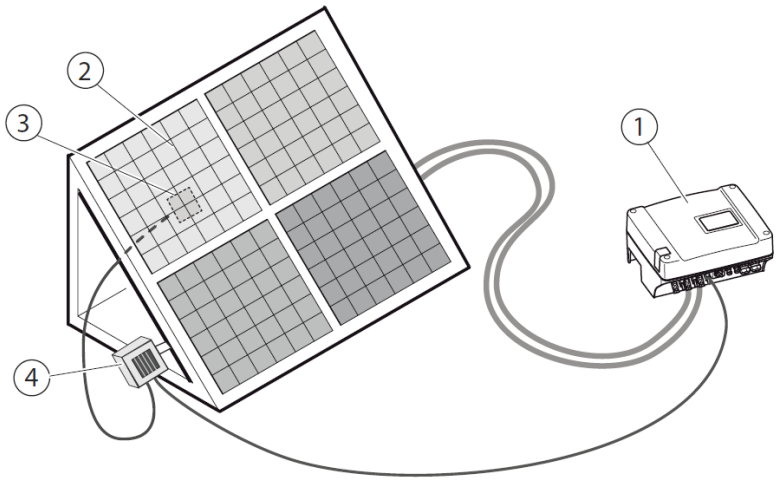

Figure 41: Typical set of monitoring devices of PIKO inverters. 1: inverter 2: PV panels 3: back surface temperature sensor 4: irradiance sensor[127]

SMA provides another monitoring system for installation with SMA inverters. Sunny sensor box consists of an irradiance sensor, an ambient sensor(PT 100) and a back panel surface sensor (PT 100) [128].

Figure 42 : SMA sensorbox [128]

Table 9: SMA irradiance sensor [128]

Sensor	amorphous
Range	0-1500W/m²
Accuracy	± 8%
Divestiture	1 W/m²

Table 10 : SMA temperature sensor [128]

Sensor	PT 100
Measuring range	-20-110°C
Accuracy	± 0,5°C
Divestiture	0.1 °C

Analogue system provide ABB with ABB monitoring and communications VSN800 Weather Station. However ABB weather station provides one more irradiance sensor which is attached in horizontal inclination.

Figure 43 : ABB weather station VSN800

Table 11 : ABB irradiance sensor

Range	0-1750W/m²
Accuracy	± 5%
Temperature range	-25 to 55°C

Table 12 : ABB temperature sensor

Measuring range	-40-80°C
Accuracy	0,3°C

It is observed that all of the manufacturers provide similar equipment and monitoring system sets. In this work the available datasets are provided by grid-connected systems which use Fronius inverters and monitoring system.

1.5 Aim and innovative features of this work

- Formulation of a methodology to manipulate datasets from grid-connected photovoltaic systems for performance evaluation and fault diagnosis without interruption in PV plant operation and without off-grid IV measurements. The aid of IR thermography to this diagnostic procedure is also examined in this work, aiming to further assist O&M procedures.
- Investigation of deviations of PV panels performance from STC values in order to check if PV manufacturers' warranties are met using real time data.
- Manipulation of big data time series of grid-connected PV system in order to give information of solar potential.
- Investigation of Airmass and clearness index impact on real time PV efficiency.
- Investigation of aerosol impact on real time PV efficiency using aerosol mass concentration, rainfall data, irradiance, temperature and electrical power of PV system.
- Investigation of dust accumulation effect in PV performance using real time data of grid-connected PV systems, aerosols mass concentration and rainfall data.
- Study degradation of PV systems by a long term analysis methodology which calculates performance metrics in order to check its evolution over time.

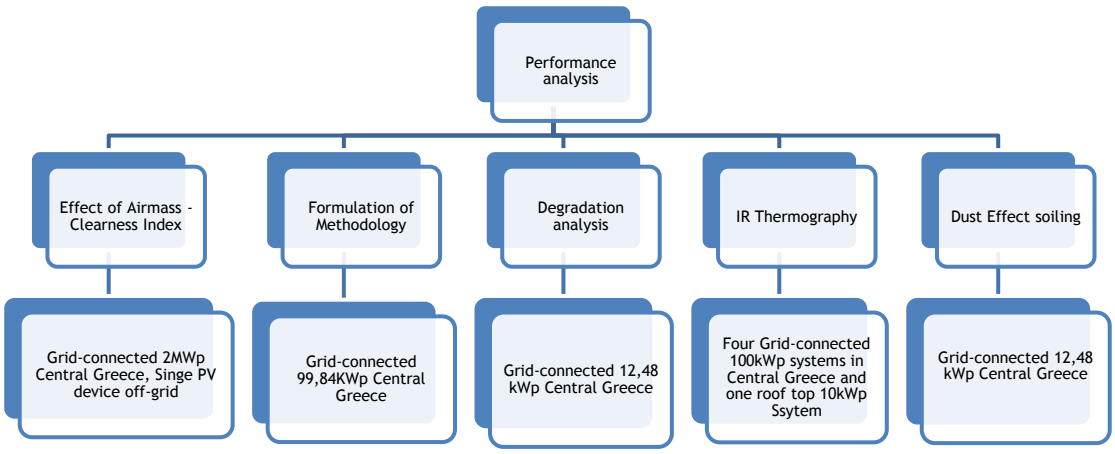

Figure 44 : Analysis objectives and respective experimental set-ups for this study

2 Literature Review

Performance analysis of grid-connected photovoltaic systems is a challenging task which is investigated by a significant number of researchers worldwide. Performance analysis applied vary widely according to its objectives, as well as the method of analysis. There are many researchers who study the prediction of photovoltaic systems energy generation and others the evaluation of systems' performance. The main researchers' objectives are study of the potential of a site [129, 130], economic assessment [131], comparisons between different types of PV technology, study of the effects of environmental conditions like humidity and dust accumulation and degradation of PV systems [111-113, 132-138].

2.1 Performance analysis of Photovoltaic systems

Estimation of solar potential has already been investigated by many researchers. Hafeznia et al, proposed a framework to estimate the solar potential for utility scale installations using spatial planning and performance simulation [139]. A challenging task is the exploitation of measurements of grid-connected PV parks in assessing solar potential or energy generation potential. In Greece, there exist many PV parks scattered across the country, and systematic data collection could create an inclusive and useful solar database. The majority of PV parks employ a typical set of sensors which collect in - plane irradiance, module temperature and power data from the inverter's inlet side. Processing of these data can be used as a tool for weather prediction and electricity generation forecasting. Several studies exploit datasets from grid connected systems for forecasting, performance evaluation and estimation of solar potential. Mellit et al, use measurements of irradiance and air temperature from a grid-connected system and with the aid of MLP network forecast 24 h ahead of solar irradiance [140]. Nespoli et al proposed a method for estimating global horizontal irradiance from AC measurements of one or more PV plants [141]. Graditi et al, used a large data set and three models, based on a neural network, a regression approach and a physical model, to forecast energy production [142]. Cervone et al, propose also an artificial neural network using a numerical weather prediction model and computed astronomical variables and the results were tested in PV stations in Italy [143]. Another example of exploitation of solar measurements in order to provide knowledge about the solar potential is a study in eastern Iran by Maleki et al.. Particularly, a geographical information system module is developed first to determine the suitable location and capacity for a stand-alone PV system in rural areas, taking into account the technical, environmental and socio-economic criteria affecting the site selection process of stand-alone PV systems [144]. On the other hand, a significant challenge is the contribution of renewable energy in buildings. To that point it is important to determine the optimal integration of solar energy in urban areas. Optimal sizing demands very good knowledge of solar potential and local environmental factors that affect photovoltaic production. Mavromatidis et al, study solar potential of a village in order to exploit solar energy using photovoltaic systems. Particularly, they proposed a model which uses Digital Elevation Models (DEM) in order to create solar availability profiles for each building examined, taking into account the different surface orientations, the neighbouring structures, but also the surrounding topography [145]. This work aims to give feedback for solar and PV production from grid connected photovoltaic systems in real conditions. The fact that this feedback concerns PV parks in real conditions gives more realistic information as

includes all type of losses and describes behavior of systems' in different environmental conditions. Furthermore, there are many approaches that study performance analysis with experimental set-ups that are not grid-connected, however operation of PV modules in MPP is a task that needs simulation. Application of the proposed methodology in combination with a GIS system and access to a large number of scattered PV parks is going to create a useful tool for sizing, forecasting of electrical loads and comparison of different technologies.

Dust accumulation is another important factor which is analyzed in 1.2.7. From a techno-economic aspect, it is important to determine whether its effect necessitates cleaning processes for PV panels. This issue is related to region characteristics and weather conditions. Hachicha et al., study the effect in a desert area and observed that rainfall contributed to improve the PV performance and decreased dust density. However, due to cementation process some dust particles tend to stick on the PV surface and could not be removed. Moreover, cleaning of PV modules cannot rely on occasional rain and it should be planned based on the regular density accumulated [146].

Triki-Lahiani et al. divide the methods of analysis in five main categories, namely electrical circuit simulation, statistical analysis, electrical signal approaches, artificial intelligence, predictive models and comparison with real models [147]. However, these categories may be combined. An important difference for each approach is the experimental set-up. Many studies based on outdoor set-ups which are PV parks in actual grid-tied operation, while other experimental set-ups are not in grid-connected operation. Other studies are based on indoors experiments, or simulation procedures. In each method of analysis, the parameters considered are the available inputs and -depending on the methodology- also the computed outputs. The selection of inputs and outputs are up to each researchers' choice and the same holds for the method of analysis, however, the available standards as IEC 61724 are employed to [120]. As far as environmental conditions are concerned , the recommended inputs by IEC61853 are irradiance in plane of array, effective irradiance, directionally resolved radiance, air temperature and wind speed [124].

As already mentioned, an important objective under investigation is PV modules degradation. Performance degradation analysis is classified as indoor and outdoor analysis. Phinikarides et al. presented a classification of methodologies for degradation analysis according to these categories. Outdoor analysis includes the calculation of PV performance metrics, IV characterization, regression modeling, normalized and scaled ratings, measurement qualifications and filtering, statistical analysis and uncertainties. Indoor analysis involves the calculation of degradation rates for PV modules subjected to accelerated aging based on weathering and PID acceleration with the aid of appropriate test conditions [148]. However, under real outdoor exposure radiation, temperature, humidity, wind and operating voltage act together, whereas under accelerated tests these parameters are varied according to a predetermined sequence which is not quite representative in order to observe the same defects [132]. Huang et al. presented a method to study the degradation process of PV models with the help of a circuit-based model of PV electrical characteristics. It was observed that the main reason of power loss was optical degradation of the PV modules, which tends to increase through time, depending on PV technology and climates [149]. Ozden et al, conducted long term outdoor testing of three different PV technologies under the same climatic conditions and calculated degradation rates from monthly efficiencies in the range 0,4 - 10,6%[150]. The term degradation rate, R_D, is defined as the rate of maximum performance reduction over time [148]. Rajput et al. studied PV degradation using

visual inspection, thermal imaging, IV and insulation resistance measurements and calculated degradation using the following formula [112]:

$$\text{Rate of Degradation}(R_d) = \frac{\text{Initial data} - \text{Final data}}{\text{Final data}} \text{ x } 100 \quad (2\text{-}1)$$

To sum up, methods of analysis are mainly based on mathematical models, on the calculation of standards' metrics IEC 61724 , the use of models of the PVUSA type [151], the use of neural networks , and the use of simulation models. Another type of analysis is based on normalization procedures [152-154]. All of the types of analysis are presented in the follow sections.

2.2 Mathematical Models

There are several models and methods of PV performance analysis in recent literature. The differences between models are related to the kind of input parameters, types of measurement equipment and type of operation, grid-connected or not. There exist three main categories for evaluation and prediction of PV performance: (i) based on real time operation data, (ii) based on off-grid measurements, and (iii) based on simulation.

Mathematical models which are described below concern either PV power or PV efficiency however calculation of PV efficiency based on PV power stems from equation (2-4).[155]

$$n = \frac{Maximum\ Electrical\ Power}{Area\ x\ \ Irrdiance} = \frac{P_{STC}}{AG_{STC}} \quad (2\text{-}2)$$

A mathematical function to compute PV efficiency for a given set of irradiance and temperature levels, proposed by Evans [156] for prediction of the PV output with a simplified procedure is the following:

$$n(T_C, G) = n_{STC}[1 + a(T_C - T_{STC}) + k \log_{10} G] \quad (2\text{-}3)$$

where n_{stc} denotes the PV efficiency on STC, a denotes the panel temperature coefficient of power, T_C denotes the temperature of PV panel, T_{STC} denotes the temperature of PV panel according to STC conditions (25°C), G denotes the irradiance on panel's surface, k the solar radiation coefficient. A simplified application of the above equation without the logarithmic term has also been proposed.

$$n(T_C, G) = n_{STC}[1 + a(T_C - T_{STC})] \quad (2\text{-}4)$$

Many researchers describe models based on this equation, using different factors each, depending on the type of model application.

Ramli et al. describe a model to study the effect of dust accumulation carrying out measurements with an experimental off-grid system and using the equation below:

$$P = P_{STC} f_{PV} \frac{G}{G_{STC}}[1 + a(T_C - T_{STC})] \quad (2\text{-}5)$$

Where P_{STC} is PV power at STC conditions, f_{PV} is a derate factor of PV, G is total irradiance, G_{STC} is irradiance at STC conditions (1000W/m^2), a is power temperature coefficient (%/°C), TC is the panel temperature and T_{STC} is panels' temperature at STC

conditions(25°C) [94]. PV panels exposed outdoor in off-grid operation using a microcontroller, a load, an ambient temperature sensor, geographical data and a global horizontal irradiance model. Results reveal that local environmental conditions, dust, rain and partial cloud, significantly reduce PV power output.

On the other hand, Nacer et al propose a model of grid-connected photovoltaic systems in family farms for electricity generation in rural areas. This model is described below.

$$P = n_{STC} n_{INV} A \, f_{DC} f_{AC} f_{AGE} f_{EXT} \frac{G}{G_{STC}} [1 + a(T_C - T_{STC})] \quad (2\text{-}6)$$

Where n_{STC} is PV performance at STC conditions, n_{INV} is inverters' performance, f_{DC} is a derate factor (typical value of 0.955), f_{AC} is a AC interconnection derate factor (typical value 0.99), f_{AGE} is a derate factor for the loss in system performance with ageing, f_{EXT} is a derate factor for external reason like dust accumulation, shading effects or snow cover, G is the total irradiance, G_{STC} is irradiance at STC conditions (1000 W/m²), a is the power temperature coefficient (%/°C), T_C is the panels' temperature and T_{STC} is the panels' temperature at STC conditions (25°C) [157]. The proposed model aids in the optimal sizing of the system and verifying the economic feasibility in applications like farms.

It is well known from manufacturers' tests that an efficiency drop happens at low irradiance levels. This is observed either from grid-connected PV systems [158] or from off –grid experimental PV systems that at small solar altitudes and consequently large values of AM there is a decrease in efficiency [159]. Thus, correlation between irradiance and power may be improved at low irradiance levels with the following two models reported in the literature[160]:

The first one is the PV form model:

$$P = \frac{G}{G_{STC}} P_{STC} [1 + a(T_C - T_{STC})] \quad (2\text{-}7)$$

For G < 125W/m²:

$$P = \frac{0.008 G^2}{G_{STC}} P_{STC} [1 + a(T_C - T_{STC})] \quad (2\text{-}8)$$

The PV form model differentiates the power computation for low irradiance levels, by employing as inputs irradiance (G) and panel's temperature (T_C) in combination with the following PV panel's technical characteristics: nominal power (P_{STC}) and temperature coefficient (a) as well as the reference values G_{STC}, T_{STC} (1000 W/m², 25°C). A similar approach is the improved bilinear interpolation model which employs a different expression for the low irradiance limit, as well as one additional coefficient, the irradiance factor k.

The improved Bilinear interpolation model takes the following form[160]:

G > 200 W/m²:

$$P = P_{STC} \left[\frac{G}{G_{STC}} [1 + a(T_C - T_{STC})] - k \frac{G_{STC} - G}{G_{STC} - 200}\right] \quad (2\text{-}9)$$

G <200 W/m²:

$$P = P_{STC}\left[\frac{G}{G_{STC}}[1 + a(T_C - T_{STC})] - k[1 - \left(1 - \frac{G}{200}\right)^4]\right] \quad (2\text{-}10)$$

Where P_{STC}, G_{STC}, T_{STC} are reference parameters, k an irradiance factor and a the panel temperature coefficient described by the manufacturer. T_c and G are measured parameters. Irradiance factor k is provided by manufacturers as a percentage reduction in efficiency at low irradiance levels (200 W/m^2). However, this factor may be computed, by conducting further characterization measurements by use of low irradiance models.

Another important model which stresses the temperature effect is described by Skoplaki et al. Skoplaki et al, propose a simple empirical expression for the electrical efficiency of a typical crystalline silicon PV cell [161]:

$$n = 0{,}12[1 - 0{,}004\left(T_{AMB} + \omega\frac{0.32}{8.91 + 2V_f}G - 25\right)] \quad (2\text{-}11)$$

Where T_{AMB} is ambient temperature, ω is defined as mounting coefficient and correlates type each mounting system with free standing(ω= type of mounting system/free-standing where values are free standing system=1, flat roof=1,2, sloped roof=1,8, façade integrated =2,4) .V_f=(V_W+0,5)/0,68 where V_W is wind speed, G is irradiance.

Akhsassi et al. proposed a mathematic model in order to evaluate PV performance of a grid connected system.

$$n_{PV} = n_{STC}[1 + a(T_C - T_{STC})][1 + \gamma \ln\frac{G}{G_{STC}}] \quad (2\text{-}12)$$

Where η_{STC} and α are the module efficiency and the temperature coefficient of maximum power, T_{STC} and G_{STC} are the reference temperature and reference solar irradiance (25 °C and 1000 W/m^2, respectively). γ is a dimensionless coefficient which is between 0.03 and 0.12 for single crystalline silicon. The experimental set up consists of 32 Sunpower (SPR-225-WHT) monocrystalline silicon panels 225 Wp. The PV power plant and its meteorological station are fitted up with sensors to monitor irradiance, wind speed, ambient and module temperatures. The meteorological parameters are recorded by a Sunny Boy Control Plus (SMA) data logger which communicates with the Sunny Sensor Box [162].

As mentioned above, most models concern real time data in grid-connected operation, on the other hand there exist models concerning off – grid operation. The two model categories have advantages and disadvantages which depend on the kind of application. In all cases a usual problem is the lack of measurements for different levels of panel temperature, irradiance and spectral distribution of radiation. In such cases, the use of appropriate models may improve prediction accuracy. A characteristic example is the lack of panel's temperature which may be substituted by use of meteorological data based on the following expression, proposed by Mavromatakis et al. [129]:

$$T_C = T_a + \frac{G}{G_{STC}}(T_1 EXP(B\,W_S) + T_2 + \Delta\theta) \quad (2\text{-}13)$$

where T_1, T_2, B, Δθ are empirical coefficients (T1=19.6° C,T2=11.6° C,B=-0.223, Δθ=3° C) and T_C, Ta are the cell's and ambient temperatures respectively and W_S the wind speed.

2.3 Performance ratio and metrics

An important performance index for a PV park is the performance ratio (PR), which is the global system efficiency with respect to the nominal installed power. Monitoring of PR of a grid-connected system correct underperforming system and reduces economic losses due to operational problems [163]. PR values are typically reported on a monthly or yearly basis. The comparison of yearly PR allows for an indicative assessment of PV park performance, although it does not account for the effect of panel temperatures and the existence of possible periods with the park disconnected from the grid. Nevertheless, PR ratio is useful to identify problems as faults in inverter operation, shading, diode failures and soiling [164]. PR was introduced by the JRC (European Joint Research Center) in order to facilitate comparisons between several PV installations and is adopted by many researchers. It is described in the IEC EN 61724 standard [120]. It can be seen as the ratio of parameters Y_f and Y_r (system yield and reference system yield, respectively), defined as follows:

$$Y_f = \frac{E}{P_{STC}} \quad \text{(kWh/kW)} \tag{2-14}$$

Where E is the net energy output and P_{STC} is the installed power at STC conditions

$$Y_R = \frac{H}{G_{STC}} \text{ (kWh/kW)} \tag{2-15}$$

Where H is the total in plane solar radiation and G_{STC} is irradiance at STC conditions ($1000W/m^2$). It represents an equivalent number of hours at the reference irradiance. This is the ideal energy produced if the system was always running at the STC efficiency.

$$\text{PR} = \frac{Y_f}{Y_r} \tag{2-16}$$

$$\text{CF} = \frac{Y_f}{8760} \tag{2-17}$$

As already mentioned, the panel temperature effects are not included in the above equations. Other researchers propose the use of temperature - corrected Y_r [165], defined as follows:

$$Y_{cr} = Y_r(1 + a(T_C - T_{STC})) \tag{2-18}$$

Where Y_r is computed from equation (2-15) , a is the panel temperature coefficient, T_c is the panel temperature and T_{STC} is the reference temperature at STC conditions.

PR analysis is focused on long term analysis, however, it is important sometimes to model the power output in real time as an index of PV performance.

Kymakis et al. applied PR and capacity factor (CF) in monitoring a PV park on the island of Crete, to draw conclusions for long term PV performance [166]. The experimental set up of this work is a grid-connected 171,36kWp PV system in Sitia Crete. The PV park supplied 229 MW h to the grid during 2007, ranging from 335.48 to 869.68 kWh. The final yield (Y_f) ranged from 1.96 to 5.07 h/d, and the performance ratio (PR) ranged from 58 to 73%, giving an annual PR of 67.36%. This work provide important information for potential of the site, however does not provide information for PV panels performance.

Dabou et al. presented a performance analysis of a 1.75 kWp grid connected photovoltaic installation in South Algeria using PR and efficiency of PV modules, system and inverter in order to study the relationship between performance and climate parameters, aging and pollution. The experimental results show that the lowest values of the system efficiency and performance ratio (10.29% and 76.5% respectively) caused by the high module temperature equal to 41.1°C in the clear day, and the fast-changing of the solar irradiance is caused by variation of clouds cover or dust storm affects the energy generated and stability of the PV system [167].

De lima et al. presented a performance analysis of a 2.2 kWp PV system in Brazil using system efficiency, performance ratio and capacity factor in order to evaluate the potential of producing electricity through photovoltaic systems in this region of Brazil. The grid connected PV system used in the present study is installed in Ceará, (latitude 3.40°S and longitude 38.33°W). The system consists of 18 modules covering a total area of 29 m^2 with an installed capacity of 4.4 kWp. The installed PV panels are Canadian Solar CS6P-245P of 245 Wp. The SMA Sunny Boy SB 2500-HF-30 inverter was used [168]. Calculation of daily average reference, array and final yields, the array capture, system and overall losses, the array, system and inverter efficiencies, the performance ratio and the capacity factor varied provide important information for systems' efficiency although factors as temperature are not examined. Consequently, the calculated performance figures of the PV panels are influenced by the panels temperature.

Congedo et al. analyzed the performance of a 960 kWp grid connected PV system in South-eastern Italy using performance ratio and the other performance indices such as AC power output and instantaneous efficiency. The study gives an aspect of how is the real performances of a PV system installed in South-eastern Italy and how the climatic conditions influence PV energy and provides a base for the comparison with other ones in different locations [169]. However, this study does not give clear conclusion about PV device performance.

Another data on a 2 kW (rooftop) solar PV plant installed in Niš (Republic of Serbia) and the equipment for the estimation of its performance and energy efficiency depending on the real climate conditions (inverter, communication system, automatic meteorological station) is studied by Milosavljevic et al. using performance ratio to investigate the solar potential in Serbia [130]. This study gives important conclusions for solar potential of Serbia where the integration of solar energy into the transmission network was considered satisfactory according to the study. The research results show that PV system works efficiently in Serbia [130]. However, this study does not draw conclusions in relation to PV panels' efficiency as the metrics used are influenced by temperature.

On the other hand, a large-scale 15MWp PV system in Mauritania was evaluated with the use of PR, CF and other factors. Elhadj et al., analyzed the performance of the plant under the meteorological conditions of region and compared their results with other studies in other regions [165].

Martín-Martínez et al, study PV performance under real conditions based on PR and its evolution over the time. The experimental set-up is based on 5 large plants in Spain and the analysis in the seasonal fluctuation in monthly PR. As far as temperature effects are concerned, a PR ambient temperature coefficient is calculated. This coefficient stemmed from the correlation of ambient temperature with PR [170].

Necaibia et al, conducted a performance analysis of a small grid connected system in a desert area using standard metrics, namely, performance ratio (PR), yield factor (YF),

reference yield (YR), capacity factor (CF) and array capture losses (LC) in order to quantify the effect of environmental parameters on system's performance, allowing comparison with other installations. The experimental set up consists of a grid-connected PV system, installed on the rooftop, with 10 modules. The PV cells technology used is mono-crystalline silicon model SM-250Wp from the Korean manufacturer S-Energy. The modules have been tilted at a fixed angle of 28.88° and oriented northward at an azimuth angle of 12°. The analysis based on seasonal and annual performance parameters and its performance have been compared with other similar grid-connected PV systems sited at different location around the world. Research results are related with temperature effects on summer season, when the performance is decreased, and the solar potential of region [171]. However, this study does not use a metric or a procedure which defines PV performance independently of the factors that affect it.

S. Seme et al. used PR metrics in order to investigate Slovenia Photovoltaic energy potential and compare with other places around the world. The results in this paper show that the performance of photovoltaic systems primarily depends on the proper inclination and azimuth angle of the photovoltaic modules, shadings, and snow barrier [172]. It is clear that PR ratio is an important critical factor for real world grid-connected PV systems efficiency, that is independent of the systems' location and scale. However, PR is influenced by the PV panels temperature and the calculation of temperature corrected ratio is proposed.

Aste et al, used PR in order to compare different types of PV technologies and the analysis is conducted in seasonal basis in order to correlate performance with climate conditions. The experimental set up of this study consists of selected PV technologies. In mounting structures characterized by a variable tilt angle and oriented with an azimuth angle of 0°. All devices are connected to a central data-logging system that stores the measurements. The DC/AC conversion is operated by a transformerless micro-inverter with MPPT tracker, that allows to monitor each PV module separately. The analysis was focused on the three different PV technologies ,PV cells (c-Si), micromorphous cells (a-Si/lc-Si) and hetero-junction with intrinsic thin layer (HIT). The analysis based on PR comparison of the three PV types [173].

Performance ratio is also used in experimental set-ups that are not grid-connected. Ustun et al, used numerous panels of different technologies and manufacturers in order to compare their efficiencies. PR is calculated for each technology and because of the fact that PV panels are in the same place with same environmental conditions, comparison is able to provide important conclusions for each technology. Particularly, technologies which are compared are c-si, mc-si, c-si(HJ), a-si/μc-si, CIGS. The results showed in Figure 45 where CIGS has the higher PR and then mc-si, c-si(HJ) are in the same levels [174].

Guerra et al, conducted a comparative analysis of grid-connected photovoltaic systems with different PV technologies based on PR metrics. Particularly, they propose calculation of PR AC according to the following equation:

$$PR_{AC} = \frac{Y_R - L_C - L_{BOS}}{Y_R} \quad (2\text{-}19)$$

Where Y_R is Reference yield , L_C is Capture losses (shadows, dirt, temperature, spectral, angular, mismatch, loss of power due to degradation, maximum power point delay, wiring, etc.), L_{BOS} is Losses in inverter, wiring and electrical connections. The photovoltaic system study is installed in Madrid on a flat roof well exposed to solar

radiation with shading of nearby buildings reduced to positions of the sun just after sunrise and before sunset. The site has a continental climate with cold winters and hot summers. The compared technologies are mc-Si, pc-Si, a-Si/μc-Si tandem, CdTe/CdS, CIS and mc-dc-si mounted on weighted fixed tilt structures. All the modules of the different technologies are coplanar with a tilt of 30° and azimuth of 19° east to optimize the spatial distribution according to the architectural requirements of the roof. Global solar irradiation data is captured by means of a thermoelectric pyranometer and a calibrated reference cell of polycrystalline silicon, module temperature is measured with a PT-1000 thermocouple sensor fixed to the backsheet of a central cell, ambient temperature and relative humidity are measured with a thermohygrometer, wind speed uses an anemometer. The results show that mc-si, p-si, CIS and mc-cd-Si technologies reach an average value of PRAC above 80%, while a-si/μc-si and CdTe/CdS remain at 74.5% and 64.3%, respectively. Furthermore, conventional technologies mc-Si and pc-Si displayed very similar thermal and energy behavior [175].

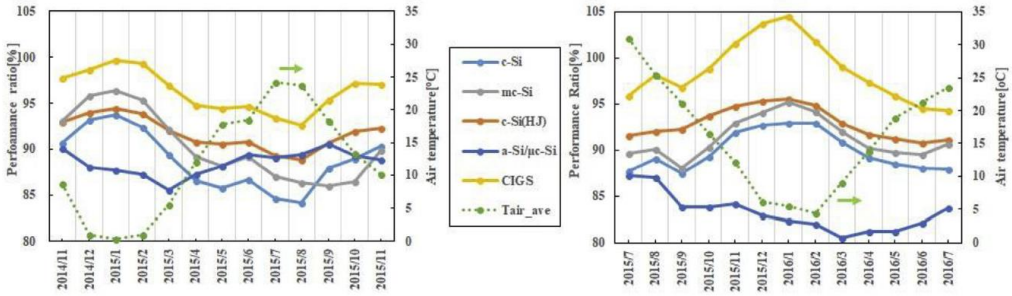

Figure 45 : Performance ratio of different technologies in Fukoshima [174]

Edalati et al, investigate performance analysis of a 11.04 kWp grid-connected photovoltaic PV system. PV system consists of 5.52 kWp common crystalline PV technology with almost similar characteristics and is established in an industrial sector of Iran. PV panels are monocrystalline silicon (mc-si) and polycrystalline silicon (p-Si) and period of analysis concern July 2013 to June 2014. Inverters are selected from SMA, model Sunny Boy 5000TL in combinations with a fully monitored with a SMA Sunny WebBox data logger integrated to a meteorological station and inverters. The available data are global solar radiation, ambient and back temperature of PV panels, DC array output power and AC array output, humidity, wind speed, and produced power in each array are recorded by the data logger and saved on a daily basis. Performance analysis is based on calculation of metrics that are referred above as performance ratio and capacity factor. Because the fact that these metrics are influenced by weather conditions and especially temperature, the use of temperature corrected PR according to NREL definition is proposed [176].

Weather corrected PR according to NREL is described by the following equation [177]:

$$PR = \frac{\sum_i P_{AC,i}}{\sum_i [P_{STC}\,(\frac{G_i}{G_{STC}})(1 - a(T_{cell\_typ\_avg} - T_{cell,i}))]} \qquad (2\text{-}20)$$

Where PR_{corr} is corrected performance ratio (unitless), P_{AC} is measured AC electrical generation (kW), P_{STC} is summation of installed modules' power rating from flash test data (kW), G_i is measured plane of array irradiance (kW/m²), i = a given point in time, G_{STC} is irradiance at standard test conditions (1000 W/m²), T_{cell} is cells' temperature

computed from measured meteorological data (°C), $T_{cell\_typ\_avg}$ is average cell temperature computed from one year of weather data using the project weather file (°C), a is temperature coefficient for power (%/°C, negative in sign) that corresponds to the installed modules.

Sometimes, the system yield in correlation with capacity factor may be used as an indicator of decreased performance for further diagnosis [178]. In that context, mathematical models that correlate the power output of PV panels with irradiance, panel temperature, AM spectrum and other factors are quite useful. Several models of this type exist in the literature, as summarized in the following paragraphs.

2.4 Neural Networks

Another way to evaluate PV park performance is by employing models with neural networks. ANN models are used in engineering analysis and predictions. The concept of ANNs is based on the learning processes of a human brain. ANN operates like a "black box" model, requiring no detailed information about the system, however it learns the relationship between the input parameters and the controlled and uncontrolled variables by studying previously recorded data, similar to the way a non-linear regression might perform [179].

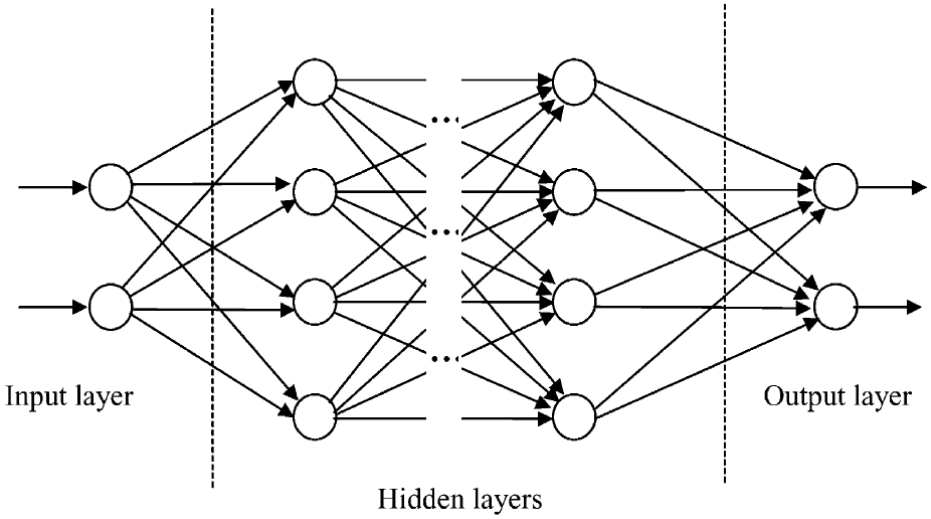

Figure 46 : Artificial network formulation [179]

The differences from all these methods are mainly related to the required number of inputs. Most of them refer to outdoor exposure of PV panels that are off- grid. Rodrigo proposed a model based on the calculation of angular, spectral and low irradiance losses. This method demands only two inputs: global irradiance on the plane of generator and PV cell temperature. It uses an artificial neural network model in combination with the Osterwald model. Both models are integrated in a single structure [180].

Vellila et al. on the other hand, proposed a neural network with one more input parameter, namely, relative humidity, which plays a significant role to PV performance . Experimental results are presented from monitoring the electrical power after exposure to external weather conditions of two different solar modules technologies, one of them a mono-crystalline 55 W silicon and the other a flexible organic solar module of 12.4 W. During the observation period the temperature, relative humidity, and irradiance were

monitored [181]. This model is employed as a prediction tool and for comparison between different technologies however this model is not able to apply in grid-connected photovoltaic systems as its experimental setup based on off-grid measurements.

Touati et al. used long term-data of PV systems in Qatar in order to investigate the effect of environment factors on PV power output and to find empirical models for PV power output using linear regression and tree decision algorithms. These empirical models confirmed that the most important parameters for PV efficiency are irradiance, accumulated dust, relative humidity, ambient temperature and panel back surface temperature [182].

Tahri et al, study the evaluation four grid-connected photovoltaic systems with different PV panel technologies. The type of technology are two mc-Si and two copper indium selenium: CIS PV panels. The analysis based on PR calculation and temperature losses, however, it is proposed a regression technique in order to correlate daily AC energy output generated by each PV power plant at given daily irradiation and daily average module temperature. The mathematical model obtained by applying a multivariable linear least square fitting is expressed as follow :

$$E_{AC} = a + bH_{MEAS} + cT_M \quad (2\text{-}21)$$

Where, E_{AC} is the daily AC energy output (expressed in kWh), H_{meas} is the daily irradiation in kWh/m^2,Tm is the daily average module temperature in °C, a is the intercept expressed in kWh, b and c are the coefficients of the multivariable regression and they are expressed in m^2 and kWh/°C respectively [183].

Rosell and Ibanez proposed a model that correlates the maximum generated power with irradiance and PV panel's temperature:

$$P_{MPP} = D_1 G + D_2 T + D_3 (\ln G)^m + D_4 T (\ln G)^m \quad (2\text{-}22)$$

where P_{MPP} denotes maximum power point of IV curve, T denotes panel's temperature and G the irradiance in plane of array. The coefficients D_1, D_2 , D_3 , D_4 , m stem from a set of measurements that is fitted by a multivariable regression equation [184].

Kazem et al. proposed four different neural computing techniques aiming to predict the energy generation of a small grid-connected photovoltaic system [185].

Dias et al, propose a model which combines irradiance and ambient temperature in mathematical equation. The available data are trained

$$P = aG + b(\frac{G}{T_{AMB}})^2 + cGT_{AMB} \quad (2\text{-}23)$$

where: P is power system output in W, G i irradiance in W/m^2; T_{AMB} is ambient temperature in C; a, b and c are regression coefficients. The data set, developed to estimate the performance of photovoltaic systems connected to the grid and mounted in opened racks without mutual shading, is related with values of power generated by the system after its conversion into AC and information from the site environment [186].

Osterwald et al. proposed a model that uses solar radiation data from a hemispherical pyranometer that are corrected by Air mass functions f(AM) (a correction with absolute airmass, pressure-corrected) [187]. Air mass functions are of the following type:

$$f(AM) = \frac{\frac{P}{G}\Big| AM}{\frac{P_{STC}}{G_{STC}}\Big| AM = 1.5} = a_0 + a_1 AM + a_2 AM^2 + a_3 AM^3 + a_4 AM^4 \quad (2\text{-}24)$$

These empirical functions are determined from outdoor measurements with test modules mounted on two-axis solar trackers and then calculated from plots of normalized calibration value (short-circuit current divided by total irradiance) versus optical Air mass. It is important to note that these functions are related to the specific location, time and are particular to each different type of PV panel [187].

2.5 Simulation

As far as simulation is concerned, several studies can be found in the literature. Simulation based on mathematical models which are used in standard simulations tools as Pspice and Matlab Simulink. The aim of these studies is either formulation of model for forecasting or for performance evaluation. Performance evaluations based on comparison of simulated values with measured values of real grid-connected system. Another goal of simulations is comparison of different PV technologies characteristics.

Anoun et al, describe four different models for simulation of PV device with accordingly different parameters. The proposed models are seven parameter model, five parameter, four parameter and ideal circuit (Figure 47). The ideal circuit is described by the following equation:

$$I = I_{ph} - I_{01}\left[exp\left(\frac{qV}{\gamma kT}\right) - 1\right] \quad (2\text{-}25)$$

Where I_{ph} is photocurrent which associated to the photo-generation of electrone-hole pairs and equals the short-circuit current I_{01} are saturation current by diffusion and by recombination respectively, k the Boltzmann constant, T the cell temperature, q the electron charge, γ_1 and the ideality factor of diode (1). This model does not account for the actual behavior of a photovoltaic cell. The four parameters circuit (γ, I_{ph}, I_0, and R_s) (Figure 47c) is described by the following equation:

$$I = I_{ph} - I_{01}\left[exp\left(\frac{q(V + IR_S)}{\gamma 1 kT}\right) - 1\right] \quad (2\text{-}26)$$

The most common model which is used by many researchers in PV modeling is One-diode model (5-parameter model) (Figure 48) and is described by the following equation:

$$I = I_{ph} - I_0\left[exp\left(\frac{q(V + IR_S)}{akT}\right) - 1\right] - \frac{V + IR_S}{R_{SH}} \quad (2\text{-}27)$$

Where I_{ph} (A) is the photocurrent associated to the photo-generation of electron-hole pairs and equals the short-circuit current if the parasitic resistances are neglected, Io is the reverse saturation or leakage current of the diode. Furthermore, series and parallel electrical resistances are usually included in the model to represent internal losses, q is the electron charge (1.60217646 $x10^{-19}$ C), k is the Boltzmann constant (1.3806503$x10^{-23}$ J/K), T (K) is the temperature of the p-n junction, and *a* is the diode ideality factor, R_S (Ω)

is the series resistance, R_{sh} (Ω) is the shunt resistance[188].

The seven-parameter (two-diode) model: describes the diffusion and recombination characteristics of the charge carriers in the material and in the space charge zone. Models parameters are I_{ph}, I_{01}, I_{02}, γ_1, γ_2, R_s, and R_{sh}. The current–voltage characteristic is described by the following equation:

$$I = I_{ph} - I_{01}\left[exp\left(\frac{q(V+IR_S)}{\gamma_1 kT_C}\right)-1\right] - I_{02}\left[exp\left(\frac{q(V+IR_S)}{\gamma_2 kT_C}\right)-1\right] - \frac{V+IR_S}{R_{sh}} \quad (2\text{-}28)$$

Where I_{01} and I_{02} are saturation current by diffusion and by recombination respectively, k (J/K) the Boltzmann constant, Tc (K) the cell temperature, q (C) the electron charge, γ_1 and γ_2 the ideality factor of diode (1) and diode (2) respectively, R_{sh} (Ω) shunt resistance characterizing the leakage currents of the junction and R_s (Ω) the series resistance representing the various resistances of the metal contacts, ohmic losses in the front surface of the cell, impurity concentrations, and junction depth [189].

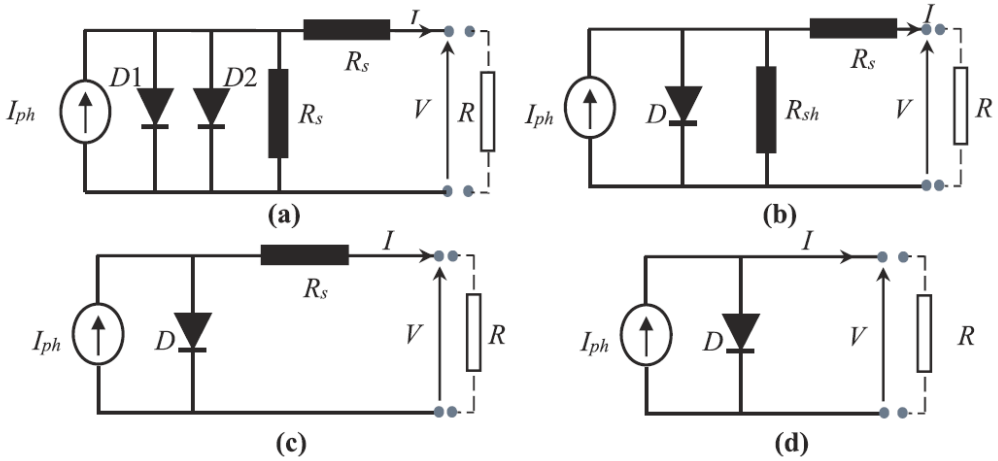

Figure 47 : a: seven parameters model, b: five parameters model, c: four parameters model d: ideal circuit [189]

Chouder et al, based on the one diode model in order to compare monitored and measured variables, and then a decision is made about the normality/abnormality of the process behavior. Inputs of the system are the measured irradiance and cell temperature which are applied to the model. The authors propose as metric for the comparison of measured values with simulated capture losses which are divided in the thermal capture and miscellaneous capture losses.

$$L_{ct\_sim} = Y_{a_{sim}}(G, 25°C) - Y_{a_{sim}}(G, T_C) \quad (2\text{-}29)$$

$$L_{C\_sim} = Y_R(G, T_C) - Y_{a_{sim}}(G, T_C) \quad (2\text{-}30)$$

$$L_{cm\_sim} = L_{C\_sim} - L_{ct\_sim} \quad (2\text{-}31)$$

where L_{ct_sim} are the simulated thermal losses, Y_{a_sim} (G, 25°C) is the normalized energy yield at real working irradiance and 25°C of temperature, and Y_{a_sim} (G, T_c) is the array yield at real working irradiance and real module temperature T_c, L_{C_sim} are the capture losses, Y_r (G, T_c) is the measured reference yield. Capture losses are calculated according to the measured energy yields and those calculated according to the simulated yields in order to check for possible faults [190].

Cuce et al. proposed a mathematical model to simulate I-V and P-V curves, to be compared with manufacturers' performance data. The considered model in this research is based on an one-diode five parameter model (Figure 48) which comprises of a solar intensity dependent current source, a p-n junction diode and two resistances (R_S and R_{SH}). The results show that energy efficiency, power conversion efficiency, and exergy efficiency logarithmically increase with increasing solar intensity and educe linearly with increasing PV cell temperature [191]. However use of this procedure does not provide conclusions for grid-connected condition and outdoor in real time operation.

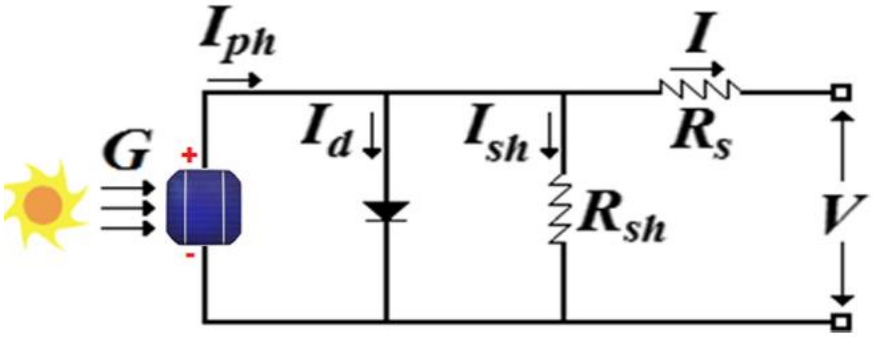

Figure 48 : Electrical circuit for simulation PV cell (one-diode model) [191]

Boutana et al, propose an explicit model to describe the behavior of PV modules which is based on a simple mathematical equation relating the current to the voltage (I-V). The model requires the estimation of ,open circuit voltage, short circuit current (I_{SC}) and a shape parameter(S). The model validation has been performed through experimental measurements for four different PV modules technologies (mono-si, multi-si, CIS,CdTe) at two different locations. The model is described by the following equations[192]:

$$I = I_{SC}\ (1 - \left(\frac{V}{V_{OC}}\right)^{S}) \qquad (2\text{-}32)$$

Gupta et al. created a model to simulate PV performance under varying real time climatic conditions: irradiation level, wind speed, temperature, humidity level and dust accumulation. Particularly, two electrical equivalent circuit are used, a single diode and double diode model. The simulation based on real time climatic models. The results show that the solar irradiation and dust accumulation have the most advantageous and disadvantageous effect on the output of PV power [193].

Faba et al. propose an one-diode model with five parameters for simulation the photovoltaic device. The purpose of this model is investigation of photovoltaic module degradation over time. The procedure based on continuous comparison with models values. The behavior of the device starts to diverge from models' behavior when degradation of panel occurs[194].

Piliougine et al. proposed a neural network using five inputs: irradiance, temperature, angle of incidence and normalized clearness index; to generate IV curves which were compared to other models, IEC 60891 procedure and measured values. Models for the grid inverter and the generator must be provided, and their outputs must be combined. The connection between both models is related to the maximum power point of the generator and how it is tracked by the inverter. That maximum power point under specific conditions of irradiance and module temperature is determined by the I–V curve of the module, which must be simulated under those conditions. Algebraic

procedures were used to simulate the I–V curve [195].

As a conclusion performance analysis which is based on simulation is able to provide information in relation with the effect of different factors on PV performance. However, these conclusions do not refer to actual conditions and grid-connected operation.

2.6 Off-grid I-V measurements

Many researchers studied the performance of PV systems conducting off-grid measurements under outdoor conditions. These measurements in most cases concern I-V, P-V curves. Furthermore , there are off-grid approaches that combine I-V curves with PR computation. This category of analysis is a comparative analysis between different technologies to study the effects of dust or other environmental factors. This section presents studies which belong to this category.

Gaglia et al. conducted off-grid measurements in order to compare outdoor operating conditions with laboratory STC conditions. The experimental set-up consists of e PV system consists of two arrays, each with four multi-crystalline PV panels. The total collecting surface is 3.5 m^2 and the total power output 392Wp. The PV system is oriented to the south with a fixed inclination of 20°. The PVs' output power, voltage and current were measured with a Hewlett Packard HP44701A digital multi-meter and digitally recorded. Significant deviations have been found between laboratory an STC conditions and outdoor exposure [196]. This study gives results at real outdoor conditions. However, the array does not operate grid-connected, lacking an MPP tracker attached to the inverter.

Tahri et al, study performance analysis of thin film PV panels under long term outdoor exposure in semi-arid climate in Saida city located in Algeria. The monitoring system was set to scan electrical and meteorological parameters. The electrical parameters of the PV modules were obtained by I-V curves using a system based on capacitor load. The analysis based on calculation of effective power according to equations below:

$$P_M^* = \frac{G P_{DC}}{G} T_f \tag{2-33}$$

$$T_f = \frac{1}{1 - a(T_M - T_M^*)} \tag{2-34}$$

Where P_{DC}, G and G∗ are the DC output power of the PV module, the irradiance, and irradiance at STC respectively, where Tm is the PV module temperature, Tm∗ is the module temperature at STC and a is the power temperature coefficient of the PV modules [197].

Carr et al, used I-V measurements and computation of PR in order to compare performance and degradation of five different photovoltaic technologies. The types of modules examined in this study are: crystalline silicon (c-Si), laser grooved buried contact (LGBC) c-Si, polycrystalline silicon (p-Si), triple junction amorphous silicon (3j a-Si) and copper indium diselenide (CIS). Researchers conducted indoor and outdoor tests. Indoor tests concern exposure in a solar simulator in order to measure STC characteristics , while outdoor tests include I-V measurements with the aid of MPP trackers. The parameters that are recorded in outdoor tests are module output power, both the plane of array (POA) and the horizontal global irradiance, back of module temperature, ambient temperature and wind speed. After the outdoor exposure conducted indoor tests in order to compare the results. During outdoor exposure PR in

yearly and monthly basis are calculated [198]. Although the method gives important results about the degradation of modules after a long period over a year, it is not easy to apply to grid-connected PV systems.

Bouraiou et al. created an experimental set up and carried out measurements in order to study the effect of climatic conditions on a desert environment and particularly the effect of partial shading and deposition of sand. The outdoor PV module performance evaluation is carried out in this work using the software and hardware of EKO instruments (MP-160I–V tracer). This tool is used for the field measurement of the IV characteristic curves and main characteristic parameters of an individual solar cell. Measured parameters voltage and current, incident solar irradiance and temperature using a pyranometer and a thermocouple. The evaluation of measurements was based on I-V and P-V characteristics and optical inspections [118]. This study draws results in outdoor desert and shading conditions which is the main goal of the study, however the inspected PV is a single ISOFOTON panel that does not operate in grid-connected operation with an MPP tracker and inverter as required for grid connection.

Guenounou et al. conducted off-grid measurements to compare yearly performance of four different PV modules in a coastal region of Algeria. The experimental set up consists of powerful electronic load from the PV-ENGINEERING company ''PVPM1000C40'' that allows plot and the data saving of the I–V characteristic of a PV panel, a reference solar cell for measuring solar irradiance and cell temperature, temperature sensor is available for measuring temperature at the back of the PV. The four panel technologies studied are micromorph silicon (μ-Si), monocrystalline silicon(Mono-Si), amorphous silicon (a-Si) and polycrystalline silicon (Poly-Si). The parameters of evaluation were P_{MAX}, I_{SC}, V_{OC}, FF, n, I_{MAX},V_{MAX} and are compared with datasheet values. Furthermore, is proposed calculation of PR. The experimental data when normalized to STC conditions and results showed significant deviations of STC values from measurements [199]. This study gives results for four different PV technologies in outdoor conditions in Algeria. However, the inspected PV panels do not operate grid-connected with an MPP tracker attached to the inverter. Instead, the study employs an electronic load, which is not equivalent to the MPP tracker of the grid-connected inverters.

Sanchez-Friera et al. conducted outdoor I-V measurements and IR thermography in order to study the degradation of crystalline silicon PV panels of an installation of 2 kWp after 12 years of exposure in Malaga, Spain. I–V curves were measured outdoors at the monitoring station of the Photovoltaic Laboratory of the University of Malaga, following the recommendations from the standard IEC 60904-1. The measurements conducted with commercial instruments. Digital multimeters are used to measure voltage and current , RTD Pt100 thermal sensors with appropriate thermal coupling to measure back panels surface, global irradiance is measured with a Kipp & Zonen pyranometer, calibrated. Conditions of measurements were global irradiance higher than 800 W/m^2; diffuse fraction lower than 10%, maximum fluctuation of irradiance during time of measurement lower than 1% and wind speed lower than 1 m/s. I-V curves were then fitted to a one-diode. Thus, the parameters for evaluation were values of the series (R_s) and shunt (R_{sh}), short-circuit current (I_{sc}), open-circuit, voltage (V_{oc}), fill factor (FF) and maximum power point current (I_{MPP}), voltage (V_{MPP}) and power (P_{MPP}). Furthermore, visual inspection were correlated with I-V curves results and infrared thermography. The results showed that peak power loss of the installation was 11.5% [200]. This study proposes a procedure, according to IEC standards, which gives significant results about degradation and other defects however conduction of IV

measurements in each PV panel demands break of operation of PV systems and thus results are not online with operation.

2.7 Other approaches of analysis

Another approach to evaluate PV performance at outdoor conditions is the use of contour maps of PR of PV panels in correlation with AM and clearness index. Nakada et al. analyzed the influence of clearness index and airmass on the sunlight and the outdoor PV performance. The experimental set-up consists of a 5kW c-Si and a 2kW a-Si PV system, facing due south with a tilt angle of 15.3°. The system is grid-connected through inverter. The measured values are direct-current output and output voltage, solar spectrum with the wavelength range of 350–1050 nm by a spectro-radiometer. Analysis based on contour maps of the spectral irradiance distribution and outdoor performance of the PV modules as a function of AM and Kt. Another metric which is used in analysis is APE (Average photon energy of solar radiation) and is calculated from measurements of spectral irradiance by dividing the irradiation by the integrated photon flux density, yielding the average energy per photon. Results show that PR of the a-Si PV panels increases with increasing APE, while that of the sc-Si PV panels increases with decreasing Tamb [158].

The performance analysis of a PV system may be a combination of the methods of sections above. Sharma et al, study the degradation of photovoltaic systems by the following techniques: (i) Visual inspection of the modules, (ii) Infra-red thermal imaging, (iii) I–V curve measurement of all modules and comparison with the initial measurements. The experimental set up consists of a roof top system which is located in the western Himalayan region of Himachal Pradesh (Latitude 31.49 N, Longitude 76.52 E, altitude is 875 m above mean sea level). The array consists of 10 modules of 100 Wp rating each connected in series, modules are mounted on a steel rack facing south and an inclination of 31 from the horizontal, a battery storage bank, and used to meet the load. The results led to significant conclusions, such as: some of the modules had serious defects in 2,5 years operation, the average annual degradation rate per year calculated from STC measurements before and after the outdoor exposure was found to be 0.51%, visual inspection and thermal imaging techniques were found to be quite effective for identifying hot spots, the method is an important tool to identify causes of degradation or failures of PV modules under actual outdoor conditions [136].

Further, there exist models based on infrared thermography during on–grid operation. Overheating of PV modules is an important factor that decreases system's efficiency. Aste et al. proposed the use of infrared cameras to identify systems' failure in building integrated systems in Italy. The experimental setup consists of selected PV technologies(a-si, c-si, HIT) , mounting structures characterized by a variable tilt angle and oriented with an azimuth angle of 0°. The available sensors measure irradiance on module plane and on horizontal plane, mean surface temperature, external temperature and electrical power. The DC/AC conversion is operated by a transformer-less micro-inverter with MPPT tracker. The analysis based on the evaluation of the modules performance in relation to the seasonal variation and PR calculation. The results of seasonal analysis show that c-Si and HIT PV panels is rather stable and predictable, while a-Si l presents widely variable seasonal performance. As far as PR is concerned, average annual PR is 96% for HIT technology and lower values for the c-Si (93%) and a-Si modules (91%) [173].

In that context, Kaden et al. proposed a model that assesses power loss based on the IR

images of panels. In this work, PID affected panels are investigated. The procedure except from IR imaging includes I-V measurements and EL imaging. The concept of the procedure is based on the analysis of the temperature difference ΔT_{PID}, which is the temperature difference of a PID affected PV panels and a non-affected PV panels. For the needs of the study, artificial PID damage was generated on different monocrystalline and multicrystalline silicon PV panels. In each PV panel IV measurements and EL imaging was conducted. IR imaging was conducted under irradiance levels of 500-1050W/m² . PV panels were kept in operation near the maximum power point. The measurements were accomplished by determining individual cell temperatures with thermocouples on the backside of PV panels. ΔT_{PID}, is the only input value of the procedure [201]. Estimation of power loss is described by the eq.(2-35).

$$\Delta P[\%] = \frac{\Delta P_{MAX}}{1 + \exp\left(-k\Delta P_{MAX}\Delta T_{PID}\right)\left(\frac{\Delta P_{MAX}}{\Delta P_0} - 1\right)} \quad (2\text{-}35)$$

ΔP is the power loss, ΔP_{max} the saturation power loss, ΔP_0 the power loss for $\Delta T_{PID}=0$ and k is a parameter describing the steepness of the curve. The parameter k depends on the level of irradiation as well as on the type of PV panels, i.e. mono- or multi-crystalline silicon [201].

Another analysis approach at outdoor conditions and on grid operation was applied to a PV system in Northern Italy. Micheli et al., proposed a procedure to convert the actual performance of the system to standard conditions, based on the filtering of data with respect to incidence angle and AM values, calculation of temperature coefficients and normalization of the data on STC values [202].

Herteleer et al, propose normalized efficiency and its long - term average for monitoring, system analysis and comparison of systems with different power ratings. The software used to program and interface with the sensors and meters is LabVIEW, with power and weather DC voltage, current. Three inverters are currently used from where measurements as voltage, current, power. Twelve PV modules are connected using SolarEdge 3.0 kW inverter, one standard mono-crystalline PV module, is connected to an ABB mini-inverter, twelve poly-crystalline silicon Solarex MSX-120 PV modules are connected to a Sungrow 3.0 kW inverter. In this study the equation below was proposed in order to compute the normalized efficiency:

$$n_{nmod} = \left(1 + k_1 \ln\left(\frac{G}{G_{STC}}\right) + k_2[\ln(\frac{G}{G_{STC}})]^2)\gamma_{syst}\Delta T_{STC}\left(1 + k_1 \ln\left(\frac{G}{G_{STC}}\right)\right. k_2[\ln(\frac{G}{G_{STC}})]^2) \quad (2\text{-}36)$$

Where G, G_{STC} are irradiance, ΔT_{STC} is the difference of measured temperature from the STC value, $\gamma_{syst}= \gamma_{module}+\gamma_{BOS}$ (γ_{module} is the PV panels temperature coefficient and γ_{BOS} a mathematical Balance-of-Systems (BOS) temperature coefficient). To calculate the normalised efficiency for monitoring purposes, an evaluation of the corresponding benefits and disadvantages with the chosen irradiance sensor is required. Normalized efficiency is similar to the Performance Ratio [152]. This approach of analysis is significant as it is applied in grid-connected systems and takes into account temperature effects.

Another approach involves a comparison between the measured and theoretical power [134, 153]. Malvoni et al, observed an increasing trend in the difference of measured and

theoretical power during the years, something that indicates a degradation in PV system, estimated at 1.12% per year. The PV 960 kWp system consists of 3000 monocrystalline silicon PV modules (Sunpower E19/320). PV panels are South-east oriented with an azimuth angle of10°and inclined at a tilt angle of 3°. There are solar irradiance sensors, PT100 type temperature sensors to measure the PV module temperature and the ambient temperature. A method to assess the degradation of the system is to determinate the difference between the measured output power and the theoretical output power. The theoretical model is provided by PVsyst which uses the one-diode model to describe the operating of a PV module, takes into account also the thermal behavior of the PV array that depends on the ambient temperature and the incident irradiance [134].

It becomes apparent from the above presentation that performance analysis of PV systems is discussed by many researchers in the recent literature. Most of the studies referred-to above, focus on grid-connected systems and employ PR calculations from monitoring system data to draw important conclusions for local solar potential or, in other cases, to study the dust effect. Nevertheless, this type of analysis is not employed to draw conclusions about PV performance deterioration through the years and correlation with STC conditions. On the other hand, researchers who carried out experimental off-grid test procedures, draw results about the correlation of outdoor exposure with STC conditions, while other researchers who used simulation models, draw similar results.

3 Correlation of actual efficiency with Air mass (Case Study 1)[1]

In this chapter, the effect of air mass on the efficiency of PV panels is investigated in more detail. This investigation could also cover the effect of different atmospheric conditions. In the present chapter, real-world efficiency data for photovoltaic panels and photovoltaic parks are correlated with the solar altitude angle (air mass) and environmental conditions.

$$n = \frac{P}{GA} \tag{3-1}$$

3.1 Experimental setup

3.1.1 Monitoring efficiency of a single PV panel

In the framework of a previous research work , a single PV module was tested outdoors in vertical, south-facing position, under actual insolation conditions in Volos, Greece (Lat 39.3604N, Long 22.9299E). Solar irradiation reaching the vertical panel surface was measured with a CMP 3e Kipp & Zonen pyranometer, placed in a vertical position, in the upper left corner of the PV panel. PV voltage and power output were controlled close to the maximum power point (MPP), by deploying a PID controller on NI Labview software [159].

Table 13 : Kyocera KD205GH-2P PV panel characteristics

PV Module Type	KD205GH-2P	
Cell Technology	Multicrystalline, 54 cells per module	
Performance at 1000 W/m²(Standard Test Conditions: Air Mass 1.5 , cell temp. 25 °C)		
Maximum Power	[W]	205
Maximum Power Voltage	[V]	26.6
Maximum Power Current	[A]	7.71
Open Circuit Voltage (V_{oc})	[V]	33.2
Short Circuit Current (I_{sc})	[A]	8.36
At 800 W/m²(Normal Conditions: AM 1.5, wind speed 1 m/s, ambient temp. 20 °C)		
Maximum Power	[W]	145
Maximum Power Voltage	[V]	23.5
Maximum Power Current	[A]	6.17
Open Circuit Voltage (V_{oc})	[V]	29.9
Short Circuit Current (I_{sc})	[A]	6.82
NOCT	[°C]	49
Power Tolerance	[%]	+5/-5

[1] A part of this chapter has been published as: Roumpakias, E., O. Zogou, and A. Stamatelos, Correlation of actual efficiency of photovoltaic panels with air mass. Renewable Energy, 2015. 74(0): p. 70-77.

Temperature Coefficient of V_{oc}		[V/°C]	$-1.20x10^{-1}$
Temperature Coefficient of I_{sc}		[A/°C]	$5.02x10^{-3}$
Temperature Coefficient of Max. Power		[W/°C]	$-9.43x10^{-1}$
Reduction of Efficiency (from 1000 to 200 W/m$^{2)}$		[%]	6.0
Length	[mm]	1500 (±2.5)	
Width	[mm]	990 (±2.5)	
Weight	[kg]	18.5	

3.1.2 Monitoring of a 2 MW PV installation

Another set of test data were collected from monitoring the year- round performance and efficiency of a 2MW PV installation in Argos, Southern Greece (Lat 37.6500N, Long 22.65222E). This installation comprises 558 strings of 13 PV panels, that is, a total of 3393 panels of 270 W_P and 3861 panels of 280 W_P. These strings are connected with 186 inverters SMA SMC11000TL. Three strings (of 13 PV panels each) are connected to each inverter. The technical data of the panels employed are presented in Table 14.

Table 14 : Suntech STP280-24Vd, STP270-24Vd, PV panel characteristics

PV Module Type	STP280-24Vd	STP270-24Vd
Electrical Characteristics		
Open-Circuit Voltage (V_{OC})	44.8V	44.5V
Optimum Operating Voltage (V_{MPP})	35.2V	35V
Short-Circuit Currents (I_{SC})	7.95A	7.71A
Optimum Operating Current (I_{MPP})	7.95A	7.71A
Maximun Power at STC (P_{MAX})	280Wp	270Wp
Operating Temperature	-40°C to+85°C	-40°C to+85°C
Maximun System Voltage	1000V DC	1000V DC
Power Tolerance	±3%	±3%
STC : Irradiance 1000W/m², Module Temperature 25°C, AM=1.5		
Mechanical Characteristics		
Solar Cell	Polycrystalline, 156x156mm	
No of Cells	72 (6x12)	
Dimensions	1956x992x50mm	
Weight	27Kg	
Temperature Coefficients		
Nominal Operating Cell Temperature (NOCT)		45±2°C
Temperature Coefficient of P_{MAX}		-(0.47±0.05)%/°C

Temperature Coefficient of V_{OC}	-(0.34±0.01)%/ °C
Temperature Coefficient of I_{SC}	(0.055±0.01)%/ °C

3.2 Results of efficiency measurements

3.2.1 Efficiency measurements with a single PV panel

Recordings of the variation of solar radiation measured by the pyranometer placed on the vertical, south-facing panel surface are shown in Figure 49 for several hours during the following days: 23, 24,26 of August, 1, 7, 8, 9, 13, and 16 September 2010 (that is, close to the Autumnal equinox). At midday (12:00-16:00), the incoming radiation to the vertical plane with clear sky varies between 400 and 570 W/m².

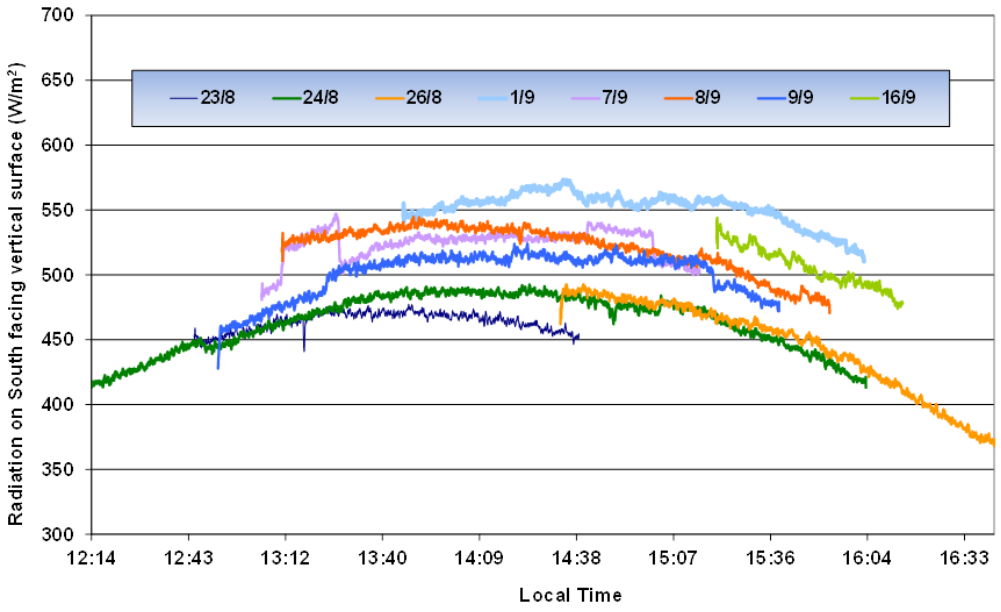

Figure 49 : Daily variation of total irradiation falling on a vertical south-facing surface during several days in August- September 2010 (Lat 39.3604, Long 22.9299E).

As regards the PV panel's efficiency, the experiments show a clear correlation with the panel temperature that is in line with the manufacturer's characteristics. On the other hand, the deterioration of panel efficiency with the drop in solar radiation seems more difficult to correlate. The above-mentioned tests indicate that sometimes the PV panel's efficiency is higher than predicted by the manufacturer's correlation with incoming solar irradiation (around noon) and sometimes is lower (late afternoon).

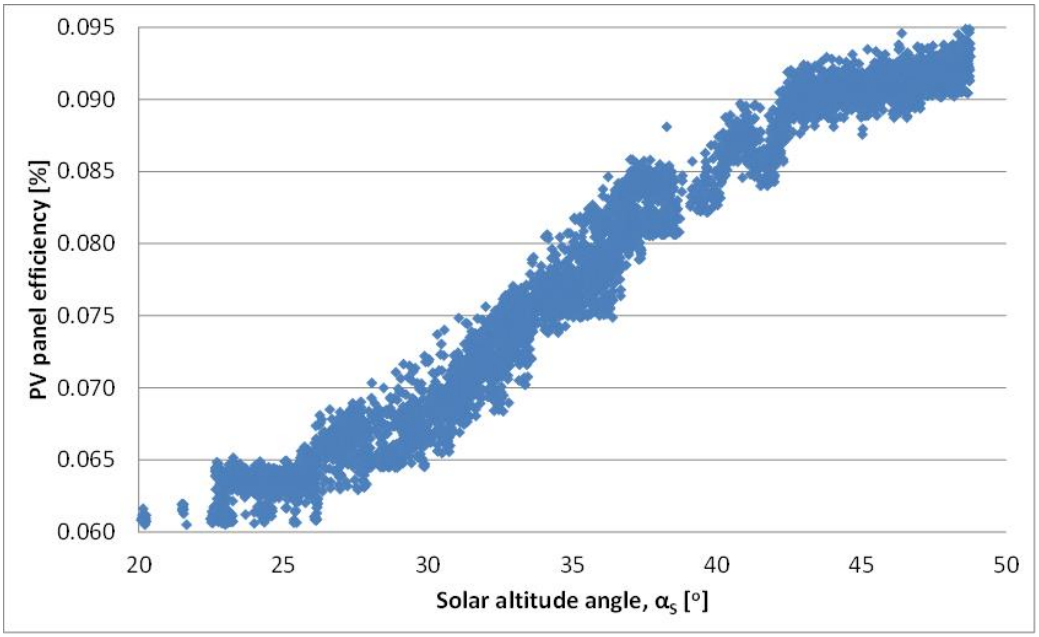

Figure 50 : Measured PV panel efficiency versus the solar altitude angle for several days of recordings in August - September 2010, Volos, Greece (Lat 39.3604N, Long 22.9299E)

A clear dependence of the panel's efficiency on solar time can be seen by a plot the measured PV panel efficiency versus the sun's altitude angle of each measurement.

Following the methodology presented in Refs.[203], we calculate the solar altitude angle, a_s using the equation:

$$\sin \alpha_S = \cos \theta_z = \cos \varphi \cos \delta \, cos\omega + \sin \varphi \sin \delta \qquad (3\text{-}2)$$

Where d is the declination angle 23.45< d < 23.45, positive declination is west of south), 4 is the latitude (39.3604N), ω is the hour angle (morning negative, afternoon positive). If we plot the measured PV panel efficiency versus the solar altitude angle, (a_s) for several days of experiments, we get the graph of Figure 50.

Although the graph is somewhat noisy, the trend is clearly observed. It seems that the difference in real air mass associated with differences in solar altitude and the aerosol present in the atmosphere, may lead to a better correlation for the efficiency drop at low incoming solar radiation levels. It should be mentioned here that the solar radiation during the morning passes through the lower layer of the troposphere above the city of Volos, and during the late afternoon it passes through the lower layer of the troposphere which is above the Volos industrial area.

3.2.2 Solar radiation and efficiency monitoring data of the 2 MWP PV installation

The results from the monitoring of the 2 MW PV park require a certain degree of processing, in order to estimate the DC power generated by the PV panels. Certain assumptions have been made in this context, regarding the efficiency of the power electronics, as well as the effect of panel temperature on efficiency [204]. The DC power generated was estimated based on the following formula:

$$P_{DC}(G,T) = P_{DCSTC} * \frac{G}{1000}(1 - a * (T - 25)) \quad (3\text{-}3)$$

where:

$P_{DC}(G,T)$: Computed DC power

P_{DCSTC} : Maximum DC power on STC

G: Measured irradiance

a: Temperature coefficient of P_{MAX}

T: Measured module temperature

At this stage, we assume that PV panel efficiency is independent from solar irradiance (or air mass).

Table 15 : Assumptions on loss coefficients for various components of the 2 MW PV park

Type of losses	respective efficiency factor
PV panels' power tolerance	0,96
AC transformer	0,97
AC cable	0,99
DC cable losses	0,99
By pass diode	0,99
Inverter	0<P<250W: n(P)=0,00032P+0.84
	0<P<1000W: n(P)=0,0000007P+0.9
	1000<P<2000W: n(P)=0,0000007P+0.966
	2000<P<4000W: n(P)=0,98
	4000<P<11000W: n(P)=0,000001P+0.982
Dust effect	0,95

The respective AC power may be calculated from the respective DC power by taking into account an additional inversion efficiency factor n, which may be estimated according to Table 15.

$$P_{AC} = \eta * P_{DC}(G,T) \quad (3\text{-}4)$$

Based on the above-mentioned calculations, the following graphs were produced presenting the theoretical performance of the specific PV park on a daily basis. On each graph, we compare the computed and measured performance, along with the irradiance variation.

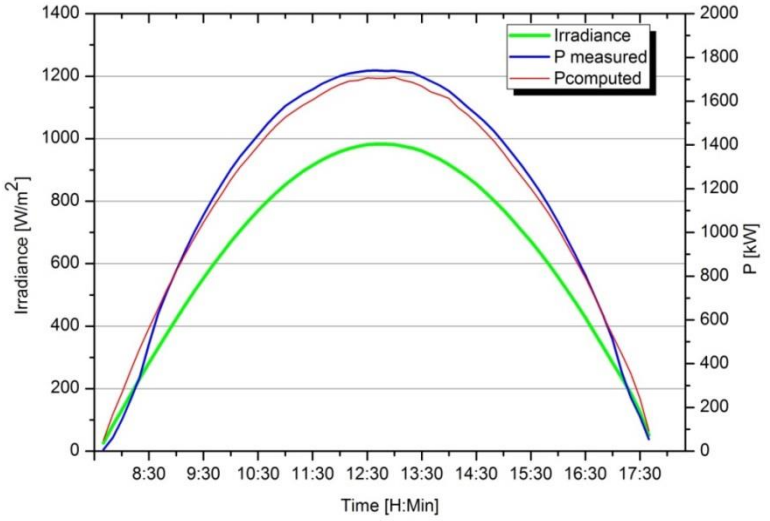

Figure 51 : Computed and measured daily performance of the PV park on February 4.

It should be mentioned here that at low insolation values, the impact of the inverter efficiency is crucial. However, inverter efficiency has been approximated as function of inverter power by means of the simplified expression of Table 15 and one should be cautious in the interpretation of the results.

A comparison between calculated (based on the measured irradiance values) and measured power produced by the park on February 4th 2010, are presented in Figure 51. February is the month with the lowest average air temperature and absolute humidity, and clear skies (outside the urban areas of course).

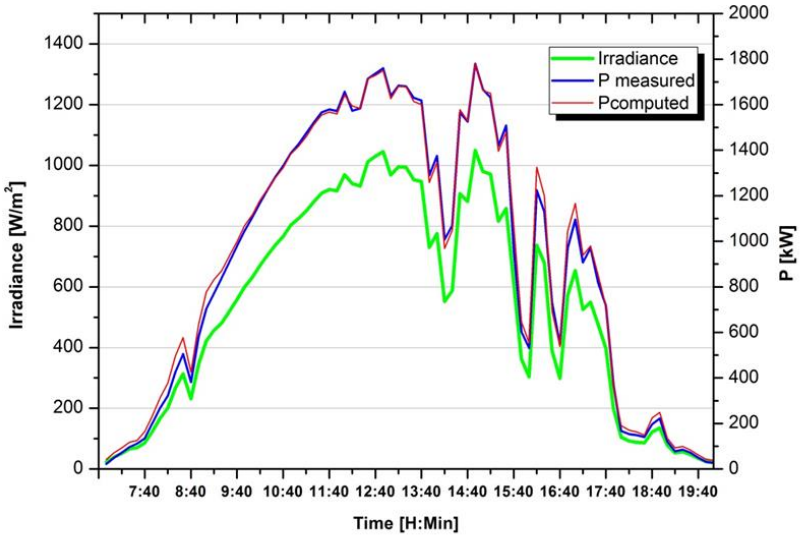

Figure 52 : Computed and measured daily performance of the PV park on May 20.

Additional graphs with comparison of calculated (based on the measured irradiance) and measured power produced by the park on characteristic days in May, August and December 2010, are presented in Figure 52 - Figure 54 respectively. Obviously, there

exist upward and downward deviations that may be attributed to the following factors:

- Irradiance measurement errors
- Power variation from MPP due to electronics
- Errors in data logging
- Other effects not included in the formulas for theoretical calculation of performance (e.g. air mass).

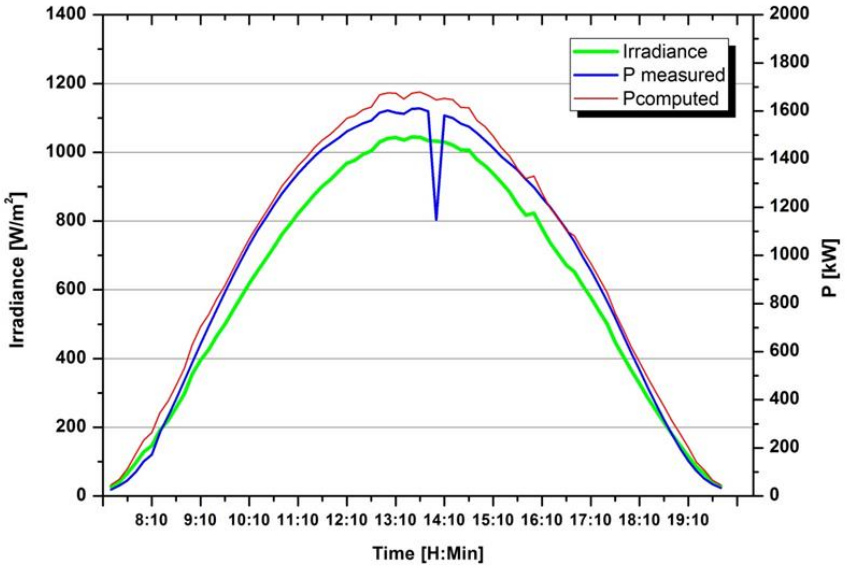

Figure 53 : Computed and measured daily performance of the PV park on August 19.

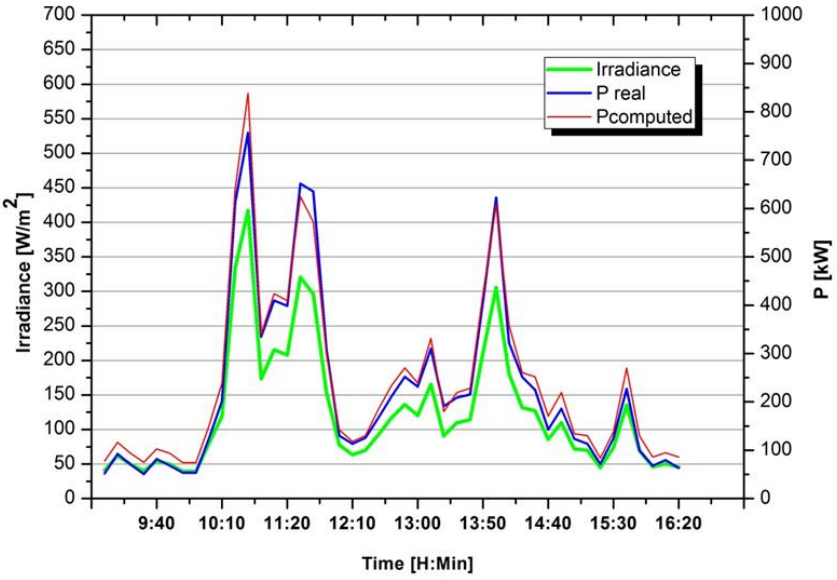

Figure 54 : Computed and measured daily performance of the PV park on December 16.

However, the most remarkable deviations between calculated and measured efficiency are observed during early morning and late afternoon Figure 51 - Figure 53. These hours are associated with high air mass and we have not yet included in our theoretical efficiency model any influence of the air mass. In order to better understand the effect of this factor, we plot in Figure 55 the PV park efficiency as function of solar altitude angle for typical clear days spanning all four seasons.

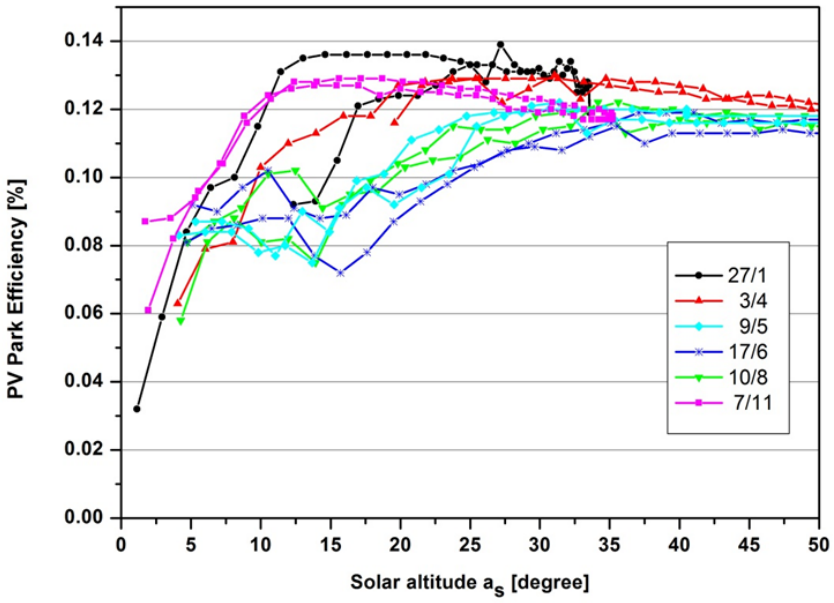

Figure 55 : PV park efficiency as function of solar altitude as for the days indicated

In this graph the PV park efficiency is seen to significantly deteriorate for solar altitude angles lower than 15 (that is, during the early morning and late afternoon hours). Less significant efficiency deterioration is observed for solar altitude angles up to 30 for specific days. These cases should be partially attributed to a lower clearness index of the atmosphere. In the following section an attempt is made to improve the modeling of PV efficiency for lower solar altitude angles and leave only the deviation that is due to a lower clearness index.

3.3 Discussion of results

During the theoretical power calculation process and its comparison with the measured power presented in the previous section, significant deviations were observed at low irradiance values.

To further understand the effect on the yearly efficiency, Figure 56 presents a comparison of the annual electricity produced by the PV park in the six solar irradiance classes selected: 10-200, 200-400, 400-600, 600-800, 800-1000, 1000-1200 W/m^2. For each class, the theoretically calculated value is also presented for comparison, as well as the total insolation falling on the panels.

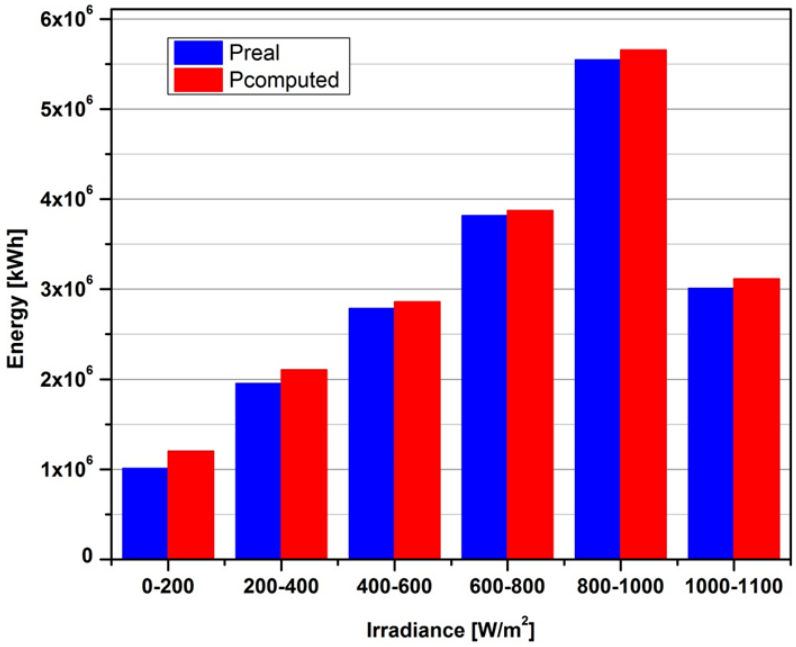

Figure 56 : Comparison of the annual electricity produced by the PV park in the six solar irradiance classes selected. For each class, the theoretically calculated value is also presented for comparison, as well as the total solar radiation falling on the panels.

It becomes apparent from Figure 56 that the most significant deviations occur in the 10-200 W/m² and 200-400 W/m² solar irradiance classes 19.1% and 7.8% respectively. Thus, the total electrical energy produced in these classes is significantly (Table 16) overestimated based on the technical data of PV performance that ignored the effect of air mass. Of course, the available measurement data do not extend to the DC part of the installation and specific assumptions had to be made regarding the power loss coefficients in the wiring and the inverter part.

Table 16 : Deviation between computed and measured energy in different irradiance classes

Irradiance Classes[W/m2]	Deviation[%]
0-200	19,1
200-400	7,8
400-600	2,7
600-800	1,5
800-1000	2,0
1000-1100	3,5

In the solar irradiance ranges exceeding 400 W/m², where Air mass is close to 1.5 the deviations between theoretical calculation and measured performance were minor. Thus, the effect of the air mass can be studied by decoupling PV park efficiency from the Air mass aided by an improved theoretical calculation model.

The correlation presented in Figure 57 is based on data from sunny days without clouds, as this can be inferred from insolation data. Theoretical and measured performance of

the PV panels is compared, as function of the solar altitude angle (in an analogous manner with the calculations presented in the context of Figure 50). In this diagram, the performance based on the measured electrical power produced (that is, including inverter and wiring losses) is displayed for comparison.

The effect of panel temperature has already been taken into account in the theoretical calculation, whereas the effects of insolation and air mass are not yet included.

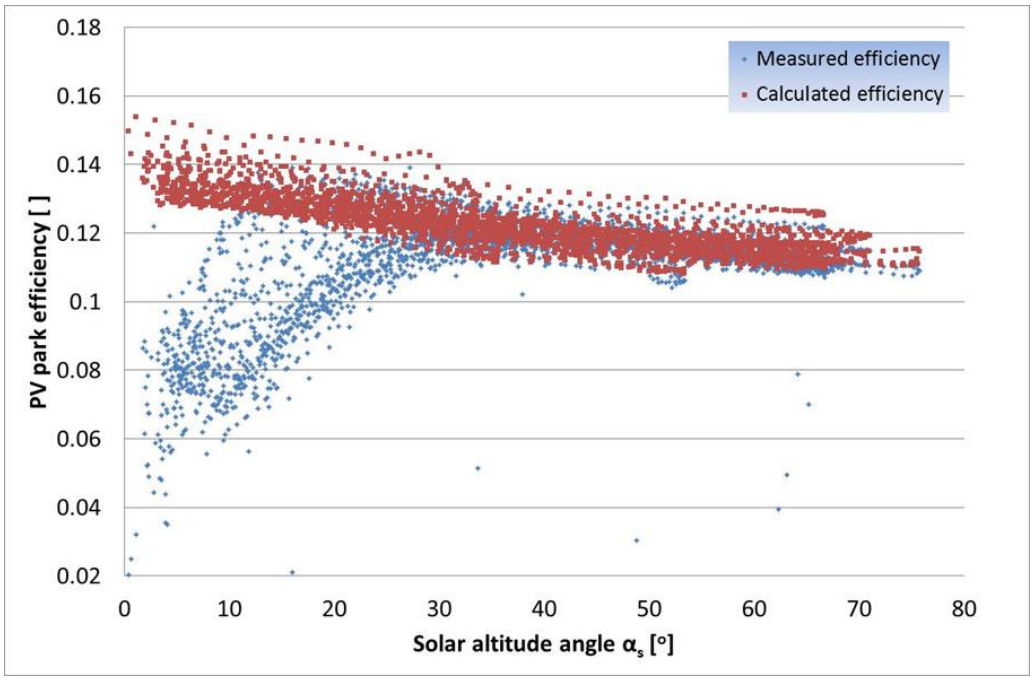

Figure 57 : Overall comparison of measured efficiency of the 2 MW PV park as function of solar altitude, with the one calculated based on the panels' technical data.

From the comparison of the calculated and measured efficiency values it can be seen that a significant overestimation of PV efficiency is done starting from 25 solar altitude and below. Moreover, the lower the solar altitude, the higher is the discrepancy between theoretical and measured efficiency. This comparison confirms the findings presented in Figure 54, as well as those of other researchers [205]. Furthermore, we observe that the PV panel temperature affects significantly electric power at high irradiance levels, which produces a negative slope in the efficiency curve at those levels. In the following section, an effort is made to further understand and model the high air mass discrepancy based on air mass calculations.

3.3.1 Detailed effect of the air mass

In this section, the effect of solar altitude and air mass on the efficiency of the panels is further investigated and an empirical model is formulated in this respect. As already mentioned, the standard Air mass of 1.5 corresponds to a solar altitude of 48°.The intensity of light traveled through the atmosphere is described by the Beer-Lambert law:

$$I(\lambda) = I_0(\lambda) * exp(-\tau(\lambda) * AM(z)) \quad (3\text{-}5)$$

where the quantity $\tau(\lambda)$ is called the characteristic optical depth of the atmosphere, AM(z) is the optical path in air measured in relative air mass and proportional to the

path traveled by light in the atmosphere, and z is the solar zenith angle.

If one focuses on Rayleigh scattering, the Rayleigh optical depth needs to be considered, which is approximated by the expression:

$$\tau(\lambda) = 0.008569/\lambda^4 \quad (3\text{-}6)$$

Where λ is in mm. This law means that shorter wavelengths are more readily scattered than longer wavelengths, i.e. blue light is scattered more than red light by gas molecules.

Modeling the atmosphere as a simple spherical shell provides a reasonable approximation of Air Mass as function of solar zenith angle and the ratio of the Earth's radius to the effective height of the atmosphere:

$$AM = \sqrt{(rcosz)^2 + 2r + 1} - rcosz \quad (3\text{-}7)$$

where the radius of the Earth R_E= 6371 km, the effective height of the atmosphere Y_{atm}≈9 km, and their ratio r = R_E/Y_{atm}≈708. That is, for the purposes of insolation calculations, the atmosphere can be considered to be effectively concentrated into around the bottom half (9 km) of the Troposphere [206].

Solar irradiance at the collector level is reduced non-linearly with increasing air mass. This dependence is further complicated due to the complex and variable atmospheric factors involved. Most high energy radiation is attenuated in the upper part of the atmosphere, that is, as we move from AM0 to AM1. For this reason, efficiency drop from AM1 to AM2 is not very significant. Furthermore significant variability is observed in atmospheric factors contributing to attenuation, e.g. water vapor, aerosol, photochemical smog. One approximate model for solar intensity versus air mass is given by:

$$I = 1.1 * I_0 * 0.7^{(AM)^{(0.678)}} \quad (3\text{-}8)$$

where solar radiation intensity external to the Earth's atmosphere I_0= 1.353 kW/m^2, and the factor of 1.1 is derived assuming that the diffuse component is 10% of the direct component. Since solar radiation is further attenuated by aerosol present in the atmosphere that can reach high concentrations in urban areas, variations of this formula exist for clean and polluted air, with respective modifications of the base and the exponent of the air mass.

In Figure 58, Air Mass is correlated to Solar Elevation, based on the above-mentioned approximation and also to solar intensity as theoretically calculated based on the expression for clear sky conditions.

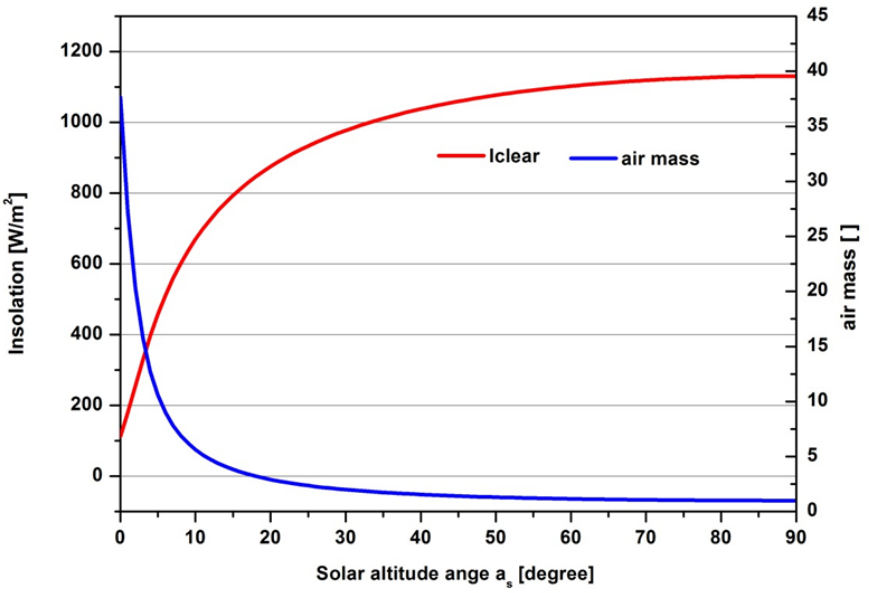

Figure 58 : Air Mass and solar intensity calculated by approximate model as function of solar altitude angle (clear sky conditions).

Obviously, the air mass increases non-linearly to very high values, when the solar altitude angle drops below 25. This observation is in line with the non-linear increase of the discrepancy between measured and calculated efficiency, when the solar altitude angle drops below 25 (see Figure 57 above). For the same day, the correlation between measured power and computed power with solar altitude is shown in Figure 59.

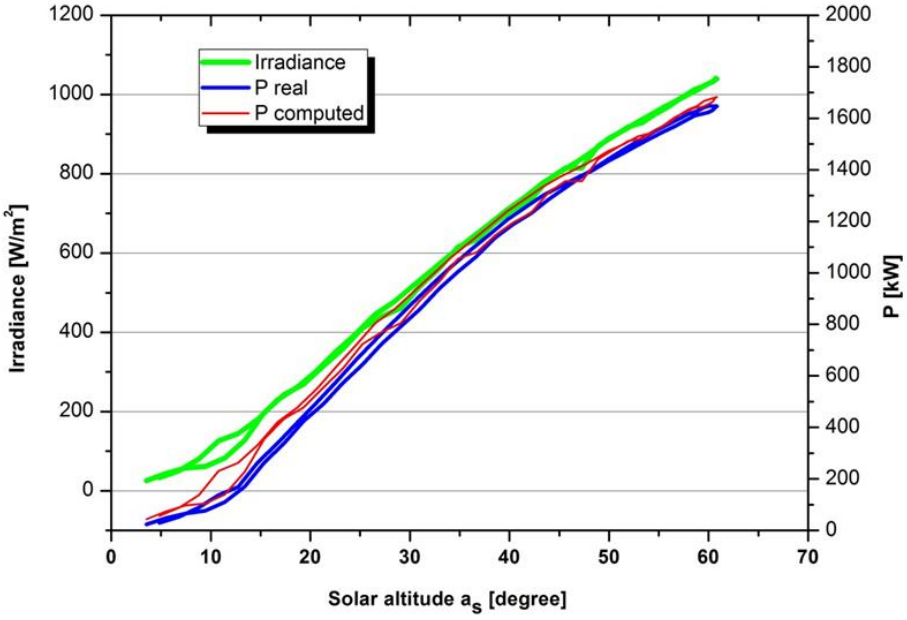

Figure 59 : Computed and measured (P real) power, irradiance versus solar altitude angle on 3 April 2011.

We can observe that when the irradiance levels lie below the line of 400W/m² the solar altitude angle is below 25. In this range, the computed power is again, significantly overestimated compared to the measured one.

The main reason for the lower PV performance in lower solar altitude angles are absorption or scattering in a particular range of solar spectrum (particular high energy wavelengths), from atmospherical aerosol and air pollution. As an example, Figure 60 (adapted from Ref. [207]) presents irradiance measurements at different hours during one clear day of May 2009 in Italy.

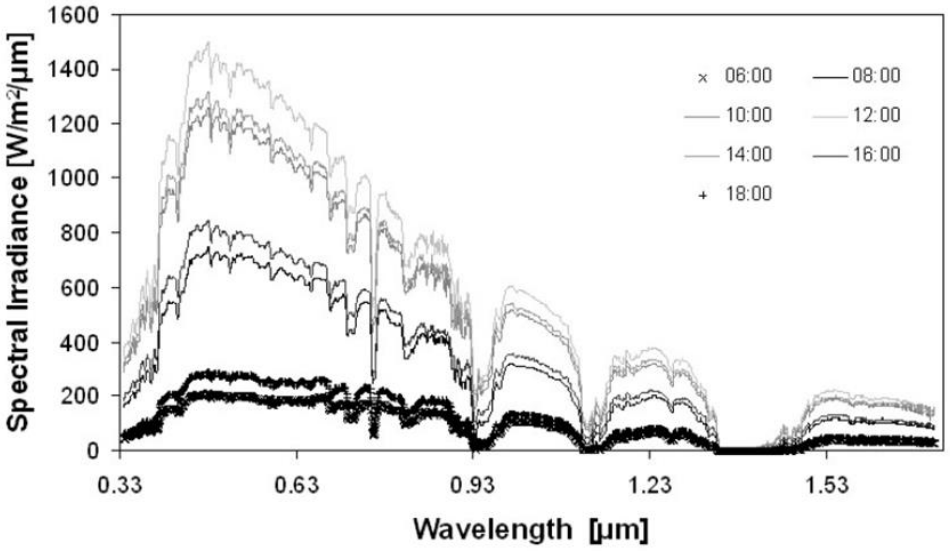

Figure 60 : Solar spectral irradiance measured at different hours on a clear day of May2009 in Italy [207]

Obviously, the attenuation in the left part of the spectrum is higher during the early morning and the late afternoon. This means that the high energy spectrum that is mainly employed by the band gap of the silicon solar cell is more severely attenuated than the average, thus leading to an apparent drop in PV panel efficiency.

These effects are further enhanced by the presence of aerosol in the troposphere in urban areas [208].

Based on the above observations, it would be interesting to model the influence of air mass on the efficiency of the module in clear sky conditions, and employ a tuning parameter to match further deviations that are due to the presence of aerosol.

As a starting point, one can model the efficiency drop due to the air mass by reducing the "effective" radiation intensity by means of the following relation:

$$I_{corr} = I_0 * Mu * exp(AM * Ex) \quad (3\text{-}9)$$

A comparison between predicted (with the additional consideration of the effect of Air Mass) and measured efficiency as function of air mass is presented in Figure 61, where the multiplier Mu is set to 0.004 and the exponent Ex is set to 0.15.

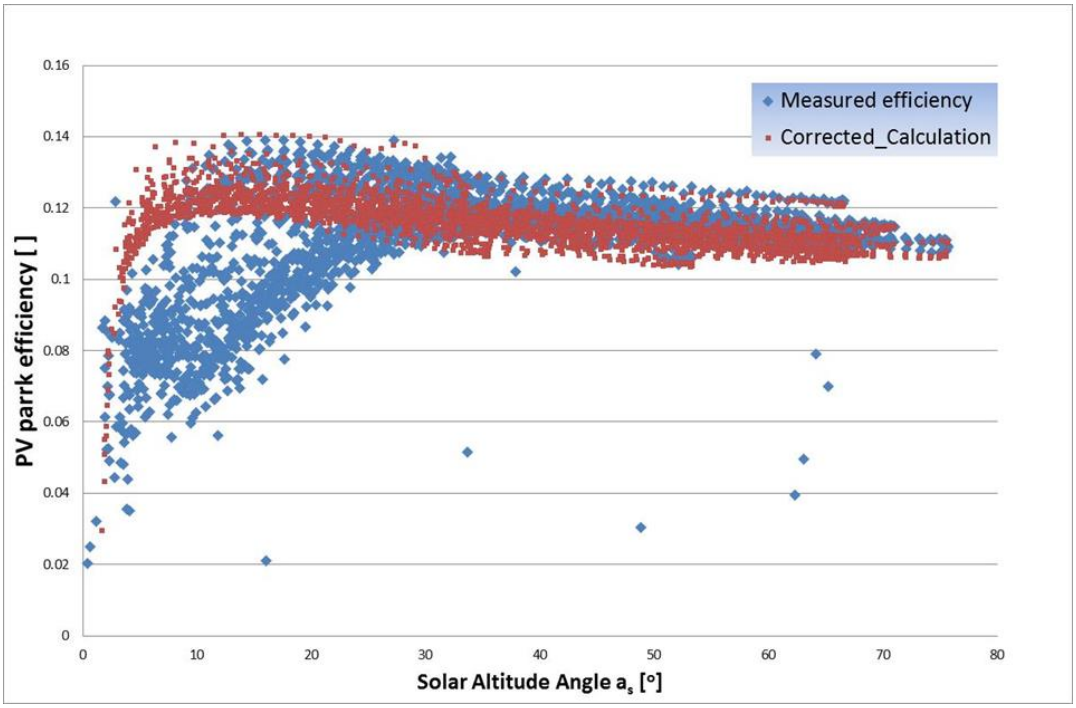

Figure 61 : A comparison with Fig. 9 shows an improved accuracy in predicting efficiency at low Solar Altitude Angles (high Air mass).

In order to check with the manufacturer's data, we take into account that the efficiency drop between 1000 and 200 W/m² insolation is stated to be 6% in Table 13 (see the respective point in the Figure, for AM=25 or solar altitude angle=10°). Obviously, there exists significant variability in efficiency drop that should be correlated to variable atmospheric conditions. This subject deserves further investigation.

3.4 Conclusions of case study

- Studies by other researchers point to the fact that PV panel efficiency drops below the values stated in the manufacturers' technical data sheets, for insolation levels below 400 W/m².
- This paper investigates the effect of the solar altitude angle on the efficiency of PV panels, based on experimental data with a single panel, as well as on data from monitoring a 2 MWp installation.
- From the analysis presented, it is concluded that there exists a non-linear reduction of efficiency in the solar irradiance range between 0 and 400 W/m2. The observed, systematic, deviations were correlated to the effect of air mass at low solar altitude angles. The remaining discrepancy could be correlated to the ambient amount of particulate matter (aerosol).
- The non-linear reduction of efficiency from the values predicted from the PV panels' manufacturer's curves results in an overestimation of the yearly electricity produced by the PV park, which was of the order of 2% for the specific installation. This percentage is by no means negligible since it affects the payback period of the installation.

4 IR Diagnostics (Case Study 2)[2]

The main objective of this chapter is to investigate optically and by IR thermography - observable faults in PV installations. A significant number of normal photographs along with the respective infrared thermographs were compiled from regions of possible faults, aiming to correlate the measured temperature field on the panel surface with optical and electrical findings. The data were extensively compared and correlated and typical results are presented here. The hot-spots that were observable at the infrared spectrum are correlated with the normal photographs of the same parts of the panels. A second objective of this work is to quantitatively assess the effect of the observed hot-spots to the electricity produced by the PV installation, as a next step towards a workable inspection methodology. Hot spots have been addressed in a number of previous studies [114], [115]. They fall into two broad categories: a) "light hot-spot" when power losses are about 4% due to a 10°C temperature difference in the cell's surface, b) "strong hot-spot" when power losses are about 10% due to a 18°C temperature difference in the cell's surface.

Measurements gathered from PV plants comprise power output data at the inverters' level and environmental data (solar irradiance, outside temperature, air velocity). However there is no way to spot defects occurring during PV operation other than those found during on-site inspections of the plants. There are a few methods that can be employed to check for damage on a panel such as electroluminescence (EL), photoluminescence (PL), IR imaging and others. Out of them, infrared thermography is the one not requiring dismounting and disconnecting of the panel from the array to be checked for defects. Through the use of IR imaging, faults and damage that are otherwise invisible to the naked eye can be seen in the form of hot-spots. The origin of hot-spots may vary and an attempt to correlate defects found during the optical and thermographic inspection of PV parks with the power output is presented in this chapter.

4.1 Experimental setup

Inspection of five PV installations was carried out. (Four PV parks of 100 kW peak power each, along with an additional roof top PV installation of 10 kW power). A FLIR Thermacam S45 camera was employed in the measurements. The camera is connected to a laptop PC by means of a firewire cable. The infrared photographs are processed by the specialized software "Thermacam Researcher"[209]. The measurements were carried out in the period from November 2014 to April 2015 in the greater area of Larissa (4 sites) and Trikala (1 site), all located in Central Greece. Measurements were carried out in a variety of meteorological conditions, comprising days with low, high and average insolation conditions.

4.2 Routine inspection procedures

A routine PV installation inspection should comprise the following 3 stages:

- Optical inspection
- Inspection by infrared thermography

[2] Parts of this chapter have been published as: E. Roumpakias, F. Bouroutzikas, A. Stamatelos (2016) On-site Inspection of PV Panels, Aided by Infrared Thermography. Advances in Applied Sciences, 2016; 1(3): 53-62

- Electrical inspection

4.2.1 Optical inspection

Optical inspection of PV installations is a useful tool that can give us a quick view of the general condition of the installation, focusing attention to possible fault regions. Significant effort has been made in the past, aiming at the compilation of an inclusive catalog of the PV system faults that are observable by optical inspection[210-212]. Moreover, specific procedures in the form of questionnaires have been compiled. One should mentioned as an example, the NREL technical report TP-5200-56154[213] which includes a detailed questionnaire for the recording of all types of problems that could be met during an optical inspection. The most usual problems observed are the following:

- Yellowing.
- Delamination.
- Bubbles.
- Cracks in the cells
- Defects in the anti-reflective coating
- Burnt cells

4.2.2 Inspection by infrared thermography, suggestions and guidelines

Inspection by use of infrared thermography is more powerful, because in the infrared spectrum one can observe certain faults that are not visible to the naked eye[114]. Infrared thermography makes visible a temperature representation of the installed panel's surface, without any need of disassembly or placement of probes. Regions of higher panel surface temperature that are readily observable at infrared (hot spots), are candidate places of faults.

The manufacturers of thermography equipment have developed technical guides for thermographic inspection, to avoid faults in the procedure that could spoil the results of the inspection[210, 213, 214]. According to these guidelines, the measurements should be made in good insolation conditions in the range of 500 – 700 W/m^2, clear sky conditions to avoid cloud shading during shooting. Measurements in calm weather conditions are required for the temperature field not to be affected by enhanced convection. The camera maybe aimed to the front or the back of the PV panel. Infrared recordings from the front of the PV panel exploit the fact that the protective glass cover has an emissivity of ε=0.85-0.90 at the wavelength range of 8-14 μm (long wave) where most of the panel's emitted power occurs. Thus the temperature field of the panel surface becomes more readable. The reflections from the sun or surrounding objects on the glass may spoil the overall infrared image. For this reason, the shooting should be done not directly perpendicular to the panel, but at 5-6° angles as shown in Figure 62. On the contrary, infrared images taken from the back of the panel take advantage of the absence of reflections, without compromising image quality, because of the fact that the tedlar polymer material of the backsheet has a high emissivity at the range of interest (ε=0.90). Shooting from the back has the disadvantage of the blocking of the view by the metallic supporting frame members, making certain parts not accessible to thermography. Due to the above reasons, shooting from the front and the back faces of the PV panel are combined, selecting the necessary viewing angles and field of view to extract useful information and avoid the problem of "false hotspots".

Figure 62: Correct viewing angles of PV panels during thermographic inspection proposed by manufacturing companies of thermographic equipment

The minimum requirements for installation and monitoring of a PV system are presented in the guideline IEC62446 [215]. This document includes a chapter devoted to thermographic inspection. Insolation conditions exceeding the 400 W/m² level are required, (ideally 600 W/m²) and steady clear sky conditions required for the temperature field to be clearly observable. Infrared shooting should be done from both sides. All PV panel arrays must be checked, with special attention to junction boxes and all electrical connections.

4.3 Electrical Inspection

Electrical inspection includes measurements with clip-on multimeters, general multimeters, PV analyzers and special equipment. Electrical inspection measurements provide an equivalent degree of performance and safety. In order to check that the PV installation works safely, it is demanded to check:

- continuity of protective earthing
- polarity of all DC cables
- insulation resistance of DC circuits

PV analyzers are able to measure the I-V curve of PV modules and string in order to compare with the I-V curve of the manufacturer's datasheet. Multimeters are able to measure the string's open circuit voltage and short circuit current. It is also useful to measure solar irradiance and panel temperature in order to compare with STC and NOCT conditions using thermal characteristics and the equations below

$$I_{SC} = I_{SC(STC)}(1 + \alpha_{isc}(T - 25)) \quad (4\text{-}1)$$

$$V_{OC} = V_{OC(STC)}(1 + \beta_{voc}(T - 25)) \quad (4\text{-}2)$$

4.4 Study of characteristic type of faults

4.4.1 Cell mismatching

An example of this type of fault can be seen in Figure 62. This photo was taken on a 2-year-old PV panel. As seen in Figure 63, some cells are very dark-colored compared to the rest of the panel's cells. Infrared thermography shows that these cells have also higher temperature than the rest of the cells. The faulty region is shown on the left of Figure 63 and the respective thermogram with the hot spot on the right. The temperature diagram produced from the processing software (bottom of Figure 64)

indicates a temperature difference of 5°C between the faulty region and the neighboring cells. The thermogram was taken from the back of the PV panel. According to the literature, the most probable cause of a hotspot is the installation of PV cells with different characteristics on the same panel [216],[217]. During the 24-month operation of the PV park to-date, no significant deterioration in the efficiency was observed. Thus, one cannot conclude if the observed difference is due to a malfunctioning of the PV panel or to an initially darker color of the cell, or even to the onset of a hot spot.

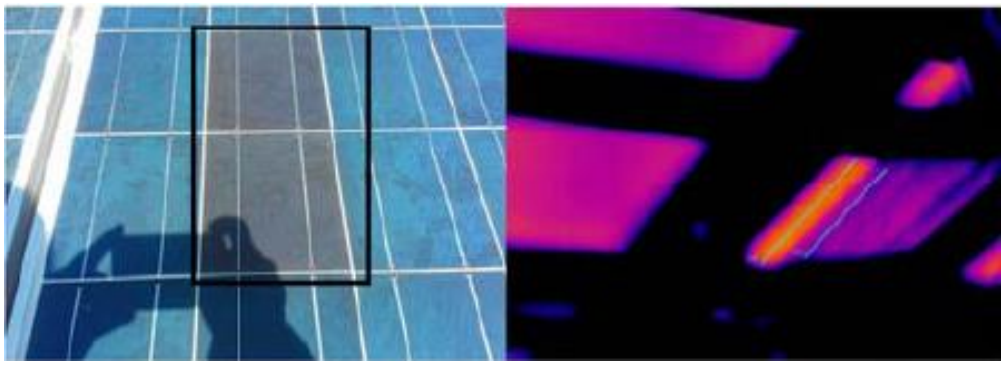

Figure 63: Normal take of a PV panel (left) and the corresponding thermography (right) taken from the back side. The cells with different color can be clearly seen and the corresponding hotspot that appears.

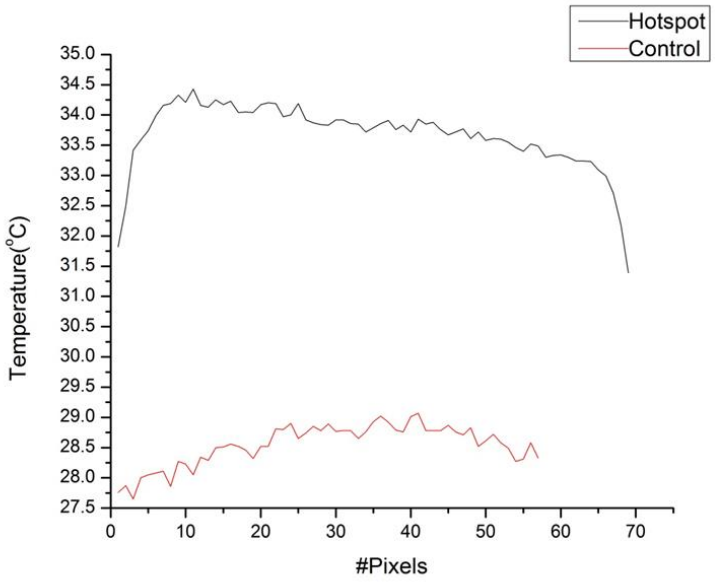

Figure 64: Temperature profiles along the two parallel, oblique lines shown on the thermogram of Figure 63 EVA membrane color discoloration (yellowing)

An observable difference in the external surface color of certain PV cells was observed in a number of panels. It should be mentioned that these are PV panels of the same manufacturer and the same age with the above-mentioned. This fault is due to the discoloration of the protective EVA (ethylene vinyl acetate) membrane, which is placed in-between the cells and the protective glass. A certain degree of discoloration (yellowing) is observed in the photo at the left of Figure 65. This yellowing of the membrane is observed in a large part of the panel's surface. According to other researchers [107, 132, 218] this phenomenon is caused by a change in the membrane's

chemical composition due to the effect of UV radiation and high temperatures. Several cells with increased temperature can be seen in the respective thermogram to the right. The temperature difference varies in the range from 4.5°C (cell #1) to 2.5°C (cells # 2, 3). The thermogram was taken from the front of the panel, because shooting from the back was hindered by the frame. It is possible that other regions exist with increased temperature. Moreover, the temperature difference could be higher than the above mentioned. This is a typical fault observed in several PV panels in this installation.

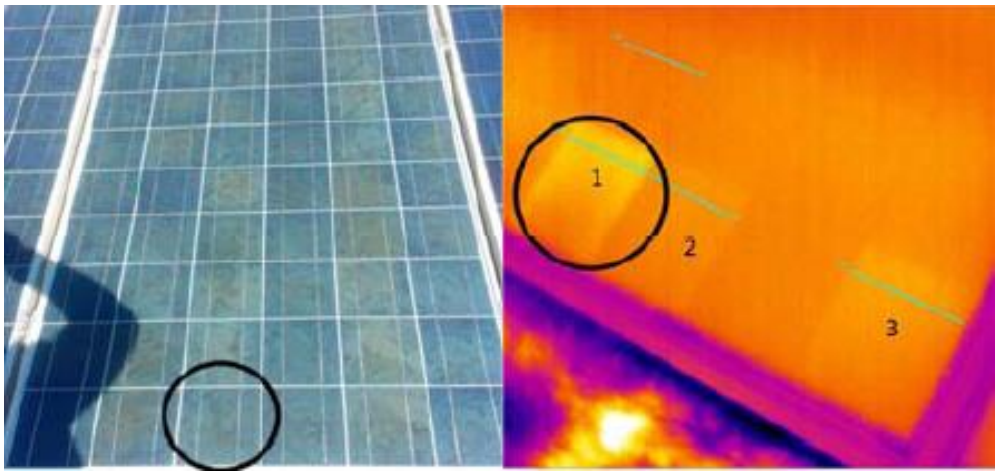

Figure 65: Normal take of a PV panel (left) and the corresponding thermography (right). The cells affected by discoloration (yellowing) can be clearly seen and the corresponding hotspots that appear.

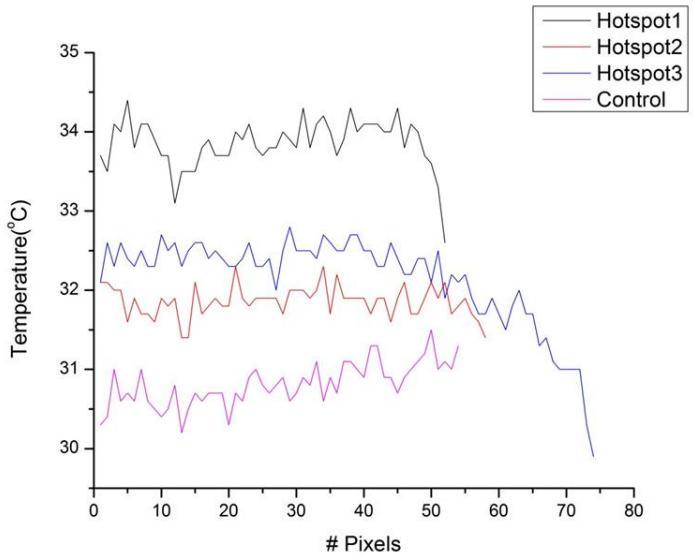

Figure 66: Temperature profiles along the six parallel lines shown on the thermogram of Figure 65

4.4.2 Mechanical damage (breakage of protective glass)

A PV panel with apparent breakage of its protective glass was spotted in the same installation. A photograph is presented in Figure 67. The protective cover has broken in two places and cracks propagated to cover most of the panel's surface. This resulted in the intrusion of humidity inside the panel structure. The results from infrared thermography revealed three hot spots with significantly higher temperature than the

neighboring cells. The temperature difference varies from 22 to 40°C (Figure 69). The image was taken from the front, in order to show a panoramic view of the panel. Closer thermograms taken from the back, revealed significantly higher temperature differences of the order of 50°C. This difference could be attributed in part to errors due to diffuse radiation from the background, during the front shootings. Moreover, the closer thermograms reveal a more detailed temperature distribution inside the cell, with regions of different temperatures in the same cell, with differences as big as 35°C. These could be due to the existence of cracks at the cell's surface, a fact that could not be confirmed due to the specific position of the panel at the highest horizontal line that was not easily accessible. The specific thermal behavior is explained in the literature [132].

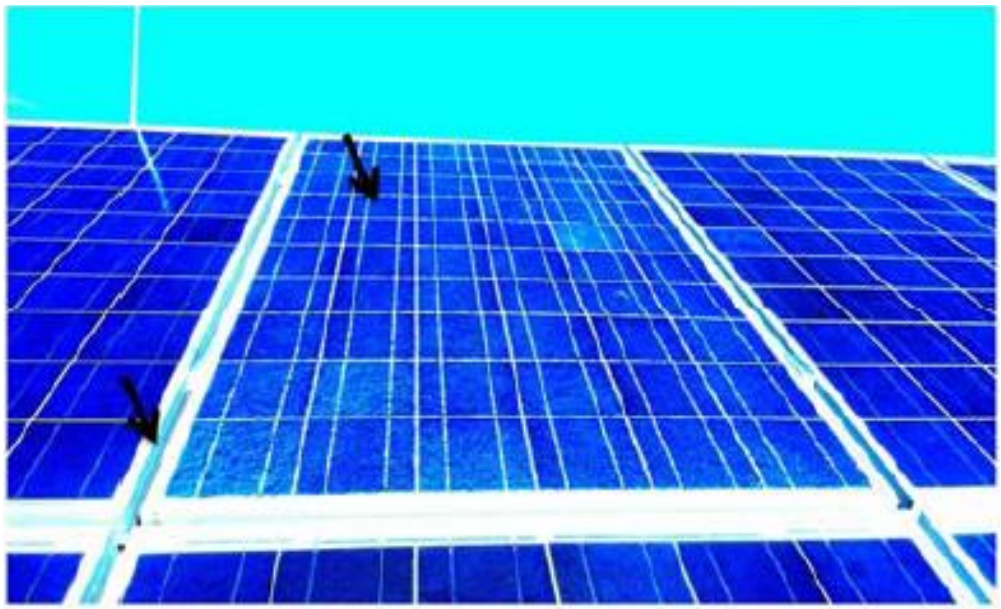

Figure 67: PV panel with mechanical damage (protective glass) in two areas highlighted by arrows.

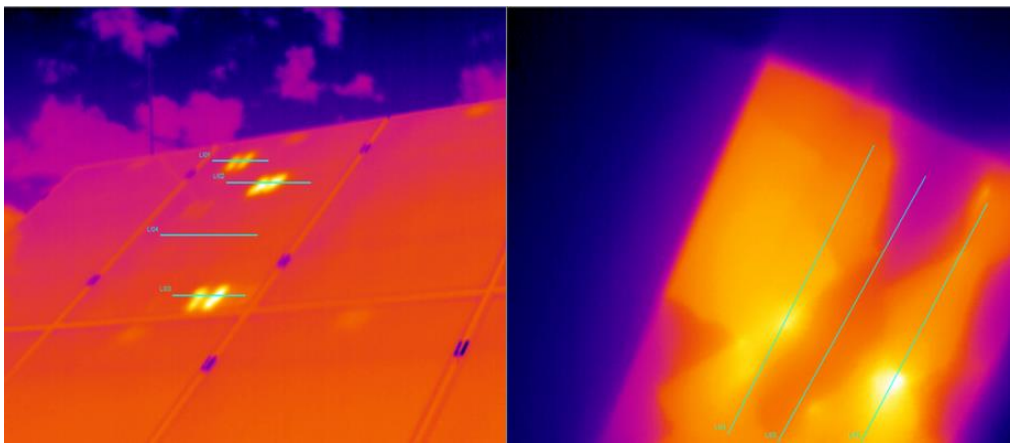

Figure 68 : Thermographic view taken from the front of the problematic PV panel with the cracked glass on the left. Close up view taken from the rear side of the same panel on the right where areas with different temperature are shown.

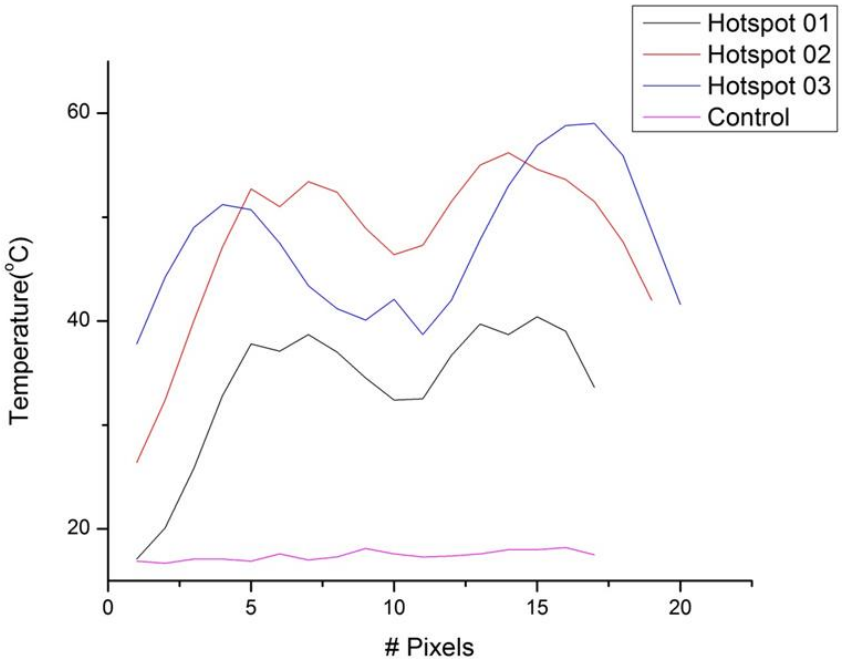

Figure 69 : Thermographic profiles of the back side of Figure 67-Figure 68

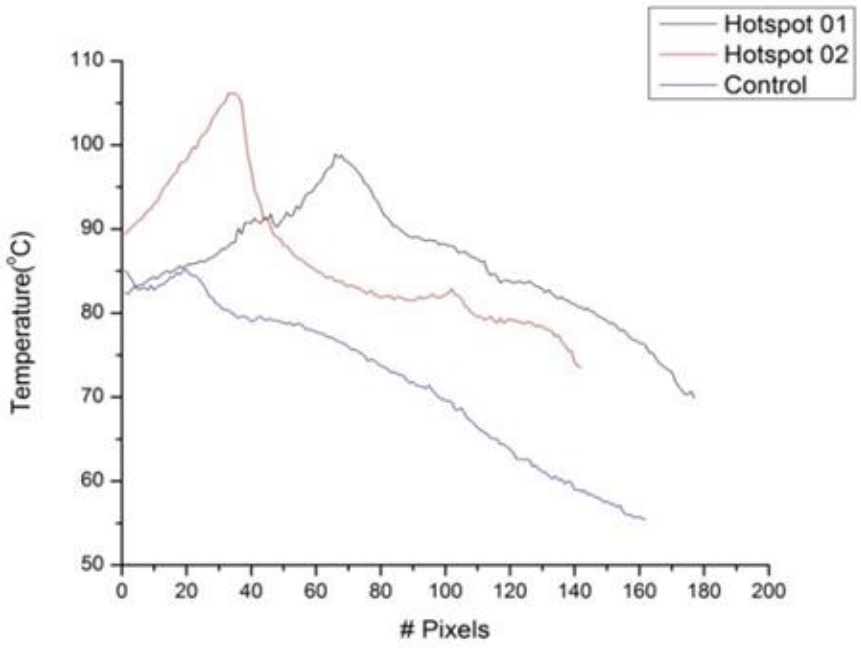

Figure 70 : Thermographic profiles of the back side of the panel of Figure 67- Figure 68

4.4.3 PID effect on PV cells

According to the findings of other researchers [116], it is possible to observe and record the phenomenon of PID by means of infrared thermography. A series of measurements were carried out in a roof-top PV installation to confirm these findings. Optical inspection of the installation did not reveal any possible faults. However, the results of

the infrared thermograms showed that a significant percentage of the installed PV panels suffered from PID. Some of the findings are observable in Figure 71. The phenomenon is especially observable with the cells that are closer to the metallic frame. The temperature difference is in the range of 3 to 4°C. Infrared thermograms were received also from the back side for confirmation. Again the processing of the thermograms indicated a temperature difference of 3°C. The same type of fault is shown in Figure 71-Figure 72.

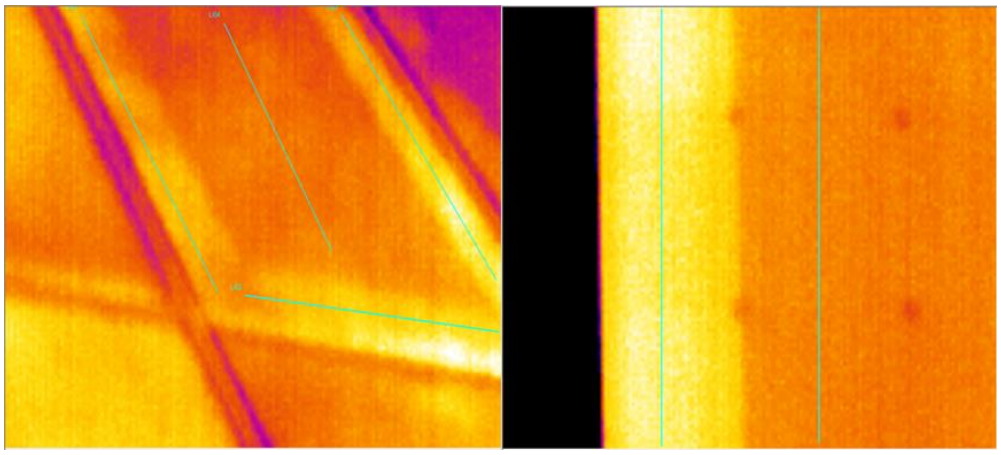

Figure 71 : Thermographs of PID affected panel. Takes from the front (left) and back side (right).

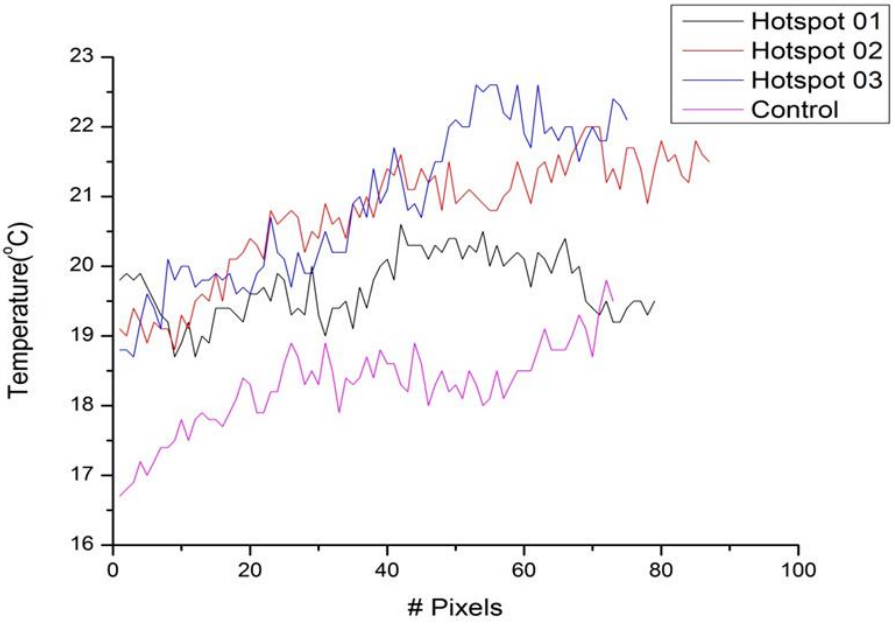

Figure 72: Temperature profiles of the front side of the PID affected panel shown on Figure 71

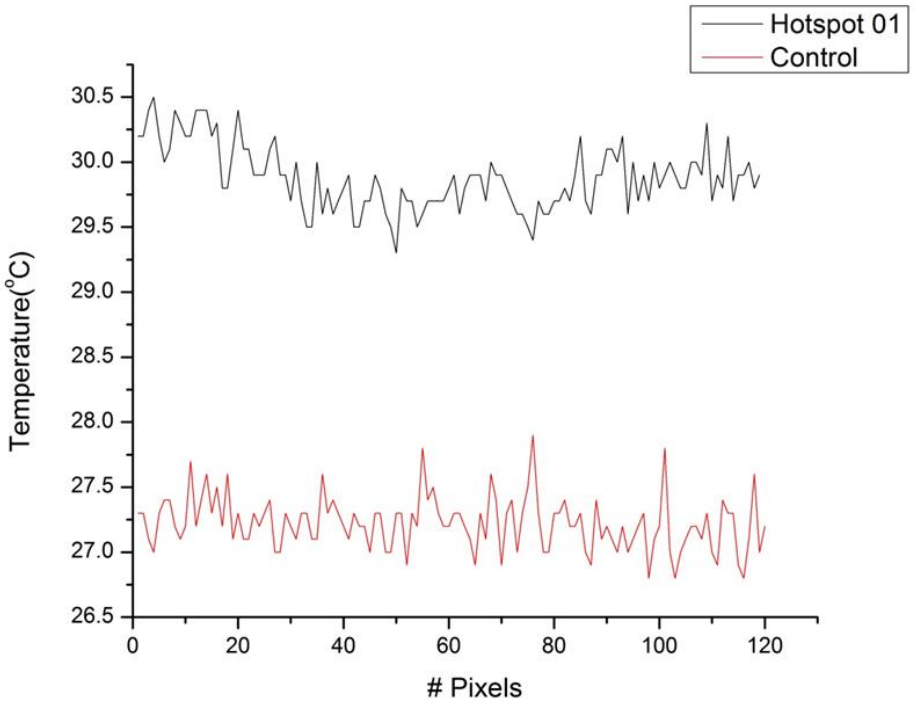

Figure 73 : Temperature profiles of the back side of the PID affected panel shown on Figure 71

4.4.4 Observable hotspots linked to no apparent optical fault

Several hot spots were found during inspection in two different PV installations, in cells with no visible faults (Figure 74, Figure 76). The temperature differences observed were of the order of 3°C (Figure 75, Figure 77, Figure 78). It is not yet confirmed if the observed hot spots point to a fault in its initial stages that is not yet visibly apparent, or if the specific type of fault is not visible to the naked eye.

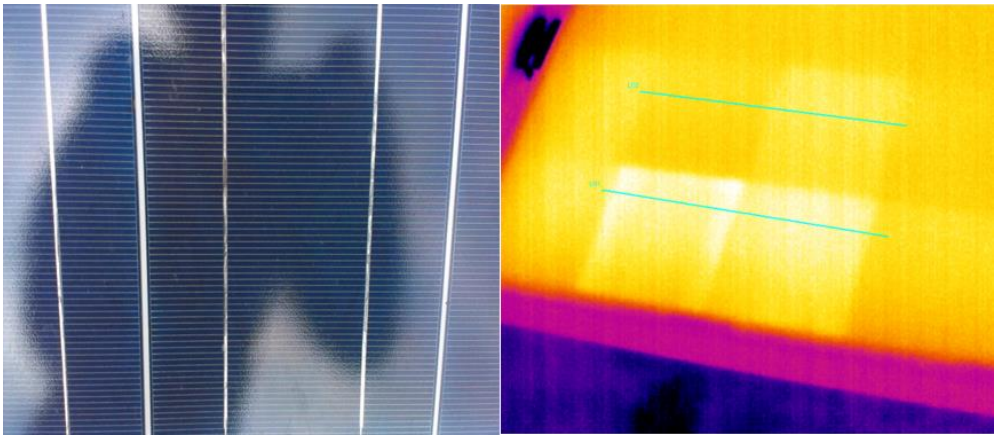

Figure 74: Hotspots appearing on a thermograph (right) of cells with no visible damage (left).

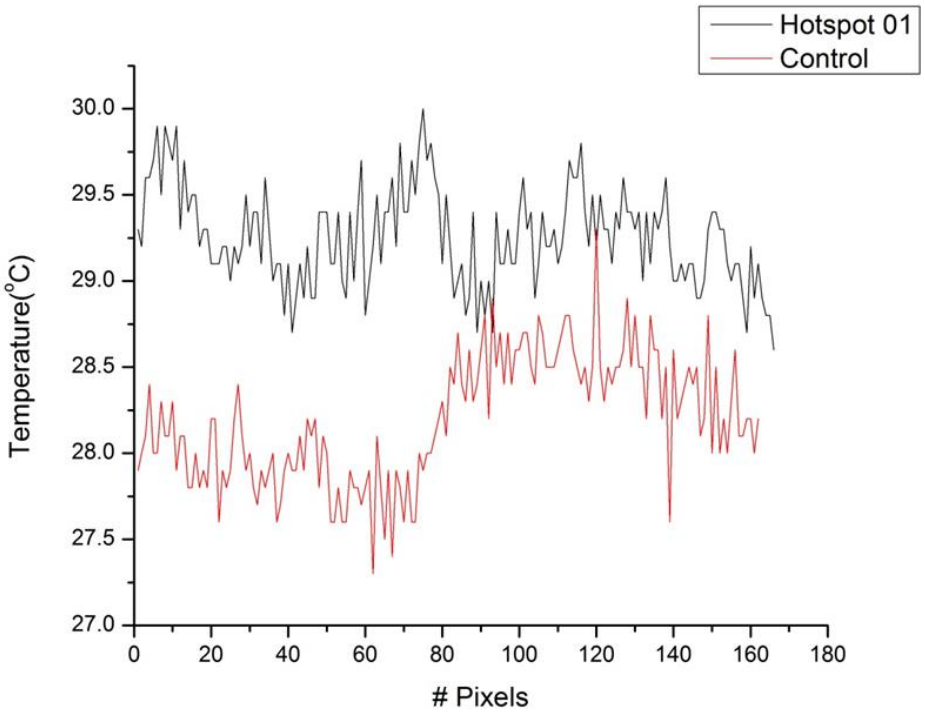

Figure 75 : Temperature profiles of the two parallel lines seen on the thermograph of Figure 74.

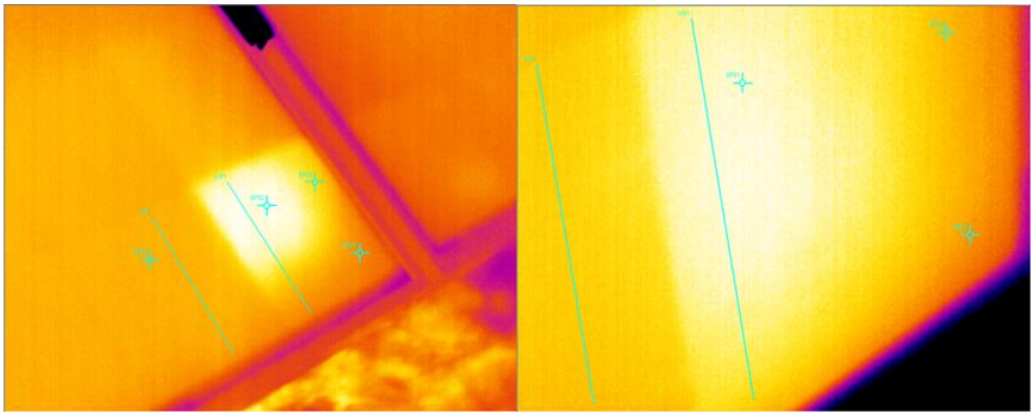

Figure 76 :Thermographs taken from the front (left) and back side (right) of a PV cell with no visible damage.

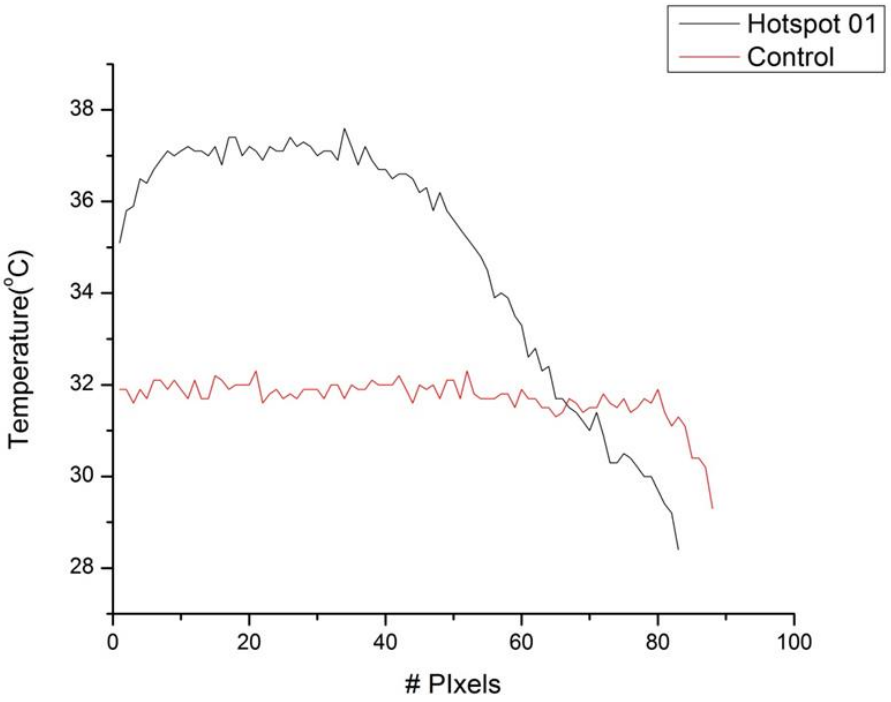

Figure 77 : Temperature profiles of the two parallel lines seen on the thermograph of Figure 76

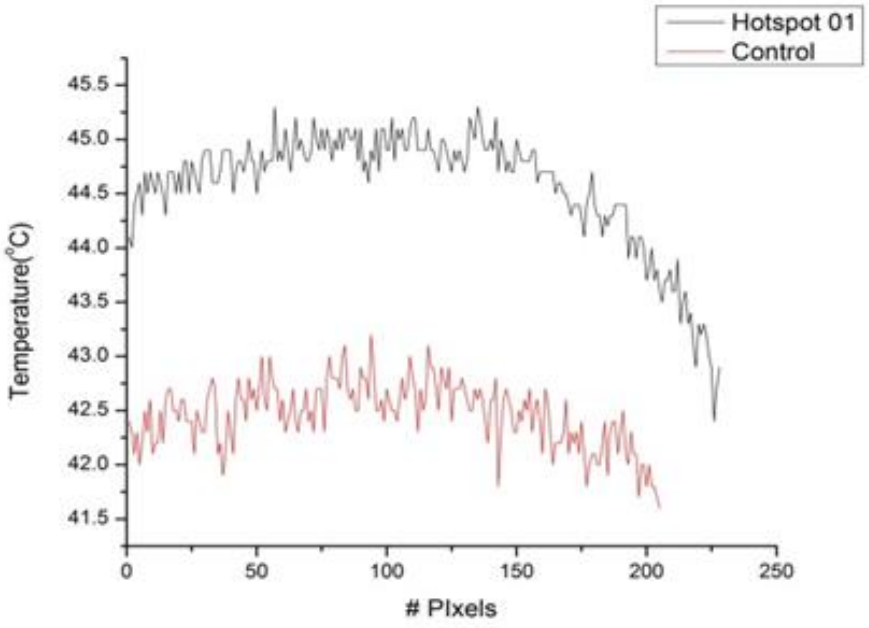

Figure 78 : Temperature profiles of the two parallel lines seen on the thermograph of Figure 76

Another case with a remarkable temperature difference without apparent optical fault is the image of Figure 79. In the specific PV panel, most of the cells have similar temperatures except for one cell that has a temperature of 80° C. However, no performance decrease is observed yet. Monitoring of this hot spot could lead to future results.

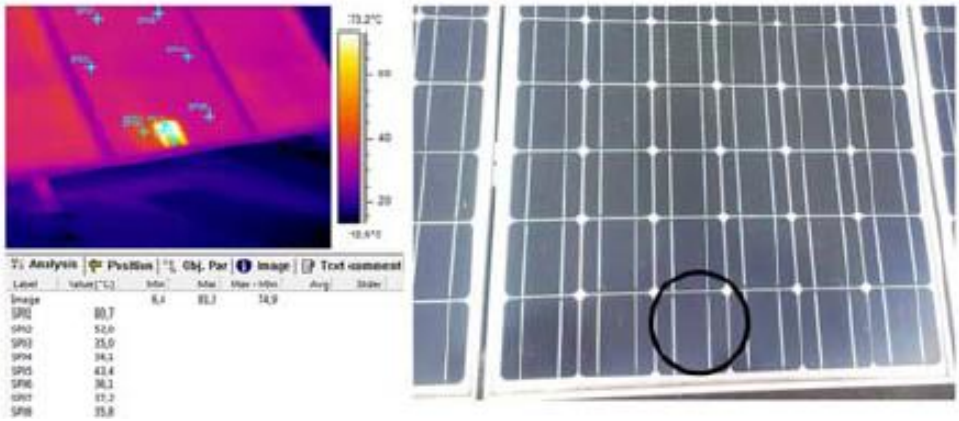

Figure 79 : IR images of PV panel that has not optical fault , however it has a cell with remarkable temperature difference.

4.5 Impact of faults on electricity generation

Monitoring data from the operation of the inverters installed on the PV park #1 (in which the faults presented in Figure 64, Figure 66, and Figure 75 were spotted) were collected and processed. The specific PV panel shown in Figure 80 is installed in the same series connected to Inv1. This specific inverter produces 5% less electric power than the rest of the inverters in this installation. This should be attributed to the faulty performance of the specific panel, because no deviation was observed in the past with these inverters. According to the above mentioned classification of hot spots, a temperature difference of 18°C may result in a 10% power loss. In the specific case, temperature differences exceed 35°C, however, the observed power losses are only 5%. This could be attributed to overproduction of the other panels in the string. Further investigation is needed. Moreover, another inverter, namely, Inv6 which is connected to PV panels shown in Figure 64, Figure 75, generates 1% less electric power compared with the rest of the inverters (apart from the above-mentioned Inv1). This slightly reduced electricity production from this series could be due to the fact that several panels from this series present a yellowing of the EVA membrane. The diagram presented in Figure 80 shows the electricity generation during the 3rd of March 2015, which was the specific day when the inspection with thermography took place. During the time interval from 11.00-13.00 where the infrared thermograms were received, it is apparent that the inverters Inv1, Inv6 produce less power. In order to confirm that this is a systematic deviation in performance, Figure 81 presents a diagram of the electricity produced during the first 10 days of March. The trend is clearly observable for all days.

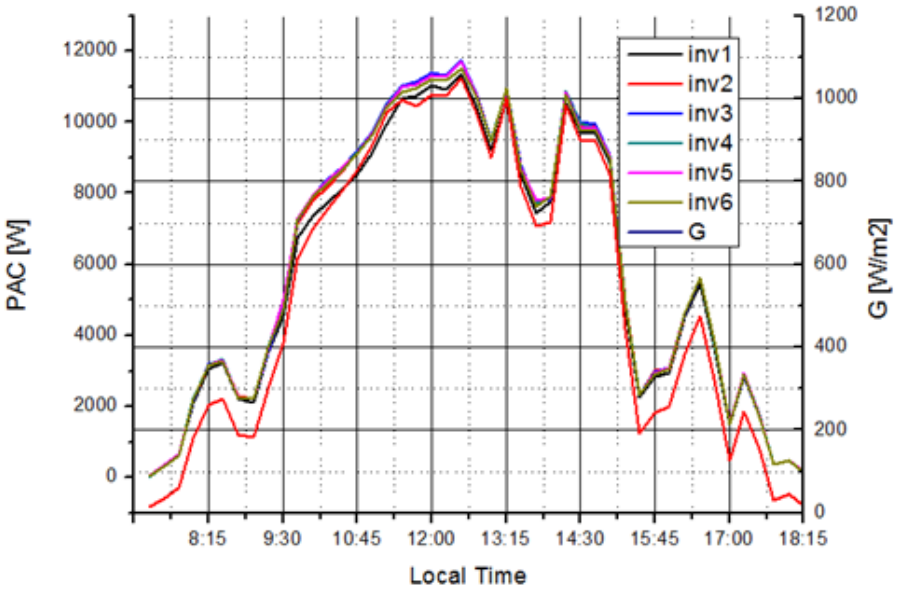

Figure 80 : Graph of daily electricity generation of a 100 kW PV plant and solar insolation on March 3rd, 2015

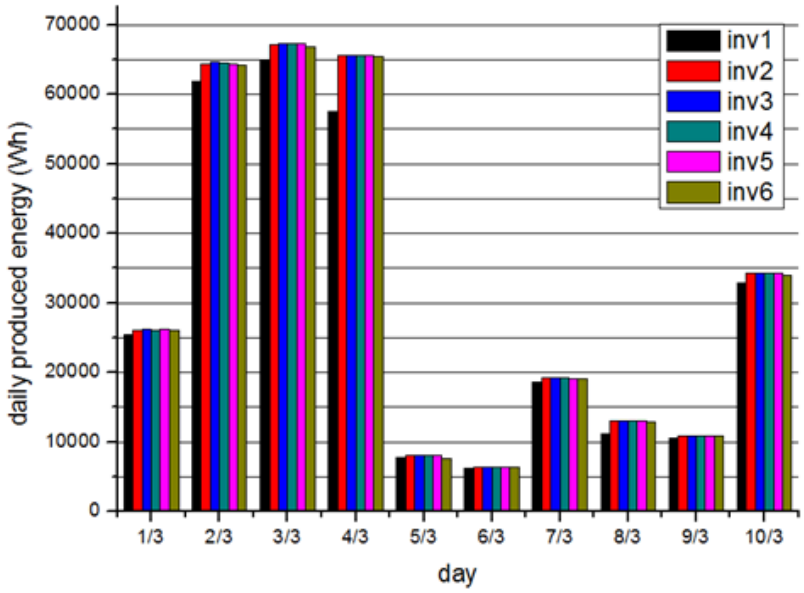

Figure 81 : Electricity generation of the same PV plant in the period from 1 to 10 March 2015.

4.6 Development of a draft diagnostics procedure

The experience gained from the carrying out of inspections, led to specific suggestions for an optimal way to schedule and carry out the respective measurements. Several standards are in preparation related to the necessary steps that should be followed during an inspection of a PV installation by infrared thermography. A "Standard for Infrared Inspection of Installed Photovoltaic (PV) Systems" was issued in 2014 by the Infraspection Institute [219]. Two additional standards are at the development stage, from the International Solar Energy Society, German Section [220] and from the International Electrotechnical Commission (IEC) [117], respectively. An optimal inspection procedure should converge on the following points:

Based on the PV panel manufacturers' suggestions, sufficient insolation conditions should prevail, between a minimum of 500 W/m^2 and an optimal level of 700 W/m^2. This was confirmed by our experience, since the faults were not observable during clouded days. Even in days with insolation close to the minimum of 500 W/m^2 several problems were met with the measurements.

- Good quality measurements were succeeded during conditions of low wind speed, where convection coefficients are lower and temperature differences more enhanced.
- The inspection must be carried out in closed circuit conditions (regular operating conditions), because the faults are only observable with electrical load.
- It is necessary to control the measurement errors whenever the measurement takes place from the PV panel's front. It should be mentioned that this type of measurement offers a panoramic view of the PV panel's surface, a fact that cannot be attained by a measurement from the back. However, front measurement induces a significant error due to the effect of diffuse radiation that should be carefully corrected by taking duplicate measurements in the respective places from the back. Measurements from different angles and different distances are very useful because their combined processing further increases resolution and the detection capability of the various faults.

This diagnostic procedure may also be employed for a pre-check of newly installed PV panels at the installation site. This is increasingly requested by several clients, because of the fact that the panels could suffer damages during shipment from the factory to the installation site.

4.7 Conclusions of the case study

- Infrared thermography supported by optical inspection was extensively applied to fault detection in 4 PV parks and 1 roof-top PV installation.
- An attempt is made to correlate observable defects on installed PV panels with hotspots appearing in IR images of the same panels.
- In most cases there is indeed a connection between observable faults and hotspots however in a few occasions such a connection cannot be made since there aren't any observable defects.
- Monitoring data from the operation of the inverters installed on one PV park were collected and processed to quantify the observable hotspots with losses in electricity production. It is found that two inverters out of six produce 5% and 1% less electric power respectively. However this is something that needs to be more extensively examined.
- The resulting experience is employed in the development of a procedure that could be routinely applied to the health monitoring of PV installations.
- This procedure may also be employed for a pre-check of newly installed PV panels on site, which is increasingly requested by the clients.

5 Methodology (Case Study 3)[3]

In this chapter, the proposed methodology for performance analysis of grid-connected PV systems in actual operating conditions is described. In contrast to the previous studies, this study aims to drawing results for PV efficiency deterioration and deviations from STC conditions, by exploiting data from the operation of grid connected PV plants. In particular, the current study focuses on a PV park's performance validation of a grid-connected 99.84 kWp PV park in Central Greece, monitored over a three year period from 2013 to 2015. This PV park presented significant variations in energy production observed from year to year. The analysis procedure has three objectives. The first is the calculation of PR, which is an important parameter for PV performance. The second is a comparative performance analysis of several of the above – mentioned models. Finally, the third objective is the application of a proposed analysis procedure to evaluate on-grid PV performance in order to explain the variations in yearly energy production and distinguish whether these variations are stemming from irradiance levels' variation or panel efficiency deterioration This has an important context in the claim of 25-years' warranties supplied by the panel manufacturers and deserves more attention in order to secure the economic results of PV parks.

5.1 Experimental setup

In this section, the available data for the PV park are presented, including location and orientation, technical data of equipment, measurement equipment and connections of the PV panels.

The specific PV park, located in Larissa (Latitude: 39.513, Longitude: 22.312), Greece, comprises 416 PV panels of 240Wp each (YL240P-29b, technical data in Table 17), connected to 8 inverters (Fronius IG Plus-150, technical data in Table 18). Four groups of 13 string series - connected panels each, are connected in parallel to each inverter (52 panels in total for each inverter, Figure 82). Photovoltaic arrays are mounted in a steady (non-tracking) mounting system with south facing orientation (surface azimuth angle γ=0°) and a tilt angle of β=30°.

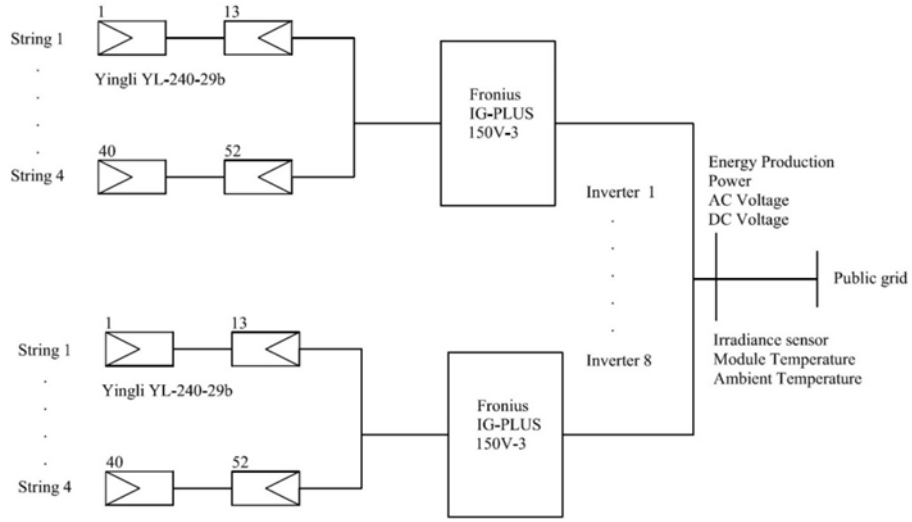

[3] This chapter has been published as: Roumpakias, E. and A. Stamatelos (2017). "Comparative performance analysis of grid-connected photovoltaic system by use of existing performance models." Energy Conversion and Management 150: 14-25.

Figure 82 : The PV park in Larissa: Basic equipment and electrical connection mode.

In order to analyze the performance of PV park, it is necessary to know of the main technical characteristics of PV panels and the inverters' efficiency data. These are presented in Table 17, Table 18 for the specific case study. An important element for the analysis procedure is the inverters' performance curve Figure 83, according to manufacturers' data.

Table 17 : Technical Data of the PV Modules

Yingli 60 cell YGE SERIES			
Module type		YL240P-29b	
		STC	NOCT
Power Output	W	240	174.3
Module efficiency	%	14.7	13.3
Voltage at P_{max}	W	29.5	26.6
Current at P_{max}	A	8.14	6.56
Open-circuit voltage	V	37.5	34.2
Short-circuit current	A	8.65	7.01
Normal operating cell temperature (NOCT)	°C	46+/-2	
Temperature coefficient of P_{max}	%/°C	-0.45	
Temperature coefficient of V_{oc}	%/°C	-0.33	
Temperature coefficient of I_{sc}	%/°C	0.06	
Temperature coefficient of V_{mpp}	%/ °C	-0.45	
Dimensions(L / W / H)	Mm	1650/990/40	
STC : 1000 W/m² irradiance , 25°C cell temperature, AM1.5 G spectrum according to EN 60904-3			
Average relative efficiency reduction of 5% at 200W/m² according to EN 60904-3			
NOCT: open-circuit module operation temperature at 800W/m² irradiance, 20°C ambient temperature, 1m/s wind speed			

Table 18 : Inverter Technical Data

Fronius IG plus 150V-3		
$P_{DC,MAX}$	W	12770
$I_{DC,MAX}$	A	55.5
$U_{DC,MIN}$	V	230
$U_{DC,START}$	V	260
$U_{DC,R}$	V	370
$U_{DC,MAX}$	V	600
$P_{AC,R}$	W	12000
$I_{AC,MAX}$	A	17.4
$U_{AC,R}$	V	3-NPE 400/230
Maximum efficiency η_{inv}	%	95.9
η_{inv} at 5% $P_{AC,R}$ (230V/370V/500V)	%	91.8/92.5/91.1
η_{inv} at 10% $P_{AC,R}$ (230V/370V/500V)	%	91.0/94.3/93.2
η_{inv} at 20% $P_{AC,R}$ (230V/370V/500V)	%	94.7/95.1/94.6
η_{inv} at 25% $P_{AC,R}$ (230V/370V/500V)	%	95.1/95.3/94.7
η_{inv} at 30% $P_{AC,R}$ (230V/370V/500V)	%	95.1/95.3/94.9
η_{inv} at 50% $P_{AC,R}$ (230V/370V/500V)	%	95.3/95.9/95.3
η_{inv} at 75% $P_{AC,R}$ (230V/370V/500V)	%	94.7/95.6/95.4
η_{inv} at 100% $P_{AC,R}$ (230V/370V/500V)	%	94.0/95.2/95.1
$P_{DC,MAX}$	W	12770
$I_{DC,MAX}$	A	55.5
$U_{DC,MIN}$	V	230
$U_{DC,START}$	V	260

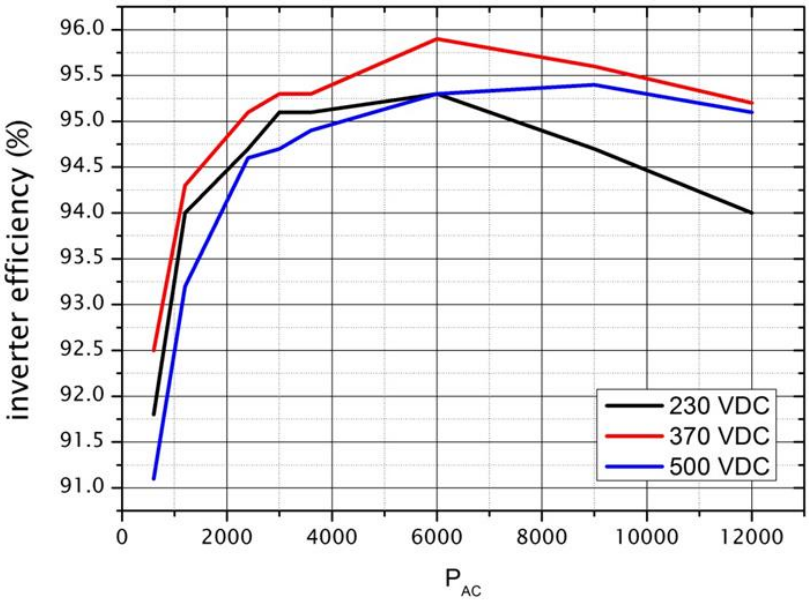

Figure 83 : Inverter performance curves at different DC voltages

Basic measurement equipment is always present in any existing PV park installation. In the specific case, there exists a thermocouple sensor whose characteristics are presented in Table 19 and an irradiance sensor, in the form of a mono-crystalline reference cell with characteristics presented in Table 20. The use of a reference cell allows better accuracy in the performance ratio evaluation than the use of pyranometers, because spectral and angular corrections are not necessary [221]. Several researchers observed faults or other performance problems using this basic equipment and the data recorded by the inverter. Yahyaoui et al. used these kind of data for fault detection and particularly, proposed a practical technique for monitoring and fault detection using data provided by the inverter and solar radiation sensor [222]. Furthermore, ElhadjSidi et al. employed this kind of data from inverters, irradiance sensors, ambient and module temperature sensors in order to analyze performance of grid-connected large scale photovoltaic system and particularly a 15 MWp system in Mauritania [165].

Table 19 : Temperature measurement equipment

Sensor	PT 100
Measuring Range	-40°C to +188°C
Accuracy	±0,8°C (in the range -40°C to +100°C)
Design	Sensor on an adhesive film for measurements on surfaces
Dimensions	32x32mm
FroniusArt.Nr.	43,0001,1190

Table 20 : Irradiance measurement equipment

Sensor	Mono-crystalline Si-sensor
Sensor voltage	75mV at 1000 W/m²
	(exact calibration voltage written on sensor)
Accuracy	±5% (average of a year)
Ambient temperature	-40°C to +85°C
Design	Sensor mounted on z-shaped aluminum profile

Dimensions	L x W x H = 55 x 55 x 10 mm
Fronius Product Nr.	43,0001,1189

Finally, measurements from sensors and inverter inlet are recorded in a data logger with a recording interval of 15 min (Table 21).

Table 21 : Main characteristics of the monitoring dataset

Recording frequency	15min
Recording period	1/1/2013 – 31/12/2015
Recorded quantities	Irradiance (W/m²) , Electric Power (W), DC Voltage (V), Ambient Temperature (°C) , Back surface Temperature (°C), AC Voltages L1,L2,L3 (V)

5.2 Analysis procedure – parameters

The performance analysis has three objectives which are described in this section. The first is the calculation of performance ratio, based on equation below which are described in 2.3, using available data from three years' operation.

$$Y_F = \frac{E}{P_{STC}} \quad \left(\frac{kWh}{kW}\right) \tag{5-1}$$

$$Y_R = \frac{H}{G_{STC}} \quad \left(\frac{kWh}{kW}\right) \tag{5-2}$$

$$PR = \frac{Y_F}{Y_R} \tag{5-3}$$

The second objective is the application of PV form model, the improved bilinear interpolation model and the Evans model which are described in section 2. Available data are used as inputs to the models in order to estimate the produced power. Particularly, all of these models use in-plane total irradiance and panels' temperature. The third objective is the formulation and testing of a proposed, improved procedure which uses irradiance, panels' temperature and data from inverter inlet, in particular AC power and DC voltage. Furthermore, this procedure takes into account the sun's position and atmospheric conditions. The procedure is described in this section.

The available datasets comprise insolation (W/m²), measured at 30° tilt angle, electric power measured at the inverter, the temperature of a typical PV panel and the DC voltage at the inverter inlet. Electric power data from each inverter are recorded, however, no significant differences exist between inverters. For this reason, it suffices to model a typical inverter in the data processing.

5.2.1 PV efficiency

$$n = \frac{P}{GA} \tag{5-4}$$

The definition of PV efficiency is defined as the ratio of power produced to the product

of irradiance times surface area [223].

The efficiency can be computed either for AC or for DC power.

5.2.2 DC power calculation

An important factor affecting PV park performance is the efficiency of the inverter. Inverter efficiency was not measured directly in the present study. Instead, available efficiency data for the specific inverter type, as supplied by the manufacturer, was used. This suffices to convert the measured AC power to DC. The inverter performance data employed in these calculations are presented in Figure 83 and Table 18, respectively. It is important to mention that the irradiance was measured by an irradiance sensor.

According to the above relationships, calculations are done for each line of the measurements' data set, with the exclusion of specific outliers in order to reduce measurement faults.

DC power is calculated from AC power based on the equation [224]:

$$P_{DC} = \frac{P_{AC}}{n_{inv}} \tag{5-5}$$

5.2.3 Temperature normalization

Another significant parameter affecting PV panel's efficiency is the operating temperature of the cell. Electrical efficiency of the cell and power output depend linearly on the operating temperature, decreasing with T_C. However, since the effect of panel temperature is not the subject of the present paper, power is normalized to 25°C (STC) panel temperature (T_C), taking into account the temperature coefficient (a) supplied by the PV panel manufacturer, as follows [205]:

$$P_{DC25} = \frac{P_{DC}}{1 + a(T_C - 25)} \tag{5-6}$$

Similarly, a normalized efficiency η_{DC25} can be computed using temperature normalized power with the aid of eq.(5-5).

5.2.4 Air mass – Clearness index

In addition to a specific panel temperature, STC conditions refer to a specific irradiance level and an Air mass of 1.5. Air mass, which is an important factor describing the atmospheric depth crossed by solar radiation, is calculated based on the time and date data recorded from the installation's data-logger and typical solar geometry equations [203]. The geographic coordinates of the PV park are additionally employed in this calculation. Clearness index, which is another important parameter characterizing optical quality of the atmosphere defined below, is also employed in the analysis procedure. Wang et al use this factor in their analysis procedure for grid-connected PV parks [225].

Air mass and Clearness index calculation is carried out as follows:

The declination angle δ is calculated from the expression:

$$\delta = 23.45\ sin[(284 + n)\frac{360}{365}] \tag{5-7}$$

The equation of time is employed to calculate time:

$$Et = 2.292(0.0075 + 0.1868cosB - 3.2077sinB \quad - 1.4615cos2B - 4.089sin2B \tag{5-8}$$

Where

$$B = (n-1)\frac{360}{365} \tag{5-9}$$

and n denotes the day of year 1≤n≤365

$$t_{SOL} = \ t_{STD} + \frac{L_{LOC} - L_{STD}}{15^{\circ}/h} + \frac{Et}{60/h} \tag{5-10}$$

where local time t_{STD} as recorded by the data-logger, geographic longitude L_{LOC} of the PV installation's location, the time-zone of the location L_{STD}, equation of time E_t, as calculated above equation (5-8) .

$$\omega = (t_{SOL} - 12)\ 15 \tag{5-11}$$

$$sin\ a_s = cos\theta_Z = cos\varphi\ cos\delta\ cos\omega + sin\varphi\ sin\delta \tag{5-12}$$

ϕ is the latitude 39.513N, ω is the hour angle, calculated based on equation (5-12).

Air mass is defined as the ratio of the mass of the atmosphere through which beam radiation passes at a specific location, day and time, to the mass it would pass through if the sun was at zenith. At sea level we define AM=1 when the sun is at zenith and AM=2 at θ_z=60°. For a zenith angle from 0 to 70° at sea level, air mass may be given to close approximation by the following expression:

$$AM = \ \frac{1}{cos\theta_z} \tag{5-13}$$

A more accurate expression for AM in different zenith angles is the following:

$$AM = \sqrt{(r\ cos\theta\ z)^2 + 2\ r + 1} - rcos\theta\ z \tag{5-14}$$

where the radius of the Earth R_E = 6371 km, the effective height of the atmosphere Y_{atm}≈ 9 km, and their ratio r = R_E / Y_{atm} ≈ 708. That is, for the purpose of insolation calculations, the atmosphere can be considered to be effectively concentrated into the bottom half (9 km) of the Troposphere[206].

Angle of incidence (AOI) is another important factor for PV efficiency. This is related to the reflection losses [195]. STC conditions in combination with irradiance 1000 W/m², AM1.5 spectrum and is implied AOI=0 [226]. AOI also affects the irradiance sensor's response. However, this effect is not examined in this study, since sensor and PV modules all have the same inclination.

$$\cos(AOI) = \cos\theta_z \cos\omega + \sin\theta_z \sin\omega \cos(\gamma_s - \gamma) \quad (5\text{-}15)$$

where irradiance G measured by the PV park monitoring system (tilt angle 30°), G_{extra} extraterrestrial radiation on the plane normal to radiation on the nth day of year, angle of incidence AOI for orientation.

Clearness index is an indicator of relative clearness of atmosphere [227] and is calculated hourly, daily or seasonally. Seasonal variations of solar irradiance can be predicted from astronomical equations. However, it is additionally affected by stochastic parameters as ground albedo, water vapor concentration, cloud optical properties and atmospheric turbidity. The effect of these stochastic parameters can be avoided with the use of the instantaneous clearness index. Calculation of clearness index is done based on the following relation:

$$Kt = \frac{G}{G_{extra}\ cosAOI} \quad (5\text{-}16)$$

where irradiance G measured by the PV park monitoring system (tilt angle 30°), G_{extra} extraterrestrial radiation on the plane normal to radiation on the nth day of year, angle of incidence AOI for orientation.

Extraterrestrial radiation on the nth day of the year is given by the equation:

$$G_{extra} = G_{SC}\ (1 + 0.033\ cos\ (\frac{360n}{365}) \quad (5\text{-}17)$$

based on the solar constant G_{SC}= 1367 W/m², and n the number of days of the year.

The computations are carried out with the available data of years 2013-2015. The results are presented in the following sections of this study, in the form of energy production, actual power and temperature - normalized efficiency. These results are compared with performance ratio results as well as with the results produced by application of other models. Computations of performance ratio are carried out and data from inverter's inlet and irradiance sensor's signal.

5.3 Results

Datasets from the monitoring of operation of a PV park for a period of three full years (2013-15), are processed and discussed in this study. This park demonstrated a significant difference in the energy produced during these three years (Figure 84). Table 6 presents the yearly energy production for 2013-2015 and the deviation from their average value. The energy production for 2015 is very close to the average value, while that for 2013 is about 7% higher and the respective for 2014 is about 7% lower than the average value. Overall, a significant decrease of 13% is observed from the first to the second year of operation. It is important to distinguish how much of this is the effect of atmospheric conditions or a decrease in efficiency, respectively.

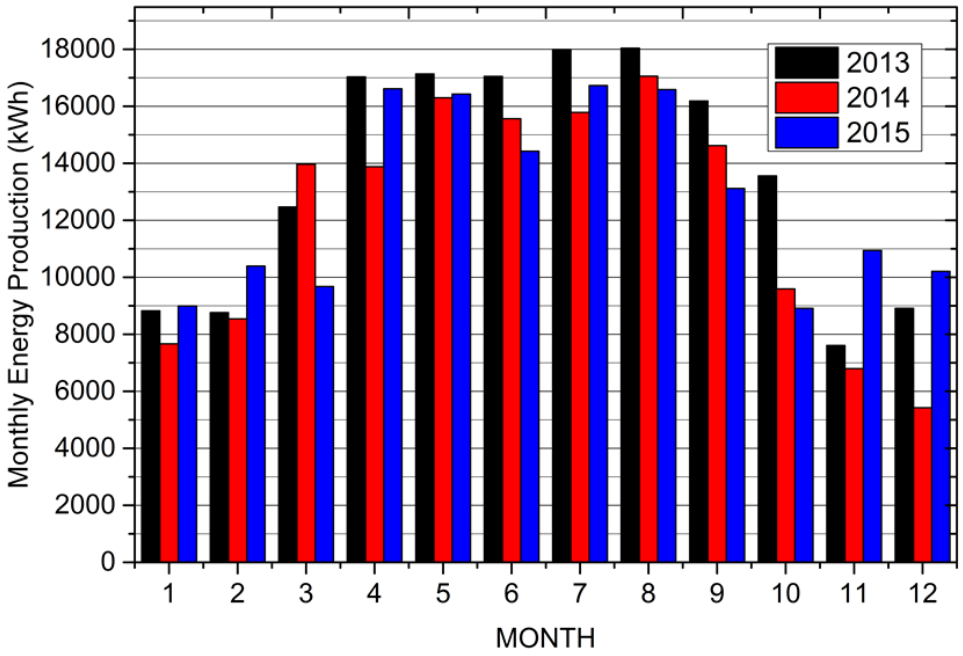

Figure 84 : Variation of monthly Energy production of the PV Park for the three year period

It was shown in Figure 82 that this PV park comprises 8 inverters with the same nominal power and with the same number of PV panels connected. For the purpose of this study, the analysis was focused to inverter 8 (Figure 85). Thus, Figure 85 and Table 22 below present the energy production to AC side for each month for the period of three years.

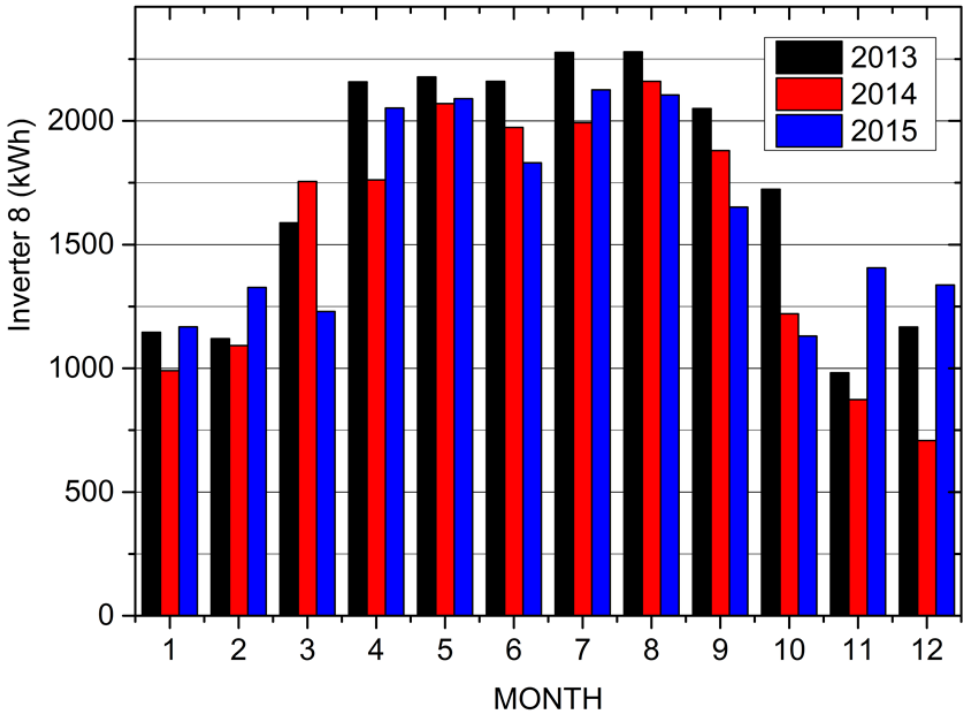

Figure 85 : Monthly Energy production of Inverter #8 for the three year period

Table 22 : Energy production and variation during the 3 - year period

Year	2013	2014	2015
Energy production (KWh)	20829	18192	19455
Energy production per Nominal power KWh/KWp/year	1669.0	1457.7	1558.9
Deviation from three years averaged production (%)	6.86	-6.67	-0.19

It is important to classify the energy production with Air mass in order to focus on the band of Air mass values that have significant effect on energy generation. From the diagram of Figure 86 it is clear that 90% of the annual production was effected with Air mass values in the range from 1 to 3. However, one should keep in mind that STC conditions (AM1.5) for which test data are available by all panels manufacturers, inherently include also spectral contribution differentiation and not only the sun's position effect, as defined by the Air Mass value.

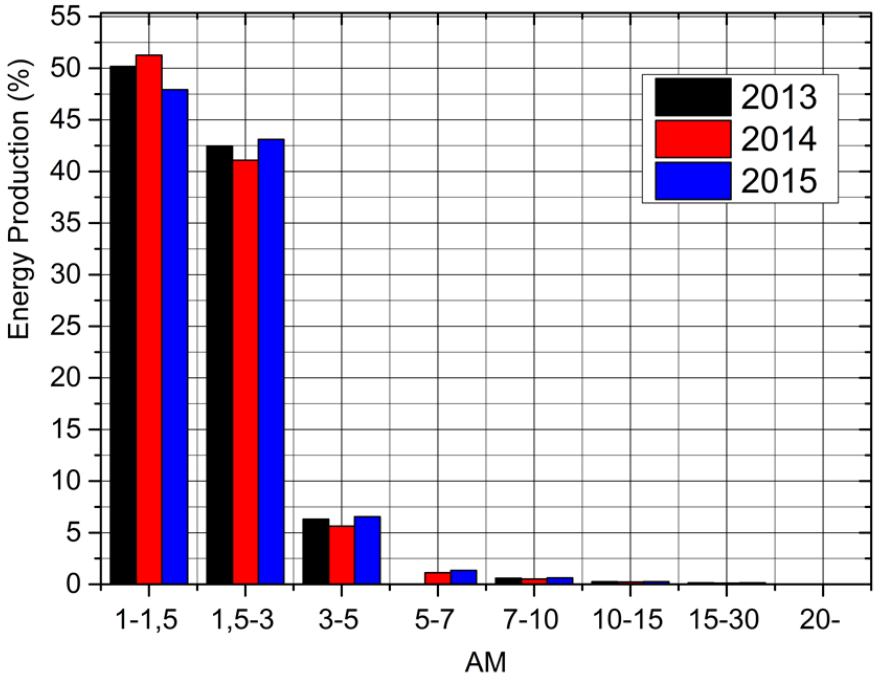

Figure 86 : Distribution of Inverter's electricity production in the various Air Mass classes

Figure 87 presents the distribution of the PV park's energy production among the various irradiance classes. Only 2% of the electricity is generated at irradiance above 1000 W/m^2.

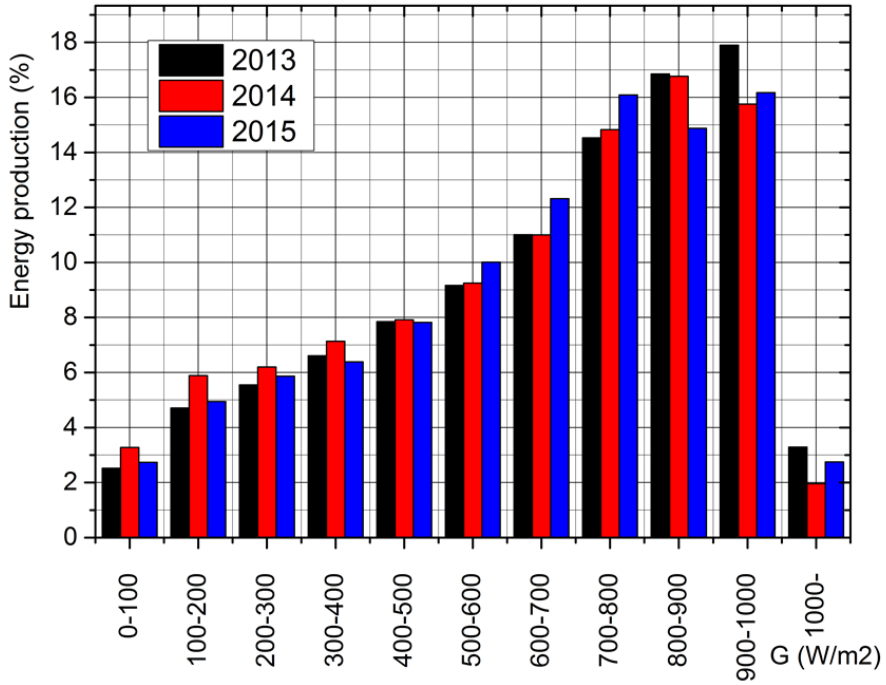

Figure 87 : Distribution of energy production in the various irradiance classes

Figure 88 presents the distribution of energy production in the various panel temperature classes. Only 6% of the electricity is produced at panels' temperatures exceeding 60°C. It is also remarkable that 10-15% of the electricity production took place at panels' temperature levels around the value of 25°C (STC conditions).

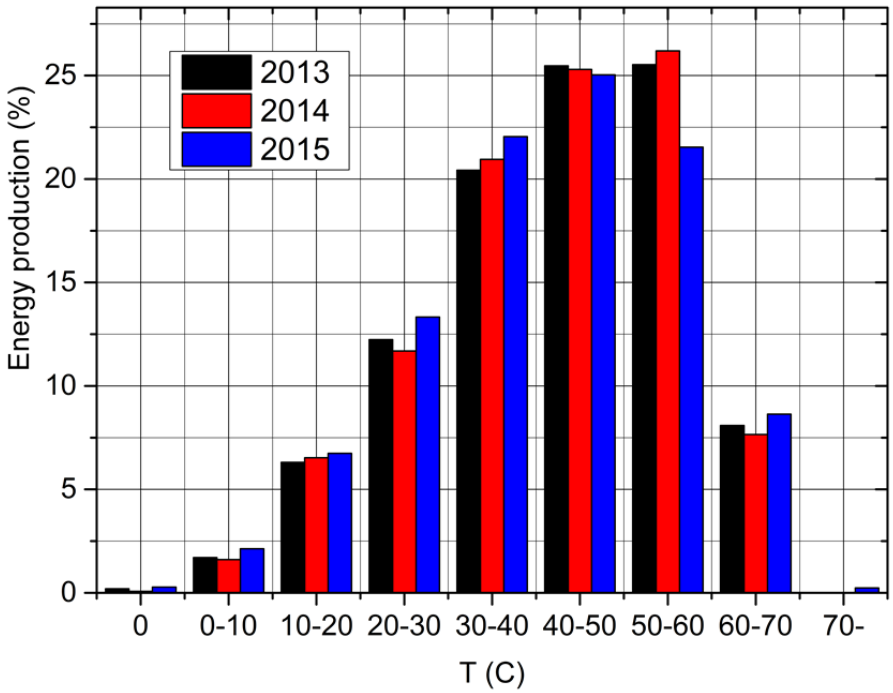

Figure 88 : Distribution of energy production in the various panel temperature classes

Figure 86 - Figure 88 show the correlation of energy production with the three parameters of STC conditions (1000W/m², 25° C PV panel temperature, AM1.5 spectrum). It is clear that real world conditions have significant differences from STC

conditions. Apart from energy production, it is important to investigate also PV performance correlation with these factors, presented Figure 89. The diagram of Figure 89 shows the total efficiency of the PV park in correlation with irradiance and panel temperature. Obviously, this diagram is not able to provide clear information about PV panel efficiency because of several factors affecting it, including inverter's efficiency, panel temperatures and measurement systems' faults.

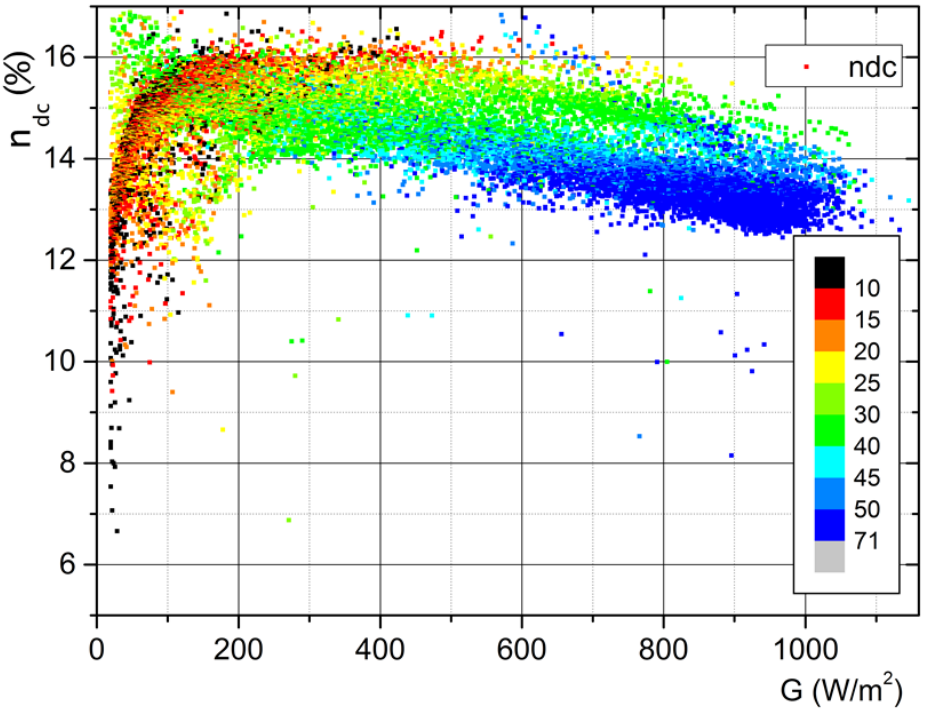

Figure 89 : Actual performance of the PV park (2013) correlated to irradiance levels and panel temperature levels during 2013.

Figure 89 shows the PV park performance which is computed from (eq. (5-4)) and is correlated with irradiance and panels' temperature. It is clear from the above diagram that the PV park's efficiency stays at acceptable levels, as the nominal efficiency at STC conditions is 14.7% according to the manufacturer's technical specifications (Table 17), however the comparison with nominal efficiency has to be conducted with normalized values. From Figure 88 and Figure 89, it becomes apparent that panel temperature plays a central role to efficiency, thus it is useful to normalize efficiency to a panel temperature of 25°C (STC conditions) in order to decouple thermal effects. It is observed in Figure 89 that real conditions are significantly different from STC conditions, except for a few points on the diagram. This fact makes the normalization and correlation with AM and clearness index mandatory.

5.4 Comparison of PV Park Performance Models

In this section, three performance models are selected for application and comparison in the specific PV park. The comparison is limited for AM < 10, based on the observation on the energy production diagram (Figure 86) that values of AM exceeding 10 have no significant impact on the production. The comparison is going to be conducted in terms of actual power and yearly energy production.

One of the models compared is the Evans model, described in the first section 2.2.

$$n(T_C, G) = n_{STC}[1 + a(T_C - T_{STC}) + k \log_{10} G] \quad (5\text{-}18)$$

This model proposes a correlation for the efficiency. Now, using a mathematical equation between efficiency and actual power (eq.(5-4)), the equation for efficiency is converted to an equation for actual power.

The second model is PV Form as described in section 2.2

$$P = \frac{G}{G_{STC}} P_{STC}[1 + a(T_C - T_{STC})] \quad (5\text{-}19)$$

For G < 125W/m²:

$$P = \frac{0.008G^2}{G_{STC}} P_{STC}[1 + a(T_C - T_{STC})] \quad (5\text{-}20)$$

The third model is an improved bilinear interpolation model as described in section 2.2 .

G > 200 W/m²:

$$P = P_{STC}\,[\frac{G}{G_{STC}}[1 + a(T_C - T_{STC})] - k\frac{G_{STC} - G}{G_{STC} - 200}] \quad (5\text{-}21)$$

G <200 W/m²:

$$P = P_{STC}\left[\frac{G}{G_{STC}}[1 + a(T_C - T_{STC})] - k[1 - \left(1 - \frac{G}{200}\right)^4]\right] \quad (5\text{-}22)$$

As far as measured power is concerned, the DC power is calculated as described in the third section 5.2.2 (equation (5-5)). It is important to observe the model's behavior at different types of days as related to the clearness of the atmosphere. First the behavior of models at actual power is presented and afterwards a comparison in terms of energy production takes place.

The following Figures present the model's behavior in terms of actual power. As a starting point, a clear sky day is selected (Figure 90). The mean and standard deviation of irradiance is 560 W/m² and 374 W/m² respectively, whereas average clearness index is 0.57. During, this day there were no significant fluctuations in cloud cover or atmospheric clearness. Evans model fits better with measured compared with the other models during all day, however models have similar behavior for irradiances below 600W/m².

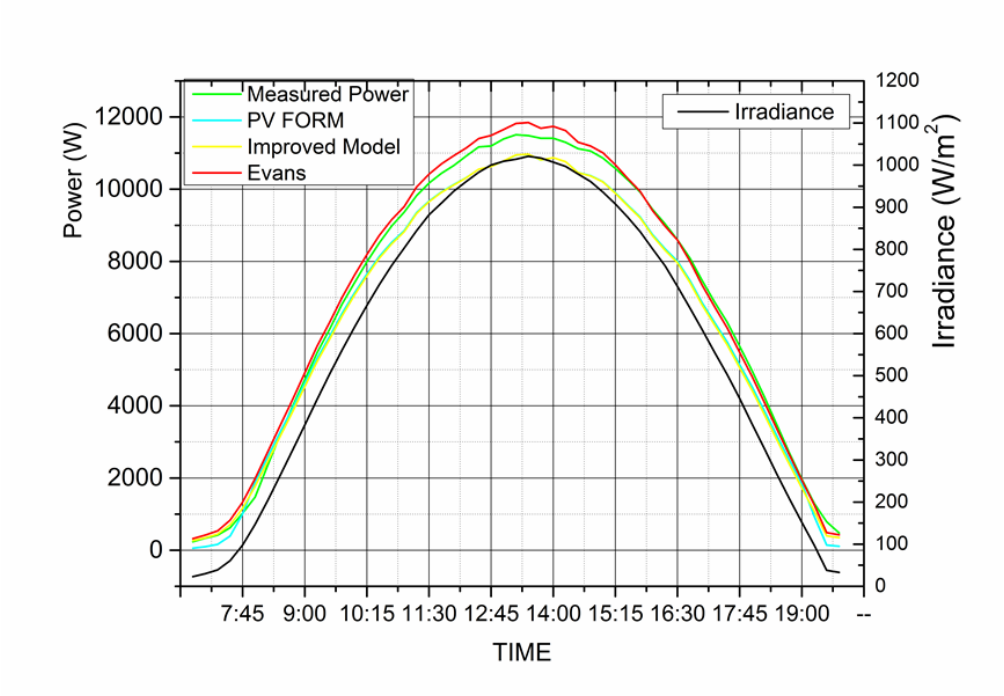

Figure 90 : Comparison of actual DC power on a day with clear sky conditions (27 May 2013).

Next, a day with significant fluctuations in atmospheric condition is selected (Figure 91). The mean and standard deviation of irradiance 374 and 281 W/m² respectively, whereas averaged clearness index is 0.34. During this day all models have similar behavior for irradiances below 600W/m², however PV form and improved bilinear interpolation model fit better during all day.

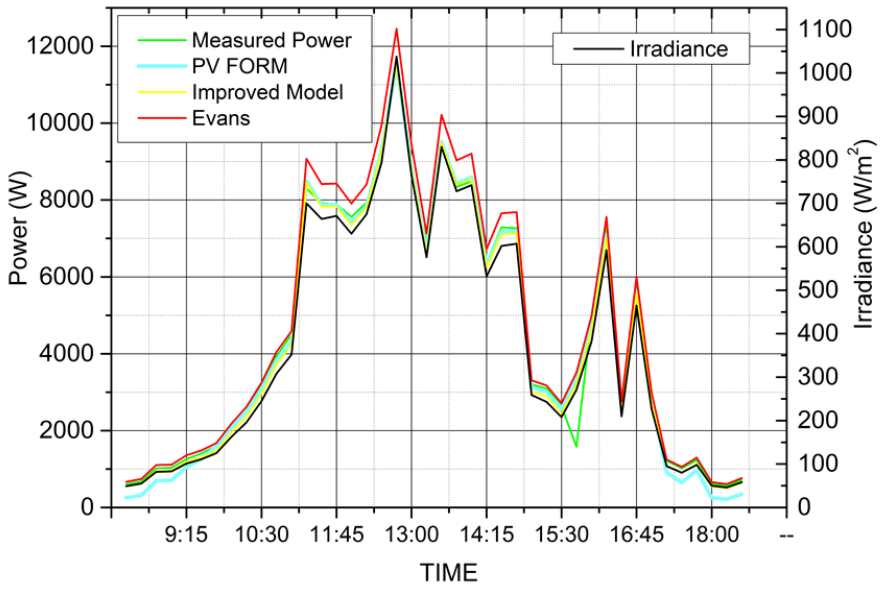

Figure 91 : Comparison of actual DC power on a day with significant irradiance fluctuations (2 October 2013).

Finally, a cloudy day is presented (Figure 92). The mean and standard deviation of irradiance is 94 and 58 W/m² respectively, whereas averaged clearness index is 0.09. During this day, there were significant fluctuations in cloud cover and low irradiance

levels. Models have relatively similar behavior during a cloudy day with an exception to irradiances between 125-200 W/m² where there is differentiation to the limits of irradiance levels which is posed by each model.

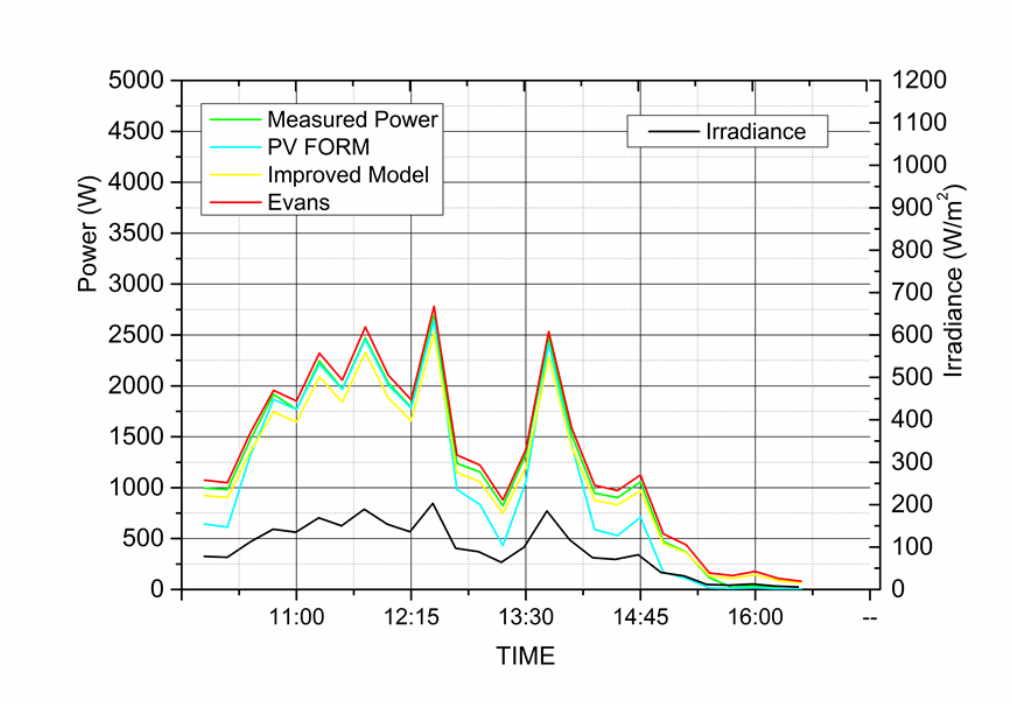

Figure 92 : Actual DC power comparison of the three models with measured power on a cloudy day (26 December 2013).

A comparison of Figure 90 - Figure 92 indicates that the Evans' model generally overestimates actual power, something that becomes also clear from the monthly energy production, Figure 93 - Figure 95. Another observation is that the PV form model and the improved bilinear interpolation model have similar behavior with exception lower irradiances levels of cloudy day as it is commented above and approximate measured performance except from irradiances over 500 W/m², something that justifies the constant difference in monthly energy production between the measured production and the one computed from these two models, as shown in Figure 93 - Figure 95.

Figure 93 - Figure 95 present monthly energy production as computed from the three models during the specific three - year period.

These Figures present the behavior of computed actual power compared to the measured one, during characteristic days of different kind, which are selected randomly. In order to quantify the differences in predictions between models, it is useful to compute the respective statistical errors in the form of the root-mean-square-error (RMSE), mean-bias-error (MBE) and (mean-absolute-error) according to the following equations [160].

$$RMSE = 100\% \cdot \frac{[\frac{1}{n}\sum_{i=1}^{n}(y_i - x_i)^2]^{1/2}}{\frac{1}{n}\sum_{i=1}^{n} x_i} \quad (5\text{-}23)$$

$$MBE = 100\% \cdot \frac{\frac{1}{n}\sum_{i=1}^{n}(y_i - x_i)}{\frac{1}{n}\sum_{i=1}^{n} x_i} \quad (5\text{-}24)$$

$$MAE = 100\% \cdot \frac{\frac{1}{n}\sum_{i=1}^{n}|y_i - x_i|}{\frac{1}{n}\sum_{i=1}^{n} x_i} \quad (5\text{-}25)$$

Where y is the modeled value and x is the measured value.

Table 23 : Statistical Parameters for Actual power computed by models

	PV Form	Improved Model	Evans Model
RMSE(%)	9.5	9.8	8.3
MBE(%)	-5.2	-5.6	2.3
MAE (%)	6.0	6.4	3.5

Table 23 presents the deviations between computed and measured values of actual power of the first year of operation. The computations concern 14386 data points in which the Air mass values were AM<5. It is clear that there exist significant deviations for all models. The main difference is that the Evans model overestimates while the other two models underestimate the actual power. Furthermore, it is important to compare the three models' predictions for the yearly energy production. These are presented in Figure 93, Figure 94, Figure 95, compared with the respective measured power.

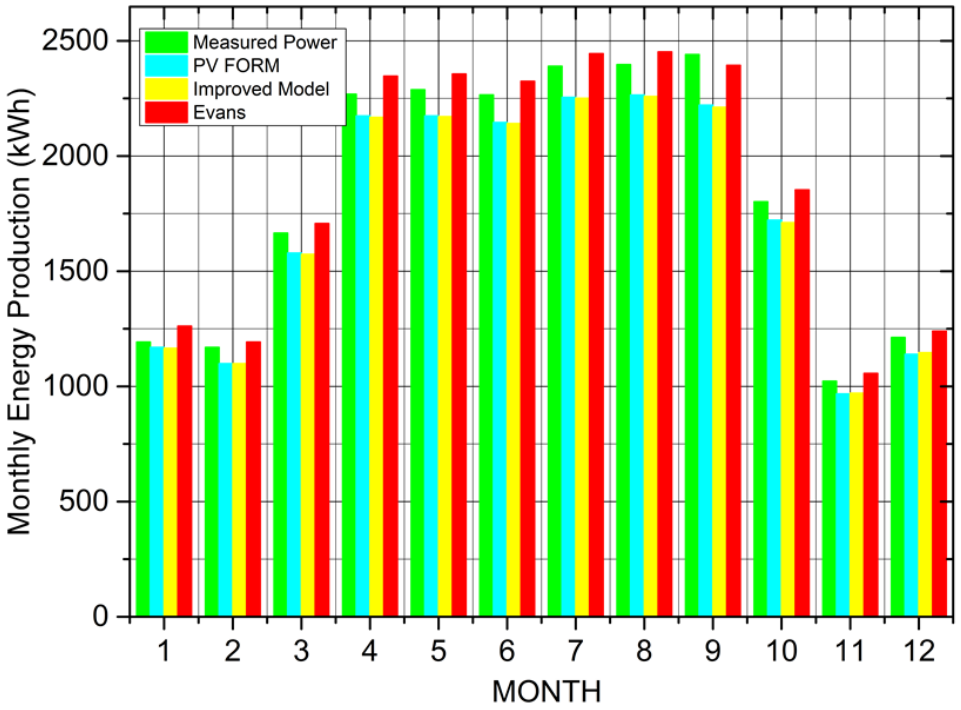

Figure 93: Monthly Energy production (DC side) computed with the three models, in comparison with the measured values for 2013.

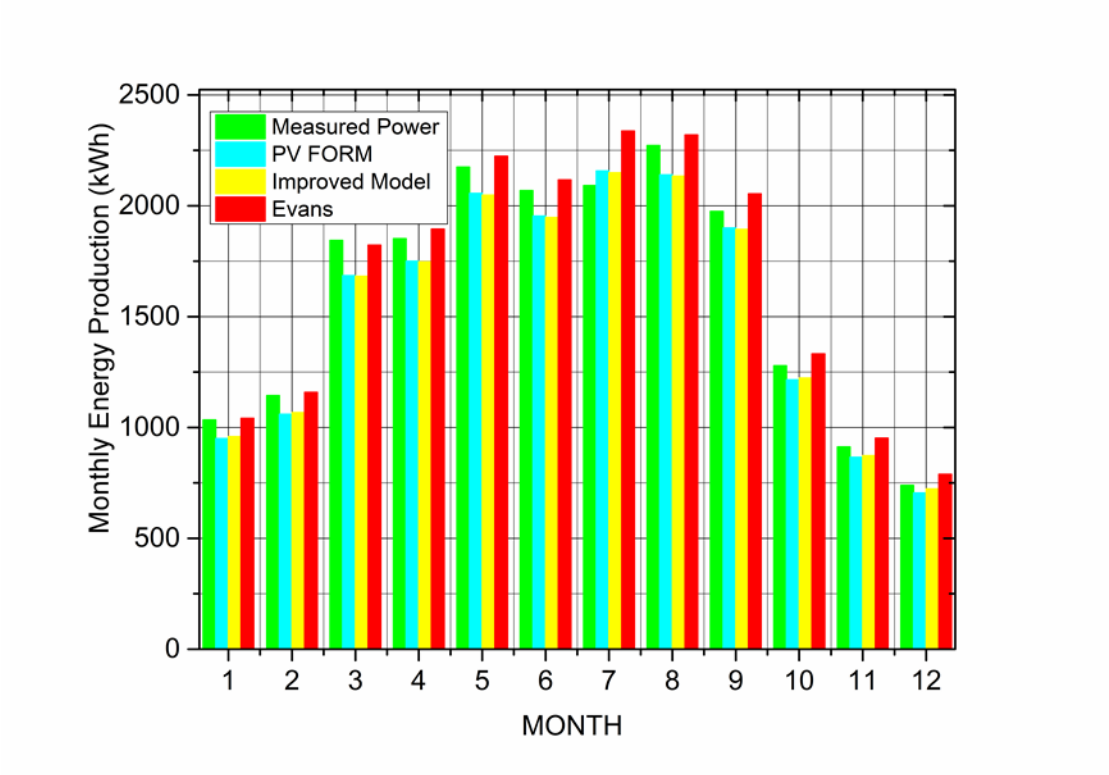

Figure 94 : Monthly Energy production (DC side) computed with the three models in comparison with the measured values for 2014

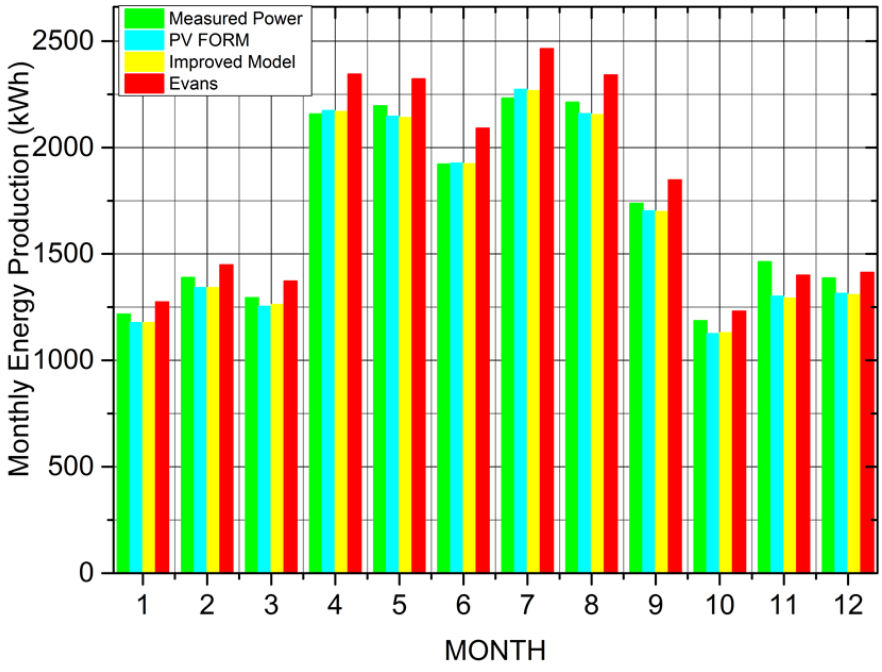

Figure 95 : Monthly Energy production (DC side) computed with the three models in comparison with the measured values for 2015

Table 24 summarizes the behavior of the three models in energy production during the 3-year period. It is clear that estimation of energy production with the aid of models is not quite accurate but there is a different deviation mode observed with each model. It

would be expected that this deviation remains constant with the passage of time. However, it is observed that the deviation of measured power for every model is not constant over the years. This fact points to a drop in efficiency as years passed. In particular, Evans model shows an overestimation of energy generation for all years, however this overestimation has an increasing trend. On the other hand, the PV form and improved bilinear models show an underestimation of energy production for all years with a decreasing trend. The deviation is computed by the equation below and it is presented in Table 24.

$$Deviation = 100\% \frac{E_C - E_M}{E_M} \quad (5\text{-}26)$$

where E_C (kWh) is the yearly energy production which is computed for each model using the available irradiance and temperature data. E_M (kWh) is measured data from inverter inlet.

Table 24 : Deviation of proposed models to energy production over this period

	Year	PV FORM (%)	Improved bilinear model (%)	Evans (%)
Deviation from measured values	2013	-5.3	-5.5	2.5
	2014	-5.1	-4.9	3.4
	2015	-3.0	-3.1	5.2

The comparison of the three models' predictions with the measured data for the specific time period does not reveal any model to be superior to the rest in matching overall the measured values. All models present significant deviations from measured values, however, the application of models can bring to the foreground the general trend for the energy production and may be used as an indicator of a possible fault in system. The first two models show a lower deviation as the PV plant yield decreases from year to year. The opposite holds for the Evans model.

Finally, it is clear that the implementation of models to this kind of data does not achieve adequately fitting with measured values, however this implementation is useful as reference value and the deviation from this value indicates a fluctuation in PV performance.

5.5 Comparison of yearly PV performance

This section discusses the significant differences in yearly energy production which are presented at Table 22. The presentation of data in Section 5.3 shows that it is not clear from AC measurements if there is a drop in PV panel efficiency. In order to investigate the reasons for these differences, the results of the PR calculation(equations(5-1)-(5-3)) and normalization to STC conditions described in Section 5.2 are presented below. The results of these two procedures are going to be correlated with the results of models' application.

The aim of the normalization is the calculation of yearly averaged efficiency in particular AM classes whose impact to energy production is shown in Figure 86. The results of calculation for each year are shown in Figure 96. Furthermore, the correlation of normalized efficiency with irradiance for random clear sky days is presented.

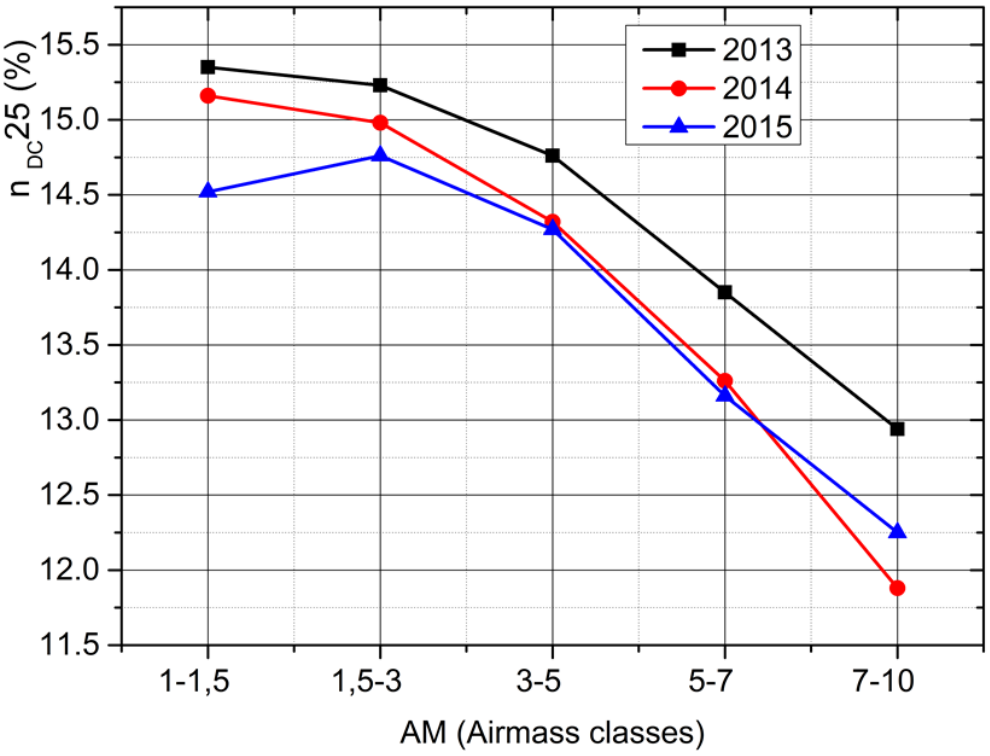

Figure 96 : Averaged normalized yearly performance distributed in the various air mass classes

Figure 96 shows that the normalized efficiency is higher than STC efficiency (14.7%), for all years, for the range 1<AM<3 where 90% of energy is produced, as shown in Figure 86. An exception is observed only with the year 2015 at 1<AM<1.5. This year, a discrepancy from the general trend is observed for the Air-mass class 1-1.5: according to the theory, efficiency should be always higher with lower Air Mass. This small discrepancy is understandable, since the normalization employed in the processing of the results and the monitoring measurements themselves are not perfect. On the other hand, Figure 96 shows a general decrease trend in normalized efficiency as the years passed. This conclusion is confirmed by the comparative analysis with the three models referred-to in section 5.6. The estimation of yearly energy production by use of the three models is shown in Figure 97, where it is compared with the measured yearly energy production. It can be additionally observed in this Figure that normalized efficiency decreases for higher values of air mass, independent of the year. Figure 96 is the essence of the proposed normalization procedure. It presents temperature - normalized efficiency in correlation with Air mass. This gives a clear picture of the averaged actual efficiency all over the year, independent of season or time of day.

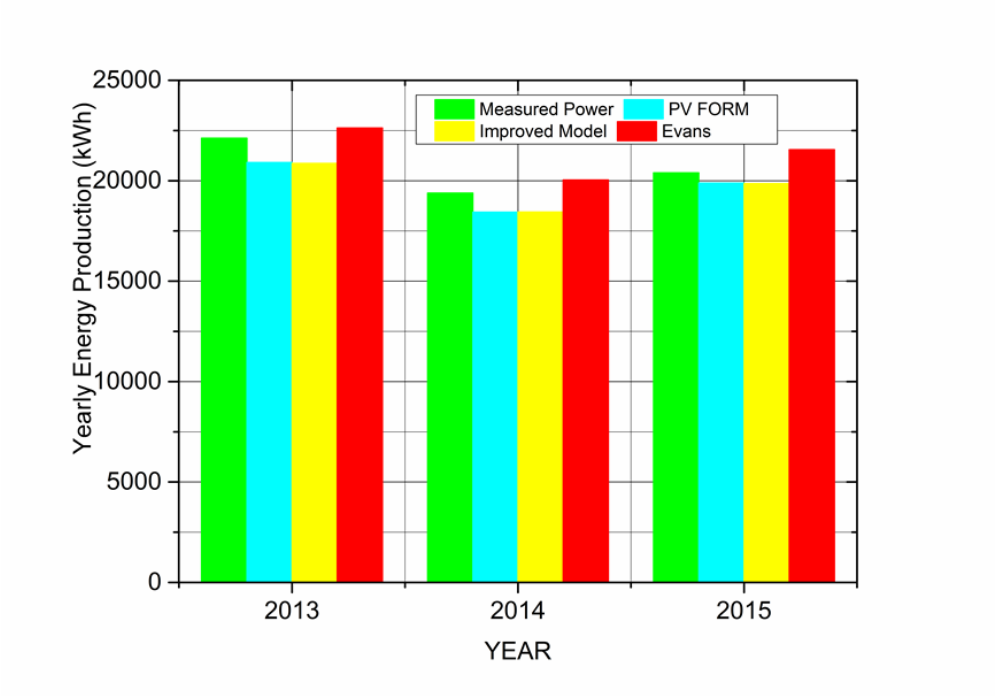

Figure 97 : Comparison of PV yearly energy production of years 2013-2015, computed with proposed models

Finally, the results of implementation of the analysis procedures described in section 5.3 are compared with the results of PR calculation. The synopsis of PR calculation is presented in

Table 25, where it is shown that PR decreases with the years. This decrease is confirmed in Figure 96 where the averaged normalized efficiency is shown to decrease with the years, with an exception for 7-10 Air mass class of the year 2014. Both methods converge to the conclusion that there is a decreasing trend in PV efficiency.

Table 25 : Performance ratio calculation

	2013	2014	2015
Y_f (kWh/Kw)	1638.5	1454.5	1532.9
Y_r(kWh/Kw)	1840.6	1648.8	1765.5
PR	0.89	0.88	0.87

In addition to the above comparisons, which concern all the available data without differentiation according to atmospheric conditions, Figure 98 shows the behavior of normalized efficiency in correlation with irradiance during clear sky days of all years.

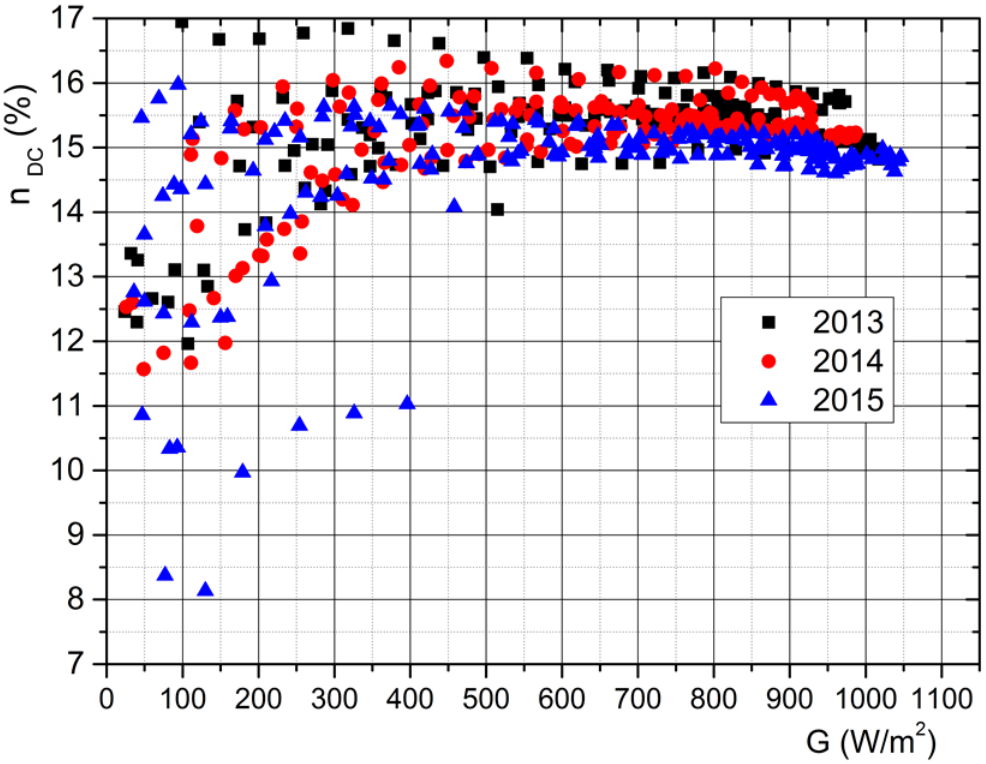

Figure 98 : Comparison of PV array performance normalized to 25°C of during clear-sky days of 2013-2015

The comparison concerns specific days selected from the dataset, based on the inspection of the daily irradiance profiles. In particular, the days selected demonstrate a smooth sinusoidal - shaped solar radiation profile without vertical perturbations indicating the presence of clouds [94]. The selected days have averaged daily clearness index between 0.5–0.65 and averaged daily irradiance ranging between 550-650 W/m².

Inspection of the diagram of Figure 98 shows that the PV panel temperature - corrected efficiency during clear - sky days is nearly constant for irradiance levels up to 400 W/m² and lies in the range between 15 – 16 %. The efficiency demonstrates significant fluctuation for lower irradiance levels between 100 - 400 W/m². At even lower irradiance levels (< 100 W/m²) there is a remarkable decrease, which is in line with what is reported in the technical datasheets (Table 17). A fact that is not quite clear from this diagram is that for irradiances greater than 400 W/m² normalized efficiency during 2015 is smaller than in the other years, a fact that converges with the conclusions of performance ratio analysis, comparative models analysis and normalization procedure (Figure 96).

5.6 Conclusions of the case study

Processing monitoring data from a grid-connected PV park using existing models and application of a proposed analysis procedure, points to a small PV performance decrease during the three year period 2013-2015. The available data included only in-plane total irradiance data and panel's temperature measured with a conventional irradiance and temperature sensor, respectively, in combination with inverters' electrical performance data.

The first objective of the analysis procedure was performance ratio calculation, which

pointed to a small drop in yearly PR from 2013 to 2015. The second objective was the application of three existing models to the available data. A comparison of the three models' computed values and the measured values shows significant deviations for all models. In terms of energy production, it was found that the PV form and the improved bilinear model underestimate the production, in contrast with Evans model. On the other hand, an agreement of all three models was observed to an efficiency decrease during the third year. Deviation between measured production and models' prediction was nearly constant for the years 2013 and 2014. However this deviation decreased for the year 2015. Thus, the application of models to this kind of data is able to give only general conclusions for the trend of the yearly energy production.

The third objective was the application of a proposed procedure which normalizes data to STC conditions. Using this procedure, the efficiency was found higher than STC conditions for the first two years, whereas during the third year a small efficiency drop from STC conditions was recorded. Despite the fact that the second year's efficiency remains higher than STC conditions, a small efficiency drop is observed compared to the first year.

The main problem to be solved was the explanation of fluctuations in yearly energy production by the use of conventional measurement equipment. This study approaches this problem by three parallel procedures and concludes that an over 10% fluctuation in yearly energy production observed during the first two years is mainly due to irradiance levels variation, whereas a very small decrease in PV performance is probable for the third year.

A convergence is observed between performance ratio analysis, normalization procedure and models' comparison to the fact that a small decrease in PV panel's efficiency right from the first year of operation is recorded. However, this decrease is covered by the terms of the manufacturer's warranty. The main advantage of the proposed comparative procedure is that it allows drawing conclusions on the PV park's performance by employing basic monitoring equipment. From now on, a challenging task arises in the study of the aging effect in older PV panels.

6 Performance analysis – Degradation[4]

As mentioned above, the majority of PV parks employ a typical set of sensors which collect in - plane irradiance, module temperature and power data from the inverter's inlet side. In this chapter the experimental setup included a grid-connected system of 99,84kWp which is performance monitored and analyzed. Aim of the proposed methodology is the performance analysis of a grid-connected system based on the values collected from a typical set of sensors. The innovative aspect of this methodology is based on the fact that it can be conveniently applied to numerous dispersed grid-connected systems and give useful results regarding solar potential, comparisons between different technologies and behavior of systems with time. An additional advantage of this type of analysis is that a systems operation shutdown is not necessary.

6.1 Experimental setup

The system studied is a grid-connected photovoltaic system of 99.84 kWp in central Greece. The system consists of 8 Inverters and 416 PV panels on the park. The technical characteristics of equipment are presented in 5.1 The available measurements are in the form of plane irradiance, back panel temperature and AC power from inverter inlet and concern 6 years (01-01-2013 – 12-31-2018) of operation. Photovoltaic systems are mounted in a fixed south facing position with 30° degrees tilt angles. The monitored performance parameters of the PV installation are recorded in a data logger at 15 minutes intervals. The main technical characteristics of the PV system are shown in 5.1. Another important element for this system is the lack of a cleaning system for the panels' surface, because its inclination in combination with frequent rainfalls allow self-cleaning. It should be mentioned additionally that during the 6-year period of analysis, there existed a certain time interval when the PV panels were covered by snow for several days.

6.2 Methodology

The analysis methodology is based on long term monitoring of several different performance metrics with time and follows three axes.

The first axis is the calculation of the daily PR and yearly PR and their comparison for the 6 years of operation. Daily PR is additionally correlated with averaged clearness index in order to investigate the atmospheric effect on PV performance.

$$Y_F = \frac{E}{P_{STC}}\left(\frac{kWh}{kW}\right) \quad (6\text{-}1)$$

$$Y_R = \frac{H}{G_{STC}}\ \left(\frac{kWh}{kW}\right) \quad (6\text{-}2)$$

$$PR = \frac{Y_F}{Y_R} \quad (6\text{-}3)$$

[4] This chapter has been published as: Roumpakias, E. and A. Stamatelos (2019). "Performance analysis of a grid-connected Photovoltaic park after 6 years of operation." Renewable Energy 141 (2019) 368-378

The second axis is the use of a mathematical model, which calculates the PV power generation, to the available data. Computed values act as reference values. The deviation of measured data from the reference values hints to possible changes in PV system's performance. The model is described by the following equations:

Improved Bilinear interpolation model [160]

G > 200 W/m² :

$$Pc = P_{STC}\left[\frac{G}{G_{STC}}[1 + a(T_C - T_{STC})] - k\frac{G_{STC} - G}{G_{STC} - 200}\right] \quad (6\text{-}4)$$

G < 200 W/m²:

$$Pc = P_{STC}\left[\frac{G}{G_{STC}}[1 + a(T_C - T_{STC})] - k[1 - \left(1 - \frac{G}{200}\right)^4]\right] \quad (6\text{-}5)$$

Where P_{STC}, G_{STC}, T_{STC} are reference parameters, k an irradiance factor and a panel temperature coefficient as stated in the manufacturer's datasheet. T_c and G are measured parameters. Irradiance factor k is provided by manufacturers as a percentage reduction in efficiency at low irradiance levels (200 W/m²). The computed values are compared with the measured ones and deviation is calculated as follows:

$$\text{Deviation } = 100\%\frac{P_C - P_{DC}}{P_C} \quad (6\text{-}6)$$

The third axis is the computation of normalized efficiency to STC conditions (G_{STC}=1000W/m², T_{STC}=25°C,). This procedure is described in [153] and includes the following three basic steps:

- Computation of DC power from available AC data from inverters' inlet based on inverters efficiency section [5.1].
- Temperature normalization according to temperature coefficients supplied by the manufacturer of the PV panels.
- The last step is the comparison of efficiency at various weather conditions and the computation of yearly average values classified with respect to Air mass [158].

The definition of weather conditions as far as clear sky is concerned, was studied by several researchers. Malvoni et al , classified days as sunny and cloudy using the clearness index and particularly, values of clearness index higher than 0.5 are considered sunny while values lower than 0.5 as cloudy days [228]. Marion, defines clear sky days as smooth sinusoidal- shaped solar radiation without vertical perturbations indicating the presence of clouds[229]. Larraneta et al, define five criteria for clear sky characterization, namely, the mean value of GHI, maximum value of GHI, line length of irradiance vs time curve, standard deviation of rate change in GHI and maximum difference between changes in GHI and clear sky time series[230].

The definition of clearness index and AM is stated below:

$$K_t = \frac{G}{G_{extra}\ cosAOI} \quad [195] \quad (6\text{-}7)$$

$$AM = COS(\ z_s\ )^{-1}\frac{P}{P_0} \quad (6\text{-}8)$$

$$\frac{P}{P_0} = \exp^{(-0.0001184h)} \quad (6\text{-}9)$$

z_s sun's zenith angle

P local air pressure

P_0 sea level air pressure

h altitude of place [225].

The results of each one of the three axes are compared and discussed in the following section. These results are presented by means of figures and summary tables in the following section.

6.3 Results and discussion

Performance analysis of the specific PV system gave significant results for PV operation during the six year period. First of all, the results give an indication of the solar potential of central Greece: In particular, yearly energy production shows a maximum deviation of 13% from the average value. This deviation could be attributed to weather conditions, faults or fluctuations in PV systems' performance. Table 26 presents the calculation of yearly PR, energy production and specific yield of the PV system. As far as PR is concerned, we observe a small yearly decrease over the years, something that is not clear from the specific yield and energy production values.

Table 26 : Summary results from the 6-year period performance analysis: Yearly PR, Degradation of PR, Energy production at inverters' inlet and Energy yield

Year	PR	R_D (%)	Energy Production (kWh)	kWh/kWp
2013	0.90	-	20904	1675.0
2014	0.89	1.12	18317	1467.7
2015	0.88	2.27	20709	1659.4
2016	0.87	3.45	19344	1550.0
2017	0.87	3.45	19485	1590.1
2018	0.87	3.45	18131	1549.6

More specific details from the analysis procedure are presented below in order to explain the observed performance fluctuations. It is significant to investigate which levels of irradiance and Air mass respectively, play an important role in energy production. The air mass factor quantifies the length of trail of the Sun's beams as they cross the atmosphere [195]. The value of air mass is calculated as described in 6.2. To this end, the percentages of energy produced in each AM class are presented in Figure 99, for all years of operation.

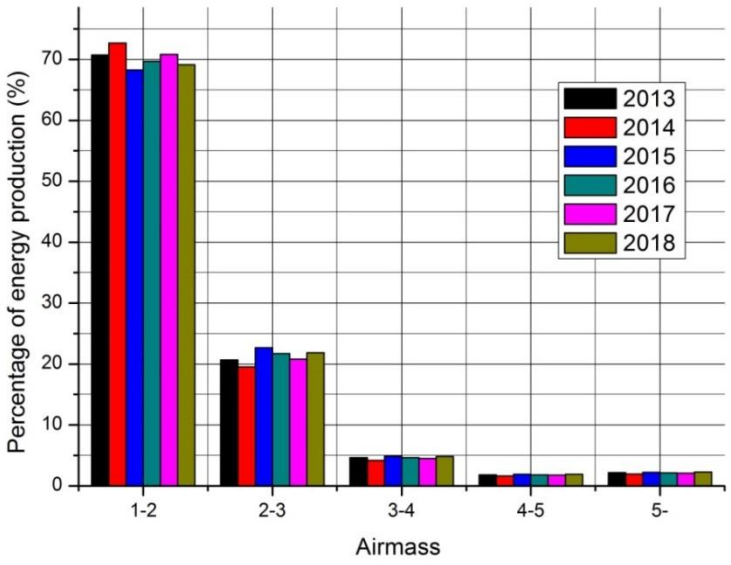

Figure 99 : Yearly energy distribution among the five AM classes in the period 1/1/2013-31/12/2018

This diagram indicates that approximately 90% of the total yearly energy production was recorded at Air mass values in the range between 1 - 3. As regards the correlation with irradiance values, 90% of total yearly energy production was recorded when irradiance values were between 200-1000W/m^2 as shown in Figure 101. Another important observation is that approximately 75-80% of energy production is generated in the period from March to October as shown in Figure 99. It is also remarkable that, for the specific site, irradiance exceeds the limit of 1000 W/m^2 only for small periods over the year, something that is observed from the energy production in this class of irradiance which fluctuates between 2-3% for all of the years according to Figure 100.

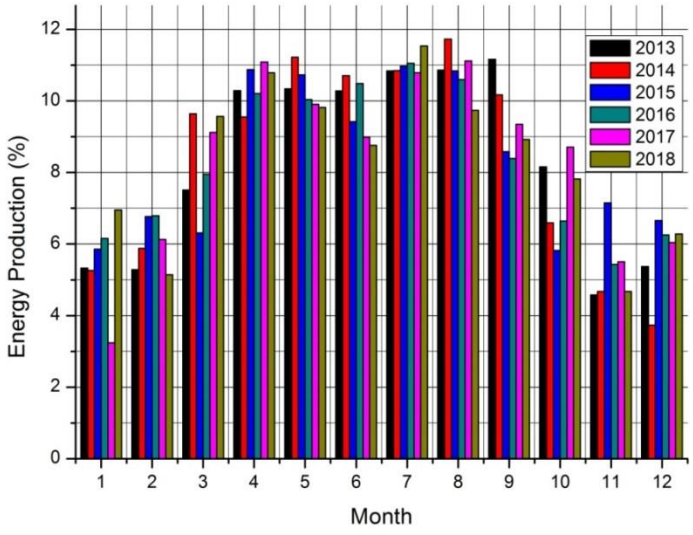

Figure 100 : Monthly energy production distribution for each year for the period 1/1/2013-

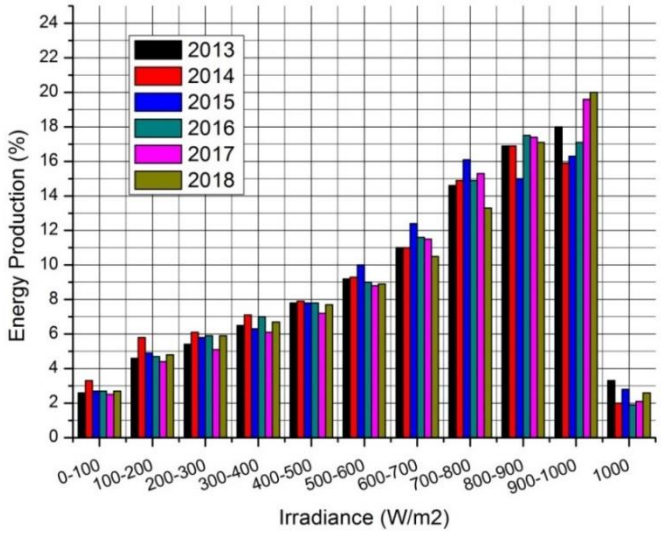

Figure 101 :Yearly energy production distribution per irradiance class for the period 1/1/2013-31/12/2018

Another important metric referenced above is the array yield which is a useful metric for the sizing of PV systems. In particular, knowledge of monthly energy array yield for several years assists the optimal sizing in off-grid systems with energy storage or in grid-connected systems with net-metering. Figure 102 shows the monthly array yields for the total monitoring period of six years. It is observed that the highest energy yield took place in September of the first year of operation (185.95 kWh/kWp), whereas the smallest value was recorded at 50kWh/kWp during January 2017. However, the smallest production was due to heavy snowfall that had covered the surface of PV panels with snow for five days.

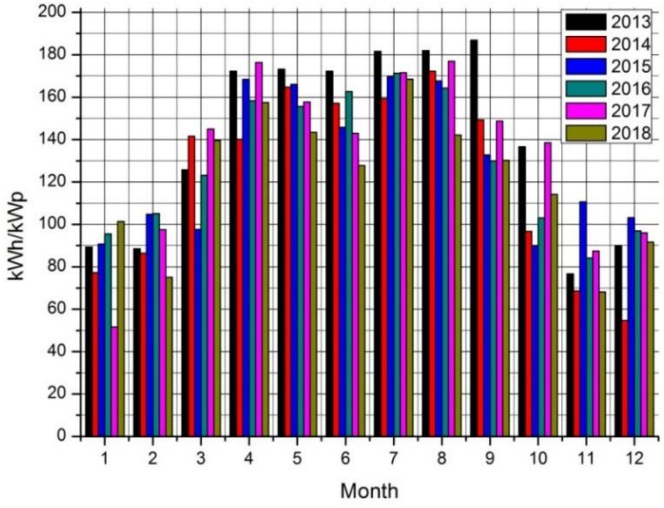

Figure 102: Monthly Energy yield in the period 1/1/2013- 31/12/2018

Array yield is a metric that cannot provide conclusions for systems' efficiency, as it does not take account of the parameters that have effect on PV systems efficiency; however it

gives an indicative view of the site's energy production potential. Efficiency is further affected by other parameters as irradiance, panels' temperature, inverters' efficiency and cleanliness of the panels' surface. Thus, the next step of analysis is the use of metrics that take into account the effect of these additional parameters. Figure 103 presents the evolution of monthly averaged back panel surface temperatures for the 6-year period. It is obvious from Figure 103 that in the period from April to October, the averaged back-surface temperature is higher than STC conditions. On the other hand, as already observed in Figure 100, 70% of the total yearly energy production is produced in these months. It is clear that temperature has a strong impact on systems' performance, therefore the use of these metrics is of significant importance.

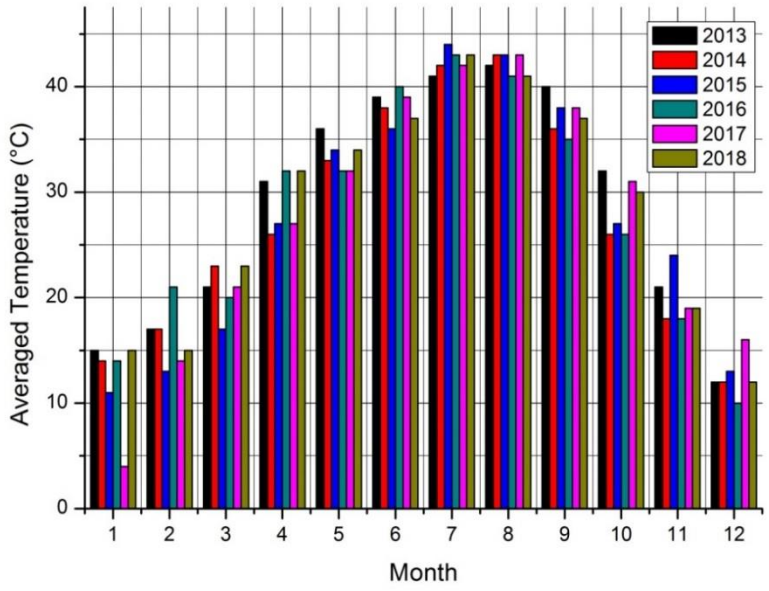

Figure 103: Monthly averaged temperatures of back panel surface for the period 1/1/2013-31/12/2018

Performance ratio is a more indicative metric for PV efficiency and its behavior in long-term analysis can provide useful conclusions. However its calculation does not include the temperature effect, which is a key variable for photovoltaic conversion process [55], and other related parameters. Figure 104 shows the correlation of PR with the clearness index during the 6 years of system's operation. The daily PR for all years fluctuated between 0.8 – 1, independently of the clearness index. Nevertheless, the yearly PR, as shown in Figure 104 and Table 26, presented a small decrease between 0 - 1.16% per year and a total decrease of 4.65% for the 6-year period.

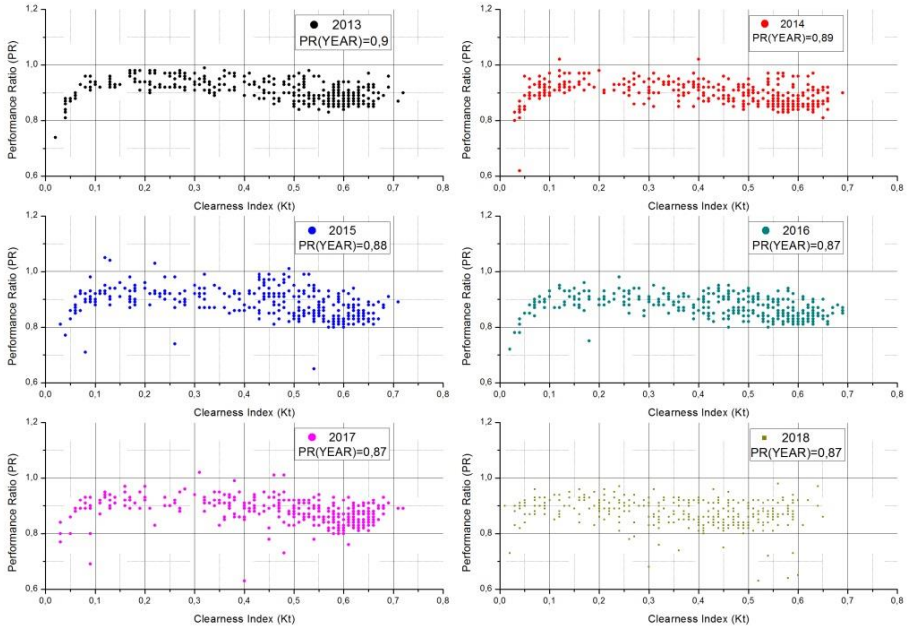

Figure 104 : Correlation of performance ratio with clearness index for each one of the 6 years of analysis.

This small decreasing trend in yearly performance ratio deserves to be examined in more detail. Thus, the second step in this analysis is the use of a mathematical model to correlate the power produced with recorded values of temperature and irradiance as described in the previous section. Table 27 presents the results as difference between computed and measured power generation as calculated by equations (6-4)-(6-6). Values of deviation are averaged in the defined AM classes for every year and presented in Figure 100. The evolution of deviation for all AM classes has a decreasing trend, a fact that hints to degradation, however this trend is not constant.

Table 27 : Deviation between measured and computed by improved bilinear model for each year in five AM classes

Year	Deviation (%)	Deviation (%)	Deviation (%)	Deviation (%)	Deviation (%)
	AM:1-2	AM:2-3	AM:3-4	AM:4-5	AM:5-10
2013	-4.03	-6.66	-17.12	-11.36	1.52
2014	-3.18	-3.37	-3.43	-2.6	4.4
2015	0.22	-2.68	-3.28	-0.99	6.74
2016	-0.75	-0.28	-0.39	-0.48	6.63
2017	-1.53	2.41	0.97	2.47	8.03
2018	0.02	-1.64	-1.84	-0.72	3.15

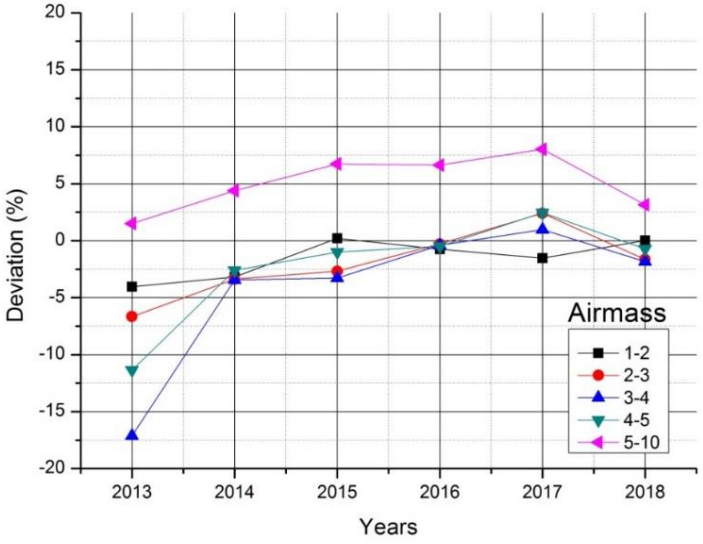

Figure 105 : Deviation between measured and computed power generation by the improved bilinear model for each year, as distributed in the five AM classes

Table 27 and Figure 105 show that values of AM in the range between 1 – 5 are underestimated whereas AM values in the range higher than 5 are overestimated. This trend is important to be examined in the future in order to observe fluctuation and particularly for the 1<AM<2, 2<AM<3 classes, in which 90% of the total yearly production takes place according to Figure 99.

The final step in this analysis is the calculation of normalized efficiency in terms of averaged values and the study of PV systems' efficiency in clear sky conditions. Figure 106 shows the monthly averaged values of normalized efficiency for the 6-year period. The values fall in the range between 13-15%. A seasonality is observed as regards the normalized efficiency, since the winter months from November to February demonstrate efficiency lower than 14% for all years.

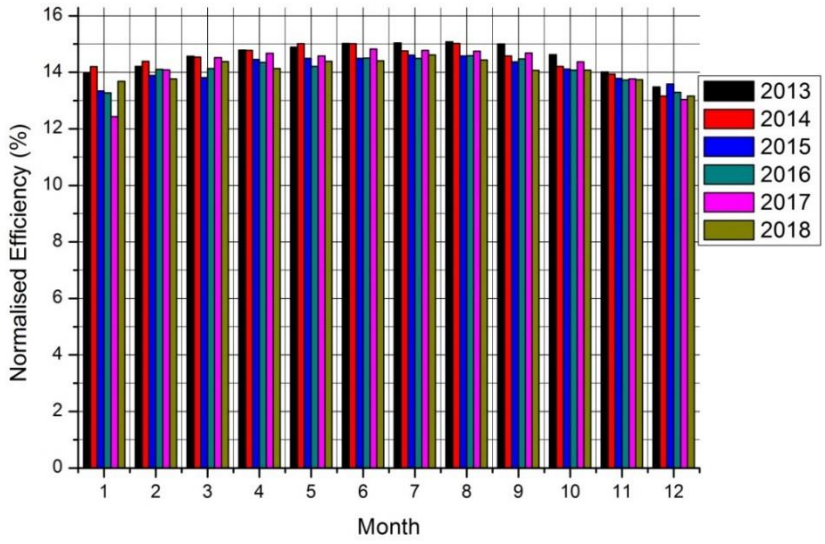

Figure 106 : Monthly averaged normalized efficiency for the period 1/1/2013- 31/12/2018

Next, normalized efficiency is inspected for clear sky days. These days meet the requirements already stated in the previous section. In particular, daily clearness index is set to not exceed 0.5 and the curve of irradiance must be smooth, sinusoidal - shaped. The number of these days found for each year is presented in Table 28. It is clear that 2014 and 2016 have significantly fewer days than the other years. An exception is also observed for 2018 .

Table 28 : Number of clear sky days

Year	Number of Clear Sky Days
2013	40
2014	28
2015	40
2016	23
2017	45
2018	30

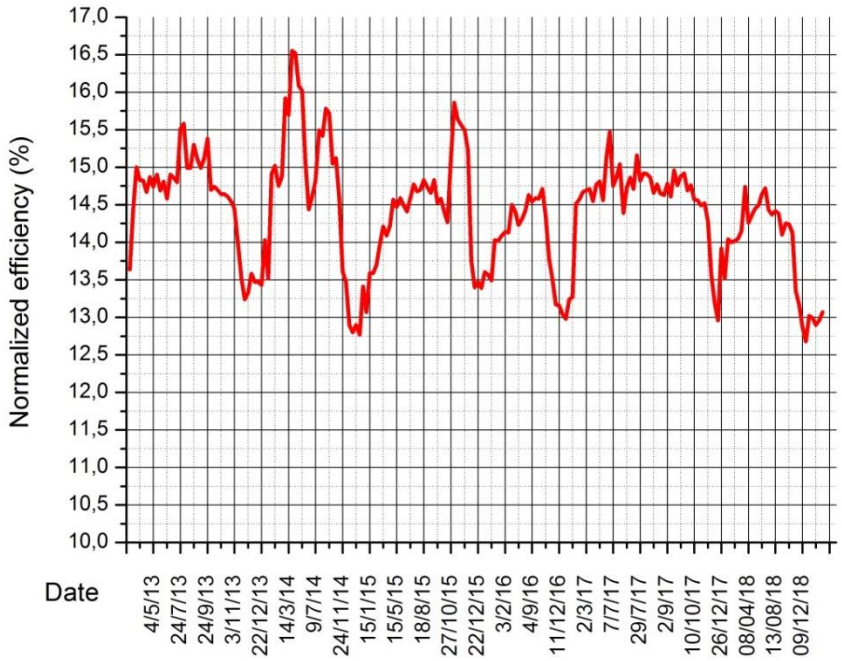

Figure 107 : Evolution of normalized efficiency for the clear sky days found in the period 1/1/2013- 31/12/2018

This diagram shows an average decreasing trend, as well as a seasonality during each year. Higher performance is observed in 2014 and –to a lesser extent- in 2013. Averaged daily normalized efficiency drops below the value of 14% during months with lower levels of irradiance and in particular for the period from November to February. Efficiency dropped below 15% during the years 2015-2018. This is to be compared to the years' 2013 and 2014 behavior. Highest efficiencies were observed during the last days of March 2014. It should be noted that this period coincides with the maximum solar activity of cycle #24, which occurred in April 2014 [231]. The evolution of the respective solar cycle is shown in Figure 108 and Figure 109.

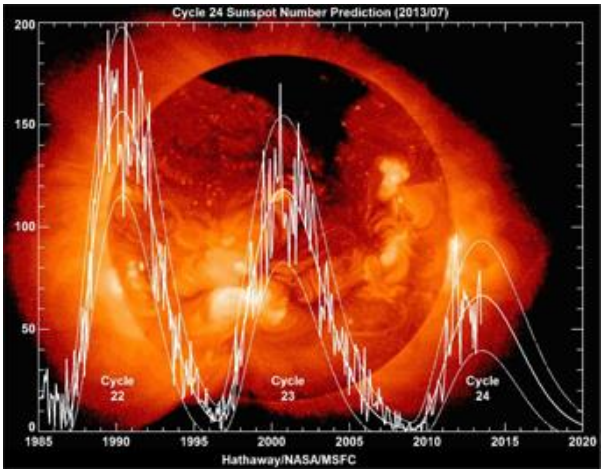

Figure 108 : Recording of the three last solar cycles (number 22, 23, 24) [231]

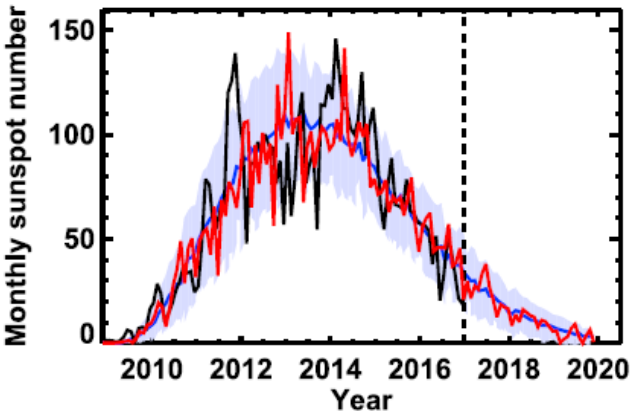

Figure 109 : Evolution of solar cycle 24. Monthly group sunspots (black curve denotes observed sunspots) [232].

Figure 110 shows averaged values of normalized efficiency for the five AM classes selected. A decreasing trend in normalized efficiency (albeit not constant) is clearly noticeable for every class of AM. However, this decrease trend is more intense for the years 2015, 2016 compared to 2017 for the first class of AM, which corresponds to 70% of total yearly energy production. Especially, the decrease for this class is remarkable for year 2015, where a degradation rate of 4.37% was reported (Table 29), which is the highest of all years for the class with 1<AM<2. It is clear that the observed decrease over the years is not the same for every class. It is remarkable that for the majority of the cases, the observed degradation rates are higher than STC value.

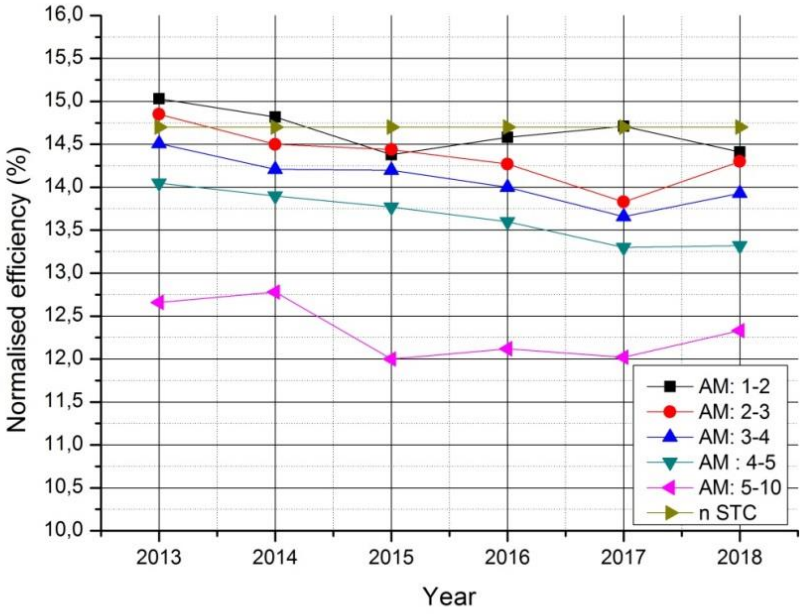

Figure 110 : Averaged normalized efficiency in five AM classes during 1/1/2013- 31/12/2018

The Air Mass classes with important effect on electricity generation are 1<AM<2, 2<AM<3 as already discussed. For these classes, the observed trend is decreasing, albeit at different rates. The degradation rate fluctuates in the range between 1.28 - 6.92%. Another important result is that for the year 2014, despite the fact that it had the lowest energy production (Table 26) and the second lower number of clear sky days (Table 28, demonstrated the lowest degradation rates. Also, year 2014 demonstrated the highest efficiency during clear sky days. This fact demonstrates the usefulness of this method in attributing the lower energy production either to weather conditions or to other causes.

Table 29 : Degradation rates of normalized efficiency with reference to the first year of operation

	R_D %	R_D %	R_D %	R_D %	R_D %
AM	2014	2015	2016	2017	2018
1-2	1.28	4.37	2.96	2.04	4.10
2-3	2.01	2.47	3.64	6.92	3.31
3-4	2.26	2.29	3.59	5.79	3.44
4-5	1.46	2.54	3.18	4.65	3.50
5-10	-0.44	4.47	3.91	4.55	3.13

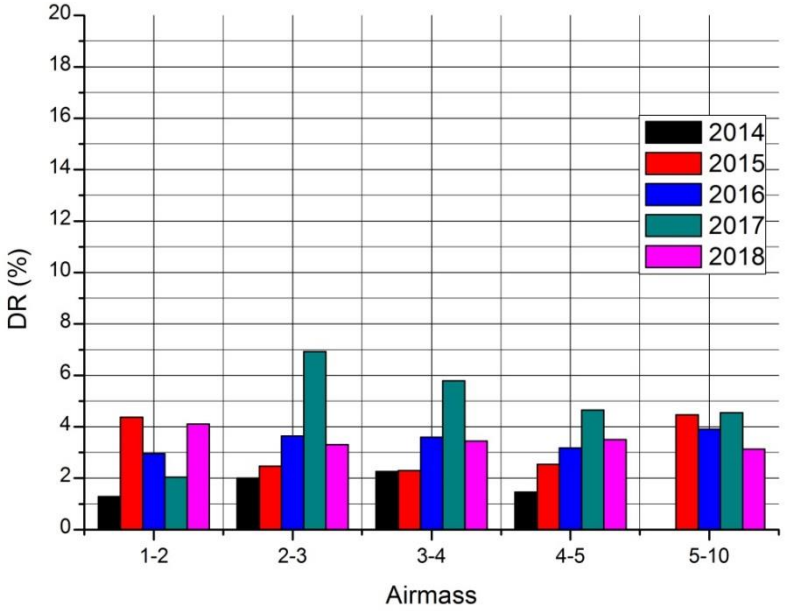

Figure 111 : Degradation rate of normalized efficiency from the first year of operation, as distributed in the five AM classes

All of the methods employed in this analysis agree to a decreasing trend in systems' efficiency (Table 30). It is not yet clear from the analysis why this decrease is not constant but it fluctuates. A characteristic example is for the class 1<AM<2 of year 2017, where the degradation rate is the lowest after that of the year 2014 (2.04%). This fact should be attributed to the soiling effect, which covers the PV modules' surface with dust. This effect cannot be taken into account by the analysis methodology, because the reference cell employed for irradiance measurements is subjected to the same levels of soiling. Furthermore, optical inspection showed that the surface of panels is cleaned by the rain, since the inclination is 30°. However, in the beginning of the specific year as reported above, the PV panels' surface had been covered by snow and the subsequent melting of the snow resulted in an effective cleaning of the panels' surface.

Table 30 : Concentrating results of the three axes of the proposed method

Year	PR	Averaged normalized efficiency AM: 1-2 (%)	Averaged deviation from models reference value AM:1-2 (%)	Averaged normalized efficiency AM: 2-3(%)	Averaged deviation from models reference value AM:2-3 (%)
2013	0.90	15.03	-4.03	14.85	-6.66
2014	0.89	14.82	-3.18	14.50	-3.37
2015	0.88	14.38	0.22	14.44	-2.68
2016	0.87	14.58	-0.75	14.27	-0.28
2017	0.87	14.71	-1.53	13.83	2.41
2018	0.87	14.41	0.02	14.30	-1.64

Table 30 shows concentrating results of each of three axes. Particularly, shows the evolution of PR during 6 years (first axis). The results of second and third axis are

focused on the AM classes which have important impact on energy production according to Figure 99. All of the metrics of each axis have the same decreasing trend compared with first year of operation.

6.4 Concluding remarks

The performance behavior of a grid-connected photovoltaic system is analyzed in this paper, by using recorded monitoring data for in - plane irradiance, AC power, PV panels' temperature and DC voltage. The methodology of analysis is based on PR metrics, a comparison with a mathematical model and calculation of normalized efficiency to STC conditions. The period of analysis concerns six years, 2013-2018. During these years, the AC energy yield varied in the range between 1467.7 – 1675.0 kWh/ kWp, AC wiring losses not included. Yearly performance ratio varied in the range 0.87 – 0.9, with a decreasing trend. When the measured values of power produced were compared with those computed by the improved bilinear model, it was observed that the deviation from the reference value had a decreasing trend over the years. This fact confirms the conclusion of PR analysis.

The final step in the analysis methodology included the calculation of normalized efficiency, the calculation of its degradation and the study of behavior in clear sky conditions. The analysis for clear sky conditions shows that normalized efficiency has a decreasing trend and a seasonality during the year. Remarkable efficiencies were recorded in some clear sky days during the end of March of 2014, a fact that could be correlated with the solar maximum of solar cycle #24. The decreasing trend over the years is validated by the final step of analysis which involves the calculation of normalized efficiency for each one of the five defined AM classes. The degradation rates of normalized efficiency for the first two AM classes, which have the highest impact on total energy production, varied in the range 1.28% - 6.92%.

The results from all three axes of the proposed methodology converge to the fact that there is a decreasing trend in PV panels' efficiency, based on the assumption that the panels' surface is cleaned by rain and snow. Soiling effects are excluded by the analysis because they equally affect the irradiance sensor. However, it is a challenging task for future investigation to monitor the PV panels surface in order to correlate with possible efficiency reduction. This would allow decoupling the effect of soiling from the remaining factors influencing PV efficiency. Correlation of normalized efficiency - especially at clear sky days - with optical inspections on PV panels and sensors surface, combined with IR imaging, could provide important conclusions for soiling.

The methodology employs simple measuring equipment to give a valid assessment of the PV system performance and produce useful performance data related to the prevailing irradiance levels, temperatures, sky conditions and energy potential of this site. An important future objective is to apply this methodology to other systems with different technologies and in different geographical regions in Greece.

7 Surface dust and Aerosol effects on the performance of Photovoltaic grid-connected systems

7.1 Introduction

The present study focuses on the impact of dust accumulation and atmospheric aerosols on PV performance. The analysis procedure is based on optical images of PV surfaces and measurements of aerosol concentration. PV performance is calculated based on monitoring data sets from a grid-connected PV installation. The main objective is to understand and qualitatively describe correlations among these factors and PV performance. The innovative aspect of this work is related to the specific application on a grid-connected PV installation in real world operation. Expanding application to a variety of grid-connected PV sites in different countries, is expected to add to our understanding of the dust and aerosols effect on PV panels' performance.

7.2 Materials and Methods

7.2.1 Experimental setup of PV system monitoring

The system studied is a 99.84 kWp grid-connected photovoltaic system located in central Greece. The installation consists of 8 inverters and a total of 416 PV panels. The technical characteristics of equipment are summarized in 5.1. Available monitoring data are in the form of plane irradiance, back panel temperature and AC power from inverter inlet and concern 6 years of operation (01-01-2013 – 04-30-2019). Additionally, a Dusttrak 8530 aerosol monitor is installed on site, in a special environmental enclosure. Photovoltaic systems are mounted in a fixed south facing position with 30 degrees tilt angle. The monitored performance parameters of the PV installation are recorded in a data logger at 15 minutes' intervals. The specific PV installation lacks a cleaning system for the panels' surfaces, because it is assumed that the panels tilt angle in combination with frequent rainfalls allow for self-cleaning. It should be mentioned additionally that during the 6-year period of analysis, an instance was observed when the PV panels were covered by snow for several days. Additionally, daily rainfall data from October 2018 to August 2019 were made available from meteorological stations in the vicinity. Furthermore, optical inspections were conducted in the period from September 2018 to August 2019 in order to assess the accumulated dust levels on the photovoltaic panels' surface.

7.2.2 Ambient PM_{10} concentration measurement setup

Previous experience with an optical particle counter, (Figure 112) TSI DustTrak 8530 [233, 234], indicated that this relatively low-cost instrument could give a very good proxy measurement of PM10, based on a measured particle count and a calibration from counts to mass for the particular aerosol of the site. This is confirmed by experience from other researchers [235, 236]. This instrument is capable of continuous measurement. It provides estimates of PM1, PM2.5 and PM10, depending on which inlet diffuser is employed. Optical particle counters tend to be more sensitive to smaller particle, due to

the nature of light scattering from aerosols [237]. One possible confounding signal that arises when using optical scattering methods is the presence of high-humidity in the sample air, with the most extreme case being fog.

The instrument was placed in an environmental enclosure (Figure 112) and requires only basic maintenance to operate under automatic control for long intervals with low total power consumption and a small footprint (main technical characteristics in Table A4, 5.1).

Figure 112 PM10 monitoring Instrument (Dusttrak 8530) placed inside its environmental enclosure.

7.3 Method of analysis

Aim of these measurements was the correlation between

- PV performance – ambient aerosol concentration and
- PV performance – dust accumulation on PV panels' surface

Based on the monitoring data of the grid-connected operation. Of course, PV performance is influenced by other factors as solar radiation, temperature and inverter efficiency. For this reason, an analysis procedure was adopted, which is based on the use of metrics, mathematical models and a normalization procedure to STC (1000W/m^2, 25°C, AM1.5 spectrum). The analysis procedure is described in detail in [153] and [238]. The analysis is based on three axes:

1. Daily Performance ratio calculation according to EN 61724
2. Use of bilinear model as reference value
3. Calculation of normalized to STC efficiency

Computation of normalized efficiency was based on irradiance and panel surface temperature measurements. Normalized efficiency is compared among days where the level of dust accumulation on the panels' surface were markedly different according to the inspections. Furthermore, normalized efficiency is compared with measured aerosol mass concentrations in order to observe possible correlations.

This first axis of the method which concern performance ratio, includes computation for days with different cleanliness of PV panels' surface. The computation is based on equations below [164]:

$$Y_F = \frac{E}{P_{STC}} \left(\frac{kWh}{kW}\right) \quad (7\text{-}1)$$

$$Y_R = \frac{H}{G_{STC}} \left(\frac{kWh}{kW}\right) \quad (7\text{-}2)$$

$$PR = \frac{Y_F}{Y_R} \quad (7\text{-}3)$$

where E is the net energy output, P_{STC} is the installed power at STC conditions, H is the total in plane solar radiation and G_{STC} is irradiance at STC conditions (1000W/m²). However, performance ratio calculation is influenced by the effect of the panel's temperature and its seasonal variations [164].Thus it is important to use additional models for the analysis procedure.

The second axis is the use of a mathematical model (improved bilinear models), which calculates the PV power generation, based on the available monitoring data. Computed values act as reference values. The deviation of measured data from the reference values hints to possible changes in PV system's performance. The model is described by the following equations [160]:

G > 200 W/m²:

$$Pc = P_{STC}\left[\frac{G}{G_{STC}}[1 + a(T_C - T_{STC})] - k\frac{G_{STC} - G}{G_{STC} - 200}\right] \quad (7\text{-}4)$$

G < 200 W/m²:

$$Pc = P_{STC}\left[\frac{G}{G_{STC}}[1 + a(T_C - T_{STC})] - k\left[1 - \left(1 - \frac{G}{200}\right)^4\right]\right] \quad (7\text{-}5)$$

Where P_{STC}, G_{STC}, T_{STC} are reference parameters, k an irradiance factor and a panels' temperature coefficient described by the manufacturer. T_c and G are measured parameters. The irradiance factor k is provided by manufacturers as a percentage reduction in efficiency at low irradiance levels (200 W/m²).

The third axis which is described in [153, 238] includes the computation of normalized efficiency which is not influenced from temperature and solar radiation. This is a metric capable of investigating other factors as dust, ageing effect or ambient aerosol concentration effect. The computation of normalized efficiency based on steps below:

DC power calculation

Computation of DC power from available AC data from inverters' inlet based on inverters efficiency in section 5.1 is based on equation [171]:

$$P_{DC} = \frac{P_{AC}}{n_{inv}} \quad (7\text{-}6)$$

Temperature normalization

Temperature normalization according to temperature coefficients supplied by the

manufacturer of the Photovoltaic panel [section 5.1] panels based on equation:

$$P_{DC25} = \frac{P_{DC}}{1 + a(T_C - 25)} \quad (7\text{-}7)$$

PV efficiency is calculated by equation (8) [171] based on the calculation of normalized PV power from equation (7).

$$n = \frac{P}{G\,A} \quad (7\text{-}8)$$

Normalized efficiency in different test conditions is useful to be correlated with Clearness Index and Airmass. The clearness index K_t may be considered as an attenuation factor of the atmosphere. On the other hand Air mass defines the direct optical path length through the Earth's atmosphere, and consequently aids performance comparison in different times and seasons of the year.

Clearness Index is defined as follows [195]:

$$K_t = \frac{G}{G_{extra}\ cosAOI} \quad (7\text{-}9)$$

The definition of AM [225] is stated below:

$$AM = COS(\ z_s\ )^{-1} \frac{P}{P_0} \quad (7\text{-}10)$$

$$\frac{P}{P_0} = \exp^{(-0.0001184h)} \quad (7\text{-}11)$$

Where, z_s is the sun's zenith angle, P is the local air pressure, P_0 the sea level air pressure and h the place's altitude.

7.4 Results and Discussion

The available datasets span a six-year operation of the grid connected system which is described in section 2. However, more intensive optical inspections in order to take pictures of PV panels' surface were conducted in the period from September of 2018 to April of 2019 while measurements of ambient aerosol concentrations were conducted during the same period. Two periods were found in which the PV panels' surfaces were heavily soiled. Furthermore, the PV panels' surfaces remained totally covered by snow during a whole week in January 2019. This fact significantly helped self - cleaning of the panels' surfaces. The following pictures present conditions on a clean surface, a lightly soiled, a medium soiled and a heavily soiled one.

7.4.1 Effect of dust accumulation on panel's surface

Comparative results of normalized efficiency in correlation with the soiling of the panel's surfaces are presented in this section. The comparisons concern conditions with different levels of soiling (based on optical inspection). For each condition, two PV cells are compared, one cleaned cell and one cell with a specific grade of soiling. The first comparison concerns clean surface conditions which act as reference regarding the behavior of normalized efficiency during a day. Figure 113 shows two clean PV cells on

18.03.2019 and two clean PV cells on 20.02.2019.

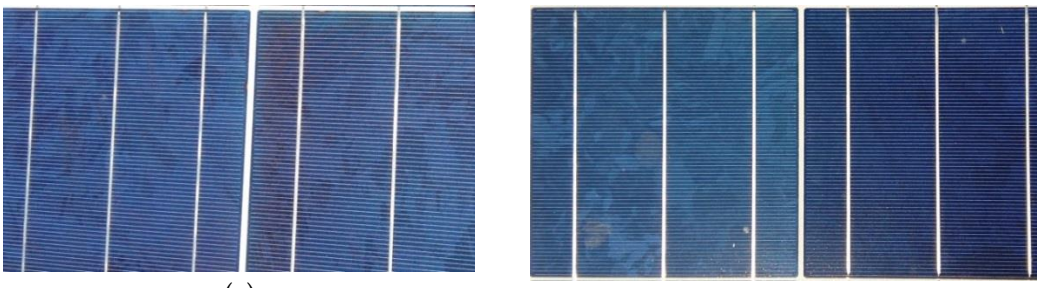

(**a**) (**b**)

Figure 113 Dust accumulation on PV panels' surface (**a**) Clean surface on 18.03.2019 (**b**) Clean surface on 20.02.2019

Figure 114 presents a comparison in normalized efficiency for the conditions of Figure 113. The diagram is completed by application of the third step of the analysis procedure described in section 2.2. Normalized efficiency is presented in correlation with time (a) and air mass (b); because air mass is not influenced by the season of year.

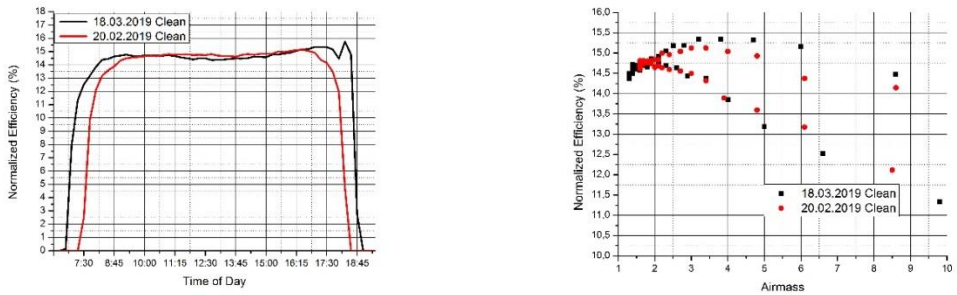

(**a**) (**b**)

Figure 114 Comparison in normalized efficiency between clean surface on 18.03.2019 and clean surface on 20.02.2019 - reference condition. (a) Normalized efficiency as function of time of day (b) Normalized efficiency as function of air mass.

No significant differences in normalized efficiency are observed. A deviation of -0.75% in averaged normalized efficiency is observed for 1<AM<3. Daily performance ratio for 18.03.2019 is 0.869 in comparison with reference condition 0.892.

The second comparison concerns a lightly soiled surface on 29.04.2019 compared to the clean surface reference conditions of 20.02.2019. Figure 115 shows two PV cells without cleaning on 29.04.2019 and the two reference PV cells on 20.02.2019.

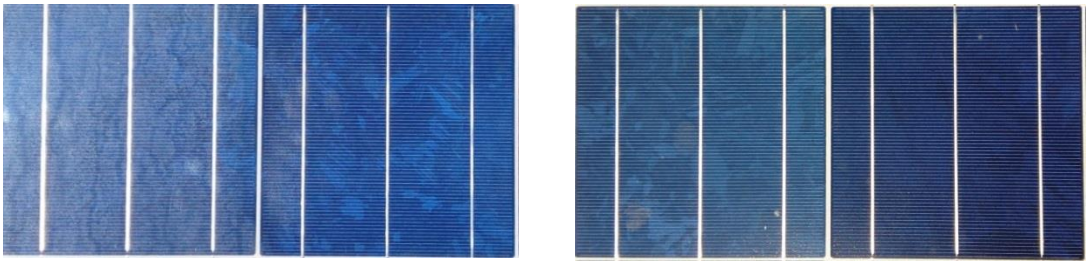

(**a**) (**b**)

Figure 115 Dust accumulation on PV panels' surface (**a**) Lightly soiled surface on 29.04.2019 (**b**) Clean PV panels' surface on 20.02.2019

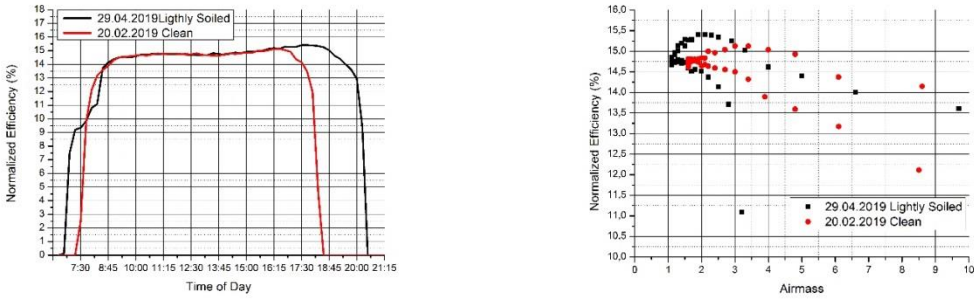

(**a**) (**b**)

Figure 116 Comparison of normalized efficiency between clean surface on 29.04.2019 and clean surface on 20.02.2019 reference condition. (a) Normalized efficiency with time of day (b) Normalized efficiency with air mass.

No significant differences in normalized efficiency are observable in Figure 116. A deviation of 0.47% in averaged normalized efficiency is observed for 1<AM<3. Daily performance ratio for 29.04.2019 was 0.866 in comparison with reference condition 0.892. The third comparison concerns a medium soiled surface on 23.08.2018 compared to the clean reference conditions on 20.02.2019. Figure 117 shows two PV cells without cleaning on 23.08.2018 and the two clean PV cells on 20.02.2019.

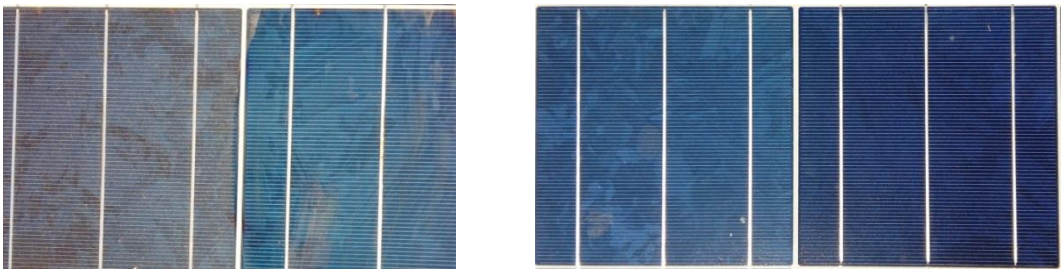

(**a**) (**b**)

Figure 117 Dust accumulation on PV panels' surface (a) Medium soiled on 23.08.2018 (b) Clean PV panels' surface on 20.02.2019

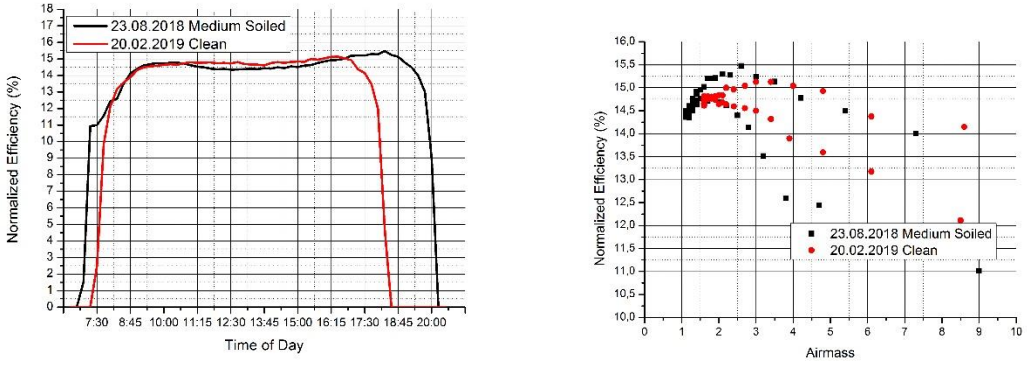

(**a**) (**b**)

Figure 118 Comparison in normalized efficiency between a medium soiled surface on 23.08.2018 and a clean surface on 20.02.2019.

No significant differences in normalized efficiency are observed in Figure 118. A deviation of -0.47% in averaged normalized efficiency is observed for 1<AM<3. Daily

performance ratio for 23.08.2019 was 0.853 in comparison with 0.892 at reference conditions. The last comparison concerns a heavily soiled surface on 24.04.2019 compared to the clean surface reference conditions of 20.02.2019. Figure 119 shows two PV cells without cleaning on 24.04.2019 and the two clean PV cells on 20.02.2019.

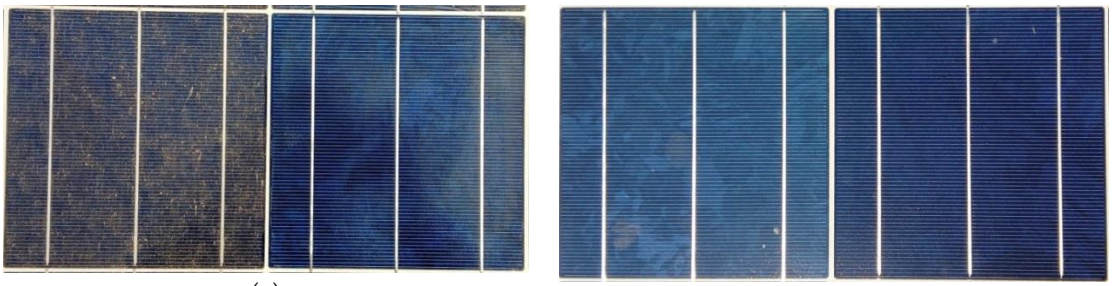

(**a**) (**b**)

Figure 119 Dust accumulation on PV panels' surface (a) Heavily soiled on 24.04.2019 (b) Clean PV panels' surface on 20.02.2019

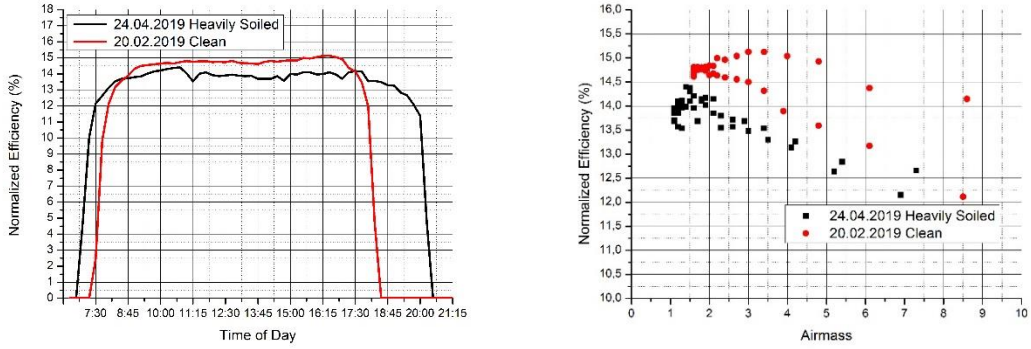

(**a**) (**b**)

Figure 120 Comparison in normalized efficiency between a heavily soiled surface on 24.04.2019 and the reference clean surface on 20.02.2019

Again, no significant differences in normalized efficiency are observed in Figure 120. A deviation of -5.6 % in averaged normalized efficiency is observed for 1<AM<3. The daily performance ratio on 29.04.2019 was 0.856 compared to 0.892 at reference conditions.

Table 31 summarizes the results for different levels of soiling for the three steps of the proposed methodology. It is clear that

Table 31 Performance metrics for five days with different level of soiling

PV panel surface	PR	Averaged Deviation from reference value 1<AM<3 (%)	Mean of normalized efficiency for the range 1<AM<3 (%)
Clean, 20-02-2019	0.892	-2.26	14.76
Clean, 18-03-2019	0.869	-1.45	14.65
Lightly Soiled, 29-04-2019	0.866	-3.2	14.83
Medium Soiled, 23-08-2018	0.853	-2.32	14.69
Heavily soiled, 24-04-2019	0.856	2.25	13.92

It is observed that conditions of medium and light soiling of the panels' surface have negligible impact on normalized efficiency, in contrast to heavy soiling which resulted

to a decrease of 5.6% on 24.04.2019. The effect of soiling on performance ratio does not show a particular trend in Table 31, however the largest value is at the reference conditions (20-02-2019), when the panels' temperatures are lower, (because PR depends on the panel's temperature). On the other hand, its comparison with the reference value (based on the mathematical model described) indicates a different behavior during the day with a heavily soiled surface (Table 31, last line), which is confirmed by the remarkable difference in normalized efficiency.

In order to observe the dust accumulation effect on the PV panel's efficiency and the effect of rainfall on the self-cleaning of PV panels, it is important to correlate daily rainfall (in mm) with normalized efficiency as shown in Figure 121.

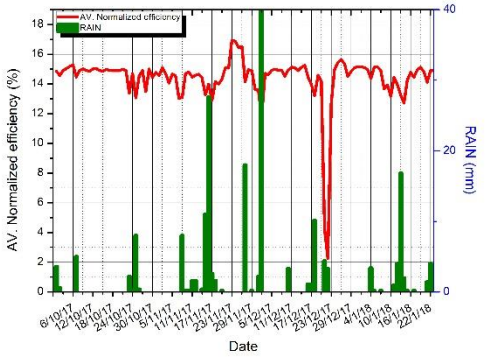

(**a**)

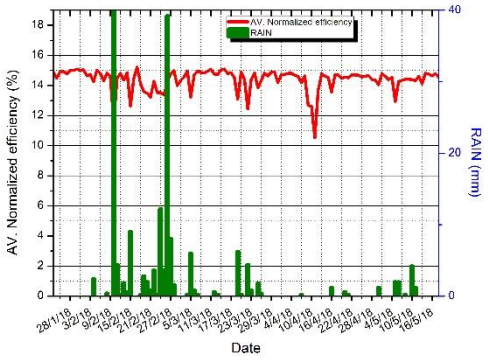

(**b**)

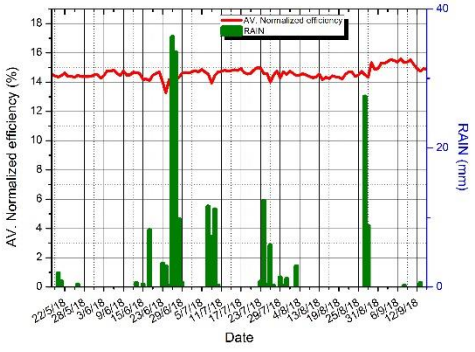

(**c**)

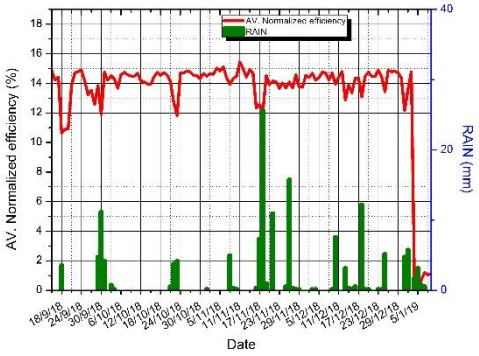

(**d**)

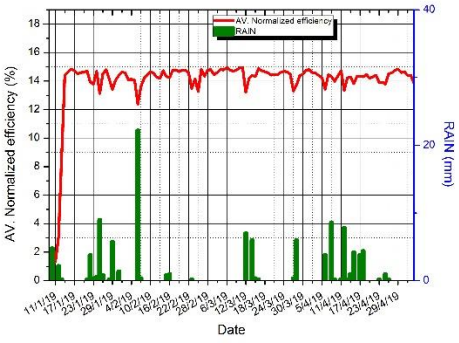

(e)

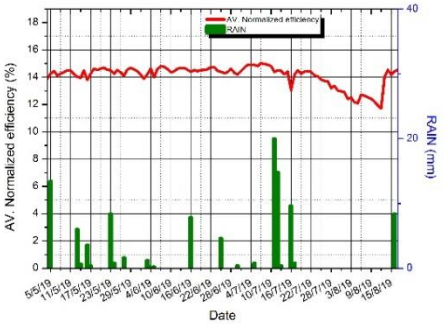

(f)

Figure 121 : Daily mm of precipitation (rainfall) in relation to the daily averaged normalized efficiency

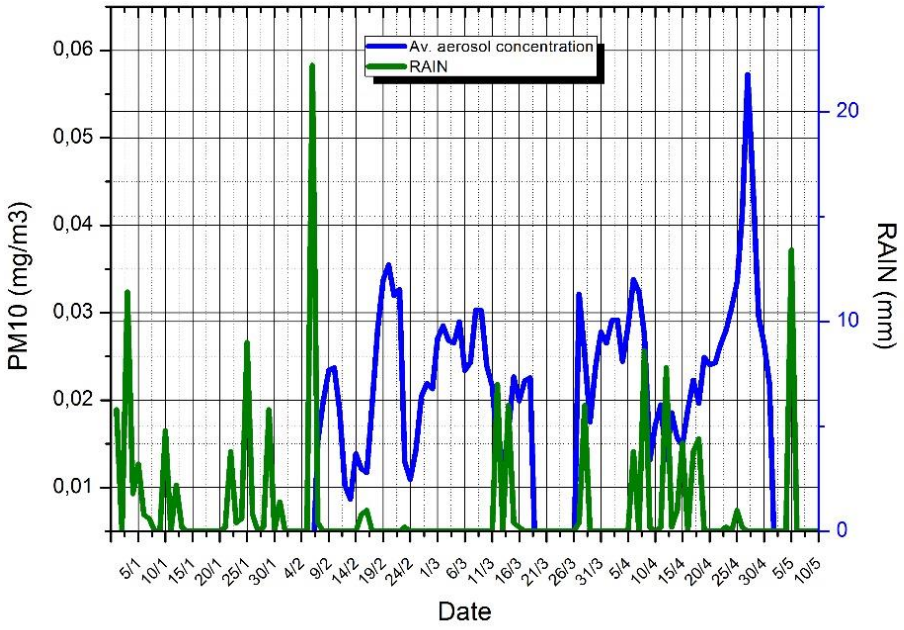

Figure 122 : Daily mm of rainfall related to daily averaged aerosol concentration \

7.4.2 Effect of ambient aerosol concentrations

Correlations among the normalized efficiency, irradiance, clearness index and aerosol concentration are attempted in this section. Three periods with recorded values of ambient aerosol concentration are examined (Figure 123).

As a starting point, the correlation between irradiance and ambient aerosol concentration is presented in Figure 123 for the specific periods: Several peaks of aerosol concentrations are recorded during the night, due to the effect of water vapor condensation in these nights [234]. Very low aerosol concentration is recorded during rainy days (Figure 122), (which obviously have very low irradiance levels), due to the nucleation and washing of particulate by the rain drops. Also, low aerosol concentration is observed in some cloudy days. The above remarks explain the lack of a straightforward correlation between irradiance and aerosol concentration. Another interesting phenomenon that is observed in these recordings is the transport of African dust in the period from 15-4-2019 to 28-4-2019, depicted in Figure 124Figure 123 (d) with an increasing trend in ambient PM10 concentration. Again, in this case, there is no obvious correlation of ambient PM10 concentration with irradiance levels.

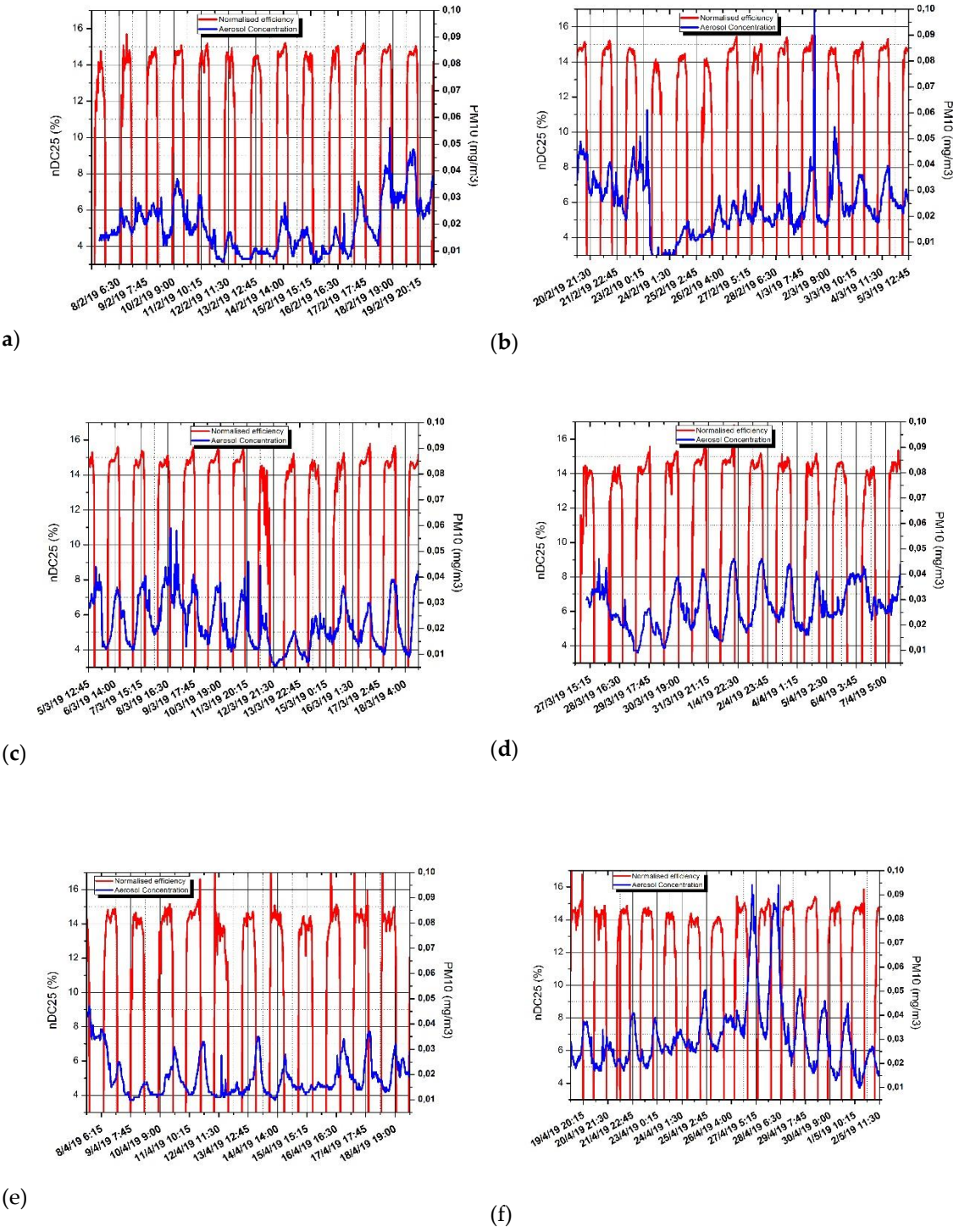

Figure 123 Aerosol concentration in comparison with Normalized efficiency (a), (b), (c) 08-02-2019 -18-03-2019. (d), (e),(f) 27-03-2019-02-05-2019

A more rational approach would be to correlate ambient aerosol concentration with clearness index, since it is possible that a portion of the particulate matter would diffuse short wavelengths of solar radiation that activate the PV panels. The same periods of study are analyzed in Figure 124-Figure 126, by presenting normalized PV efficiency as function of atmospheric aerosol concentration (PM10) with clearness index as additional parameter.

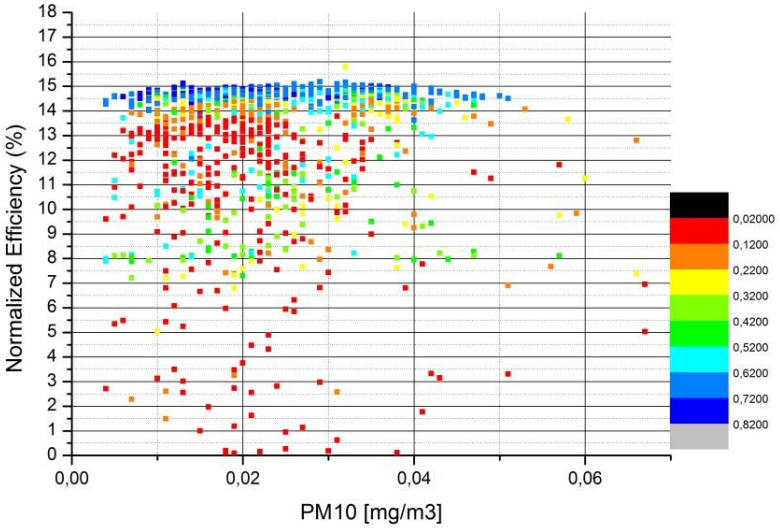

Figure 124 Correlation between PV normalized efficiency, aerosol concentration and clearness index for the period 03.12.2018-02.01.2019.

Figure 124 presents a correlation for the winter season 2018-19. As expected, high normalized efficiency figures are associated with high values of clearness index. They are generally associated with PM10 concentrations below the levels of 40 μg/m^3. Higher PM10 concentrations do not coincide with high normalized efficiency.

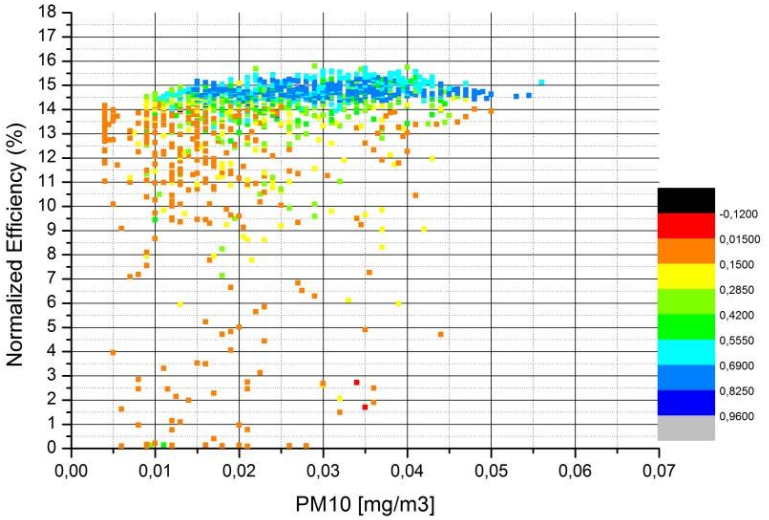

Figure 125 Correlation between PV normalized efficiency, aerosol concentration and clearness index from 07.02.2019-18.03.2019

Figure 125 presents a correlation for the beginning of spring 2019. Again, high normalized efficiency figures are associated with high values of clearness index, but the highest efficiency values occur with moderate values of clearness index. They are generally associated with PM_{10} concentrations below the levels in the range 10-50 μg/m3. Higher PM_{10} concentrations were not observed for this period.

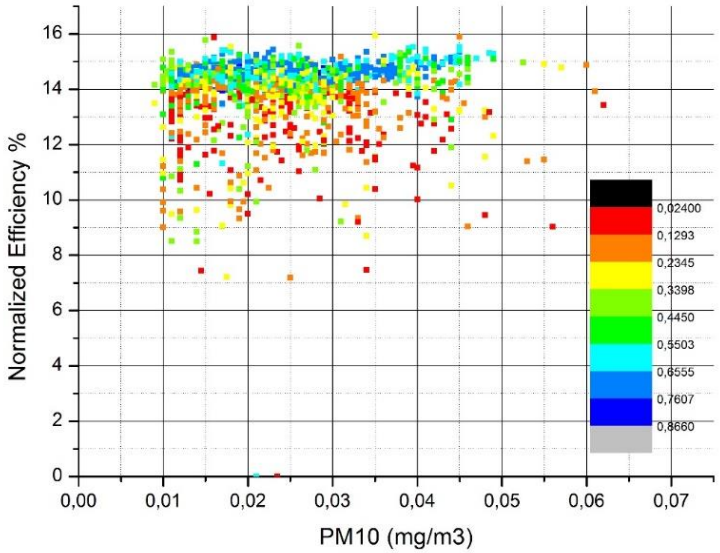

Figure 126 Correlation between PV normalized efficiency, aerosol concentration and clearness index from 27.03.2019-02.05.2019.

Figure 126 presents a correlation for the spring of 2019. High normalized efficiency figures are generally associated with high values of clearness index, but also occur with moderate values of clearness index. They are generally associated with PM_{10} concentrations below 50 μg/m³. However, high normalized efficiency figures are also observed during the days with highest transport of African dust.

7.5 Conclusions

This paper studied the effect of dust accumulation and ambient aerosol concentration levels on the performance of a grid-connected photovoltaic system. The method of analysis is based on three axis: calculation of PR, use of a bilinear model as reference value and calculation of normalized efficiency. The amounts of dust accumulated on the panels were not measured, thus the results are only qualitative. There are photographs which show the dust on PV panels' surface comparing with a reference situation in which surface was clean. The results show that dust accumulation has remarkable impact on efficiency. When the PV panels' surface was heavily soiled, a decrease of 5.6% in normalized efficiency was estimated. During the specific period the transport of large quantities of African dust was observed in the region. On the other hand, the impact of ambient aerosol concentration levels on PV efficiency is more complex and requires further study. Aerosol scattering of different wavelengths is possible to affect PV efficiency, however this fact may be related to the specific spectral response of PV cells. High normalized efficiency figures in general coincide with PM10 concentration not exceeding 50 μg/m³. On the other hand, lower clearness index is more directly correlated with lower normalized efficiency. Further investigation is necessary with spectral irradiance measurements in order to be able to correlate absorption or scattering in particular ranges of solar spectrum from atmospheric aerosols.

8 Concluding Remarks

From the analysis presented, it is concluded that there exists a non-linear reduction of efficiency in the solar irradiance range between 0 and 400 W/m2. The observed, systematic, deviations were correlated to the effect of air mass at low solar altitude angles. The remaining discrepancy could be correlated to the ambient amount of particulate matter (aerosol). The non-linear reduction of efficiency from the values predicted from the PV panels' manufacturer's curves results in an overestimation of the yearly electricity produced by the PV park, which was of the order of 2% for the specific installation. This percentage is by no means negligible since it affects the payback period of the installation.

Monitoring data from the operation of the inverters installed on one PV park were collected and processed to quantify the observable hotspots with losses in electricity production. It is found that two inverters out of six produce 5% and 1% less electric power respectively. However this is something that needs to be more extensively examined.

A comparison of the three models' computed values and the measured values shows significant deviations for all models. In terms of energy production, it was found that the PV form and the improved bilinear model underestimate the production, in contrast with Evans model. On the other hand, an agreement of all three models was observed to an efficiency decrease during the third year. Deviation between measured production and models' prediction was nearly constant for the years 2013 and 2014. However this deviation decreased for the year 2015. Thus, the application of models to this kind of data is able to give only general conclusions for the trend of the yearly energy production.

The main problem to be solved was the explanation of fluctuations in yearly energy production by the use of conventional measurement equipment. This study approaches this problem by three parallel procedures and concludes that an over 10% fluctuation in yearly energy production observed during the first two years is mainly due to irradiance levels variation, whereas a very small decrease in PV performance is probable for the third year.

A convergence is observed between performance ratio analysis, normalization procedure and models' comparison to the fact that a small decrease in PV panel's efficiency right from the first year of operation is recorded. However, this decrease is covered by the terms of the manufacturer's warranty. The main advantage of the proposed comparative procedure is that it allows drawing conclusions on the PV park's performance by employing basic monitoring equipment. From now on, a challenging task arises in the study of the aging effect in older PV panels.

The period of analysis concerns six years, 2013-2018. During these years, the AC energy yield varied in the range between 1467.7 – 1675.0 kWh/ kWp, AC wiring losses not included. Yearly performance ratio varied in the range 0.87 – 0.9, with a decreasing trend. When the measured values of power produced were compared with those computed by the improved bilinear model, it was observed that the deviation from the reference value had a decreasing trend over the years. This fact confirms the conclusion of PR analysis.

The analysis for clear sky conditions shows that normalized efficiency has a decreasing

trend and a seasonality during the year. Remarkable efficiencies were recorded in some clear sky days during the end of March of 2014, a fact that could be correlated with the solar maximum of solar cycle #24. The decreasing trend over the years is validated by the final step of analysis which involves the calculation of normalized efficiency for each one of the five defined AM classes. The degradation rates of normalized efficiency for the first two AM classes, which have the highest impact on total energy production, varied in the range 1.28% - 6.92%.

The results show that dust have remarkable impact when PV panels' surface was heavily soiled and estimated a decrease of 5.6% in normalized efficiency. It should be mentioned that significant African dust transport was observed in the region during this period.

Aerosol concentration do not have a direct impact on PV efficiency. However lower clearness index is correlated with lower normalized efficiency. This fact needs further investigation with spectral irradiance measurements in order to correlate performance with absorption or scattering in a particular range of solar spectrum from aerosols.

The results from all three axes of the proposed methodology converge to the fact that there is a decreasing trend in PV panels' efficiency, based on the assumption that the panels' surface is cleaned by rain and snow. Soiling effects are excluded from the analysis because they equally affect the irradiance sensor. However, it is a challenging task for future investigation to monitor the PV panels surface in order to correlate with possible efficiency reduction. This would allow decoupling the effect of soiling from the remaining factors influencing PV efficiency. Correlation of normalized efficiency - especially on clear sky days - with optical inspections on PV panels and sensors surface, combined with IR imaging, could provide important conclusions for soiling.

The resulting experience is employed in the development of a procedure that could be routinely applied to the health monitoring of PV installations. This procedure may also be employed for a pre-check of newly installed PV panels on site, which is increasingly requested by the clients. In combination with IR thermography the analysis procedure which is presented in sections 5, 6 is proposed in order to evaluate systems' performance, observe faults and draw conclusions for Photovoltaic performance under real world operation.

A challenging task is the application of methodology in different PV installations in Greek Territory in order to draw conclusions for the solar potential, PV behavior, degradation analysis. There are many PV grid-connected parks which are equipped with measurement devices that are described in this work and consequently only the application of the proposed methodology is required. This could be a useful GIS tool for PV technology.

REFERENCES

1. Union, E. *Directives*. Available from: https://ec.europa.eu/energy/en/topics/energy-strategy-and-energy-union/2020-energy-strategy.
2. *Global market outlook*. Available from: http://www.solarpowereurope.org/.
3. Huld, T., R. Müller, and A. Gambardella, *A new solar radiation database for estimating PV performance in Europe and Africa.* Solar Energy, 2012. **86**(6): p. 1803-1815.
4. Coria, G., F. Penizzotto, and R. Pringles, *Economic analysis of photovoltaic projects: The Argentinian renewable generation policy for residential sectors.* Renewable Energy, 2019. **133**: p. 1167-1177.
5. MARKET, O.O.E. *RES&CHP MONTHLY STATISTICS*. Available from: http://www.lagie.gr/en/feed-in-tariffs/res-chp/res-chp-monthly-statistics/.
6. Pablo-Romero, M.d.P., et al., *An overview of feed-in tariffs, premiums and tenders to promote electricity from biogas in the EU-28.* Renewable and Sustainable Energy Reviews, 2017. **73**: p. 1366-1379.
7. Gu Choi, D., et al., *Is the concept of 'grid parity' defined appropriately to evaluate the cost-competitiveness of renewable energy technologies?* Energy Policy, 2015. **86**: p. 718-728.
8. Cho, D. and J. Valenzuela, *Scheduling energy consumption for residential stand-alone photovoltaic systems.* Solar Energy, 2019. **187**: p. 393-403.
9. Marino, C., et al., *Energetic and economic analysis of a stand alone photovoltaic system with hydrogen storage.* Renewable Energy, 2019. **142**: p. 316-329.
10. Eltawil, M.A. and Z. Zhao, *Grid-connected photovoltaic power systems: Technical and potential problems—A review.* Renewable and Sustainable Energy Reviews, 2010. **14**(1): p. 112-129.
11. Rao, R.R., M. Mani, and P.C. Ramamurthy, *An updated review on factors and their inter-linked influences on photovoltaic system performance.* Heliyon, 2018. **4**(9): p. e00815.
12. Ma, J., et al., *Approximate Single-Diode Photovoltaic Model for Efficient I-V Characteristics Estimation*. Vol. 2013. 2013. 230471.
13. Hegedus, S. and A. Luque, *Handbook of Photovoltaic Science and Engineering, Second Edition*. 2011. p. 1-38.
14. Ibn-Mohammed, T., et al., *Perovskite solar cells: An integrated hybrid lifecycle assessment and review in comparison with other photovoltaic technologies.* Renewable and Sustainable Energy Reviews, 2017. **80**: p. 1321-1344.
15. *Crystalline Silicon Solar Cells and Modules*, in *Handbook of Photovoltaic Science and Engineering*. p. 255-306.
16. Jackson, F., *Planning & Installing Photovoltaic Systems*. 2007, London: earthscan.
17. Płaczek-Popko, E., *Top PV market solar cells 2016.* Opto-Electronics Review, 2017.

25(2): p. 55-64.

18. Parida, B., S. Iniyan, and R. Goic, *A review of solar photovoltaic technologies.* Renewable and Sustainable Energy Reviews, 2011. **15**(3): p. 1625-1636.

19. Yang, J., A. Banerjee, and S. Guha, *Amorphous silicon based photovoltaics—from earth to the "final frontier".* Solar Energy Materials and Solar Cells, 2003. **78**(1): p. 597-612.

20. Gay, R.R., *Status and prospects for CIS-based photovoltaics.* Solar Energy Materials and Solar Cells, 1997. **47**(1): p. 19-26.

21. *First Solar Series 6™*

Thin Film Modules. 2018 2018 04031_PD_BR_21AUG18]; Available from: http://www.firstsolar.com/en-EMEA/Modules/Our-Technology.

22. Bosio, A., G. Rosa, and N. Romeo, *Past, present and future of the thin film CdTe/CdS solar cells.* Solar Energy, 2018. **175**: p. 31-43.

23. Fauzi, I.F., M. Mohamad Shahimin, and M. Mazalan, *Simulation of cadmium telluride solar cells structure*. 2011. 392-396.

24. SANYO, P., *DATASHEET HIT PANASONIC.*

25. ALEO. *Data sheet*. Available from: https://www.aleo-solar.com/types-of-solar-panels/.

26. CanadianSolar. *Datasheets*. Available from: https://www.canadiansolar.com/en/solarPanels/detail/53.

27. LG. *DATASHEET*. Available from: https://www.lg.com/global/business/solar/neon-2.

28. REC. *DATASHEET*. Available from: https://recgroup.com/en.

29. LUXOR. *DATASHEET ECOLINE*. Available from: https://www.luxor-solar.com/en/solar-modules/eco-line.html.

30. HYUNDAI. *DATASHEET*. Available from: https://www.hyundaisolar.com.au/.

31. Sunpower. *Datasheet*. 2019; Available from: https://us.sunpower.com/products/solar-panels.

32. Suntech. *Datasheet*. 2018; Available from: http://www.suntech-power.com/productInfo.html?type=1726.

33. Panasonic. *Datasheet*. Available from: https://panasonic.net/lifesolutions/solar/download/index.html.

34. QCELLS, H. *DATASHEET*. Available from: https://www.hanwha-qcells.com/.

35. TRIENERGIA. *DATASHEET*. Available from: https://www.trienergia.com/.

36. FRONTIER, S. *DATASHEET*. Available from: http://www.solar-frontier.com/eng/.

37. Yingli. *Datasheet*. Available from: http://www.yinglisolar.com/en/.

38. Sharp. *Datasheet*. Available from: https://www.sharp.co.uk/cps/rde/xchg/gb/hs.xsl/-/html/solar-modules.htm.

39. FIRSTSOLAR. *DATASHEET*. Available from: http://www.firstsolar.com/en-

EMEA/.

40. KANEKA, *DATASHEET.*

41. Sasitharanuwat, A., et al., *Performance evaluation of a 10kWp PV power system prototype for isolated building in Thailand.* Renewable Energy, 2007. **32**(8): p. 1288-1300.

42. Silvestre, S., et al., *Evaluation of the performance and degradation of crystalline silicon-based photovoltaic modules in the Saharan environment.* Energy, 2018. **152**: p. 57-63.

43. Tossa, A.K., et al., *Energy performance of different silicon photovoltaic technologies under hot and harsh climate.* Energy, 2016. **103**: p. 261-270.

44. Kichou, S., et al., *Analysis of the behaviour of cadmium telluride and crystalline silicon photovoltaic modules deployed outdoor under humid continental climate conditions.* Solar Energy, 2018. **171**: p. 681-691.

45. ASTM, *E 948 – 95 (Reapproved 2001) Standard Test Method for Electrical Performance of Photovoltaic Cells Using Reference Cells Under Simulated Sunlight*. 2001.

46. ASTM, *G173 - 03 Standard Tables for Reference Solar Spectral Irradiances: Direct Normal and Hemispherical on 37° Tilted Surface*. 2012.

47. Osterwald, C.R., *llf-1 - Standards, calibration and testing of PV modules and solar cells A2 - Markvart, Tom*, in *Solar Cells*, L. Castañer, Editor. 2005, Elsevier Science: Oxford. p. 451-474.

48. Strutt, J., *On the scattering of light by small particles. .* Philosophical Magazine, 1871. **Series 4**(41): p. 447-454.

49. Mie, G., *Beiträge zur Optik trüber Medien, speziell kolloidaler Metallösungen. .* Annalen der Physik, Vierte Folge, 1908. **Band 25**(3): p. 377–445.

50. Roumpakias, E., *Efficiency of PV installations in real world operating conditions. MSc Thesis*, in *Mechanical Engineering Department, University of Thessaly*. 2012.

51. Gueymard, C.A. and H.D. Kambezidis, *5 - Solar spectral radiation*, in *Solar Radiation and Daylight Models (Second Edition)*, T. Muneer, C. Gueymard, and H. Kambezidis, Editors. 2004, Butterworth-Heinemann: Oxford. p. 221-301.

52. Dubey, S., J.N. Sarvaiya, and B. Seshadri, *Temperature Dependent Photovoltaic (PV) Efficiency and Its Effect on PV Production in the World – A Review.* Energy Procedia, 2013. **33**: p. 311-321.

53. Said, S.A.M., et al., *The effect of environmental factors and dust accumulation on photovoltaic modules and dust-accumulation mitigation strategies.* Renewable and Sustainable Energy Reviews, 2018. **82**: p. 743-760.

54. Skoplaki, E. and J.A. Palyvos, *On the temperature dependence of photovoltaic module electrical performance: A review of efficiency/power correlations.* Solar Energy, 2009. **83**(5): p. 614-624.

55. Skoplaki, E. and J.A. Palyvos, *Operating temperature of photovoltaic modules: A survey of pertinent correlations.* Renewable Energy, 2009. **34**(1): p. 23-29.

56. Garcia, M.C.A. and J.L. Balenzategui, *Estimation of photovoltaic module yearly*

temperature and performance based on Nominal Operation Cell Temperature calculations. Renewable Energy 2004. **29** p. 1997–2010.

57. del Cueto, J.A., *Comparison of energy production and performance from flat plate PV module technologies deployed at fixed tilt*. 2002. 1523-1526.

58. Alonso-Abella, M., et al., *Analysis of spectral effects on the energy yield of different PV (photovoltaic) technologies: The case of four specific sites.* Energy, 2014. **67**: p. 435-443.

59. Kumar, R. and L. Umanand, *Estimation of global radiation using clearness index model for sizing photovoltaic system.* Renewable Energy, 2005. **30**(15): p. 2221-2233.

60. Santos, J.M., J.M. Pinazo, and J. Cañada, *Methodology for generating daily clearness index index values Kt starting from the monthly average daily value Kt. Determining the daily sequence using stochastic models.* Renewable Energy, 2003. **28**(10): p. 1523-1544.

61. Mellit, A., et al., *Methodology for predicting sequences of mean monthly clearness index and daily solar radiation data in remote areas: Application for sizing a stand-alone PV system.* Renewable Energy, 2008. **33**(7): p. 1570-1590.

62. Woyte, A., R. Belmans, and J. Nijs, *Fluctuations in instantaneous clearness index: Analysis and statistics.* Solar Energy, 2007. **81**(2): p. 195-206.

63. Nakada, Y., et al., *Influence of clearness index and air mass on sunlight and outdoor performance of photovoltaic modules.* Current Applied Physics, 2010. **10**(2, Supplement): p. S261-S264.

64. Norton, M., A.M.G. Amillo, and R. Galleano, *Comparison of solar spectral irradiance measurements using the average photon energy parameter.* Solar Energy, 2015. **120**: p. 337-344.

65. Green, M.A., et al., *Solar cell efficiency tables (version 39).* Progress in Photovoltaics: Research and Applications, 2012. **20**(1): p. 12-20.

66. Perez-Lopez, J.J., F. Fabero, and F. Chenlo, *Experimental Solar Spectral Irradiance Until 2500 nm: Results and Influence on the PV Conversion of Different Materials.* Prog. Photovolt: Res. Appl., 2007. **15**: p. 303–315.

67. Zdanowicz, T., T. Rodziewicz, and M.Z. Waclawek. *Effect of air mass factor on the performance of different type of PV modules*. in *Photovoltaic Energy Conversion, 2003. Proceedings of 3rd World Conference on*. 2003.

68. Virtuani, A., H. Muellejans, and E. Dunlop, *Comparison of indoor and outdoor performance measurement of recent commercially available solar modules*. Vol. 19. 2011. 11-20.

69. Koussa, M., et al., *Measured and modelled improvement in solar energy yield from flat plate photovoltaic systems utilizing different tracking systems and under a range of environmental conditions.* Applied Energy, 2011. **88**(5): p. 1756-1771.

70. Koussa, M., et al., *Sun Tracker Systems Effects on Flat Plate Photovoltaic PV Systems Performance for Different Sky States: A Case of an Arid and Hot Climate.* Energy Procedia, 2012. **18**(0): p. 839-850.

71. Sidek, M.H.M., et al., *Automated positioning dual-axis solar tracking system with precision elevation and azimuth angle control.* Energy, 2017. **124**: p. 160-170.

72. Tian, W., et al., *Effect of urban climate on building integrated photovoltaics performance.* Energy Conversion and Management, 2007. **48**(1): p. 1-8.

73. Malathy, S. and R. Ramaprabha, *Comprehensive analysis on the role of array size and configuration on energy yield of photovoltaic systems under shaded conditions.* Renewable and Sustainable Energy Reviews, 2015. **49**: p. 672-679.

74. Bingöl, O. and B. Özkaya, *Analysis and comparison of different PV array configurations under partial shading conditions.* Solar Energy, 2018. **160**: p. 336-343.

75. Satpathy, P.R. and R. Sharma, *Power loss reduction in partially shaded PV arrays by a static SDP technique.* Energy, 2018. **156**: p. 569-585.

76. Shamseldein, M., M. Kazerani, and M.M.A. Salama, *Optimal Photovoltaic Array Reconfiguration to Reduce Partial Shading Losses.* Sustainable Energy, IEEE Transactions on, 2013. **4**: p. 145-153.

77. Sullivan, C.R., J.J. Awerbuch, and A.M. Latham, *Decrease in Photovoltaic Power Output from Ripple: Simple General Calculation and the Effect of Partial Shading.* Power Electronics, IEEE Transactions on, 2013. **28**(2): p. 740-747.

78. Anzalchi, A. and A. Sarwat, *Overview of technical specifications for grid-connected photovoltaic systems.* Energy Conversion and Management, 2017. **152**: p. 312-327.

79. Xiao, B., et al., *Modular Cascaded H-Bridge Multilevel PV Inverter With Distributed MPPT for Grid-Connected Applications.* IEEE Transactions on Industry Applications, 2015. **51**(2): p. 1722-1731.

80. Mahela, O.P. and A.G. Shaik, *Comprehensive overview of grid interfaced solar photovoltaic systems.* Renewable and Sustainable Energy Reviews, 2017. **68**: p. 316-332.

81. Sangwongwanich, A., et al. *Impacts of PV array sizing on PV inverter lifetime and reliability*. in *2017 IEEE Energy Conversion Congress and Exposition (ECCE)*. 2017.

82. Vignola, F., F. Mavromatakis, and J. Krumsick, *Performance of PV inverters*. Vol. 1. 2008.

83. Gupta, A., Y.K. Chauhan, and R.K. Pachauri, *A comparative investigation of maximum power point tracking methods for solar PV system.* Solar Energy, 2016. **136**: p. 236-253.

84. Luoma, J., J. Kleissl, and K. Murray, *Optimal inverter sizing considering cloud enhancement.* Solar Energy, 2012. **86**(1): p. 421-429.

85. Hussin, M.Z., et al. *Sizing ratio of inverter and PV array for a-Si FS GCPV system in Malaysia's perspectives*. in *2012 IEEE Control and System Graduate Research Colloquium*. 2012.

86. Chen, S., et al., *Determining the optimum grid-connected photovoltaic inverter size.* Solar Energy, 2013. **87**: p. 96-116.

87. Mondol, J.D., Y.G. Yohanis, and B. Norton, *Optimal sizing of array and inverter for grid-connected photovoltaic systems.* Solar Energy, 2006. **80**(12): p. 1517-1539.

88. Rodrigo, P.M., R. Velázquez, and E.F. Fernández, *DC/AC conversion efficiency of grid-connected photovoltaic inverters in central Mexico.* Solar Energy, 2016. **139**: p. 650-665.

89. *TIGO ENERGY presents steps to maximize PV solar*

production over the system lifetime. Photovoltaics international, 2008.

90. Kaldellis, J.K. and A. Kokala, *Quantifying the decrease of the photovoltaic panels' energy yield due to phenomena of natural air pollution disposal.* Energy, 2010. **35**(12): p. 4862-4869.

91. Darwish, Z.A., et al., *Effect of dust pollutant type on photovoltaic performance.* Renewable and Sustainable Energy Reviews, 2015. **41**: p. 735-744.

92. Ullah, A., et al., *Investigation of optimal tilt angles and effects of soiling on PV energy production in Pakistan.* Renewable Energy, 2019. **139**: p. 830-843.

93. Saidan, M., et al., *Experimental study on the effect of dust deposition on solar photovoltaic panels in desert environment.* Renewable Energy, 2016. **92**: p. 499-505.

94. Ramli, M.A.M., et al., *On the investigation of photovoltaic output power reduction due to dust accumulation and weather conditions.* Renewable Energy, 2016. **99**: p. 836-844.

95. Massi Pavan, A., A. Mellit, and D. De Pieri, *The effect of soiling on energy production for large-scale photovoltaic plants.* Solar Energy, 2011. **85**(5): p. 1128-1136.

96. Pulipaka, S. and R. Kumar, *Analysis of irradiance losses on a soiled photovoltaic panel using contours.* Energy Conversion and Management, 2016. **115**: p. 327-336.

97. Beattie, N.S., et al., *Understanding the effects of sand and dust accumulation on photovoltaic modules.* Renewable Energy, 2012. **48**: p. 448-452.

98. Javed, W., B. Guo, and B. Figgis, *Modeling of photovoltaic soiling loss asa function of environmental variables.* Solar Energy, 2017. **157**: p. 397-407.

99. Abderrezek, M. and M. Fathi, *Experimental study of the dust effect on photovoltaic panels' energy yield.* Solar Energy, 2017. **142**: p. 308-320.

100. Adıgüzel, E., et al., *Prediction of dust particle size effect on efficiency of photovoltaic modules with ANFIS: An experimental study in Aegean region, Turkey.* Solar Energy, 2019. **177**: p. 690-702.

101. Kaldellis, J.K. and P. Fragos, *Ash deposition impact on the energy performance of photovoltaic generators.* Journal of Cleaner Production, 2011. **19**(4): p. 311-317.

102. Kaldellis, J.K. and M. Kapsali, *Simulating the dust effect on the energy performance of photovoltaic generators based on experimental measurements.* Energy, 2011. **36**(8): p. 5154-5161.

103. Mussard, M. and M. Amara, *Performance of solar photovoltaic modules under arid climatic conditions: A review.* Solar Energy, 2018. **174**: p. 409-421.

104. Sartelet, K., et al., *Representation of aerosol optical properties using a chemistry transport model to improve solar irradiance modelling.* Solar Energy, 2018. **176**: p. 439-452.

105. Gutiérrez, C., et al., *Impact of aerosols on the spatiotemporal variability of photovoltaic energy production in the Euro-Mediterranean area.* Solar Energy, 2018. **174**: p. 1142-1152.

106. Neher, I., et al., *Impact of atmospheric aerosols on photovoltaic energy production*

Scenario for the Sahel zone. Energy Procedia, 2017. **125**: p. 170-179.

107. Ndiaye, A., et al., *Degradations of silicon photovoltaic modules: A literature review.* Solar Energy, 2013. **96**: p. 140-151.

108. Oreski, G. and G.M. Wallner, *Evaluation of the aging behavior of ethylene copolymer films for solar applications under accelerated weathering conditions.* Solar Energy, 2009. **83**: p. 1040-1047.

109. Sharma, V. and S.S. Chandel, *Performance and degradation analysis for long term reliability of solar photovoltaic systems: A review.* Renewable Sustainable Energy Review, 2013. **27**: p. 753-767.

110. Jordan, D.C. and S.R. Kurtz, *Photovoltaic Degradation Rates — An Analytical Review.* Progress in Photovoltaics: Research and Applications, 2012.

111. Limmanee, A., et al., *Degradation analysis of photovoltaic modules under tropical climatic conditions and its impacts on LCOE.* Renewable Energy, 2017. **102**: p. 199-204.

112. Rajput, P., et al., *Degradation of mono-crystalline photovoltaic modules after 22years of outdoor exposure in the composite climate of India.* Solar Energy, 2016. **135**: p. 786-795.

113. Han, H., et al., *Analysis of the Degradation of Monocrystalline Silicon Photovoltaic Modules After Long-Term Exposure for 18 Years in a Hot–Humid Climate in China.* IEEE Journal of Photovoltaics, 2018. **8**(3): p. 806-812.

114. Hoyer, U., et al., *Analysis of PV modules by electroluminescence and IR thermography*, in *24th European Photovoltaic Solar Energy Conference*. 2009: Hamburg, Germany.

115. Acciani, G., O. Falcone, and S. Vergura. *Typical Defects of PV-Cells*. in *IEEE international symposium on industrial electronics (ISIE)*. 2010. Bari, Italy.

116. Berghold, J., et al., *Potential Induced Degradation of solar cells and panels.*

117. Köntges, M. *Reviewing the practicality and utility of electroluminescence and thermography*. 2014; Available from: http://www.nrel.gov/pv/pdfs/2014_pvmrw_33_kontges.pdf.

118. Bouraiou, A., et al., *Analysis and evaluation of the impact of climatic conditions on the photovoltaic modules performance in the desert environment.* Energy Conversion and Management, 2015. **106**: p. 1345-1355.

119. Roumpakias, E., F. Bouroutzikas, and A. Stamatelos, *On-site Inspection of PV Panels, Aided by Infrared Thermography.* Advances in Applied Sciences, 2016. **Vol. 1**(No. 3): p. pp. 53-62.

120. Bergmann, A., ed. *Photovoltaikanlagen*. 2011, VDE VERLAG Berlin - Offenbach.

121. Osterwald, C.R., *Chapter III-2 - Standards, Calibration, and Testing of PV Modules and Solar Cells*, in *Practical Handbook of Photovoltaics (Second Edition)*. 2012, Academic Press: Boston. p. 1045-1069.

122. Cañete, C., J. Carretero, and M. Sidrach-de-Cardona, *Energy performance of different photovoltaic module technologies under outdoor conditions.* Energy, 2014. **65**: p. 295-302.

123. Emery, K. and R. Smith, *Monitoring System Performance NREL/PR-5200-50643*, in *PV Module Reliability Workshop*, NREL, Editor. 2011.

124. Huld, T., et al., *Data sets for energy rating of photovoltaic modules.* Solar Energy, 2013. **93**: p. 267-279.

125. Wittkopf, S., et al., *Analytical performance monitoring of a 142.5kWp grid-connected rooftop BIPV system in Singapore.* Renewable Energy, 2012. **47**: p. 9-20.

126. Aristizabal, A.J., et al. *Development of Equipment for Monitoring PV Power Plants, using Virtual Instrumentation*. in *Photovoltaic Energy Conversion, Conference Record of the 2006 IEEE 4th World Conference on*. 2006.

127. KOSTAL. *DATASHEET*. Available from: https://www.kostal-solar-electric.com/el-gr/products/tools-and-software/monitoring.

128. SMA, *DATASHEET.*

129. Mavromatakis, F., et al., *Modeling the photovoltaic potential of a site.* Renewable Energy, 2010. **35**(7): p. 1387-1390.

130. Milosavljević, D.D., T.M. Pavlović, and D.S. Piršl, *Performance analysis of A grid-connected solar PV plant in Niš, republic of Serbia.* Renewable and Sustainable Energy Reviews, 2015. **44**: p. 423-435.

131. Bianchini, A., et al., *Performance analysis and economic assessment of different photovoltaic technologies based on experimental measurements.* Renewable Energy, 2016. **85**: p. 1-11.

132. Chandel, S.S., et al., *Degradation analysis of 28 year field exposed mono-c-Si photovoltaic modules of a direct coupled solar water pumping system in western Himalayan region of India.* Renewable Energy, 2015. **78**: p. 193-202.

133. Han, H., et al., *Degradation analysis of crystalline silicon photovoltaic modules exposed over 30 years in hot-humid climate in China.* Solar Energy, 2018. **170**: p. 510-519.

134. Malvoni, M., M.G. De Giorgi, and P.M. Congedo, *Study of degradation of a grid connected photovoltaic system.* Energy Procedia, 2017. **126**: p. 644-650.

135. Quansah, D.A. and M.S. Adaramola, *Ageing and degradation in solar photovoltaic modules installed in northern Ghana.* Solar Energy, 2018. **173**: p. 834-847.

136. Sharma, V. and S.S. Chandel, *A novel study for determining early life degradation of multi-crystalline-silicon photovoltaic modules observed in western Himalayan Indian climatic conditions.* Solar Energy, 2016. **134**: p. 32-44.

137. Tabatabaei, S.A., D. Formolo, and J. Treur, *Analysis of performance degradation of domestic monocrystalline photovoltaic systems for a real-world case.* Energy Procedia, 2017. **128**: p. 121-129.

138. Tanesab, J., et al., *Seasonal effect of dust on the degradation of PV modules performance deployed in different climate areas.* Renewable Energy, 2017. **111**: p. 105-115.

139. Hafeznia, H., H. Yousefi, and F. Razi Astaraei, *A novel framework for the potential assessment of utility-scale photovoltaic solar energy, application to eastern Iran.* Energy Conversion and Management, 2017. **151**: p. 240-258.

140. Mellit, A. and A.M. Pavan, *A 24-h forecast of solar irradiance using artificial neural*

network: Application for performance prediction of a grid-connected PV plant at Trieste, Italy. Solar Energy, 2010. **84**(5): p. 807-821.

141. Nespoli, L. and V. Medici, *An unsupervised method for estimating the global horizontal irradiance from photovoltaic power measurements.* Solar Energy, 2017. **158**: p. 701-710.

142. Graditi, G., S. Ferlito, and G. Adinolfi, *Comparison of Photovoltaic plant power production prediction methods using a large measured dataset.* Renewable Energy, 2016. **90**: p. 513-519.

143. Cervone, G., et al., *Short-term photovoltaic power forecasting using Artificial Neural Networks and an Analog Ensemble.* Renewable Energy, 2017. **108**: p. 274-286.

144. Maleki, A., et al., *A novel framework for optimal photovoltaic size and location in remote areas using a hybrid method: A case study of eastern Iran.* Energy Conversion and Management, 2017. **153**: p. 129-143.

145. Mavromatidis, G., K. Orehounig, and J. Carmeliet, *Evaluation of photovoltaic integration potential in a village.* Solar Energy, 2015. **121**: p. 152-168.

146. Hachicha, A.A., I. Al-Sawafta, and Z. Said, *Impact of dust on the performance of solar photovoltaic (PV) systems under United Arab Emirates weather conditions.* Renewable Energy, 2019. **141**: p. 287-297.

147. Triki-Lahiani, A., A. Bennani-Ben Abdelghani, and I. Slama-Belkhodja, *Fault detection and monitoring systems for photovoltaic installations: A review.* Renewable and Sustainable Energy Reviews, 2018. **82**: p. 2680-2692.

148. Phinikarides, A., et al., *Review of photovoltaic degradation rate methodologies.* Renewable and Sustainable Energy Reviews, 2014. **40**: p. 143-152.

149. Huang, C. and L. Wang, *Simulation study on the degradation process of photovoltaic modules.* Energy Conversion and Management, 2018. **165**: p. 236-243.

150. Ozden, T., B.G. Akinoglu, and R. Turan, *Long term outdoor performances of three different on-grid PV arrays in central Anatolia – An extended analysis.* Renewable Energy, 2017. **101**: p. 182-195.

151. Dias, C.L.d.A., et al., *Performance estimation of photovoltaic technologies in Brazil.* Renewable Energy, 2017. **114**: p. 367-375.

152. Herteleer, B., et al., *Normalised efficiency of photovoltaic systems: Going beyond the performance ratio.* Solar Energy, 2017. **157**: p. 408-418.

153. Roumpakias, E. and A. Stamatelos, *Comparative performance analysis of grid-connected photovoltaic system by use of existing performance models.* Energy Conversion and Management, 2017. **150**: p. 14-25.

154. Roumpakias, E. and A. Stamatelos, *Performance analysis of a grid-connected Photovoltaic park after 6 years of operation.* Renewable Energy, 2019.

155. Emery, K.A. and C.R. Osterwald, *Solar cell efficiency measurements.* Solar Cells, 1986. **17**(2): p. 253-274.

156. Evans, D.L., *Simplified method for predicting photovoltaic array output.* Solar Energy, 1981. **27**(6): p. 555-560.

157. Nacer, T., et al., *Feasibility study of grid connected photovoltaic system in family farms*

for electricity generation in rural areas. Renewable Energy, 2016. **96, Part A**: p. 305-318.

158. Roumpakias, E., O. Zogou, and A. Stamatelos, *Correlation of actual efficiency of photovoltaic panels with air mass.* Renewable Energy, 2015. **74**(0): p. 70-77.

159. Zogou, O. and H. Stapountzis, *Experimental validation of an improved concept of building integrated photovoltaic panels.* Renewable Energy, 2011. **36**(12): p. 3488-3498.

160. Marion, B. *Comparison of predictive models for photovoltaic module performance*. in *Photovoltaic Specialists Conference, 2008. PVSC '08. 33rd IEEE*. 2008.

161. Skoplaki, E., A.G. Boudouvis, and J.A. Palyvos, *A simple correlation for the operating temperature of photovoltaic modules of arbitrary mounting.* Solar Energy Materials and Solar Cells, 2008. **92**(11): p. 1393-1402.

162. Akhsassi, M., et al., *Experimental investigation and modeling of the thermal behavior of a solar PV module.* Solar Energy Materials and Solar Cells, 2018. **180**: p. 271-279.

163. Khalid, A.M., et al., *Performance ratio – Crucial parameter for grid connected PV plants.* Renewable and Sustainable Energy Reviews, 2016. **65**: p. 1139-1158.

164. Marion, B., et al., *Performance parameters for grid-connected PV systems*, in *Photovoltaic Specialists, IEEE Conference*. 2005. p. 1601-1606.

165. Elhadj Sidi, C.E.B., et al., *Performance analysis of the first large-scale (15 MWp) grid-connected photovoltaic plant in Mauritania.* Energy Conversion and Management, 2016. **119**: p. 411-421.

166. Kymakis, E., S. Kalykakis, and T.M. Papazoglou, *Performance analysis of a grid connected photovoltaic park on the island of Crete.* Energy Conversion and Management, 2009. **50**(3): p. 433-438.

167. Dabou, R., et al., *Monitoring and performance analysis of grid connected photovoltaic under different climatic conditions in south Algeria.* Energy Conversion and Management, 2016. **130**: p. 200-206.

168. de Lima, L.C., L. de Araújo Ferreira, and F.H.B. de Lima Morais, *Performance analysis of a grid connected photovoltaic system in northeastern Brazil.* Energy for Sustainable Development, 2017. **37**: p. 79-85.

169. Congedo, P.M., et al., *Performance measurements of monocrystalline silicon PV modules in South-eastern Italy.* Energy Conversion and Management, 2013. **68**: p. 1-10.

170. Martín-Martínez, S., et al., *Performance evaluation of large solar photovoltaic power plants in Spain.* Energy Conversion and Management, 2019. **183**: p. 515-528.

171. Necaibia, A., et al., *Analytical assessment of the outdoor performance and efficiency of grid-tied photovoltaic system under hot dry climate in the south of Algeria.* Energy Conversion and Management, 2018. **171**: p. 778-786.

172. Seme, S., et al., *Analysis of the performance of photovoltaic systems in Slovenia.* Solar Energy, 2019. **180**: p. 550-558.

173. Aste, N., C. Del Pero, and F. Leonforte, *PV technologies performance comparison in temperate climates.* Solar Energy, 2014. **109**: p. 1-10.

174. Ustun, T.S., et al., *Performance analysis of PV panels based on different technologies after two years of outdoor exposure in Fukushima, Japan.* Renewable Energy, 2019. **136**: p. 159-178.

175. Adrada Guerra, T., et al., *Comparative Energy Performance Analysis of Six Primary Photovoltaic Technologies in Madrid (Spain).* Energies, 2017. **10**: p. 772.

176. Edalati, S., M. Ameri, and M. Iranmanesh, *Comparative performance investigation of mono- and poly-crystalline silicon photovoltaic modules for use in grid-connected photovoltaic systems in dry climates.* Applied Energy, 2015. **160**: p. 255-265.

177. Dierauf, T., et al., *Weather-Corrected Performance Ratio*. 2013: United States.

178. Khatib, T., K. Sopian, and H.A. Kazem, *Actual performance and characteristic of a grid connected photovoltaic power system in the tropics: A short term evaluation.* Energy Conversion and Management, 2013. **71**: p. 115-119.

179. Kalogirou, S.A., *Artificial neural networks in renewable energy systems applications: a review.* Renewable and Sustainable Energy Reviews, 2001. **5**(4): p. 373-401.

180. Rodrigo, P., et al., *A new method for estimating angular, spectral and low irradiance losses in photovoltaic systems using an artificial neural network model in combination with the Osterwald model.* Solar Energy Materials and Solar Cells, 2012. **96**(0): p. 186-194.

181. Velilla, E., J. Valencia, and F. Jaramillo, *Performance evaluation of two solar photovoltaic technologies under atmospheric exposure using artificial neural network models.* Solar Energy, 2014. **107**: p. 260-271.

182. Touati, F., et al., *Long-term performance analysis and power prediction of PV technology in the State of Qatar.* Renewable Energy, 2017. **113**: p. 952-965.

183. Tahri, F., A. Tahri, and T. Oozeki, *Performance evaluation of grid-connected photovoltaic systems based on two photovoltaic module technologies under tropical climate conditions.* Energy Conversion and Management, 2018. **165**: p. 244-252.

184. Rosell, J.I. and M. Ibáñez, *Modelling power output in photovoltaic modules for outdoor operating conditions.* Energy Conversion and Management, 2006. **47**(15–16): p. 2424-2430.

185. Kazem, H.A. and J.H. Yousif, *Comparison of prediction methods of photovoltaic power system production using a measured dataset.* Energy Conversion and Management, 2017. **148**: p. 1070-1081.

186. Dias, C., et al., *Performance Estimation of Photovoltaic Technologies in Brazil*. Vol. 114. 2017.

187. Osterwald, C.R., K.A. Emery, and M. Muller, *Photovoltaic module calibration value versus optical air mass: the air mass function.* Progress in Photovoltaics: Research and Applications, 2014. **22**(5): p. 560-573.

188. Boutana, N., et al., *Assessment of implicit and explicit models for different photovoltaic modules technologies.* Energy, 2017. **122**: p. 128-143.

189. Aoun, N. and N. Bailek, *Evaluation of mathematical methods to characterize the electrical parameters of photovoltaic modules.* Energy Conversion and Management, 2019. **193**: p. 25-38.

190. Chouder, A. and S. Silvestre, *Automatic supervision and fault detection of PV*

systems based on power losses analysis. Energy Conversion and Management, 2010. **51**(10): p. 1929-1937.

191. Cuce, E., et al., *An accurate model for photovoltaic (PV) modules to determine electrical characteristics and thermodynamic performance parameters.* Energy Conversion and Management, 2017. **146**: p. 205-216.

192. Boutana, N., et al., *An explicit I-V model for photovoltaic module technologies.* Energy Conversion and Management, 2017. **138**: p. 400-412.

193. Gupta, A. and Y.K. Chauhan, *Detailed performance analysis of realistic solar photovoltaic systems at extensive climatic conditions.* Energy, 2016. **116**: p. 716-734.

194. Faba, A., S. Gaiotto, and G.M. Lozito, *A novel technique for online monitoring of photovoltaic devices degradation.* Solar Energy, 2017. **158**: p. 520-527.

195. Piliougine, M., et al., *Modelling photovoltaic modules with neural networks using angle of incidence and clearness index.* Progress in Photovoltaics: Research and Applications, 2015. **23**(4): p. 513-523.

196. Gaglia, A.G., et al., *Energy efficiency of PV panels under real outdoor conditions–An experimental assessment in Athens, Greece.* Renewable Energy, 2017. **101**: p. 236-243.

197. Tahri, A., et al., *Analysis of thin film photovoltaic modules under outdoor long term exposure in semi-arid climate conditions.* Solar Energy, 2017. **157**: p. 587-595.

198. Carr, A.J. and T.L. Pryor, *A comparison of the performance of different PV module types in temperate climates.* Solar Energy, 2004. **76**(1): p. 285-294.

199. Guenounou, A., A. Malek, and M. Aillerie, *Comparative performance of PV panels of different technologies over one year of exposure: Application to a coastal Mediterranean region of Algeria.* Energy Conversion and Management, 2016. **114**: p. 356-363.

200. Sánchez-Friera, P., et al., *Analysis of degradation mechanisms of crystalline silicon PV modules after 12 years of operation in Southern Europe.* Progress in Photovoltaics: Research and Applications, 2011. **19**(6): p. 658-666.

201. Kaden, T., K. Lammers, and H.J. Möller, *Power loss prognosis from thermographic images of PID affected silicon solar modules.* Solar Energy Materials and Solar Cells, 2015. **142**: p. 24-28.

202. Micheli, D., et al., *Analysis of the outdoor performance and efficiency of two grid connected photovoltaic systems in northern Italy.* Energy Conversion and Management, 2014. **80**(0): p. 436-445.

203. Duffie, J.A. and W.A. Beckmann, *Solar Engineering for Thermal Processes*. 1980, New York: John Wiley and Sons Inc.

204. King, D.L., W.E. Boyson, and J.A. Kratochvil. *Analysis of factors influencing the annual energy production of photovoltaic systems*. in *Photovoltaic Specialists Conference, 2002. Conference Record of the Twenty-Ninth IEEE*. 2002.

205. Parretta, A., A. Sarno, and L.R.M. Vicari, *Effects of solar irradiation conditions on the outdoor performance of photovoltaic modules.* Optics Communications, 1998. **153**(1–3): p. 153-163.

206. Schoenberg, E., *Theoretische Photometrie, g) Über die Extinktion des Lichtes in der*

Erdatmosphäre. In Handbuch der Astrophysik., 1929. **vol II.** (Berlin: Springer erste Hälfte.).

207. CORNARO, C. and A. ANDREOTTI. *Solar spectral irradiance measurements relevant to photovoltaic applications*. in *Proceedings of the Third International Conference on Applied Energy*. 2011. Perugia, Italy, 16-18 May 2011.

208. Gueymard, C. and H. Kambezidis, *Solar Spectral Radiation: Chapter 5 in "Solar Radiation and Daylight Models"*, T. Muneer, Editor. 2004, Elsevier, Butterworth Heinemann.

209. AB, F.S., *ThermaCAM Researcher Pro 2.8 SR-3*. 2006, FLIR Systems.

210. Ancuta, F. and C. Cepisca, *Failure Analysis Capabilities for PV Systems.* Models and Methods in Applied Sciences.

211. Kaplani, E., *Detection of Degradation Effects in Field-Aged c-Si Solar Cells through IR Thermography and Digital Image Processing.* International Journal of Photoenergy, 2012.

212. Munoz, M.A., et al., *Early degradation of silicon PV modules and guaranty conditions.* Solar Energy 2011.

213. Corinne, E., et al., *Development of a Visual Inspection Data Collection Tool for Evaluation of Fielded PV Module Condition*. 2012, National Rewenable Energy Laboratory (NREL).

214. FLIR. *Thermal imaging cameras: a fast and reliable tool for testing solar panels*. Available from: http://www.flir.co.uk/instruments/building/display/?id=41872.

215. IEC, *Grid connected photovoltaic systems – Minimum requirements for system documentation, commissioning tests and inspection*. 2009, IEC: Geneva, Switzerland.

216. Djordjevic, S., D. Parlevliet, and P. Jennings, *Detectable faults on recently installed solar modules in Western Australia.* Renewable Energy, 2013. **67**: p. 215-221.

217. Herrmann, W., W. Wiesner, and W. Vaaßen, *HOT SPOT INVESTIGATIONS ON PV MODULES - NEW CONCEPTS FOR A TEST STANDARD AND CONSEQUENCES FOR MODULE DESIGN WITH RESPECT TO BYPASS DIODES.*

218. Pern, F.J. and A.W. Czanderna, *Characterization of ethylene vinyl acetate (EVA) encapsulant: Effects of thermal processing and weathering degradation on its discoloration.* Solar Energy Materials and Solar Cells, 1992. **25**: p. 3-23.

219. Institute, I. *Standard for Infrared Inspection of Installed Photovoltaic (PV) Systems*. 2014; Available from: http://www.infraspection.com/infrared-standards.html.

220. International Solar Energy Society, G.S. *Thermografie – Auffälligkeiten erkennen, bevor Leistungsminderungen auftreten oder Schäden entstehen*. 2014; Available from: http://www.dgs-berlin.de/en/projects/bundesweitabgeschlossen/dkethermografie.html.

221. Polo, J., W.G. Fernandez-Neira, and M.C. Alonso-García, *On the use of reference modules as irradiance sensor for monitoring and modelling rooftop PV systems.* Renewable Energy, 2017. **106**: p. 186-191.

222. Yahyaoui, I. and M.E.V. Segatto, *A practical technique for on-line monitoring of a photovoltaic plant connected to a single-phase grid.* Energy Conversion and

Management, 2017. **132**: p. 198-206.

223. Ayompe, L.M., et al., *Measured performance of a 1.72 kW rooftop grid connected photovoltaic system in Ireland.* Energy Conversion and Management, 2011. **52**(2): p. 816-825.

224. Wirth, G., et al., *Modeling the maximum power output of a distributed PV fleet.* Progress in Photovoltaics: Research and Applications, 2015. **23**(9): p. 1164-1181.

225. Wang, H., et al., *Seasonal performance comparison of three grid connected photovoltaic systems based on different technologies operating under the same conditions.* Solar Energy, 2017. **144**: p. 798-807.

226. Donovan, M., B. Bourne, and J. Roche. *Efficiency VS. irradiance characterization of PV modules requires angle-of-incidence and spectral corrections*. in *Photovoltaic Specialists Conference (PVSC), 2010 35th IEEE*. 2010.

227. Waide, P.A. and B. Norton, *Variation of Insolation Transmission With Glazing Plane Position and Sky Conditions.* Journal of Solar Energy Engineering, 2003. **125**(2): p. 182-189.

228. Malvoni, M., et al., *Improvements in the predictions for the photovoltaic system performance of the Mediterranean regions.* Energy Conversion and Management, 2016. **128**: p. 191-202.

229. Marion, B. *Influence of atmospheric variations on photovoltaic performance and modeling their effects for days with clear skies*. in *2012 38th IEEE Photovoltaic Specialists Conference*. 2012.

230. Larrañeta, M., et al., *Identifying periods of clear sky direct normal irradiance.* Renewable Energy, 2017. **113**: p. 756-763.

231. Hathaway, D.D. *Solar Cycle Prediction* 2013; Available from: https://solarscience.msfc.nasa.gov/predict.shtml.

232. Jiang, J. and J. Cao, *Predicting solar surface large-scale magnetic field of Cycle 24.* Journal of Atmospheric and Solar-Terrestrial Physics, 2018. **176**: p. 34-41.

233. TSI, *Model 8530/8531/8532 DUSTTRAK II Aerosol Monitor, Operation and Service Manual. 2009, P/N 6001893, Revision D*. 2010.

234. Zogou, O. and A. Stamatelos, *Analysis of Data From Ambient PM10 Concentration Monitoring in Volos in the Period 2005-2010.* American Journal of Environmental Engineering, 2012. **2**(4): p. 97-108.

235. Heal, M.R., et al., *Intercomparison of five PM10 monitoring devices and the implications for exposure measurement in epidemiological research.* Journal of Environmental Monitoring, 2000. **2**(5): p. 455-461.

236. Chow, J.C., et al., *Comparability between PM2.5 and Particle Light Scattering Measurements.* Environmental Monitoring and Assessment, 2002. **79**(1): p. 29-45.

237. Kokhanovsky, A., *Aerosol Optics: Light Absorption and Scattering by Particles in the Atmosphere.* . 2008, Chichester UK: Springer/ Praxis Publishing.

238. Roumpakias, E. and A. Stamatelos, *Performance analysis of a grid-connected photovoltaic park after 6 years of operation.* Renewable Energy, 2019. **141**: p. 368-378.